



Thesis titled:

Studies into Selected Organic Anions and Cumulenenic Systems of Interstellar Significance

submitted for the Degree of Doctor of Philosophy (Ph.D.)

by

Andrew Michael McAnoy

B.Sc.(Hons)

of the

Department of Chemistry



**THE UNIVERSITY
OF ADELAIDE
AUSTRALIA**

February 2003

CONTENTS

PREFACE

Contents	i
Abstract	iv
Statement of Originality	v
Acknowledgements	vi

CHAPTER 1

EXPERIMENTAL METHODS FOR THE STUDY OF GAS PHASE IONS

1. INTRODUCTION	1
2. GENERATION OF IONS FOR MASS SPECTROMETRIC STUDY	2
3. MASS SPECTROMETRY	11
4. POSITIVE ION BEHAVIOUR	24
5. NEGATIVE ION BEHAVIOUR	25

CHAPTER 2

THEORETICAL METHODS FOR THE STUDY OF MOLECULAR SYSTEMS

1. INTRODUCTION	29
2. APPLICATION OF QUANTUM THEORY TO CHEMICAL PHENOMENA	29
3. CALCULATION OF CHEMICAL PROPERTIES	37

CHAPTER 3

SELECTED REARRANGEMENTS OF DEPROTONATED ORGANIC ANIONS

1. INTRODUCTION	41
2. RESULTS AND DISCUSSION	43
A. Loss of CO from Deprotonated Methyl Benzoate	43
B. Loss of CO ₂ from <i>Ortho</i> Deprotonated Methyl Phenyl Carbonate	61
3. EXPERIMENTAL	70
A. Mass Spectrometric Methods	70
B. Synthetic Procedures	71
C. Theoretical Methods	71

CHAPTER 4**THEORETICAL STUDIES OF POTENTIAL INTERSTELLAR ANIONS**

	ABSTRACT	73
1.	INTRODUCTION	74
A.	Molecules in the Interstellar Medium	74
B.	Anion Formation in the Interstellar Medium	81
2.	RESULTS AND DISCUSSION	87
A.	The C_nH Series	87
B.	The $C_{n-1}CH_2$ Series	96
C.	The C_nO Series	103
D.	The Possible Detection of C_nH^- , $C_{n-1}CH_2^-$, and C_nO^- as Interstellar Species	110
E.	Conclusions	114
3.	THEORETICAL METHODS	115

CHAPTER 5**FORMATION OF C_3 FROM THE LINEAR $[CCC]^-$ ANION IN THE GAS PHASE**

1.	INTRODUCTION	116
2.	RESULTS AND DISCUSSION	118
3.	EXPERIMENTAL	134
A.	Mass Spectrometric Methods	134
B.	Synthetic Procedures	135
C.	Theoretical Methods	135

CHAPTER 6**GENERATION OF BOROCUMULENIC SYSTEMS IN THE GAS PHASE**

1.	INTRODUCTION	137
2.	RESULTS AND DISCUSSION	139
A.	Formation of CCBO and $[CCBO]^+$ from $[CCBO]^-$ in the Gas Phase	139
B.	Formation of CCCCBO in the Gas Phase	157
C.	Borocumulenes of CCBCC connectivity	167
3.	EXPERIMENTAL	176
A.	Mass Spectrometric Methods	176
B.	Synthetic Methods	177
C.	Theoretical Methods	179
4.	APPENDIX	180

CHAPTER 7

SUMMARY AND CONCLUSIONS

1. EXPERIMENTAL STUDIES	181
2. THEORETICAL STUDIES	185

REFERENCES

186

List of Publications

ix

ABSTRACT

Energised organic anions in the gas phase may undergo fragmentation or rearrangement providing valuable information about the structure and intrinsic stability of the system. In this regard, the deprotonated anions of methyl benzoate and methyl phenyl carbonate have been investigated. These two systems were found to undergo rearrangements resulting in the losses of CO and CO₂ respectively. Experimental and theoretical studies into these processes have been carried out.

The identification of over 120 non-terrestrial molecules has led to considerable interest in interstellar and circumstellar chemistry. This thesis describes theoretical and experimental studies into processes of cumulenenic molecules, some of which are known interstellar molecules. We have carried out a systematic theoretical investigation into the possible radiative electron attachment to known interstellar molecules. These results suggest that within interstellar environs the C_nH, C_{n-1}CH₂ and C_nO series of molecules may capture an electron to form the corresponding stable anions. Experimentally, the anion of the interstellar cumulene C₃ was generated with the linear connectivity and was converted into the corresponding neutral in a ⁻NR⁺ experiment. Complete rearrangement of the carbons was observed; this process was investigated experimentally and theoretically.

Other neutral cumulenenic species, which have not been detected in the interstellar medium, are also of interest. Here we also describe efforts to generate various borocumulenes and borocumulene oxides in the gas phase, namely; CCBO, CCCCBO and CCBCC. The generation of these species and their rearrangements are discussed.

STATEMENT OF ORIGINALITY

This work contains no material which has been accepted for the award of any other degree, in any university or other tertiary institution and, to the best of my knowledge and belief, contains no material previously published or written by another person, except where due reference is made in the text.

I give consent to this copy of my thesis, when deposited in the University Library, being made available for loan and photocopying.

Andrew Michael McAnoy

14/2/03

Date

ACKNOWLEDGEMENTS

No significant scientific work can be carried out in isolation. It is therefore appropriate for me to acknowledge those persons who were involved in the science described in these pages. Also, this is an opportunity to thank family and friends who, despite not contributing to the science detailed here (and indeed may not fully understand it), have helped me through the last three years to this important milestone.

I would first like to acknowledge my supervisor Professor John Bowie, who has had a major role in all of the chemistry described here. Professor Bowie is an outstanding scientist; his extensive knowledge of gas phase ion chemistry has been an invaluable resource for my postgraduate studies. His genuine enthusiasm for scientific research has continually motivated me during my candidature. I also would like to thank Professor Bowie for the opportunity to participate in collaborative work with researchers from other institutions, as well as his support that has allowed me to travel to attend various conferences and conduct research overseas.

Dr Suresh Dua has been a pivotal part of the research from these laboratories over the past decade and this work is no different. I would therefore like to acknowledge his significant contribution to the chemistry described herein. Suresh's guidance has been instrumental in the development of my own scientific skills. His advice and encouragement has always been most appreciated. I am grateful for his friendship over the years that I have known him. I wish him, along with his family, all the best in his recent career change.

During my years in the Bowie group I was also fortunate enough to know Dr Stephen Blanksby. Steve was charged with the role of introducing me to theoretical calculations. These beginnings lead to a collaborative project after he left the group, and I thank him for

his participation (via many emails) in the MNRAS article as well as his advice on many other scientific matters. I wish him well as he begins his academic career.

Also noteworthy is Tom Blumenthal, who has the painstaking task of keeping the ZAB mass spectrometer running. In addition, he also teaches postgraduate students the operation and maintenance of the instrument and for this I am very much appreciative. This leads me to thank other members of the Bowie research group who over the years have helped provide a happy and productive work environment. In particular, I must mention Dr Sam Peppe and Craig Brinkworth. Sam has been a great friend and colleague and I thank him for his camaraderie and wish him well for the future. Our many lively discussions on scientific and political issues will be missed. My longest co-conspirator Craig has been a constant source of encouragement. I thank Craig for his friendship and for reminding me (by example) that it is ok to have dreams no matter how far fetched they may be. Additionally, I would like to express my gratitude to other group members; Pinmanee (Charm) Boontheung, Mark Fitzgerald, Margit Apponyi, Tara Pukala and Vita Maselli. It has been a pleasure working with such spirited people.

I am also very thankful to Professor Helmut Schwarz and members of his research group at the Technical University of Berlin. The Schwarz group were extremely welcoming and I very much enjoyed the time that I spent with them both academically and socially. My three months in Berlin both broadened and advanced my knowledge greatly. I would in particular like to thank Dr Detlef Schröder for his contribution to parts of the science presented here.

The Department of Chemistry at the University of Adelaide also deserves praise. The advice and expertise of the academic and general staff as well as fellow students have often

been invaluable. I also must acknowledge financial support of the University of Adelaide who awarded me a postgraduate stipend. Also, for allowing me to visit the Berlin laboratories I acknowledge an ARC linkage grant, Deutsche Forschungsgemeinschaft and Fonds der Chemischen Industrie for funding.

I would like to convey my appreciation to those individuals who have spent a considerable amount of time reading through parts or the whole of this thesis. These people include Professor John Bowie, Dr Sam Peppe, Dr Suresh Dua, Mark Fitzgerald and Craig Brinkworth.

This leaves only family and friends to graciously acknowledge for their kind thoughts and best wishes during the past three years. I thank all of my family and friends for their support during my university studies - especially during a number of trying times. It stands to reason that I must single out the support of my loving wife Sarah. As I make this significant academic accomplishment, the role that she played in me achieving it cannot be understated. I thank her dearly for all of her support and encouragement during the past three years, and for filling my life with purpose and joy each day.

CHAPTER 1

EXPERIMENTAL METHODS FOR THE STUDY OF GAS PHASE IONS

1. INTRODUCTION

Mass spectrometry is a field of research that is as fascinating as it is practical. This is exemplified by its routine involvement throughout many areas of chemistry, including (i) the analysis and detection of natural or synthetic compounds, and (ii) fundamental gas phase ion studies of unstable or short-lived species, such as reactive intermediates and interstellar molecules. Accurate mass measurements are routinely used as part of the chemical characterisation of organic compounds or natural products. While this is an important application of mass spectrometry it is not the end of its usefulness as an analytical technique with the fragmentations observed able to provide important structural data, such as for the sequence determination of amino acid residues in peptides.

Perhaps of more fundamental interest is the study of the stability and reactivity of a chemical system free from any solvent effects. Reaction mechanisms can be elucidated by the generation of reactive intermediates in the gas phase followed by analysis of the observed fragmentations. This may be aided by use of labelling experiments to determine which atoms are involved in a particular reaction. Mass spectrometry has also been central to the investigation of non-terrestrial molecular species. These seemingly unstable molecules and ions detected in interstellar clouds and circumstellar envelopes can be generated and interrogated by a variety of mass spectrometric experiments.

One of the most important considerations for mass spectrometric studies is the initial generation of the ion of interest, since this may require careful selection, and possibly even the synthesis, of a suitable precursor. A number of methodologies for generation of ions have been developed, some of which will be discussed here with particular emphasis on the generation of negative ions.

2. GENERATION OF IONS FOR MASS SPECTROMETRIC STUDY

i. Electron Impact

Electrons, generated by heating a tungsten wire in the source of the mass spectrometer, are accelerated by a small voltage* and confined to a narrow helical path by a weak magnetic field (*ca.* 300 gauss).¹ Interaction of such electrons with gas phase molecules, M can often impart enough energy to the system to effect ionisation to the molecular cation M⁺ (Scheme 1.1).



SCHEME 1.1

This process of ionisation is known as electron impact (EI) and is the oldest and most widely used method for generating positive ions.² EI ionisation, estimated to occur for

* By convention the voltage used for standard reference mass spectra with electron accelerated to 70 eV.

0.1% of all sample molecules, involves a vertical electronic transition as governed by the Franck-Condon principle (*ie.* the process occurs without rearrangement of any nuclei within the molecule). Therefore, ions formed by EI can be either a bound radical cation or an unbound radical cation dissociating directly to products.³ Both these possibilities are depicted in the Morse potential energy curves of Figure 1.1.

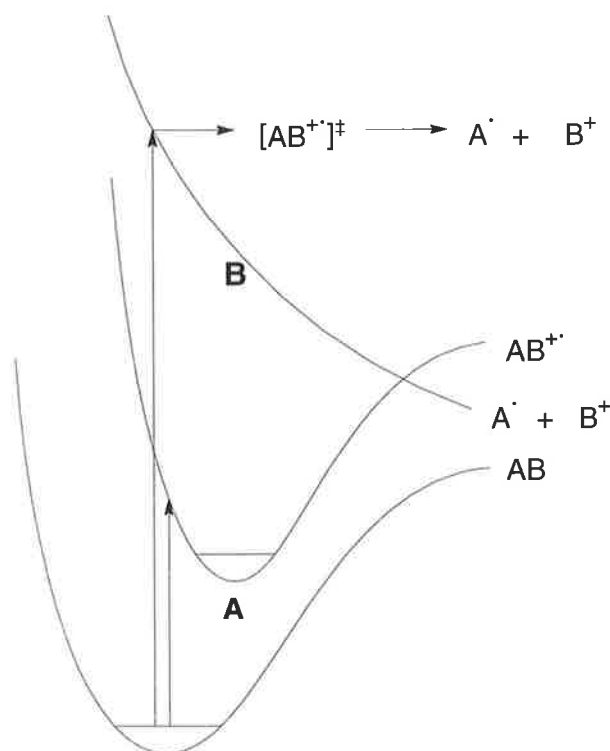
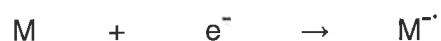


FIGURE 1.1 Morse potential energy curves for a diatomic neutral substrate molecule, AB. Vertical ionisation by electron impact (EI) results in either **(A)** a bound radical cation, AB^+ , or **(B)** an unbound radical cation dissociating directly to products $A\cdot$ and B^+ (dissociative ionisation).

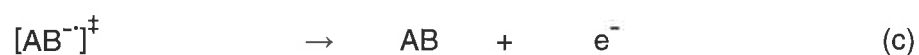
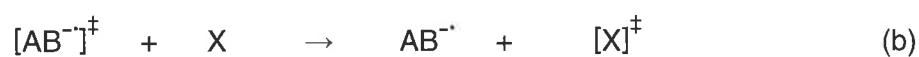
ii. Resonance Capture

When M has a positive electron affinity, interaction with electrons can lead to electron capture by the neutral species forming the radical anion $M^{\cdot-}$ (Scheme 1.2). This process, referred to as resonance capture, is highly dependent on the nature of M, but is typically about 100 times less probable than EI ionisation.



SCHEME 1.2

Radical anions formed by resonance capture usually possess significant internal energies and therefore the system undergoes an energy lowering process. A number of energy lowering processes are outlined for a diatomic molecule AB in Scheme 1.3.



SCHEME 1.3

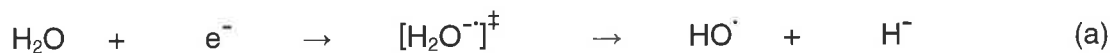
A stabilised radical anion $AB^{\cdot-}$ will result when the excess internal energy of $[AB^{\cdot-}]^{\ddagger}$ is released by either *radiative emission* [Scheme 1.3 (a)] or *collisional stabilisation* [Scheme 1.3 (b)]. Alternatively, $[AB^{\cdot-}]^{\ddagger}$ may undergo *electron detachment* [Scheme 1.3 (c)], *ion pair formation* [Scheme 1.3 (d)], or *dissociation* [Scheme 1.3 (e)].

Resonance capture can be encouraged by increasing the pressure in the source resulting in a greater number of interactions between the sample and the electron beam. In addition, the production of low energy electrons [see Scheme 1.3 (c) and (d)] promotes further electron capture by sample molecules increasing the overall yield of radical anions.

iii. Negative Ion Chemical Ionisation (NICI)

Higher source pressures increase the occurrence of ion-molecule reactions. This observation has been successfully exploited in negative ion chemical ionisation (NICI),⁴ a method for generating even-electron anions with relatively low internal energies. NICI involves an ion-molecule reaction between a reagent anion and a neutral sample molecule M. A typically used reagent gas is water, which undergoes resonance capture and readily dissociates to give a hydride ion and a hydroxy radical [Scheme 1.4 (a)]. The hydride anion readily deprotonates another water molecule forming dihydrogen and the hydroxide ion [Scheme 1.4 (b)]. The hydroxide ion thus formed can then react with the neutral molecule M, usually by deprotonation to generate the $[M - H]^-$ anion [Scheme 1.4 (c)]. The partial pressure of the reagent gas is sufficiently higher than that of the vaporised sample, such that (primary) ionisation by the electron beam involves the reagent gas with minimal primary ionisation of the sample. This in turn increases the number of ion-

molecule reactions between the reagent ion and the sample molecule. NICI is commonly referred to as a *soft* ionisation method as it forms even electron (closed shell) anions with low internal energies.



SCHEME 1.4

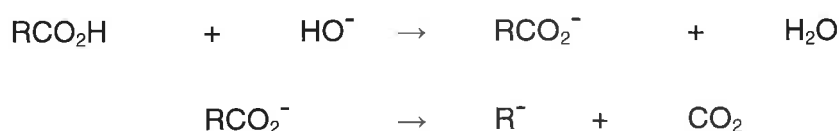
iv. Generation of Isomeric Anions

Generation of a particular anion of interest by NICI as outlined above can prove to be problematic if the neutral precursor molecule has multiple acidic sites or if the charged centre is required to be on an atom with no acidic hydrogens. The most useful method to overcome such problems involves a $\text{S}_{\text{N}}2(\text{Si})$ reaction between the fluoride anion and a precursor molecule possessing a trimethylsilyl (TMS) group at the required anionic site as first proposed by De Puy *et al.*⁵ (Scheme 1.5). It was later shown that other gas phase bases, such as the hydroxide anion, can also effect an $\text{S}_{\text{N}}2(\text{Si})$ reaction with TMS leading to a site-specific anion.⁶



SCHEME 1.5

Decarboxylation of a gas phase carboxylate anion will also lead to a site specific anion⁷ as shown in Scheme 1.6. Deprotonation of a suitable carboxylic acid to the carboxylate anion can, if formed with sufficient internal energy, undergo decarboxylation forming the site-specific anion. This method can be somewhat limiting since, in cases where the carboxylate anion does not acquire sufficient energy during deprotonation, collisional activation may be required for decarboxylation.

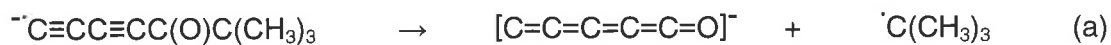


SCHEME 1.6

v. Ionisation by Dissociation

Simple homolytic cleavages can occur for both closed shell and radical anions. These processes result in the formation of a smaller charged fragment and a neutral. This process is typified by the collision induced radical loss of an alkyl group, R from deprotonated benzyl ethers of the form $[\text{PhCHOR}]^-$, to give PhCHO^- , the benzaldehyde radical anion.⁸ Similar homolytic cleavages can occur without excitation in the source of a mass spectrometer and thus be exploited as method of generation of specific negatively charged ions of interest. An example is the generation of the C_5O^- radical anion⁹ from a closed shell anion by radical loss of the *tert*-butyl group [Scheme 1.7 (a)]. Similarly, diazo-substituted systems $\text{RC}(\text{N}_2)\text{R}^1$ readily undergo dissociative electron capture to give the

radical anion $[\text{RCR}^1]^-$ and dinitrogen in good yield [Scheme 1.7 (b)].¹⁰ This method has been used for the generation of the radical anion $[\text{CH}_3\text{COCH}]^-$.¹¹



SCHEME 1.7

vi. Chemical Ionisation with the Oxygen Radical Anion

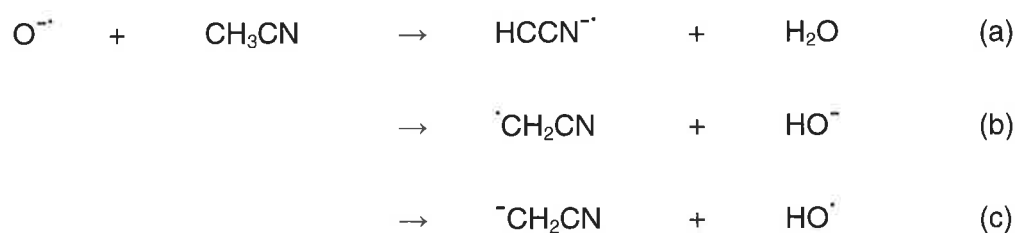
The importance of dissociative electron attachment in negative ion gas phase studies extends to the formation of reagent ions for chemical ionisation. The reagent ion O^- can be generated in the source of a mass spectrometer by dissociative electron capture of nitrous oxide [Scheme 1.8].^{12,13} The reactions of the oxygen radical anion have been reviewed.¹⁴



SCHEME 1.8

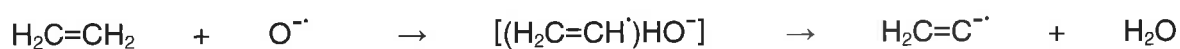
Dawson and Jennings studied the production of radical anions by reaction of a number of organic substrates with O^- .¹⁵ One of the best understood reactions of this type is the reaction between O^- and acetonitrile. This gives three products following transfer of H^\cdot

and/or H^+ to O^- . These processes are shown in Scheme 1.9; $a : b : c = 6 : 1 : 3$ (ion cyclotron resonance spectrometer)¹⁵ and $13 : 1 : 3$ (flowing afterglow instrument).¹⁶



SCHEME 1.9

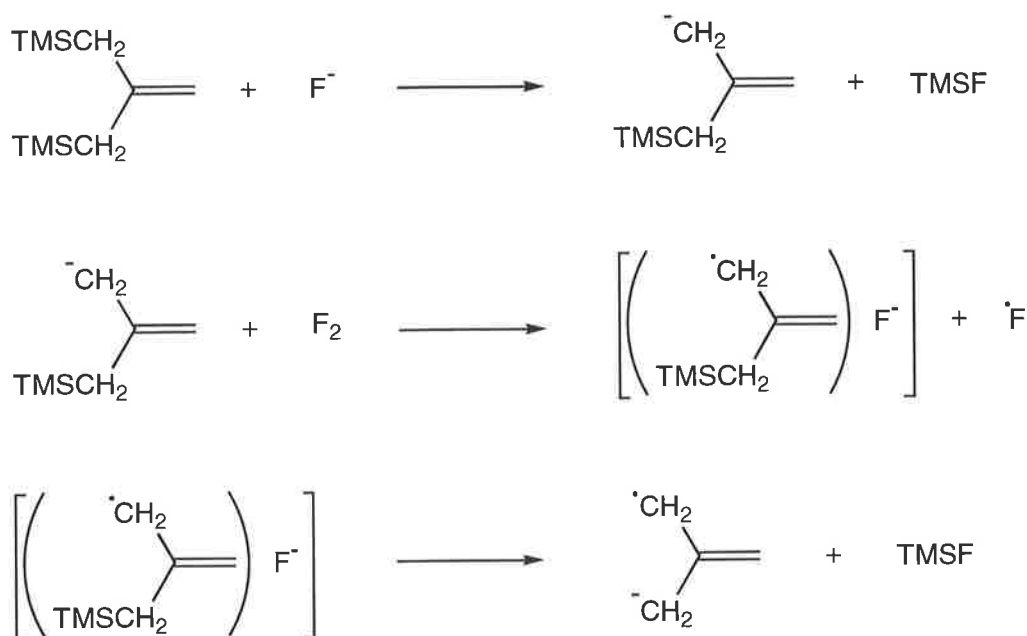
Radical anions of vinylidene and labelled vinylidene, $\text{H}_2\text{C}=\text{C}^-$ and $\text{D}_2\text{C}=\text{C}^-$, have been generated by the reaction between O^- and labelled ethylene ($\text{H}_2\text{C}=\text{CD}_2$).¹⁷ No $[\text{HC}=\text{CD}]^-$ species is observed.¹⁷ This clearly shows that O^- removes two hydrogens from the same carbon atom. The mechanism for this process is thought to occur stepwise where hydrogen atom abstraction precedes proton abstraction (Scheme 1.10), since abstraction of a hydrogen atom from ethylene is endothermic by less than $0.5 \text{ kcal mol}^{-1}$, whereas proton abstraction is endothermic by almost 25 kcal mol^{-1} .^{18,19}



SCHEME 1.10

vii. Double Desilylation

An extension of the single desilylation method (used to generate anions with specific charged centres by removal of a TMS group), the double desilylation method involves the removal of two TMS groups from an organic substrate resulting in the formation of a radical anion. This method has been used for the selective generation of distonic^{*20} radical anions, for example *para* benzyne,²¹ oxyallyl,¹¹ and trimethylene methane²² radical anions have all been studied using this technique. Generation of the trimethylene methane radical anion, shown in Scheme 1.11, illustrates the general mechanism for this methodology.



SCHEME 1.11

* Distonic anions have a charged centre and an unpaired electron residing on different atoms.

3. MASS SPECTROMETRY

i. The VG ZAB 2HF Mass Spectrometer

The mass spectrometer used in the investigation of ions discussed in this thesis is the VG ZAB 2HF mass spectrometer (Figure 1.1). The VG ZAB 2HF is a two-sector instrument consisting of a magnetic sector (B) that precedes an electric sector (E). Denoted BE this arrangement is referred to the reverse geometry²³ as compared with the conventional geometry of EB or Nier-Johnson geometry.²⁴ The reverse geometry arrangement allows for the selection, using the magnetic sector, of an ion of interest (the *parent* ion), which may subsequently undergo fragmentation and its mass spectrum recorded by scanning the electric sector. An experiment of this type is known as *mass-analysed ion kinetic energy* (MIKE) experiment and is briefly discussed below.

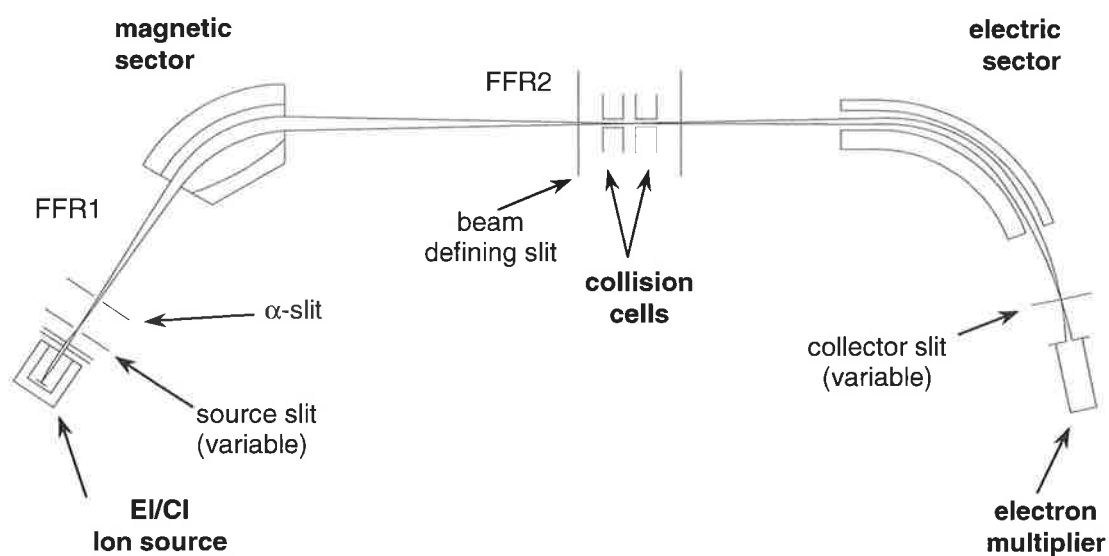


FIGURE 1.2 Schematic diagram of the VG ZAB 2HF reverse geometry two-sector mass spectrometer at the University of Adelaide.

ii. Mass-analysed Ion Kinetic Energy Spectrometry

Ions formed in the source of the VG ZAB 2HF mass spectrometer are accelerated to 7 kV toward the magnetic sector. The kinetic energy of the ions entering the magnetic sector is equal to the potential energy loss of the ions. This can be expressed as Equation 1.1, where z is the charge of the ion, V is the applied voltage (7 kV), m is the mass of the ion and v is the velocity of the ion.

$$zV = mv^2/2 \quad \text{EQUATION 1.1}$$

As the ions traverse the magnetic sector a force is exerted on them which is both orthogonal to the direction of motion and the magnetic field B . This results in deviation of the ions along a circular path of radius r according to Equation 1.2. Combining Equations 1.1 and 1.2 gives Equation 1.3, an expression for the mass to charge ratio of an ion. The radius of the magnetic sector is fixed by a slit placed at exit of the magnetic sector and the potential applied is 7 kV. Thus the magnetic field strength can be adjusted such that only ions with a charge to ratio m/z are allowed to pass through to the next field free region (FFR) and on to the electric sector.

$$mv/z = Br \quad \text{EQUATION 1.2}$$

$$m/z = B^2r^2/2V \quad \text{EQUATION 1.3}$$

The electric sector is also designed to deviate ions of energy E in a circular path of radius r according to Equation 1.4. Therefore scanning the electric sector separates ions on the

basis of their kinetic energy ($mv^2/2$) to produce a mass-analysed kinetic energy (MIKE) spectrum (the general term MS^n is used to describe experiments involving n mass separations). A MIKE experiment can be regarded as an MS^2 , or simply MS/MS.

$$mv^2/2 = 2zEr \quad \text{EQUATION 1.4}$$

The MS/MS data thus obtained may show the parent together with any fragment or *daughter* ions formed in the second field free region. The initial parent ion has a fixed amount of kinetic energy; this must be divided between any products formed in the ratio of their respective masses. As an illustration, when the parent ion AB^- decomposes to ion A^- and neutral B in the second field free region, the energy of ion A^- (E_{A^-}) and energy of AB^- (E_{AB^-}) is related to the mass of A (M_{A^-}) and the mass of the AB^- (M_{AB^-}) as shown in Equation 1.5.

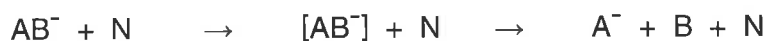
$$M_{A^-} / M_{AB^-} = E_{A^-} / E_{AB^-} \quad \text{EQUATION 1.5}$$

iii. Collisional Induced Dissociation

In mass spectrometry, ions may be classified as stable, unstable or metastable. An ion that is accelerated out of the ion source and detected after traversing the magnetic and electric sectors is classified as stable. Unstable ions simply decompose in the ion source, while metastable ions are accelerated out of the source, but have enough internal energy to spontaneously decompose before being detected. Decompositions occurring in the second

field free region give rise to daughter ions in a MIKE experiment described above.²⁵ In order to observe a similar mass spectrum (MS/MS) of anionic systems consisting of mainly stable ions, the parent anions may be excited by collision of the ions with a neutral gas.²⁶ As eluded to earlier, anions produced by the NICI method are formed with low internal energies and often do not fragment spontaneously. Therefore, the anions formed by NICI are allowed to collide with a neutral gas in one of the two collision cells located in the second field free region (Figure 1.2) resulting in *collisionally activated* (CA) MS/MS data. This process is also referred to as *collisional induced dissociation* (CID).

In CID experiments carried out in the VG ZAB 2HF instrument, the translational kinetic energy of a parent ion (AB^-) is about 7 kV. Such collisions with neutral gas (N) lead to vertical electronic excitation.^{25,27} The highly energetic ion produced may then undergo dissociation (Scheme 1.12). The energy imparted to the parent ion in such a high energy collision is less than 10 eV in most instances,^{25,27} although some processes requiring up to 16 eV have been observed to occur under CID conditions.²⁸

**SCHEME 1.12**

Along with dissociation occurring upon collisional excitation the potential exists for other (undesirable) processes such as ion scattering and/or electron detachment* of the parent

* Electron detachment of anions is central to charge reversal and neutralisation-reionisation mass spectrometry (see later discussion).

ion. The nature of the collision gas used in CID experiments and its pressure in the collision cell are therefore extremely important in obtaining good results. The ideal situation is for the maximum number of ions to undergo a single collision with the neutral gas, with only a minority of ions undergoing multiple collision processes.* It has been shown that inert atomic gases such as helium and argon, are most efficient for CID because of low inclinations of ion scattering and electron detachment.²⁹ The reduction in intensity of the parent ion beam with introduction of the collision gas provides an insight into the collision conditions in the collision cell. It has been estimated that when the intensity reduction is 10 - 20%, the probability of a single collision is between 20 to 50%, with multiple collisions being of low probability. These conditions are referred to as *single collision conditions*.³⁰

Fragment ions formed in the second field region, either by collisional induced dissociation or metastable decomposition, can gain some additional energy in the form of translational (kinetic) energy from the decomposing parent ion. This phenomenon, known as *kinetic energy release*,²⁵ is a result of the drift between the neutral and ion fragments after dissociation. If the drift of the ion is in the same direction as the ion beam it will be observed to have slightly higher kinetic energy and appear at slightly higher m/z in the mass spectrum. Ions for which the drift is in the opposite direction to that of the main beam will be observed to possess slightly lower kinetic energies and therefore will be observed at a slightly lower m/z value in the mass spectrum. The overall effect is an altered peak shape of the fragment ion peak. The magnitude of the kinetic energy release is very much dependent on the mechanism of ion fragmentation and can be useful in the elucidation of the mechanism of unimolecular decompositions.²⁵

* An examiner has indicated that it is important to state that these high energy collisions are non-momentum transfer events.

iv. Charge Reversal Mass Spectrometry

Not all negative ions undergo significant collision induced dissociation to be useful in structural determination of the anion. Bowie and Blumenthal^{31,32} found that anions, under CID conditions, can be charge stripped of two electrons to form the corresponding cation - a process now known as *charge reversal* (CR) mass spectrometry. Charge reversal involves charge stripping incident negative ions (AB^-) in a high energy collision with a neutral gas (N) forming the corresponding positive ions (Scheme 1.13). The energy loss in conversion of the anion to the cation can be measured in an MS/MS experiment.^{33,34} The CR process may occur provided that the energy E imparted to the anion during collision is at least equal to the sum of the electron affinity (EA) and ionisation energy (IE) of the corresponding neutral (Equation 1.6). Some early applications of the CR process have been reviewed.³⁵



SCHEME 1.13

$$E = EA_{(AB)} + IE_{(AB)} \quad \text{EQUATION 1.6}$$

As mentioned earlier (see CID section) collision processes are considered to occur by a vertical Franck-Condon transition. It follows that CR is also a vertical process and that the cation formed has the same structure (at least initially) as that of the anion. In analogy to

CID experiments, the nature of the collision gas is of great importance with regards to the resolution of the CR experiment. Oxygen has been found to best favour the CR process for two reasons, (i) it readily captures an electron during collision and (ii), it minimises fragmentations of the reionised species and as such is referred to as a *soft* target gas.³⁶

A promising result from investigations into the CR process is that the spectrum produced is often characteristic of the parent anion and can even successfully distinguish isomeric anions. For example, the CR spectra of the isomeric anions $\text{CH}_2=\text{C}=\text{CH}^-$, $\text{CH}_3\text{C}\equiv\text{C}^-$ and *cyc*- $\text{CH}_2\text{CH}=\text{CH}^-$ are distinctive.³⁷

For completeness it should be mentioned here that charge inversion of cations has been observed to occur in high energy collisions between a cation and a neutral gas resulting in an observed negative ion signal.³⁸ The applicability of this method is limited since two-electron attachment by a collisional process is an extremely improbable event. As a consequence, the charge states are often included in the nomenclature for a charge reversal experiment, *viz* $^-\text{CR}^+$ and $^+\text{CR}^-$, for charge inversion of negative and positive incident ions.

v. Neutralisation-Reionisation Mass Spectrometry

The formation of neutrals by collisional electron detachment of an incipient anion has been mentioned above as an undesirable process during a CID experiment, where neutralisation is avoided by use of a noble gas in the collision cell. It follows that neutrals can be investigated using the VG ZAB HF mass spectrometer, or equivalent, in an experiment similar to the CID or CR experiments. This may seem somewhat contradictory in light of the preceding discussions and obviously the neutrals themselves cannot be detected in a

two-sector instrument, however ionisation of the neutrals can then allow their detection by the electric sector. This process, pioneered by McLafferty in the early 80s,³⁹ has been further developed and is now known as *neutralisation-reionisation* (NR)⁴⁰⁻⁴³ mass spectrometry. Using a reverse sector instrument, such as the VG ZAB HF, the NR experiment (see Figure 1.3) is carried out with a mass selected anion by collision with an appropriate target gas in the first of the tandem collision cells located in the second field free region. Provided that the energy, $E_{neutralisation}$ imparted on the anion during the collision process is greater than the electron affinity (EA) of the neutral but not more than the sum of the EA and ionisation energy (IE) of the neutral, then some ions in the beam are neutralised (Equation 1.7). This process is not 100% effective and accurate control of the energy imparted to the ion during collision is not possible, with the result that some anions with sufficient energy can undergo two-electron oxidation to form the cation (see CR section).

$$EA_{(AB)} < E_{neutralisation} < [EA_{(AB)} + IE_{(AB)}] \quad \text{EQUATION 1.7}$$

The application of an electric potential orthogonal to the flight path of the beam and between the two collision cells results in deflection of all ionic species leaving a pure neutral beam. The neutral beam is then reionised by a further collision event as it traverses the second of the tandem collision cells. The reionised species, together with any fragment ions, can then be detected by scanning the electric sector as with a standard MS/MS experiment.

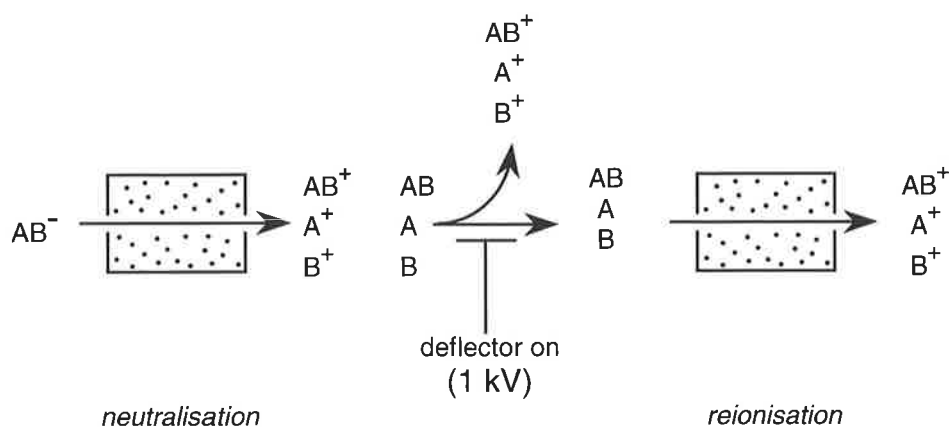


FIGURE 1.3 Simplified schematic diagram of the neutralisation-reionisation ($^-NR^+$) experiment.

The charge transitions illustrated in Figure 1.3 are for the case where the incipient ion is negatively charged and the product ions are positively charged. There are other charge permutations possible, and it is for this reason that the charged state of the incipient and product ions are included in the nomenclature, to give four possible NR experiments *viz.*, $^-NR^+$, $^-NR^-$, $^+NR^+$ and $^+NR^-$. By far the most common of these experiments are $^-NR^+$ and $^+NR^+$. The $^-NR^-$ and $^+NR^-$ are of limited application because of the difficulty of inducing electron attachment to a neutral species during the collision process.⁴⁴ The choice of target gas is important and depends upon the particular experiment to be performed. Xenon⁴⁵ and benzene³⁸ are often used in NR for charge transitions requiring attachment of an electron, although vaporised metals such as mercury and sodium can also be used.⁴⁶ For charge stripping events, such as neutralisation of an anion or reionisation of a neutral to the corresponding cation, oxygen is often used as the target gas since it readily captures electrons and is a soft target gas minimising fragmentations.^{36*} This is particularly important for NR since the stability of the transient neutral AB can only be inferred when a (recovery) signal corresponding to the reionised neutral, usually AB^+ , is observed.

* See also C. Aubry and J. Holmes, *J. Am. Soc. Mass Spectrom.*, 2001, 12, 23.

Demonstrating the stability of a transient neutral is one of the most favoured features of the NR process, whereby stability can generally be inferred by attainment of a recovery signal, or at least stability on the time scale of the experiment. The effective lifetime of the neutral is the time taken for it to traverse the distance between the two collision cells. In most instruments the distance d between the two collision cells is *ca.* 50 mm. The velocity of the neutral is the same as the incipient ion, so for an ion accelerated to 7 keV the neutral formed will traverse the distance between the cells in the order of microseconds (Equation 1.8).

$$t = d / (2eV / m)^{1/2} \quad \text{EQUATION 1.8}$$

Geometrical changes during neutralisation and reionisation are negligible and consequently Franck-Condon factors apply in each step of the NR process and affect the observed fragmentations.^{47,48} A diagram depicting how Franck-Condon factors can affect the NR process is illustrated in Figure 1.4. For simplicity, the ${}^+NR^+$ experiment of AB^+ is used as an example since only the neutral and cation energy surfaces need to be considered. When AB and AB^+ are both bound with respect to dissociation, and are similar in geometry, the Franck-Condon overlap is favourable [Figure 1.4 (a)]. The neutral can therefore be formed with minimum excess internal energy upon neutralisation, and reionisation back to the cation may also occur with little excess energy, in turn resulting in a large recovery signal. In systems where the neutral and cation have different geometries, the Franck-Condon overlap is unfavourable [Figure 1.4 (b)], resulting in significant excess internal energy upon both neutralisation and reionisation.⁴⁹ In this case, fragmentations are much more

likely, and often result in significant or perhaps even total reduction in the abundance of the recovery signal.

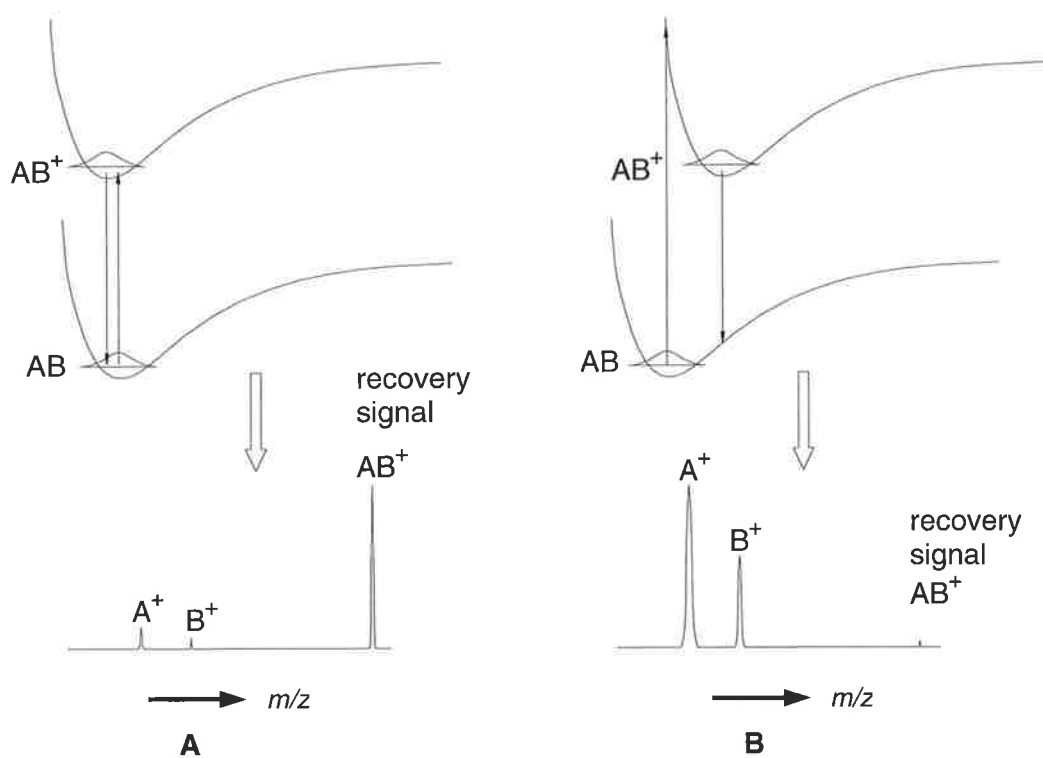


FIGURE 1.4 Simplified diagrams depicting the affect of Franck-Condon factors during a ${}^+NR^+$ experiment where (A) the geometries of the neutral and cation are similar and (B) geometries of neutral and cation are different.

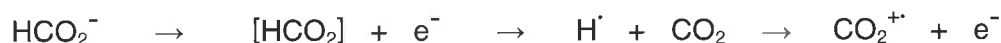
vi. Neutral Ion Decomposition Difference

*Neutral ion and decomposition difference (NIDD)*⁵⁰ is a useful technique designed to infer more information about the neutral formed in the conventional NR configuration. When interpreting a ${}^-NR^+$ spectrum, fragment peaks observed may be a composite of both cationic and neutral processes. The premise behind NIDD is to subtract from the ${}^-NR^+$

peaks, the magnitude of the peaks that arise from cationic processes. This can be achieved easily since fragment peaks in a $\bar{\text{C}}\text{R}^+$ experiment are normally due to cationic processes, since the anion is converted directly to the cation.⁵⁰ Normalisation of both $\bar{\text{C}}\text{R}^+$ and $\bar{\text{N}}\text{R}^+$ spectra followed by subtraction of the $\bar{\text{C}}\text{R}^+$ peaks from the $\bar{\text{N}}\text{R}^+$ peaks gives the NIDD spectrum (Equation 1.8, where I_i is the intensity of peak i). The NIDD spectrum shows both positive and negative peaks where the positive peaks infer a neutral process, while negative peaks correspond to cationic processes. It should be noted that the $\bar{\text{C}}\text{R}^+$ and $\bar{\text{N}}\text{R}^+$ experiments should be carried out under the same experimental conditions to allow the comparison of spectra in this manner. This can be achieved by obtaining by first running a $\bar{\text{N}}\text{R}^+$ experiment (deflector on) and then immediately running a $\bar{\text{C}}\text{R}^+$ experiment (deflector off).

$$I_i(\text{NIDD}) = [I_i(\text{NR})/\sum I_i(\text{NR})] - [I_i(\text{CR})/\sum I_i(\text{CR})] \quad \text{EQUATION 1.8}$$

NIDD is of most value when the $\bar{\text{N}}\text{R}^+$ and $\bar{\text{C}}\text{R}^+$ are noticeably different as in the case of the formate anion, HCO_2^- .⁵⁰ In this system the $\bar{\text{C}}\text{R}^+$ spectrum shows a large recovery signal while little recovery signal is observed in the $\bar{\text{N}}\text{R}^+$ spectrum. NIDD analysis shows that an observed CO_2^+ peak (*ie.* loss of H) in $\bar{\text{N}}\text{R}^+$ is predominantly due to a neutral process. Theory predicts hydrogen radical loss from neutral HCO_2 occurs with little activation required, and therefore the neutral decomposes upon formation leaving the CO_2 to be reionised (Scheme 1.14).



SCHEME 1.14

vii. Neutralisation Collisional Activation Reionisation

In the late 1980s, following on from their earlier work on NR mass spectrometry, McLafferty and co-workers⁵¹ modified the conventional NR configuration to allow for collisional activation of neutrals during a NR experiment. The alteration involved addition of a third collision cell such that an incident ion is (i) neutralised in the first collision cell, (ii) collisionally activated in the second cell and (iii) reionised in the third cell. Deflection of ions in between collisions ensures that only collisionally activated neutrals are observed (Figure 1.5). The ability to further excite the neutral once formed allows the stability of transient neutrals to be interrogated significantly more than in a conventional NR experiment.

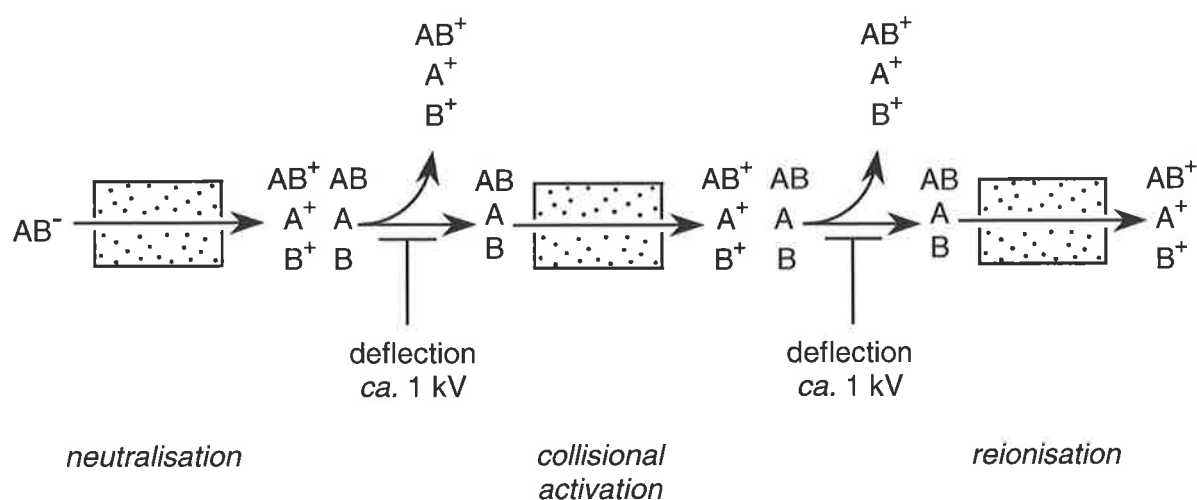


FIGURE 1.5 Schematic diagram of the altered NR configuration as used for NCR experiments

Despite the additional collision event required for NCR this method has successfully demonstrated the stability of the neutral H_2CClH , which upon activation does not undergo rearrangement to the more stable H_3CCl isomer.^{52-54*} Conversely, the diradical neutral CH_2OCH_2 , stable on the NR time scale, isomerises upon collisional excitation to oxirane.⁵⁵

4. POSITIVE ION BEHAVIOUR

Mass spectrometry has become a powerful tool in structure determination. The behaviour, in particular the fragmentations, of positively charged ions has been extensively studied, with numerous texts existing on the subject.⁵⁶⁻⁵⁹ It is not the intent here to fully describe this work, but rather to describe, in brief, two general categories of fragmentations of positive ions.

i. Simple Homolytic Cleavage

Radical cations, which may be formed by EI ionisation, undergo facile homolytic bond cleavages forming a stable cation and neutral radical. Although the charge may be distributed to either fragment, the fragment that results in the more stable cation typically retains the charge. For example, ionised methyl benzoate fragments by cleavage of the C-OMe bond to form the phenyl acyl cation and the methoxide radical (Scheme 1.15).

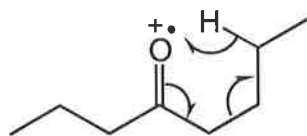
* ref. 54 also suggests that simple cationic ions do not form stable neutrals under NR conditions.



SCHEME 1.15

ii. Rearrangement Reactions

Rearrangements reactions of radical cations can result in the loss of an even electron fragment. The best known of such processes is arguably the McLafferty rearrangement. The McLafferty rearrangement proceeds via a γ -hydrogen transfer to the carbonyl oxygen of ionised ketones followed by elimination of an alkene; for simplicity, it can be viewed as occurring via a six-membered transition state (Scheme 1.16).



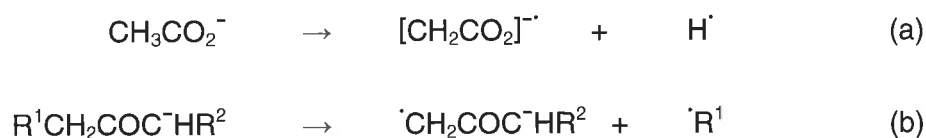
SCHEME 1.16

5. NEGATIVE ION BEHAVIOUR

Collision induced fragmentations of closed shell anions have been extensively studied and have been the subject of review.^{60,61} These studies allow for the broad categorisation of their behaviour as follows.

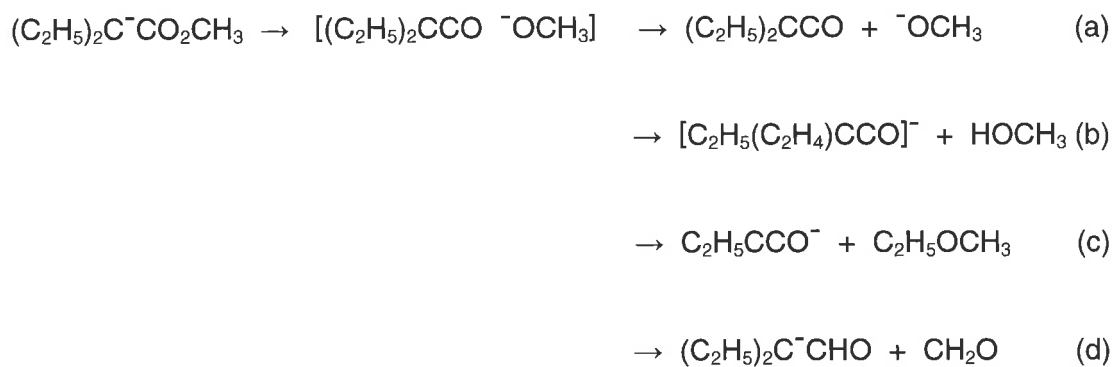
i. Simple Homolytic Cleavage

Loss of a hydrogen radical from organic anions is not an uncommon occurrence, especially when the resulting radical anion is resonance stabilised - as is the case for deprotonated acetic acid [Scheme 1.17 (a)]. The formation of a stabilised radical anion can also drive other radical losses [*eg.* Scheme 1.17 (b)].

**SCHEME 1.17**

ii. Ion-Neutral Complex Formation

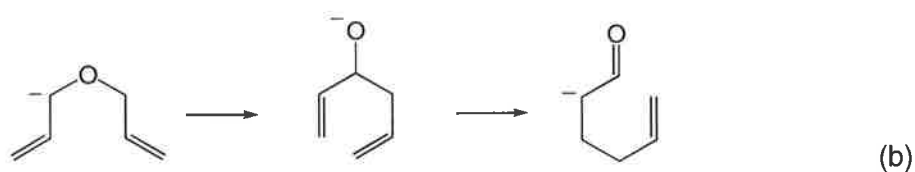
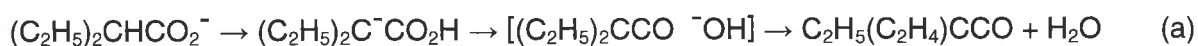
An ion-neutral complex⁶² is held together by hydrogen bonding and ion-induced dipole interactions and is initially formed by heterolytic cleavage of the parent anion. The ion-neutral complex may decompose by direct displacement of the anion [Scheme 1.18 (a)], or decomposition may occur subsequent to some other process including, (i) deprotonation [Scheme 1.18 (b)], (ii) S_N2 displacement [Scheme 1.18 (c)], or (iii) hydride transfer [Scheme 1.18 (d)].



SCHEME 1.18

iii. Rearrangement Reactions

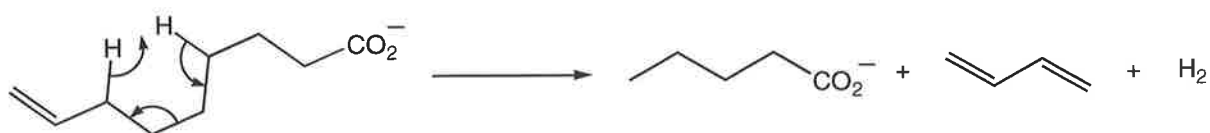
If the simple fragmentations described above are unfavourable, the $[\text{M} - \text{H}]^-$ anion may undergo collision induced rearrangement to another anionic species from which any of the above mentioned fragmentations may proceed more easily. This may involve a simple proton transfer [eg. Scheme 1.19 (a)] or a more complex skeletal rearrangement [eg. Scheme 1.19 (b)].⁸



SCHEME 1.19

v. Charge-Remote Processes

Charge-remote processes are different to the processes described above in that the reaction site is remote from and uninfluenced by the charged centre.^{63,64} The classical example of a charge-remote process is the Gross rearrangement (Scheme 1.20), which involves rearrangement of a long alkyl chain away from the charged site. Charge-remote rearrangements are generally high energy processes and generally occur only when no simple fragmentations are energetically feasible.



SCHEME 1.20

v. Charge Inversion

One might consider that the processes that occur upon CR or NR to be similar to those described above for positive ions but it is in fact more complex. For example, early on it was observed that the CR^+ spectrum of the nitrobenzene radical anion is notably different to that of nitrobenzene radical cation formed by IE.³¹ This was attributed to the different internal energies of the ions formed in each case.

CHAPTER 2

THEORETICAL METHODS FOR THE STUDY OF MOLECULAR SYSTEMS

1. INTRODUCTION

The use of quantum theory is widespread in most areas of chemistry. Advances in super-computing facilities and the advent of quantum chemistry packages with graphical user-interfaces has allowed for molecular orbital theory to be more widely exploited by the experimental chemist. The origins of computational chemistry involved investigations of pre-existing phenomena, whereas now computational chemistry can be used to pre-empt an experimental investigation. Quantum chemistry can be used to determine the structures of any neutral or ionic species of interest and investigate their stability, including short-lived reactive intermediates and transition states - a task not easily accomplished using experimental techniques. Quantum chemical methods are used in concert with experimental data throughout this thesis and a brief discussion on the theory and the methods used follows.

2. APPLICATION OF QUANTUM THEORY TO CHEMICAL PHENOMENA

i. The Schrödinger Equation

The properties of a particular nuclear arrangement at thermodynamic equilibrium can be calculated using *ab initio* molecular orbital theory.⁶⁵⁻⁶⁹ The time-independent Schrödinger equation is pivotal to molecular orbital theory (Equation 2.1, where H is the Hamiltonian operator, ψ is the wavefunction, and E is the electronic energy of the system).

$$H\psi = E\psi \quad \text{EQUATION 2.1}$$

The wavefunction is a mathematic function requiring knowledge of the spatial and spin coordinates of the electrons and the coordinates of the nuclei. The modulus squared of the wavefunction, $|\psi|^2$ (ie. $\psi^*\psi$ if ψ is complex) can be physically interpreted as the probability of finding an electron in a given region of space. The Hamiltonian operator consists of terms for the kinetic and potential energies of all particles in the molecular system. The electronic and nuclear motions can be considered separately according to the *Born-Oppenheimer* approximation.⁷⁰ This is a reasonable assumption since nuclei are many times more massive than electrons and thus the nuclei move more slowly than electrons. Nuclei are considered to be stationary for a given geometry of a molecular system and therefore nuclear-nuclear repulsion can be ignored. The solution to Equation 2.1 using the reduced Hamiltonian and the electronic wavefunction, gives the electronic potential energy of the molecular system. The Schrödinger equation in this form is still extremely complex for all but the simplest molecular systems. A number of theories have been developed to calculate an approximate solution to the Schrödinger equation by applying various assumptions in order to simplify the calculation and make it applicable for a more diverse range of molecular systems.

ii. The Hartree-Fock Approximation

Hartree-Fock (HF) theory^{71,72} describes the electronic wavefunction ψ as a linear combination of molecular orbitals ϕ , which are in turn described as a linear combination

of one-electron functions called basis functions χ (Equation 2.2). Basis functions are centred on nuclei and can essentially be considered to approximate atomic orbitals.

$$\phi_i = \sum c_{ik} \chi_k \quad \text{EQUATION 2.2}$$

The coefficients c_{ik} are optimised iteratively using the self-consistent field (SCF) procedure. This involves solving the electronic energy for each electron separately and the determination of interactions between particles. New molecular orbitals are produced for each electron such that the electronic energy is decreased. This cycle is repeated until two consecutive cycles are found to have essentially the same electronic energy. HF theory simplifies this procedure by averaging the repulsive interactions of all other electrons. Physically this means that movement of an electron is independent of the position of any other electron in the molecular system. In real molecular systems electrons move with respect to each other to reduce electron-electron repulsion in a process known as *electron correlation*. HF theory neglects this correlation energy and therefore cannot accurately predict the exact (non-relativistic) energy of a system. The difference between the energy of a system at the HF limit, E_{HF} and the exact (non-relativistic) energy, E_o is known as the correlation energy, E_{corr} (Equation 2.3).

$$E_{corr} = E_o - E_{HF} \quad \text{EQUATION 2.3}$$

Electron correlation accounts for about 0.5% to 1% of the energy of the system. In the majority of cases reasonable geometries can be obtained using HF theory despite the

absence in the method of a treatment for electron correlation. However, the electron correlation energy must be included in the calculated energy in order to obtain reasonable energies. A number of so-called post-HF methods have been developed to take account of electron correlation. The level of sophistication to which the calculation approaches the electron correlation problem is directly related to the time spent on the computation and the computational resources required.

iii. Møller-Plesset Perturbation Theory

A commonly used post-HF *ab initio* method is *Møller-Plesset perturbation* (MP) theory.⁷³ MP theory essentially applies a correction to the HF solution. The Hamiltonian of the HF solution is taken to be the zeroth order approximation, H_0 which differs from that of a more accurate solution, H_{MPn} by a small perturbation, $\lambda H'$ (Equation 2.4). The perturbation is a series of terms taking into account the correlation energy. Second, third, fourth and even fifth orders of perturbation available and are referred to as MP2, MP3, MP4 and MP5 respectively.

$$H_{MPn} = H_0 + \lambda H' \quad \text{EQUATION 2.4}$$

iv. Coupled Cluster Theory

Perhaps the most sophisticated approach to the incorporation of electron correlation into an *ab initio* method is that of *coupled cluster* (CC) theory.^{74,75} Unlike MP theory, which applies a correction to the Hamiltonian operator of the HF solution, CC theory applies an

exponential operator, e^T on the HF wavefunction, ψ_{HF} resulting in a more accurate representation of the true electronic wavefunction. The ψ_{CC} wavefunction (Equation 2.5) is a function of all possible excitations of electrons from occupied to unoccupied molecular orbitals.

$$\psi_{CC} = e^T \psi_{HF} \quad \text{EQUATION 2.5}$$

The cluster operator T is the sum of *one, two, three,*, N -electron excitation operators, $T_1, T_2, T_3, \dots, T_N$ respectively, where N equals the number of electrons in the system (Equation 2.6).

$$T = T_1 + T_2 + T_3 + \dots + T_N \quad \text{EQUATION 2.6}$$

It is not feasible to do a calculation considering all possible excitations of electrons from occupied to unoccupied molecular orbitals for all but the smallest systems. Therefore, a number of predefined CC methods are included in most *ab initio* packages, viz (i) CCD (coupled cluster doubles), (ii) CCSD (coupled cluster singles and doubles), and (iii) CCSDT (coupled cluster singles, doubles and triples), where the method is derived from the inclusion of (i) T_2 , (ii) T_1 and T_2 , and (iii) T_1, T_2 and T_3 excitation operators. The CCSDT method is very costly of time and computer resources and thus most *ab initio* packages include a variation of this method, which simplifies the contribution of the triple excitations, eg. CCSD(T).⁷⁶

v. Density Functional Theory

A totally different approach to computational chemistry attempts to determine the electron probability density, ρ rather than the electronic wavefunction, ψ . This approach is known as density functional theory (DFT).⁷⁷ Central to DFT is the Hohenberg-Kohn⁷⁸ theorem stating that it is possible to describe the ground-state energy as functionals of the electron probability density, ρ . The one-electron equations as described by Kohn-Sham orbitals⁷⁹ can be solved iteratively in much the same way as using the SCF procedure. The electronic energy of the system, E_{system} is separated into terms determined by the charge density, $E_{charge\ density}$ and the exchange-correlation energy, $E_{ex-corr}$ (Equation 2.7). The charge density terms account for kinetic energy as well as electron-nuclear attractions and electron-electron repulsions. The exchange-correlation terms account for electron correlation (as described above), and electron exchange compensates for electrons having opposite spins.

$$E_{system} = E_{charge\ density} + E_{ex-corr} \quad \text{EQUATION 2.7}$$

The *local density approximation* (LDA) provides the initial functional for most DFT methods. However the LDA itself does not adequately describe molecular systems, so gradient corrected exchange functional and correlation functional have been introduced by Becke⁸⁰ and Perdew⁸¹ respectively to give the LDA-BP functional. The pairing of exchange and correlation functional defines the DFT method, in this case the BP method. Similarly replacing the Perdew correlation functional with that of Lee, Yang and Parr,⁸² defines the popular BLYP method. DFT calculations incorporate electron correction in a manner not significantly greater in computational cost than that for a HF calculation.

vi. Hybrid Density Functional Theory

Electron exchange is better described using the HF-SCF approach as compared to DFT methods. This has led to definitions of hybrid functionals that combine terms from both DFT and HF methods thereby mimicking HF exchange energies. This approach, known as hybrid density functional theory (DFT-HF), was introduced by Becke⁸³ as a way to obtain consistently reliable computational results using reasonably modest computational resources and time. Arguably the B3LYP method⁸⁴ is the best DFT-HF method giving accurate results for a large range of molecular systems. The B3LYP method combines LDA, HF, B and, LYP functionals, E_{LDA} , E_{HF} , E_B , and E_{LYP} respectively, as a linear combination to give the exchange-correlation functional, $E_{ex-corr}$ (Equation 2.8). The coefficients in Equation 2.8 were determined semi-empirically based on the values that were able to reproduce experimental values for heats of formation. While other DFT-HF methods are available, few are comparable to the B3LYP method.

$$\text{(B3LYP)} E_{ex-corr} = 0.8 E_{LDA} + 0.2 E_{HF} + 0.72 E_B + 0.81 E_{LYP} \quad \text{EQUATION 2.8}$$

vii. Basis Sets

The set of one-electron basis functions (see earlier) used in a calculation is known as its basis set. The addition of a basis set to a theoretical method (*eg.* HF or MP2) defines the level of theory of the calculation. Therefore it is necessary to have an understanding of basis sets and their effects on the reliability, accuracy and expense of a calculation.

One-electron basis functions are centred on nuclei and can essentially be considered to approximate atomic orbitals, as described previously (Equation 2.2). A linear combination of basis functions describes a molecular orbital. In turn a linear combination of molecular orbitals describes the electronic wavefunction. Basis sets therefore dictate the regions of a molecule or atom that an electron can populate. In quantum theory the probability of finding an electron is only unity when $|\psi|^2$ is integrated over infinite space. Basis functions restrict the electrons to specific regions of space close to the nucleus. By increasing the number of basis functions less restriction is placed on the electrons allowing for a more accurate approximation of the electronic wavefunction.

Quantum chemistry packages include many predefined basis sets, which differ in the number and type of basis functions allocated to each atom. Some basis sets also allow for the size of the basis function to increase by including two or three sizes of each valence basis function. These are referred to as *split-valence* basis sets and are usually denoted as *double-zeta* (two sizes) or *triple-zeta* (three sizes). The *6-31G* basis set is one of the simplest split-valence basis sets. Defined as a *double-zeta* basis set, the *6-31G* basis set assigns two *1s*-type functions of different size to the H and He atoms, whereas atoms Li-Ne are assigned a total of nine basis functions; one *1s*-type basis function and two different sizes of *2s*, *2p_x*, *2p_y*, *2p_z*-type basis functions.

Although double and triple zeta basis sets allow for changes in the size of basis function, the shape of basis functions remains restricted. This restriction is overcome by adding basis functions of higher angular momentum than required to describe the electronic ground state of the system. More succinctly, by placing *d*-type functions on the second row atoms and *p*-type functions on hydrogen atoms, the orbitals are able to change shape. This better describes the bonding in the system and in turn results in a better approximation

of the electronic wavefunction. The $6-31G(d)$ basis is a common example of this, in which a set of d -type basis functions is added to the $6-31G$ basis set for second row atoms. Additionally, p -type basis functions may be placed on hydrogen atoms by including a p in the basis set definition, an example is the $6-31G(d,p)$ basis set. Systems comprised of electrons far removed from the nuclei of the molecular system are better described with the inclusion of diffuse s and p -type functions. Such systems include those containing a lone pair of electrons, an anionic centre, or hydrogen bonding. The inclusion of diffuse functions in a basis set is designated by the inclusion of a $+$ in the definition, so that $6-31+G(d)$ is the $6-31G$ basis set with polarisation and diffuse functions added to all non-hydrogen atoms. To include diffuse functions on hydrogen atoms a second $+$ is added to the basis set [*ie.* $6-31++G(d)$]. The prefix *aug* is used to add diffuse functions to non-Pople basis sets such as the correlation consistent *double-zeta* basis set of Dunning to give *aug-cc-pVDZ*, here the p represents addition of polarisation functions.

3. CALCULATION OF CHEMICAL PROPERTIES

i. High-Level Energies

In most cases, stable geometries of molecular systems are adequately described by the use of modest theoretical methods. However, energy calculations are much more dependent on the level of theory used. The typical protocol for theoretical investigations is to optimise the geometry of a system using a modest level of theory and to subsequently carry out a single point energy calculation at a higher level of theory. An example of this methodology is the CCSD(T)/aug-cc-pVDZ//B3LYP/6-31G(d) level, defining a theoretical

study with CCSD(T) energies using B3LYP geometries. In this manner accurate energies can be determined for a much more affordable cost in computational resources.

Results for geometries and other parameters presented in this thesis have been carried out using the HF, B3LYP or MP2 methods, usually with the modest basis set 6-31G(d). DFT-HF (and DFT) has been demonstrated as extremely cost effective in predicting geometries and other properties of molecular systems.⁸⁵ In particular the B3LYP method with a modest basis set has allowed the calculation of vibrational frequencies of over 100 molecules with an average deviation of less than 50 cm^{-1} .⁸⁶ When appropriate, a single point energy calculation is carried out using large basis sets, such as B3LYP/aug-cc-pVDZ, for determination of accurate energies. The CCSD(T)/aug-cc-pVDZ level of theory is also used for single point energy calculations to determine highly accurate energies.

ii. Rates of Reactions

The Arrhenius equation (Equation 2.9) states that the rate constant of a reaction, k is a product of an exponential energy term and a pre-exponential A factor term. The exponential term is comprised of terms for the activation energy, E_a the gas constant, R and the temperature, T . The A factor allows for entropy contributions of a process to be considered in the rate determination, that is, how accessible is the reaction channel and how probable is the reaction.

$$k = A \exp\left(\frac{-E_a}{RT}\right)$$

EQUATION 2.9

To determine the probability in such a manner would require an intimate knowledge of the potential energy surface of the process in question, such as the width of the reaction coordinates for each step into and out of the transition state and reactive intermediate together with the curvature of the reaction coordinate. Often such studies are not feasible due to the system size and available computer resources. However, when considering competing reaction pathways then comparison of the relative vibrational partition functions, as determined by transition state theory, for the transition state in each of the processes may give some insight into the relative pre-exponential factors for both processes. For example, the competitive processes; (i) six centred cyclisation, and (ii) seven centred cyclisation of the gas phase 5,6-epoxyhexoxide, has been determined using this approach to favour the six-membered transition state.⁸⁷ Since the energetics of both processes are similar [35 and 39 kJ mol⁻¹ respectively at the MP2(FC)/6-31G(d) level of theory] this indicates the importance of the pre-exponential *A* factor.

Using transition state theory,⁸⁸ the *A* factor for a uni-molecular process is given by a term dependent on the partition function densities of the reactant, Q_R and the transition state, Q_T (Equation 2.10, where k_B is Boltzman's constant and h is Planck's constant).

$$A = \left(\frac{k_B T}{h} \right) \left(\frac{Q_T}{Q_R} \right) \quad \text{EQUATION 2.10}$$

The partition function density is an approximate measure of the number of energy states accessible to a particular molecule at a given temperature. Translational, rotational, vibrational and electronic states can be considered separately for determination of the partition function density as shown in Equation 2.11.

$$Q = Q_{\text{Trans}} Q_{\text{Rot}} Q_{\text{Vib}} Q_{\text{Elec}} \quad \text{EQUATION 2.11}$$

When the reaction occurs on a single potential energy surface, $Q_{\text{Elec}} = 1$. Further simplification can be made for uni-molecular rearrangements since Q_{Trans} of the reactant and the transition state are identical and can then be factored out of the expression. This can also be considered to be true for Q_{Rot} , at least in a qualitative approximation. Thus, relative A factors can be approximated by simply evaluating Q_{Vib} for the reactant and the transition state. The vibrational partition function is given by Equation 2.12, where ν_n is the harmonic vibrational frequency of mode n (for a non linear molecule and excluding the reaction coordinate $1 \leq n \leq 3n - [6n + 1]$), λ is a scaling factor for vibrational modes.⁸⁹ The partition function density can then be evaluated from *ab initio* frequency calculations.

$$Q_{\text{Vib}} = \prod_{n=1}^{3n-(6+1)} \left[\frac{1}{1 - \exp\left(-\frac{h\lambda\nu_n}{k_B T}\right)} \right] \quad \text{EQUATION 2.12}$$

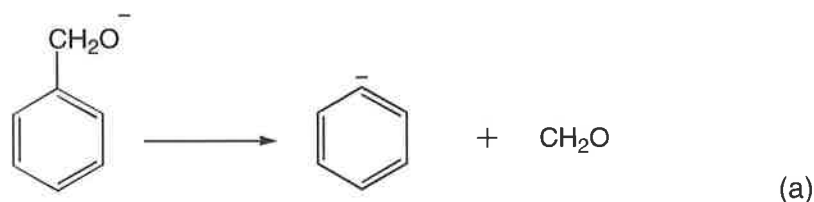
CHAPTER 3

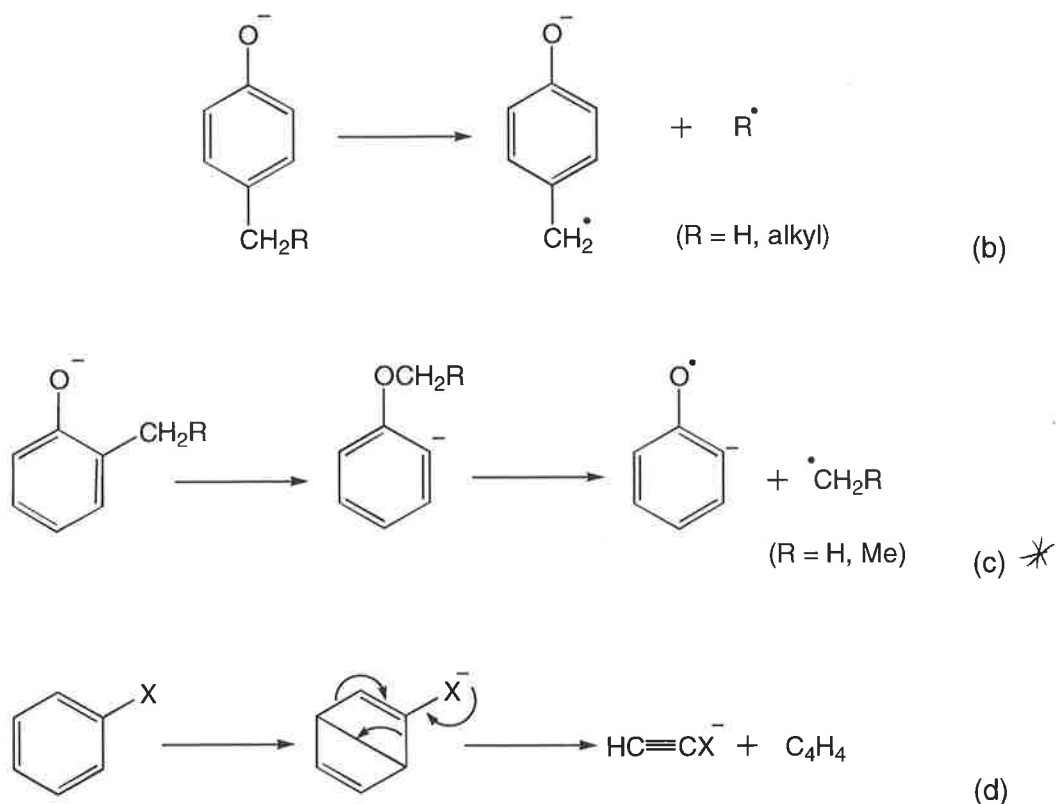
SELECTED REARRANGEMENTS OF DEPROTONATED ORGANIC ANIONS

1. INTRODUCTION

As outlined in chapter one, MS/MS data from deprotonated organic anions can be quite characteristic and therefore useful in structure determination. In many cases simple bond cleavages result, however when these processes are unfavourable the deprotonated anion may (i) rearrange to another anionic species from which a simple cleavage is favourable, (ii) undergo skeletal rearrangement, often similar to analogous rearrangement processes of anions in solution, or (iii) undergo a charge-remote process (*ie.* a process which occurs remote from and uninfluenced by the charged centre).

A number of deprotonated substituted phenyl systems have been investigated and illustrate these fragmentations. For example, the benzyloxy anion undergoes simple cleavage resulting in loss of formaldehyde⁹⁰ [Scheme 3.1 (a)], while alkylphenoxide anions fragment by loss of an alkyl radical [Scheme 3.1 (b)] which may be preceded by rearrangement⁹¹ [Scheme 3.1 (c)]. A more complex retro-cleavage of the phenyl ring occurs when there is no simple fragmentation which can occur [Scheme 3.1 (d)].⁶⁰





SCHEME 3.1

The collision induced mass spectrum (MS/MS) of deprotonated methyl benzoate shows loss of CO from the parent anion $[(\text{C}_6\text{H}_4)^-\text{CO}_2\text{Me}]$. Research into this unusual rearrangement reaction commenced as part of the author's honours requirement⁹² however time constraints left the investigation incomplete. The experimental results are revisited here and two possible mechanisms are proposed. In an attempt to distinguish between the two proposed mechanisms a theoretical investigation of the system is presented. Furthermore, it is possible that an analogous system, deprotonated methyl phenyl carbonate $[(\text{C}_6\text{H}_4)^-\text{OCO}_2\text{Me}]$, may undergo loss of CO_2 by a similar process to that of the CO loss in the $(\text{C}_6\text{H}_4)^-\text{CO}_2\text{Me}$ system. Experimental and theoretical investigations were carried into this possibility and are also described here.

* An examiner has suggested that the distonic radical/anion should have - and - interchanged.

2. RESULTS AND DISCUSSION

A. Loss of CO from Deprotonated Methyl Benzoate

i. Experimental Studies

Upon collision the deprotonated methyl- d_3 benzoate anion loses CO (Figure 3.1). Other reported losses of CO from deprotonated esters include that of dimethyl succinate⁹³ and acyloxy acetates.⁹⁴ The loss of CO in these cases occurs via the formation of an ion-neutral complex in which MeOCO^- acts as a methoxide donor. The mass spectra of several deprotonated anions of other unsaturated esters were carried out and were found to undergo simple fragmentation processes. For example, deprotonated methyl phenylacetate fragments by loss of MeOH [Scheme 3.2 (a)]. In contrast, deprotonated cyclopentadienyl methyl ester loses Me^\cdot [Scheme 3.2 (b)], while aromatic radical anions of the general formula $[\text{ArCO}_2\text{R}]^\cdot$ fragment by the characteristic cleavage sequence $\text{M}^\cdot - \text{R}^\cdot - \text{CO}_2$.⁹⁵

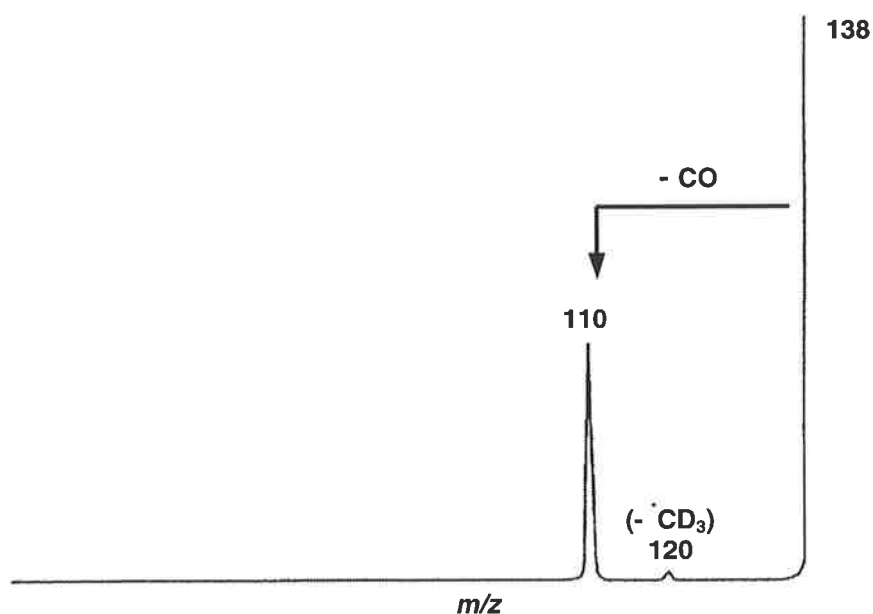
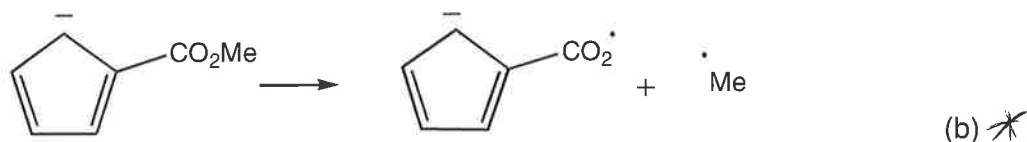
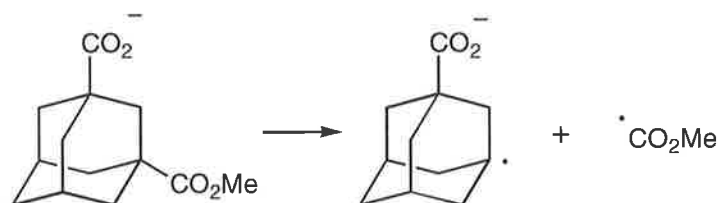


FIGURE 3.1 Collision induced mass spectrum (MS/MS) of the $[\text{M} - \text{H}]^-$ ion of methyl- d_3 benzoate. For experimental conditions see Experimental Section.



SCHEME 3.2

The possibility that the loss of CO from deprotonated methyl benzoate is a charge-remote^{63,64,96} process needs to be considered. The collision induced mass spectrum (MS/MS) of the demethylated dimethyl ester of 1,3 adamantane dicarboxylic acid was therefore recorded to see whether CO is lost. While a charge-remote radical cleavage occurred in this system (Scheme 3.3) no loss of CO was observed. It therefore seems unlikely from the experimental data that the loss of CO from deprotonated methyl benzoate can be a charge-remote reaction. It appears that this is a charge-initiated process of a closed shell aromatic anion and that the charged centre is required to be on the aryl ring.



SCHEME 3.3

In principle, deprotonation of methyl-*d*₃ benzoate could occur at any position on the phenyl ring. If the loss of CO from methyl-*d*₃ benzoate is charge-initiated, is the reaction initiated by the charge being at the *ortho* position, or can it also occur for isomers where the charge

* An examiner has suggested that the aliphatic radical anion should have a methyl group interchanged.

is localised on the *meta* or *para* position? This was investigated both indirectly as well as directly. First, the collision induced mass spectrum (MS/MS) of the analogous system methyl 2,4,6-trifluorobenzoate was examined. This system was chosen since deprotonation is only possible at the *meta* position of the aromatic ring. The mass spectrum (MS/MS) of the $[M - H]^-$ ion shows two major fragmentations $[(M - H)^- - HF]$ and $[(M - H)^- - MeCO_2]$ in the ratio of 2 : 1, but no loss of CO was observed. This result suggests that perhaps *meta* deprotonated methyl benzoate may not undergo loss of CO.

In order to confirm this proposal the DePuy⁵ method (see Chapter 1) was used to unequivocally generate the *ortho* $(C_6H_4)^-CO_2Me$ anion by the $S_N2(Si)$ reaction between HO^- and *ortho* $TMS(C_6H_4)CO_2Me$. The collision induced dissociations of the *ortho* desilylated anion (Figure 3.2) are identical to those of deprotonated methyl benzoate (Figure 3.1); in particular, both spectra show pronounced loss of CO.

The collision induced mass spectra (MS/MS) of the (similarly generated) *meta* and *para* $(C_6H_4)^-CO_2Me$ anions are also shown in Figure 3.2. Both spectra show loss of Me together with ~~minor~~^{major} loss of CO.

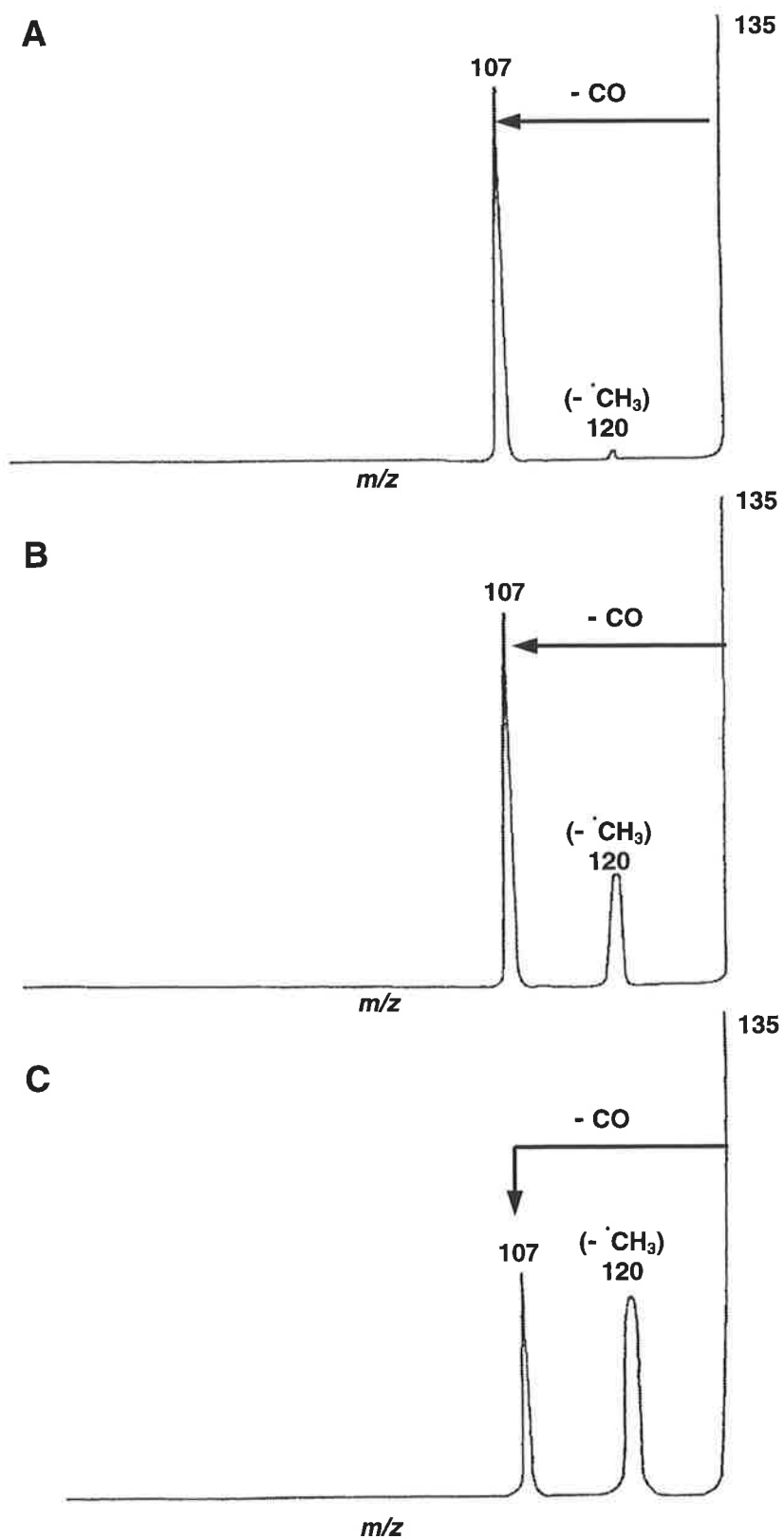
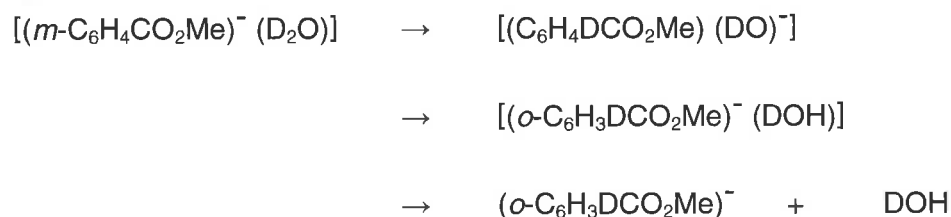


FIGURE 3.2 Collision induced mass spectra (MS/MS) of the $[M - \text{TMS}]^-$ anions from (A) *ortho*, (B) *meta* and (C) *para* trimethylsilyl-methyl benzoate. For experimental conditions see Experimental Section.

A qualitative comparison of the m/z 107 and m/z 120 peaks, corresponding to the processes $[(C_6H_4)^-CO_2Me - CO]$ and $[(C_6H_4)^-CO_2Me - Me]$ respectively, showed the following ratios: *ortho* (100 : 3), *meta* (100 : 28) and *para* (100 : 91). The energy of Me \cdot loss is comparable in each case, so the relative extent of CO loss is *ortho* > *meta* >> *para*. The kinetic energy released for the loss of CO from each isomeric $(C_6H_4)^-CO_2Me$ anion was investigated by measuring the peak width at half height of the m/z 107 fragment anions in the three CID spectra (Figure 3.2). The peak widths were found to be different in each case [*ortho* (28.0 ± 0.5 V), *meta* (32.9 ± 0.5 V) and *para* (35.7 ± 0.5 V)] indicating that either (i) the structures and/or energies of the three m/z 107 ions are different, or (ii) the modes of formation of the ions are different.²⁵ The m/z 107 ions, from each $(C_6H_4)^-CO_2Me$ isomer, are also formed in the ion source of the mass spectrometer. These three source formed m/z 107 ions each have identical mass spectra, exemplified by the dominant loss of CH_2O . The loss of CH_2O to give a peak at m/z 77 is characteristic of the deprotonated anisole anion $[(C_6H_4)^-OMe]$,^{97,98} the formation of which is consistent with the loss of CO from $(C_6H_4)^-CO_2Me$. Furthermore, the peak widths at half height of the resulting m/z 77 ions ($C_6H_5^-$), corresponding to loss of CH_2O from the three source formed $(C_6H_4)^-OMe$ (m/z 107) ions, are the same in each case within experimental error (33.5 ± 0.5 V). These kinetic energy release experiments suggest that the losses of CO from the *ortho*, *meta* and *para* $(C_6H_4)^-CO_2Me$ anions result in formation of the same (probably *ortho*) $(C_6H_4)^-OMe$ anion, but that the energetics of formation of the *ortho* $(C_6H_4)^-OMe$ anion by loss of CO from the *ortho*, *meta*, *para* deprotonated methyl benzoate anions are different. It is proposed that the loss of CO is a fragmentation of the *ortho* $(C_6H_4)^-CO_2Me$ anion and that losses of CO from the *meta* and *para* isomers is preceded by rearrangement of each of these anions to the *ortho* isomer.

ii. *Para, Meta, and Ortho* Interconversion

Interconversion of *meta* and *para* isomers of deprotonated methyl benzoate to the *ortho* anion may be a result of (i) rearrangement of the ring carbons, (ii) rearrangement of the ring hydrogens, or (iii) proton exchange between $(\text{C}_6\text{H}_4)^-\text{CO}_2\text{Me}$ and H_2O in an anion-neutral complex formed in the source of the mass spectrometer. The last of these possibilities can be tested experimentally by using D_2O as the reagent gas for anion formation. If an anion-water complex is formed and does allow for proton exchange then incorporation of deuterium into the anion will result (Scheme 3.4). No deuterium was incorporated into the anion and therefore this process is not operable in this system.



SCHEME 3.4

Carbon rearrangement in neutral benzene is a highly energetic process and has been studied both experimentally and theoretically. The energies of benzvalene and prismane relative to benzene are calculated (at the RMP2/6-31G(d) level of theory) to be +313 and +492 kJ mol^{-1} respectively.⁹⁹ The barrier for ring opening of benzvalene is calculated to be 116 kJ mol^{-1} (at the B3LYP/DZP level of theory)¹⁰⁰⁻¹⁰² and measured experimentally to be 122.6 kJ mol^{-1} .¹⁰³ We have calculated the reaction coordinates for the corresponding carbon rearrangements of the C_6H_5^- system at the B3LYP/6-311+G(d,p)//HF/6-31+G(d) level of theory; these results are shown in Figure 3.3.

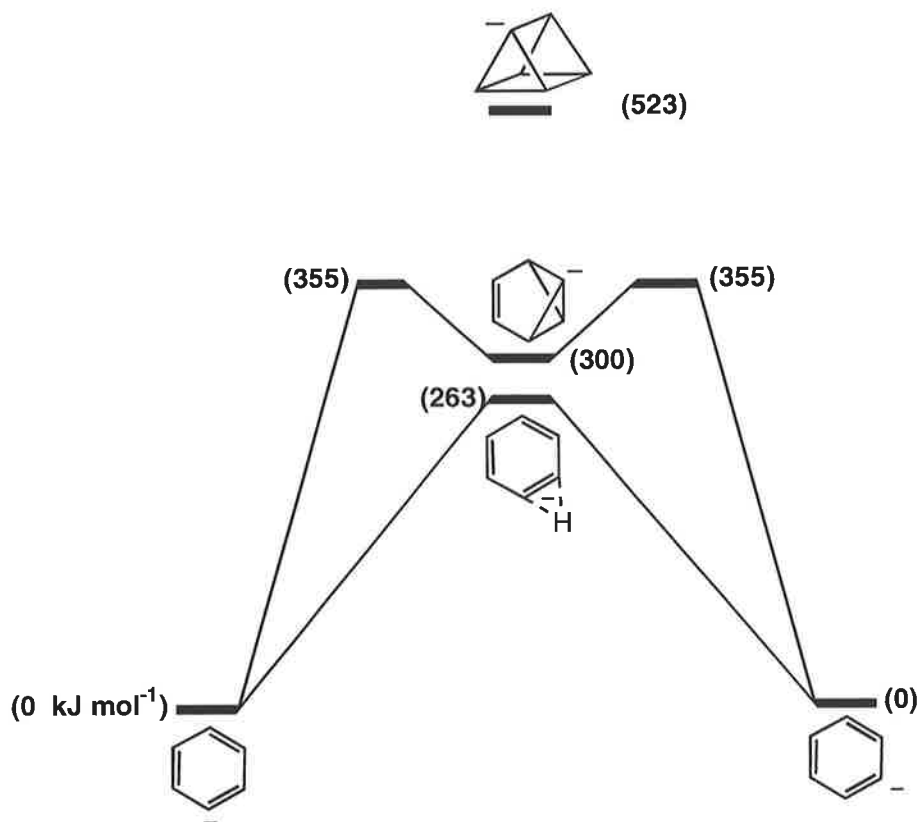
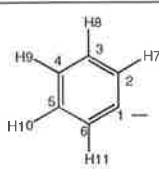
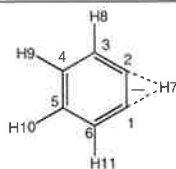
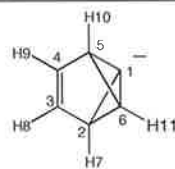
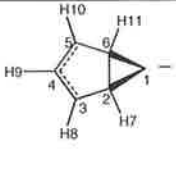
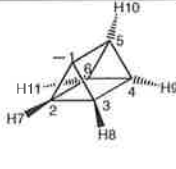


FIGURE 3.3 Calculated rearrangement pathways for the degenerate * interconversion of the phenyl anion. For full details see Table 3.1.

At this level of theory, the benzvalene anion lies 300 kJ mol⁻¹ above the phenyl anion, and the transition state for interconversion of the two is 355 kJ mol⁻¹ above the phenyl anion. The corresponding prismane anion is 523 kJ mol⁻¹ less stable than the phenyl anion. Anion scrambling via a degenerate H transfer mechanism has also been investigated at the B3LYP/6-311+G(d,p)//HF/6-31+G(d) level of theory with the transition state requiring 263 kJ mol⁻¹ above the phenyl anion. Though anion scrambling through degenerate H transfer is a high-energy process, it is more energetically favourable than that for carbon scrambling and therefore more likely to occur in the deprotonated methyl benzoate system.

* An examiner has asked whether this might be a stepwise rearrangement proceeding through [(C₆H₅) H⁻]. Should this process be operable, scrambling of H should be observed. Such scrambling did not occur (cf. Scheme 3.4).

TABLE 3.1 Calculated properties of stationary points for the interconversion of the $C_6H_5^-$ anion as shown in Figure 3.3.

					
Energy (Hartrees) ^a	-231.575561	-231.475534	-231.461480	-231.440187	-231.376405
Relative Energy (kJ mol ⁻¹)	0.0	263	300	355	523
C_2C_1 (Å) ^b	1.417	1.435	1.580	1.504	1.545
C_3C_2	1.394	1.394	1.500	1.455	1.546
C_4C_3	1.391	1.397	1.332	1.386	1.503
C_5C_4	1.391	1.391	1.501	1.383	1.507
C_6C_5	1.394	1.397	1.495	1.502	1.546
H_7C_2	1.084	1.288	1.080	1.083	1.082
H_8C_3	1.082	1.082	1.077	1.074	1.081
H_9C_4	1.080	1.081	1.077	1.079	1.082
$H_{10}C_5$	1.082	1.081	1.080	1.076	1.081
$H_{11}C_6$	1.084	1.082	1.086	1.093	1.082
$C_3C_2C_1$ (°)	124.8	119.4	111.3	129.6	92.7
$C_4C_3C_2$	120.3	120.2	105.1	107.5	89.1
$C_5C_4C_3$	117.9	120.4	105.1	111.7	60.8
$C_6C_5C_4$	120.3	120.4	109.6	113.1	89.1
$H_7C_2C_1$	118.7	56.1			129.7
$H_7C_2C_3$				121.5	118.7
$H_8C_3C_2$	120.1	121.1	126.4	124.0	133.8
$H_9C_4C_3$	121.0	120.1	128.4	125.4	127.8
$H_{10}C_5C_4$	119.5	119.5	121.5	125.7	130.4
$H_{11}C_6C_5$	116.4	118.7	135.3	119.6	130.2
$C_4C_3C_2C_1$			31.8	40.7	-1.2
$C_5C_4C_3C_2$			0.0	8.3	-90.2
$C_6C_5C_4C_3$			-29.1	4.5	59.6
$H_7C_2C_3C_4$			179.5	-166.1	-152.5
$H_8C_3C_4C_5$			178.8	155.6	116.2
$H_9C_4C_3H_8$			0.0	-171.0	-0.8
$H_{10}C_5C_4H_9$			-0.7	-176.7	0.8
$H_{11}C_6C_5H_{10}$			-24.0	139.2	0.5

a. Energies calculated at the B3LYP/6-311++G(d,p) level of theory and include zero point correction (calculated from HF/6-31+G(d) vibrational frequencies). b. Geometries optimised at the HF/6-31+G(d) level of theory.

The barriers for the *para* → *meta* and *meta* → *ortho* H transfer reactions for the $(C_6H_4)^-CO_2Me$ system were calculated at the B3LYP/6-311++G(d,p)//HF/6-31G(d) level of theory and found to be 280 and 276 kJ mol⁻¹ respectively (Figure 3.4). It is proposed

that the interconversion of *para*, *meta* and *ortho* isomers proceeds via a H transfer mechanism. Thus the loss of CO ratio *ortho* > *meta* >> *para* can be explained since the *para* → *ortho* interconversion requires two steps as opposed to one step for the *meta* → *ortho* interconversion.

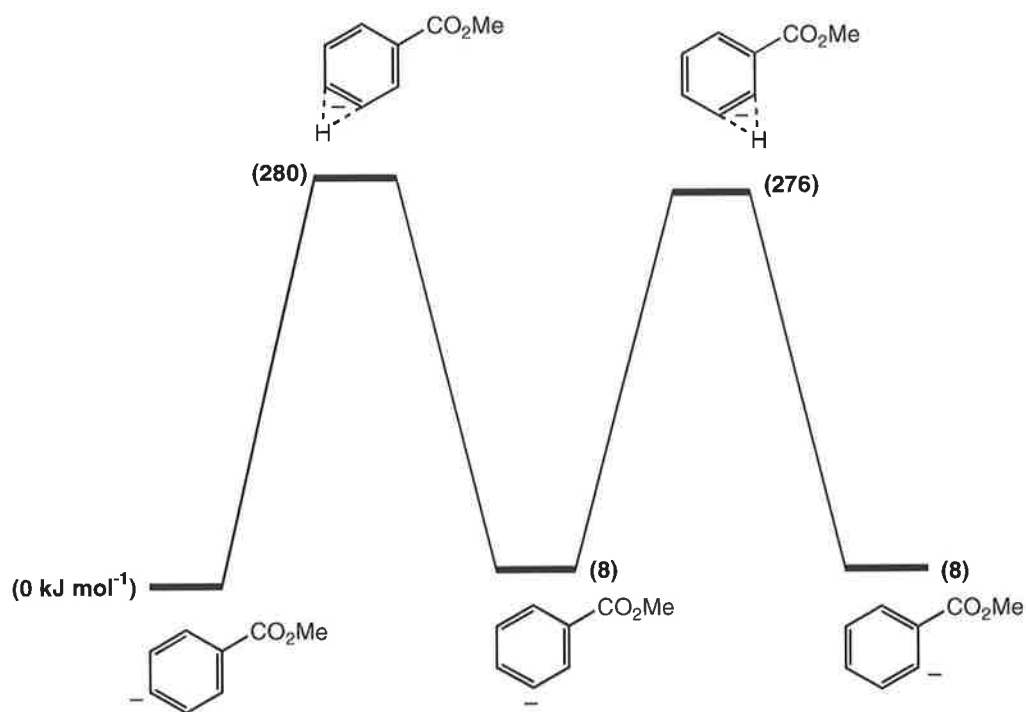
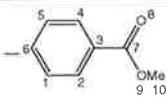
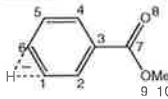
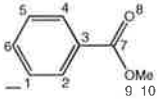
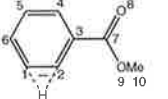
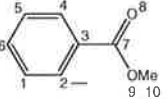


FIGURE 3.4 Calculated rearrangement pathway for 1,2 H transfer of deprotonated methyl benzoate. Full details are given in Table 3.2.

TABLE 3.2 Calculated properties of stationary points for the interconversion of the $(\text{C}_6\text{H}_4)^-\text{CO}_2\text{Me}$ anion as shown in Figure 3.4.

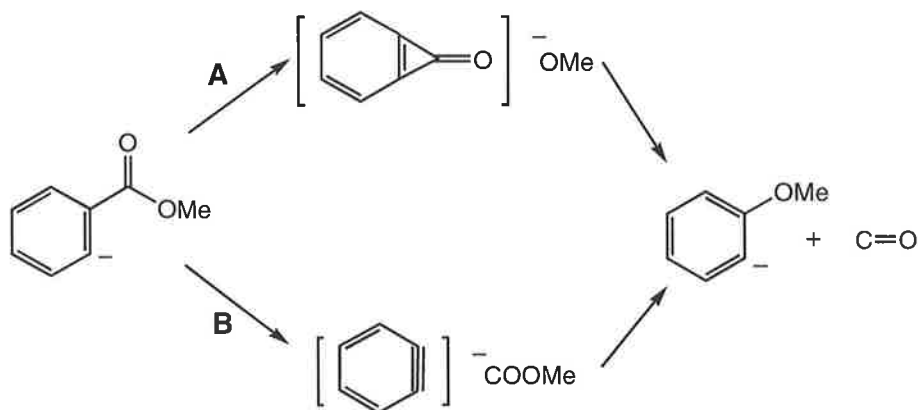
					
Energy (Hartrees) ^a	-459.61927	-459.511163	-459.616346	-459.509115	-459.616230
Relative Energy (kJ mol ⁻¹)	0.0	268.5	8.7	273.5	8.5
C_2C_1 (Å) ^b	1.385	1.390	1.417	1.441	1.425
C_3C_2	1.401	1.405	1.400	1.393	1.413
C_4C_3	1.400	1.399	1.398	1.407	1.408
C_5C_4	1.384	1.387	1.382	1.380	1.377
C_6C_5	1.422	1.399	1.400	1.405	1.401
C_7C_3	1.464	1.474	1.480	1.482	1.487
O_8C_7	1.203	1.202	1.202	1.205	1.209
O_9C_7	1.345	1.341	1.338	1.332	1.332
C_{10}O_9	1.403	1.404	1.404	1.401	1.399
HC_1		1.292		1.291	
$\text{C}_3\text{C}_2\text{C}_1$ (°)	120.3	120.2	124.8	119.6	112.2
$\text{C}_4\text{C}_3\text{C}_2$	117.6	120.0	119.9	119.9	124.4
$\text{C}_5\text{C}_4\text{C}_3$	120.5	120.7	118.1	120.3	120.3
$\text{C}_6\text{C}_5\text{C}_4$	124.7	119.7	120.3	120.5	118.2
$\text{C}_7\text{C}_3\text{C}_2$	123.0	122.4	122.7	123.3	121.3
$\text{O}_8\text{C}_7\text{C}_3$	126.3	126.0	125.7	125.1	125.0
$\text{O}_9\text{C}_7\text{O}_8$	120.0	120.1	120.2	120.1	119.7
$\text{C}_{10}\text{O}_9\text{C}_7$	117.1	113.8	117.1	117.1	117.1
HC_1C_6		56.0			
HC_1C_2				55.8	

a. Energies calculated at the B3LYP/6-311++G(d,p) level of theory and include zero point correction (calculated from HF/6-31+G(d) vibrational frequencies). b. Geometries optimised at the HF/6-31G(d) level of theory.

iii. Mechanism for Loss of CO from *Ortho* $(\text{C}_6\text{H}_4)^-\text{CO}_2\text{Me}$

Two possible mechanisms may account for the loss of CO from the *ortho* anion of methyl benzoate as outlined in Scheme 3.5. Mechanism **A** involves cyclisation by intramolecular attack of the carbonyl carbon forming a $[(\text{C}_6\text{H}_4)\text{CO}^-\text{OMe}]$ ion-neutral complex followed by nucleophilic substitution prior to loss of CO. The second mechanism **B** involves formation of a [benzyne MeOCO^-] ion-neutral complex, followed by a cine-substitution, with MeOCO^- acting as a MeO^- donor. No obvious experimental probe can be used to distinguish between these two mechanisms. A theoretical approach is therefore needed

and so the optimised reaction coordinates along both pathways were calculated at the B3LYP/6-311++G(d,p)//HF/6-31+G(d) level of theory.



SCHEME 3.5

The cyclisation mechanism is complex involving four steps with the first (A) having a barrier of 199 kJ mol^{-1} (Figure 3.5). The second transition state differs in energy to the first by only 3 kJ mol^{-1} ; this is due to a flat region of the potential energy surface in the vicinity of the $[(\text{C}_6\text{H}_4)\text{CO}^- \text{OMe}]$ complex where the $^- \text{OMe}$ anion requires little energy to move and reorientate itself about the ring. Subsequent ring-opening and dissociation of CO yields *ortho* deprotonated anisole, a reaction endothermic by 85 kJ mol^{-1} .

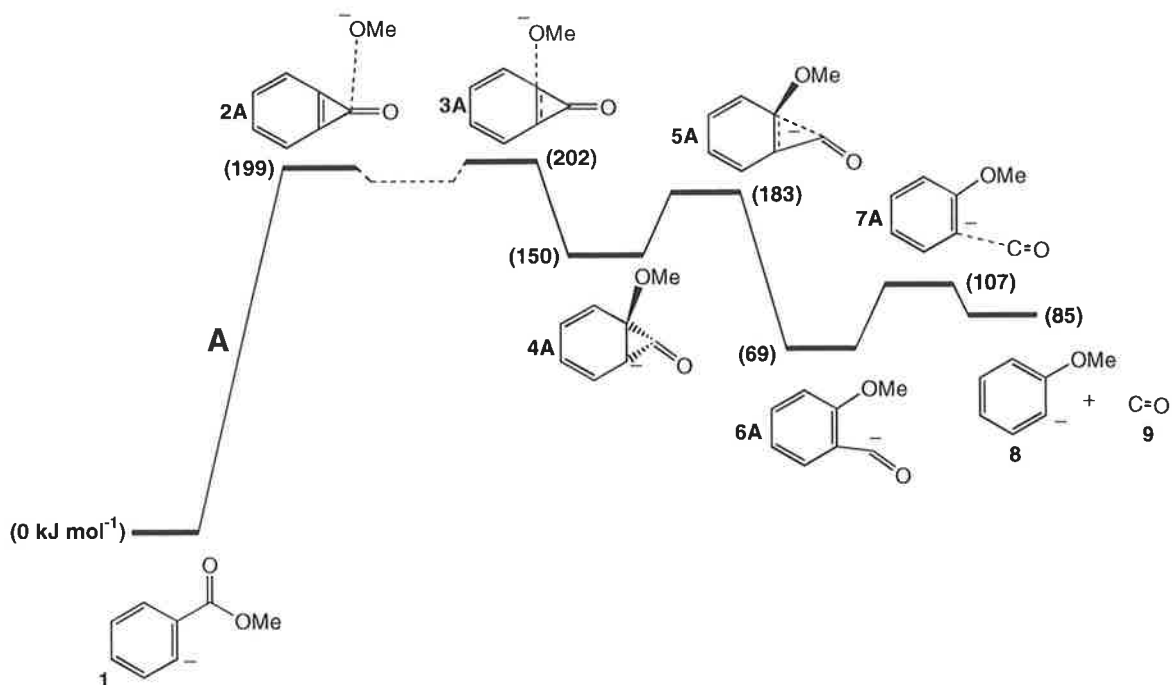


FIGURE 3.5 Calculated reaction coordinates for the cyclisation mechanism (A). Full details are given in Table 3.3 and 3.4.

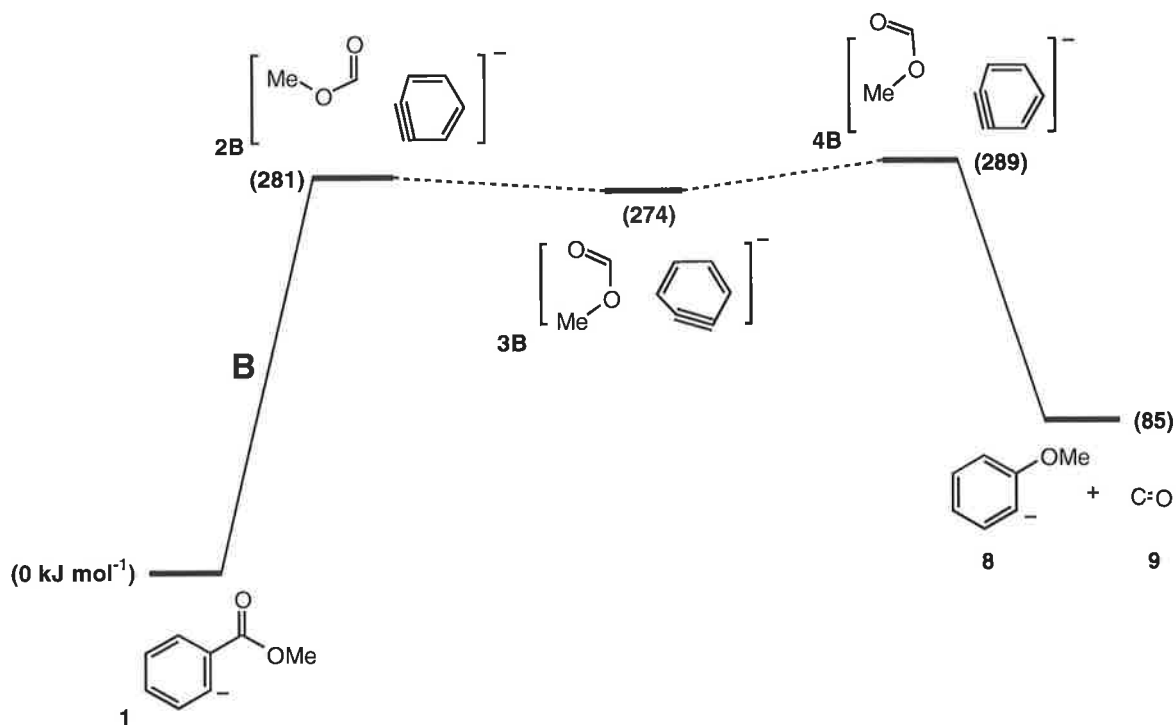
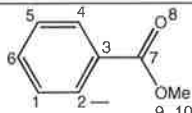
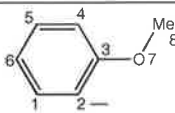
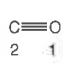


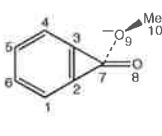

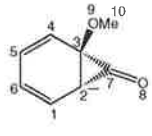
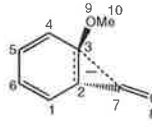
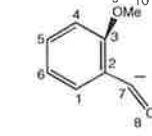
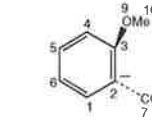
FIGURE 3.6 Reaction coordinates for the benzyne cine-substitution mechanism (B). Full details are given in Table 3.3 and 3.5.

TABLE 3.3 Calculated properties of reactant and products shown in Figures 3.5 and 3.6

			
	1	7	8
Energy (Hartrees) ^a	-459.489448	-346.113713	-113.343499
E_{reactant} (kJ mol ⁻¹)	0.0		
E_{products} (kJ mol ⁻¹)	85.0		
O_2C_1 (Å) ^b			1.113
C_2C_1	1.425	1.409	
C_3C_2	1.413	1.399	
C_4C_3	1.408	1.393	
C_5C_4	1.377	1.389	
C_6C_5	1.401	1.389	
C_7C_3	1.487		
O_7C_3		1.388	
O_8C_7	1.209		
C_8O_7		1.390	
O_9C_7	1.332		
C_{10}O_9	1.399		
$\text{C}_3\text{C}_2\text{C}_1$ (°)	112.2	112.0	
$\text{C}_4\text{C}_3\text{C}_2$	124.4	125.4	
$\text{C}_5\text{C}_4\text{C}_3$	120.3	119.5	
$\text{C}_6\text{C}_5\text{C}_4$	118.2	119.3	
$\text{C}_7\text{C}_3\text{C}_2$	121.3		
$\text{O}_7\text{C}_3\text{C}_2$		121.8	
$\text{O}_8\text{C}_7\text{C}_4$	125.0		
$\text{C}_8\text{O}_7\text{C}_3$		118.3	
$\text{O}_9\text{C}_7\text{C}_8$	119.7		
$\text{C}_{10}\text{O}_9\text{C}_7$	117.1		

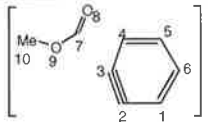
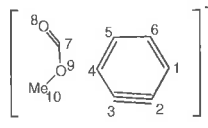
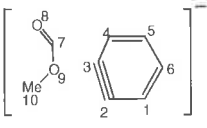
a. Energies calculated at the B3LYP/6-311++G(d,p) level of theory and include zero point correction (calculated from HF/6-31+G(d) vibrational frequencies). b. Geometries optimised at the HF/6-31+G(d) level of theory.

TABLE 3.4 Calculated properties of intermediates and transition states for the cyclisation mechanism as shown in Figure 3.5.

						
	2A	3A	4A	5A	6A	7A
Energy (Hartrees) ^a	-459.41373	-459.41281	-459.43233	-459.41976	-459.46349	-459.44887
Relative Energy (kJ mol ⁻¹)	199	201	150	183	68	107
C ₂ C ₁ (Å) ^b	1.395	1.426	1.442	1.477	1.396	1.481
C ₃ C ₂	1.352	1.370	1.496	1.511	1.397	1.474
C ₄ C ₃	1.395	1.435	1.493	1.424	1.394	1.346
C ₅ C ₄	1.378	1.351	1.341	1.370	1.385	1.436
C ₆ C ₅	1.420	1.454	1.466	1.458	1.389	1.397
C ₇ C ₂	1.440	1.389	1.355	1.296	1.614	1.313
C ₈ C ₇	1.194	1.207	1.222	1.181	1.223	1.181
O ₉ C ₃	2.666	2.102	1.422	1.412	1.370	1.380
C ₁₀ O ₉	1.346	1.348	1.389	1.391	1.406	1.383
C ₃ C ₂ C ₁ (°)	123.6	123.8	123.8	120.3	116.5	114.9
C ₄ C ₃ C ₂	123.6	121.2	113.3	112.4	121.4	121.8
C ₅ C ₄ C ₃	114.0	114.6	119.2	121.9	120.5	122.6
C ₆ C ₅ C ₄	122.4	123.1	121.9	119.9	119.3	116.6
C ₇ C ₂ C ₃	62.0	62.1	62.5	86.4	123.4	121.2
O ₈ C ₇ C ₂	147.8	151.0	151.9	173.3	110.0	177.2
O ₉ C ₃ C ₂	75.3	118.7	121.6	120.5	123.1	111.9
C ₁₀ O ₉ C ₃	144.4	116.6	114.7	115.2	116.7	118.8
C ₄ C ₃ C ₂ C ₁	0.0	-11.7	-21.4	-30.6	-0.9	0.0
C ₅ C ₄ C ₃ C ₂	-2.1	8.7	17.8	8.2	0.9	0.0
C ₆ C ₅ C ₄ C ₃	2.1	-1.0	-3.8	14.5	-0.2	0.0
C ₇ C ₂ C ₃ C ₄	-175.6	148.9	113.2	114.0	-179.4	180.0
O ₈ C ₇ C ₂ C ₃	-147.5	-172.2	-171.1	-171.2	-162.8	180.0
O ₉ C ₃ C ₂ C ₁	115.2	99.0	117.3	113.3	-178.0	180.0
C ₁₀ O ₉ C ₃ C ₂	111.5	27.7	-58.0	-64.8	-67.6	180.0

a. Energies calculated at the B3LYP/6-311++G(d,p) level of theory and include zero point correction (calculated from HF/6-31+G(d) vibrational frequencies). b. Geometries optimised at the HF/6-31+G(d) level of theory.

TABLE 3.5 Calculated properties of intermediates and transition states for the benzyne mechanism as shown in Figure 3.6.

			
	2B	3B	4B
Energy ^a	-459.382419	-459.385171	-459.379626
Relative Energy (kJmol ⁻¹)	281	274	288
C ₂ C ₁ (Å) ^b	1.417	1.408	1.418
C ₃ C ₂	1.251	1.366	1.250
C ₄ C ₃	1.360	1.400	1.359
C ₅ C ₄	1.398	1.408	1.397
C ₆ C ₅	1.405	1.394	1.409
C ₇ C ₄		3.581	3.320
O ₈ C ₇	1.221	1.203	1.204
O ₉ C ₇	1.416	1.492	1.480
C ₁₀ O ₉	1.397	1.391	1.392
C ₃ C ₂ C ₁ (°)	110.1	114.0	109.6
C ₄ C ₃ C ₂	105.6	140.0	143.4
C ₅ C ₄ C ₃	121.3	105.5	105.7
C ₆ C ₅ C ₄	121.9	121.9	121.2
C ₇ C ₃ C ₂	146.0		
C ₇ C ₄ C ₃		169.1	96.8
O ₈ C ₇ C ₄		174.9	175.1
O ₈ C ₇ C ₃	98.4		
O ₉ C ₇ C ₈	113.1	11.9	112.3
C ₁₀ O ₉ C ₇	118.7	118.4	118.5

a. Energies calculated at the B3LYP/6-311++G(d,p) level of theory and include zero point correction (calculated from HF/6-31+G(d) vibrational frequencies). b. Geometries optimised at the HF/6-31+G(d) level of theory.

The reaction coordinate diagram for the benzyne cine-substitution mechanism (**B**) is shown in Figure 3.6. This is a simpler process than the cyclisation mechanism with formation of the [benzyne MeOCO⁻] complex being followed directly by formation of products. The simplicity of this mechanism avoids any potential bottle necks in subsequent steps along the reaction pathway (*cf.* mechanism **A**) however the barrier to the rate limiting transition state for mechanism **B** is 289 kJ mol⁻¹, some 87 kJ mol⁻¹ more than that for mechanism **A**.

The cyclisation process **A** is favoured in terms of the energy barrier to the rate determining transition state. However, energetics alone are not sufficient to accurately predict whether

a particular reaction will occur in preference to another. The pre-exponential Arrhenius factors for both processes need to be ascertained since the rate of a reaction is governed by the Arrhenius equation (Equation 3.1).

$$k = A \exp\left(\frac{-E_a}{RT}\right) \quad \text{EQUATION 3.1}$$

Comparison of the relative probabilities of the two possible processes **A** and **B** requires an intimate knowledge of the potential energy surface for both processes. Such studies are not feasible for a system of this size. However, comparison of the relative vibrational partition functions, as determined by transition state theory, for the first transition state in each of the processes shown in Figures 3.5 and 3.6 may give some insight into the relative pre-exponential factors for both processes,^{87,104,105} as discussed earlier (see Chapter 2).

The partition function density is an approximate measure of the number of energy states accessible to a particular molecule at a given temperature. The first step in each of the processes **A** and **B** can be simplified, at least in a qualitative sense, such that the partition function requires consideration of vibrational states only. Since the reactant is the same in each process we only need to consider the vibrational partition function density for the two transition states. The vibrational partition function is given by Equation 3.2, where ν_n is the harmonic vibrational frequency of mode n (for a non linear molecule and excluding the reaction coordinate $1 \leq n \leq 3n - [6n + 1]$), λ is a scaling factor for HF/6-31G+(d) vibrational modes.⁸⁹ The partition function density can then be evaluated from *ab initio* frequency calculations.

$$Q_{vib} = \prod_{n=1}^{3n-(6+1)} \left[\frac{1}{1 - \exp\left(-\frac{h\nu_n}{k_B T}\right)} \right] \quad \text{EQUATION 3.2}$$

The computed frequencies and partition functions are given in Table 3.6. The difficulties of including low frequencies (which may act as rotations) in such an analysis have been reported.^{106,107} When all frequencies are considered, the pre-Arrhenius factors for the first transition state of the benzyne mechanism is four times larger than that of the cyclisation process providing an upper limit on the ratio. While this can only be considered in a qualitative sense it does suggest that the simpler benzyne mechanism has a larger entropic factor than the cyclisation mechanism.

TABLE 3.6 Vibrational Partition Functions for Transition States 2A and 2B

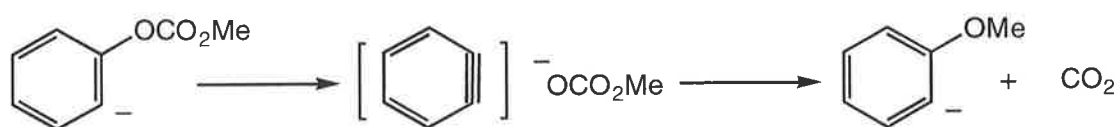
Transition State 2A				Transition State 2B			
cm ⁻¹	Q' vib	cm ⁻¹	Q' vib	cm ⁻¹	Q' vib	cm ⁻¹	Q' vib
63	4.1394	1242	1.0042	38	6.5088	1158	1.0061
92	3.0050	1244	1.0042	59	4.3730	1204	1.0050
100	2.8028	1247	1.0041	99	2.8205	1227	1.0045
112	2.5641	1282	1.0035	105	2.6986	1274	1.0037
183	1.8067	1289	1.0034	134	2.2487	1309	1.0031
269	1.4412	1399	1.0021	185	1.7914	1340	1.0027
293	1.3802	1401	1.0021	342	1.2851	1411	1.0020
394	1.2144	1584	1.0009	361	1.2553	1530	1.0012
499	1.1251	1607	1.0008	443	1.1657	1594	1.0009
548	1.0984	1609	1.0008	466	1.1473	1596	1.0009
584	1.0827	1626	1.0008	480	1.1373	1630	1.0008
688	1.0507	1626	1.0008	666	1.0560	1644	1.0007
771	1.0347	1770	1.0004	691	1.0501	1649	1.0007
807	1.0295	1785	1.0004	759	1.0366	1724	1.0005
823	1.0274	1980	1.0002	845	1.0248	1997	1.0002
843	1.0250	2870	1.0000	902	1.0192	3178	1.0000
972	1.0140	2907	1.0000	926	1.0172	3225	1.0000
1063	1.0094	2976	1.0000	966	1.0144	3230	1.0000
1079	1.0087	3325	1.0000	1074	1.0089	3321	1.0000
1103	1.0078	3345	1.0000	1075	1.0088	3343	1.0000
1113	1.0075	3375	1.0000	1096	1.0081	3362	1.0000
1181	1.0055	3378	1.0000	1122	1.0072	3374	1.0000

iv. Conclusions

The loss of CO from the *ortho* anion of methyl benzoate is a charge initiated process resulting in the formation of the *ortho* anisole anion. The *meta* and *para* forms of deprotonated methyl benzoate undergo 1,2 hydrogen transfer(s) to form the *ortho* isomer which subsequently loses CO. Experimental and theoretical data available do not allow differentiation between the two mechanisms proposed in Scheme 3.5. While the cyclisation process appears to be favoured on energetic grounds, the benzyne cine-substitution process has the higher Arrhenius A factor and therefore is more entropically favoured.

B. Loss of CO₂ from *Ortho* Deprotonated Methyl Phenyl Carbonate

The benzyne cine-substitution reaction (Scheme 3.5, mechanism B) for loss of CO from deprotonated methyl benzoate is an attractive proposal: unfortunately it cannot be substantiated in that particular system for the reasons outlined above. It would be of interest to construct an analogous system in which a benzyne-ion complex might lead to a cine-substitution product. In such a system the benzyne reaction should be kinetically and thermodynamically more favourable than the analogous process of the (C₆H₄)⁻CO₂Me system. The deprotonated methyl phenyl carbonate system would seem to meet these prerequisites, with the anticipated benzyne process shown in Scheme 3.6. In this system the formation of the benzyne-ion complex seems to be a plausible process, MeOCO₂⁻ is a good MeO⁻ donor and overall the loss of CO₂ is only endothermic by 6 kJ mol⁻¹ (cf. 85 kJ mol⁻¹ for loss of CO from (C₆H₄)⁻CO₂Me). A cyclisation process similar to that for (C₆H₄)⁻CO₂Me might also occur in this system (see later discussion).

**SCHEME 3.6****i. *Ortho*, *Meta* and *Para* (C₆H₄)⁻OCO₂Me**

The *ortho*, *meta* and *para* (C₆H₄)⁻OCO₂Me anions were generated in the ion source of the mass spectrometer from their corresponding trimethylsilyl derivatives by S_N2(Si) processes. The collision induced mass spectra (MS/MS) of the three isomers are shown in Figure 3.7.

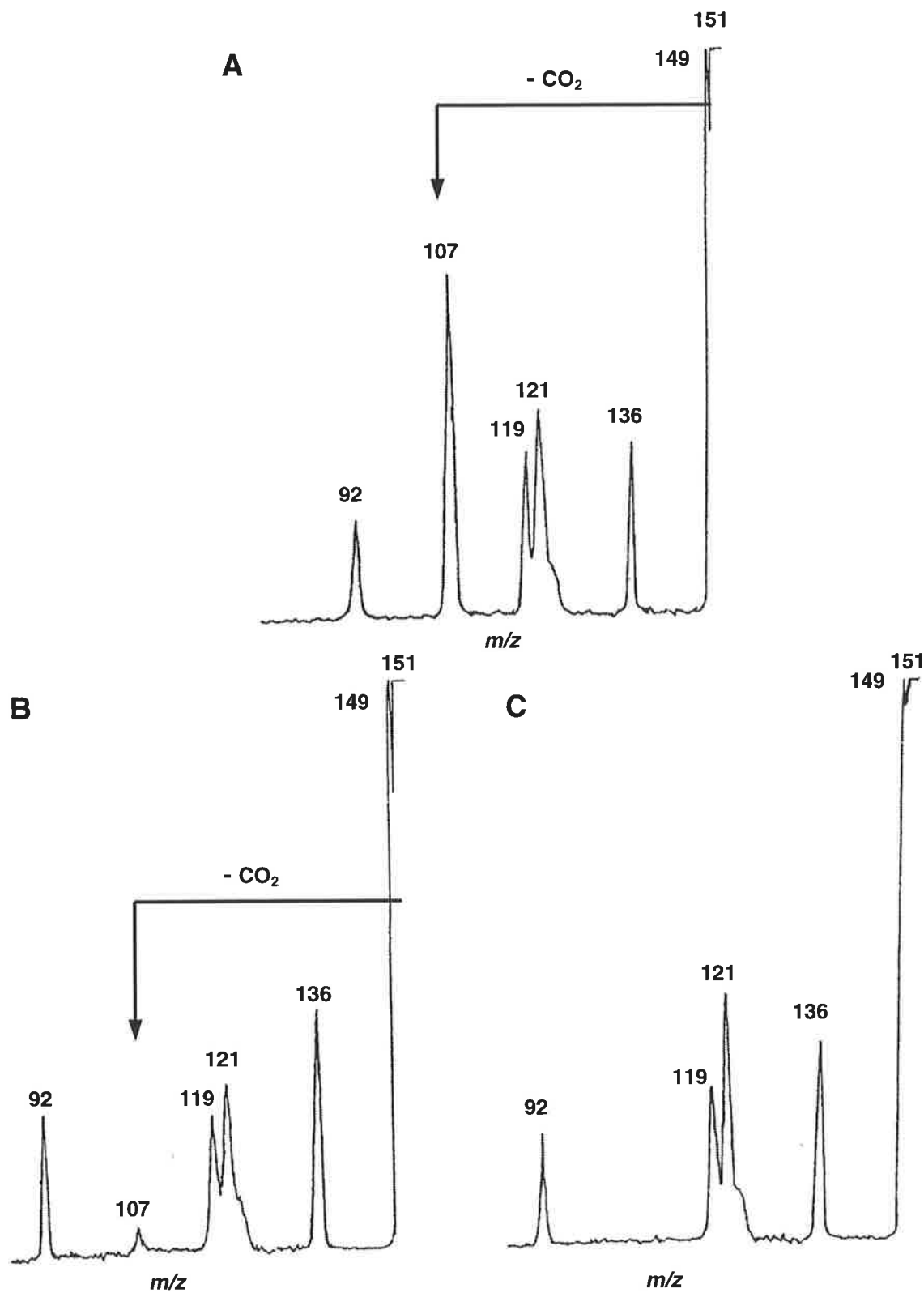
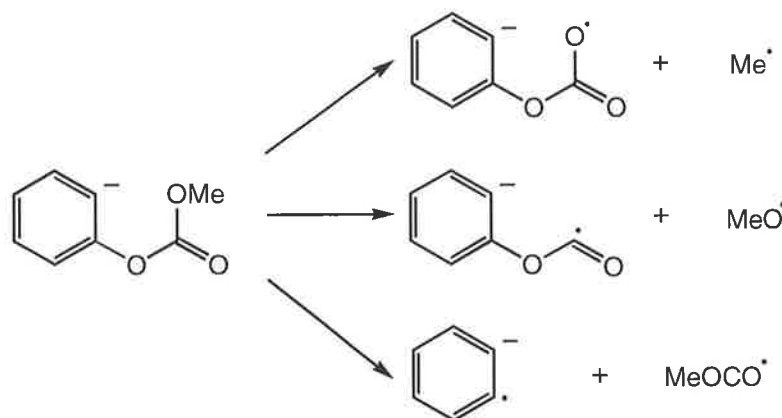


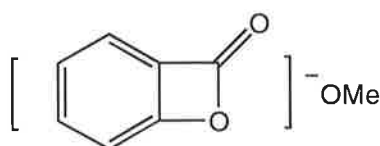
FIGURE 3.7 Collision induced mass spectra (MS/MS) of the $[M - TMS]^-$ anions from (A) *ortho*, (B) *meta* and, (C) *para* trimethylsilyl-methyl phenyl carbonate. For experimental conditions see Experimental Section.

Loss of CO₂ is observed in the CID mass spectrum of the *ortho* isomer, but it is accompanied by a number of other processes not observed in the CID mass spectrum of deprotonated methyl benzoate. No significant loss of CO₂ is observed from the *meta* or *para* anions, unlike the cognate *meta* and *para* (C₆H₄)⁻CO₂Me where losses of CO are observed. Other reactions of the (C₆H₄)⁻OCO₂Me anions include the losses of radicals and neutrals: Me[•], MeO[•], MeOCO[•], CH₂O and MeOH. The observed relative abundances of the ions formed by these losses are similar for each of the three isomers and appear to occur independently of the position of the charge. These processes must either be charge-remote processes and/or anion induced processes occurring after an interconversion process (eg. 1,2-H transfer as described in the preceding section). It has been shown that ester groups (-CO₂R) fragment by charge-remote processes involving competitive losses of R[•], RO[•], and ROCO[•] to form distonic radical anions.¹⁰⁸ For example, the 1,3 di-substituted adamantane anion shown in Scheme 3.3 is an anionic system where the charged centre is positioned on carbon 1 and the methyl ester functionality is on carbon 3. Reactions of the ester (losses of Me[•], MeO[•] and MeOCO[•]) may be charge-remote processes. It is therefore proposed that radical losses from the three isomeric deprotonated phenyl carbonates are charge-remote radical cleavages (shown for the *ortho* isomer in Scheme 3.7).



SCHEME 3.7

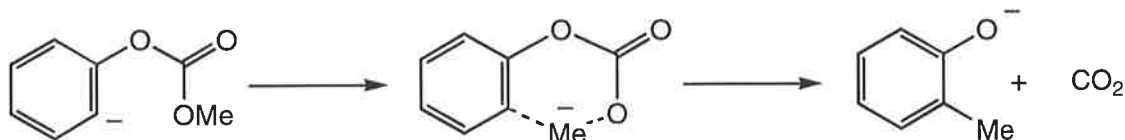
The losses of MeOH and CH₂O are either charge-remote processes of MeO[•] or charge-induced processes of MeO⁻. Neither of these losses were observed in the earlier study of charge-remote processes using 1,3 di-substituted adamantanes.¹⁰⁸ The MeO⁻ ion of the intermediate ion-neutral complex formed by cyclisation of the deprotonated methyl phenyl carbonate system (Scheme 3.8) could effect either deprotonation of, or hydride donation to the cyclic lactone, thus explaining the losses of MeOH and CH₂O.



SCHEME 3.8

This study was initiated in order to explore a system similar to that of methyl benzoate, and to see whether a benzyne cine-substitution reaction occurs for the chosen system. Methyl phenyl carbonate appears to be a good choice for such a study since the anticipated loss of CO₂ is observed from the *ortho* isomer. The absence of CO₂ loss in the *meta* and *para* isomers may be attributed to different kinetic and thermodynamic factors in the

$(\text{C}_6\text{H}_4)^-\text{OCO}_2\text{Me}$ system compared with the $(\text{C}_6\text{H}_4)^-\text{CO}_2\text{Me}$ system. Does the loss of CO_2 from the *ortho* isomer occur by a benzyne cine-substitution mechanism or via a cyclisation mechanism through the intermediate shown in Scheme 3.8? In either case the reaction is analogous to that involving loss of CO in the $(\text{C}_6\text{H}_4)^-\text{CO}_2\text{Me}$ system, and the resulting product anion should be *ortho* $(\text{C}_6\text{H}_4)^-\text{OMe}$ (m/z 107). As discussed earlier, the mass spectrum (MS/MS) of the *ortho* $(\text{C}_6\text{H}_4)^-\text{OMe}$ anion is dominated by loss of formaldehyde. The mass spectrum (MS/MS) of the source formed m/z 107 ion from *ortho* $\text{C}_6\text{H}_4^-\text{OCO}_2\text{Me}$ does not show loss of formaldehyde. Thus the loss of CO_2 in the deprotonated methyl phenyl carbonate system is not analogous to the previously described loss of CO from the deprotonated methyl benzoate system. What is the mechanism for this loss of CO_2 ? The only other plausible mechanism involves methyl migration through a six-centred transition state resulting in the formation of the product *ortho* methyl phenoxide (cresol) anion as shown in Scheme 3.9.



SCHEME 3.9

The collision induced (MS/MS) and charge reversal ($^-\text{CR}^+$) mass spectra of isomeric cresol anions have been reported.¹⁰⁹ The CID mass spectra are very weak and only show radical losses of H^\cdot and Me^\cdot . The mass spectrum (MS/MS) of the source formed m/z 107 ion, formed by loss of CO_2 from *ortho* $(\text{C}_6\text{H}_4)^-\text{OCO}_2\text{Me}$, does not show loss of Me^\cdot but, as mentioned above, this product peak is of small abundance and is likely to be lost in the

background noise. The $\bar{\text{C}}\text{R}^+$ mass spectra of authentic samples of the *ortho* anisyl anion and the *ortho* cresol anion are different enough in the high mass region to allow for characterisation of the source formed m/z 107 ion. The high mass regions of these two $\bar{\text{C}}\text{R}^+$ spectra (*ortho* anisyl and *ortho* cresol) are shown in Figure 3.8: also shown is the high mass region of the $\bar{\text{C}}\text{R}^+$ spectrum of the m/z 107 formed from loss of CO_2 from *ortho* $(\text{C}_6\text{H}_4)\bar{\text{O}}\text{CO}_2\text{Me}$. The $\bar{\text{C}}\text{R}^+$ spectrum of the m/z 107 product ion matches that of the *ortho* cresol anion and is reproducible. Thus, the loss of CO_2 occurs by methyl migration, through a six-centred transition state (Scheme 3.9) to form the cresol anion.

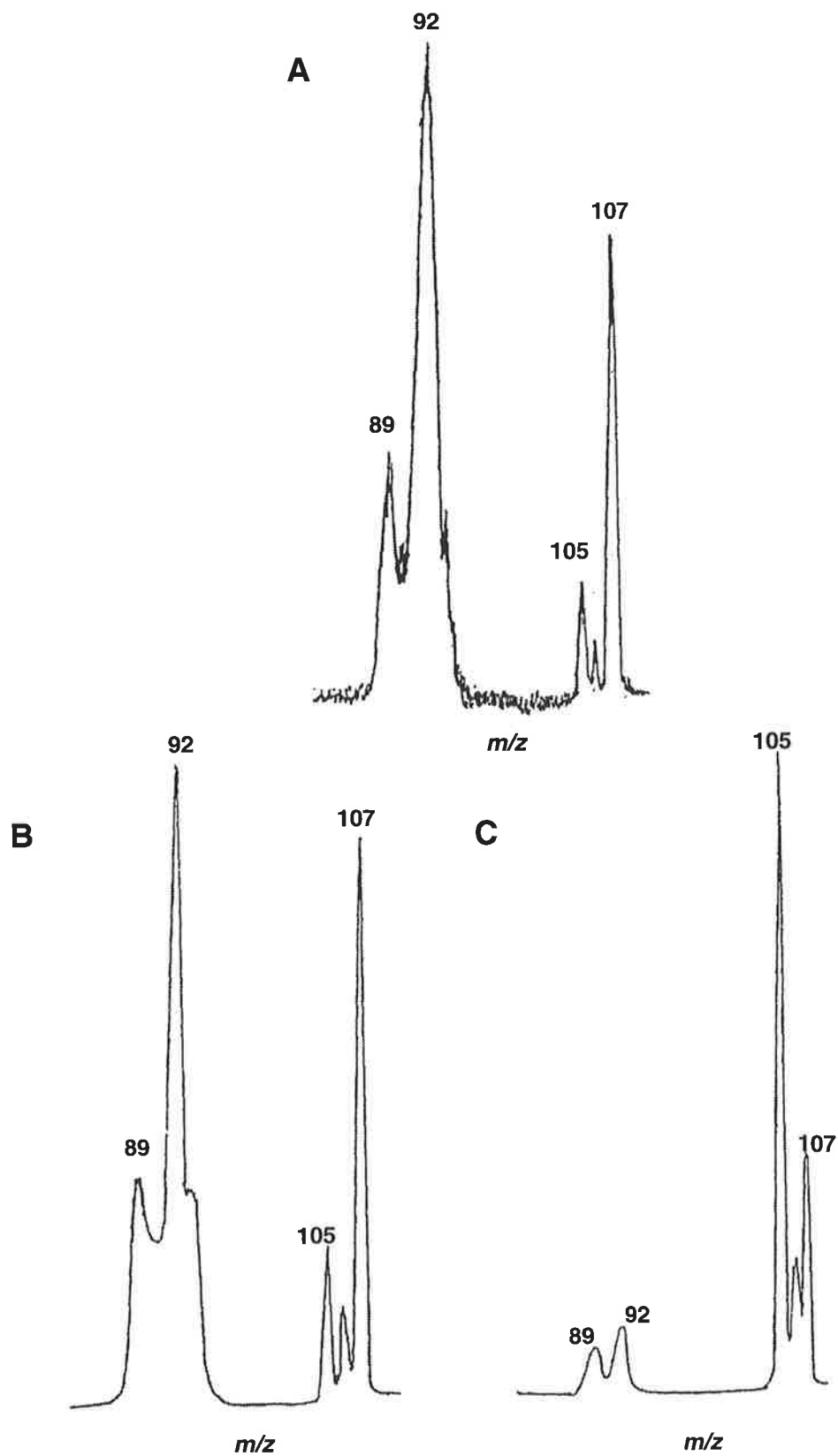


FIGURE 3.8 High mass region of three ${}^{-}\text{CR}^{+}$ spectra of: (A) m/z 107 anion formed by loss of CO_2 from *ortho* $(\text{C}_6\text{H}_4)^{-}\text{OCO}_2\text{Me}$, (B) the *ortho* cresol anion and, (C) the *ortho* anisole anion. For experimental conditions see Experimental Section.

ii. Mechanism for Loss of CO₂

The methyl migration process described above has been investigated using theoretical calculations. In principle, the methyl transfer can be either a concerted or stepwise process. Theoretical calculations at the B3LYP/6-311++G(d,p)//HF/3-21+G(d) level of theory have found stationary points only along the stepwise path, no stationary points corresponding to the concerted process were found to exist at the level of theory used. The stepwise process for loss of CO₂ is summarised in Figure 3.9. The barrier to Me migration via a six-membered transition state is 191 kJ mol⁻¹. The reaction is strongly exothermic and the intermediate (at -296 kJ mol⁻¹) is formed with sufficient excess energy to allow loss of CO₂ to form the product *ortho* cresol anion.

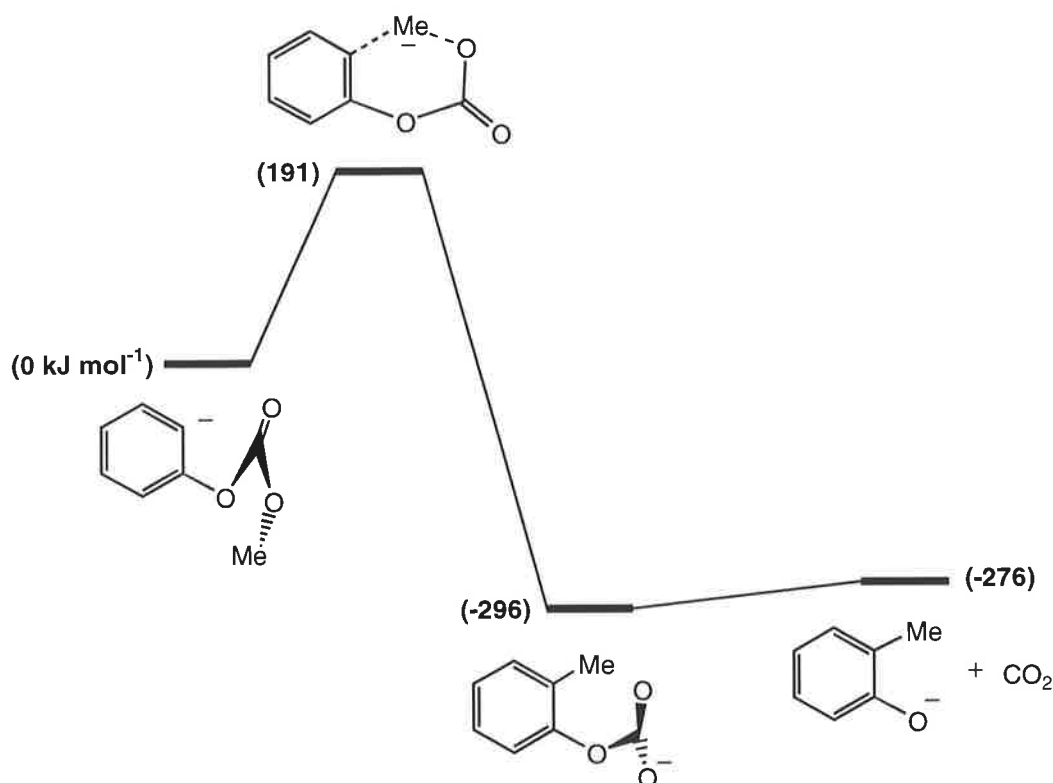
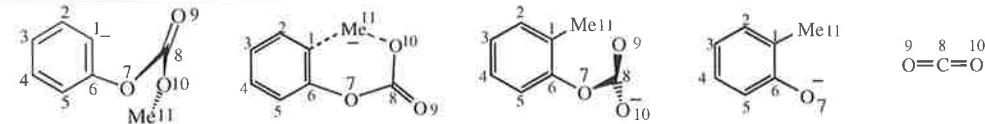


FIGURE 3.9 Calculated reaction pathway for the loss of CO₂ from the *ortho* (C₆H₄)⁻OCOO₂Me anion. Full details are given in Table 3.7.

TABLE 3.7 Calculated properties of stationary points for the Me transfer reaction of methyl phenyl carbonate as shown in Figure 3.9.


Energy (Hartrees) ^a	-534.73410	-534.66125	-534.84690	-346.20291	-188.63621
Relative Energy (kJ mol ⁻¹)	0	191	-296	-276	
C ₂ C ₁ (Å) ^b	1.419	1.406	1.388	1.378	
C ₃ C ₂	1.392	1.391	1.389	1.388	
C ₄ C ₃	1.392	1.389	1.386	1.391	
C ₅ C ₄	1.389	1.387	1.386	1.381	
C ₆ C ₅	1.379	1.387	1.383	1.433	
O ₇ C ₆	1.466	1.457	1.379	1.300	
C ₈ O ₇	1.352	1.416	1.478		
O ₉ C ₈	1.209	1.228	1.236		1.599
O ₁₀ C ₈	1.354	1.301	1.247		1.599
C ₁₁ O ₁₀	1.461	1.888			
C ₁₁ C ₁	2.265	1.511	1.433		
C ₃ C ₂ C ₁ (°)	123.7	123.3	121.4	122.3	
C ₄ C ₃ C ₂	120.2	119.6	119.5	117.7	
C ₅ C ₄ C ₃	118.9	119.6	119.7	121.1	
C ₆ C ₅ C ₄	117.6	119.3	120.5	122.3	
O ₇ C ₆ C ₅	113.8	123.8	120.6	122.7	
C ₈ O ₇ C ₆	121.6	153.0	119.1		
O ₉ C ₈ O ₇	125.7	114.3	122.1		
O ₁₀ C ₈ O ₉	121.5	126.6	133.1	180.0	
C ₁₁ C ₁ C ₆	90.7	119.6	117.3		
C ₁₁ O ₁₀ C ₈	120.3	105.1			

a. Energies calculated at the B3LYP/6-311++G(d,p) level of theory and include zero point correction (calculated from HF/3-21+G(d) vibrational frequencies). b. Geometries optimised at the HF/3-21(d) level of theory.

iii. Conclusions

The deprotonated methyl phenyl carbonate system was investigated following on from the previous study on deprotonated methyl benzoate, since it was proposed that loss of CO₂ might occur via a benzyne mechanism. While loss of CO₂ is observed to occur from the *ortho* deprotonated methyl phenyl carbonate it is only a minor process from the *meta* and *para* analogues. The loss of CO₂ was shown to occur by the methyl migration pathway shown in Scheme 3.9.

3. EXPERIMENTAL

A. Mass Spectrometric Methods

All mass spectra were recorded using a modified VG ZAB HF mass spectrometer with BE configuration (where B and E represent magnetic and electric sectors, respectively) equipped with tandem collision cells between B and E. The instrument was used in negative ion chemical ionisation mode. Samples were introduced via a heated septum inlet to give an operating pressure inside the source housing of 5×10^{-6} Torr. Typical source conditions were as follows: source temperature 200°C , repeller voltage -0.5 V, ion extraction voltage 7 kV, mass resolution $m/\Delta m \geq 1500$. All slits were fully open in order to minimize mass discrimination. The reagent ion HO^- was generated by electron impact on H_2O (introduced through the heated septum inlet to give an operating pressure of *ca.* 5×10^{-5} Torr). The estimated total pressure in the ion source is 0.1 Torr. Negative ion chemical ionisation by HO^- effected either (i) deprotonation of a neutral organic substrate, or (ii) desilylation of a neutral trimethylsilylated substrate (by analogy to the method developed by DePuy *et al.*⁵).

Collision induced dissociation (CID) of B-mass selected ions was effected by collision with argon gas in one of the collision cells at a pressure of 10^{-6} Torr. This reduces the main beam to 80% of the initial value, producing essentially single collision conditions.³⁰ The resulting ions were recorded by scanning E.

Charge reversal (${}^{-}\text{CR}^+$)^{31,35,110} of B-mass selected anions was effected by collision with oxygen in one of the collision cells, allowing 80% transmittance of the main beam and thus producing essentially single collision conditions.³⁰ ${}^{-}\text{CR}^+$ spectra were then recorded as for

the CID experiment except that the polarity of the electric sector was reversed to allow detection of positive ions.

B. Synthetic Procedures

Methyl benzoate, methyl phenylpropiolate, methyl phenyl carbonate and *ortho* cresol are commercial samples and were used without further purification. The three isomeric methyl (trimethylsilyl) benzoates,¹¹¹⁻¹¹³ three isomeric methyl (trimethylsilylphenyl) carbonates,¹¹⁴⁻¹¹⁷ *ortho* trimethylsilylanisole¹¹⁸ and 1-methoxycarbonylcyclopenta-1,3-diene¹¹⁹ were prepared by known methods. (Methyl-*d*₃) benzoate (*d*₃ = 99%) was prepared by esterification of benzoyl chloride with methanol-*d*₄.¹²⁰

C. Theoretical Methods

Geometries were optimised using the Hartree-Fock (HF) method^{71,72} combined with either the 6-31+G(d) or 3-21+G(d) basis set. Stationary points on the potential energy surface were characterised as either minima (no imaginary frequencies) or transition states (one imaginary frequency) by calculation of the frequencies using analytical gradient procedures. Intrinsic reaction coordinate (IRC) calculations were used to examine the reaction path on the potential energy surface leading away from a given transition state, thus confirming connection between minima and the transition state. The calculated frequencies were used to determine zero-point energies which were scaled⁸⁹ by 0.9135 [HF/6-31+G(d)] or 0.9207 [HF/3-21G+(d)] and then used as a zero-point energy correction for the electronic energetic calculated at the respective level of theory as well as at higher

levels of theory. Higher level single point energies were calculated for each stationary point at the B3LYP/6-311++G(d,p) level of theory to obtain more accurate and reliable energies. The B3LYP method^{83,84} has proven to be an effective, reliable and cost effective theoretical method and such are particularly suited to large systems such those studied here. Calculations were carried out using the Gaussian 94 suite of programs¹²¹ with the Power Challenge supercomputer of the South Australian Computing Centre (The University of Adelaide) and the Beowulf computing cluster at the South Australian Computational Chemistry Facility (The University of Adelaide).

CHAPTER 4

THEORETICAL STUDIES OF POTENTIAL INTERSTELLAR ANIONS

ABSTRACT

Terzieva and Herbst¹²² reported a theoretical investigation showing that carbon cumulenes, C_n (where $n \geq 6$) can undergo efficient radiative attachment of an electron to form the corresponding anions. More recently, Barckholtz, Snow and Bierbaum¹²³ demonstrated that C_n^- ($n = 2, 4 - 10$) and C_nH^- ($n = 2, 4, 6, 7$) anions do not react efficiently with molecular hydrogen, implying that detectable abundances of cumulenenic anions may exist in the interstellar medium. We have carried out a systematic theoretical investigation examining possible anionic candidates for detection in the interstellar medium, highlighting properties that are pertinent to their interstellar detection. The extraordinary electron affinities of the series of interstellar molecules investigated [C_nH , $C_{n-1}CH_2$ and C_nO ($n = 2 - 10$)] suggest that efficient radiative attachment of an electron can occur under interstellar conditions. In addition, the large dipole moments of the corresponding anions indicate that their interstellar detection should be possible by radio astronomy. The results reported here have appeared in *Monthly Notices of the Royal Astronomical Society*,¹²⁴ a contribution which should serve as a guide to future laboratory experiments and astronomical surveys into these anions.

1. INTRODUCTION

A. Molecules in the Interstellar Medium

The vast expanse of the visible universe encloses massive localised regions of matter known as *galaxies*. While the matter within our own galaxy is predominantly concentrated into the stars that dominate our night sky, about 10% of the galactic mass is attributed to the matter in regions between the stars, or the *interstellar medium*. This interstellar matter is unevenly distributed, showing a propensity to condense into massive dusty, gaseous structures - the so-called *interstellar clouds*. Based on their opacity to ultraviolet-visible radiation, interstellar clouds can be broadly categorised as either; *dense*, *translucent* or *diffuse* depending on their density.¹²⁵⁻¹²⁸

Diffuse clouds have gas densities between 10^2 and 10^4 particles cm^{-3} and their temperatures range from 50 to 100 K.¹²⁵⁻¹²⁷ In regions of diffuse interstellar clouds, starlight from nearby background stars is able to penetrate the cloud and allow for the gas component of the cloud to be probed by optical absorption spectroscopy. Accordingly, such studies have determined that the gas component of diffuse clouds is primarily made up of neutral atomic species. The elemental abundance of the gas generally resembles that of stars, that is, predominately hydrogen. In addition, the helium concentration of the gas is about 10% that of hydrogen, while concentrations of carbon, nitrogen and oxygen are 0.1 - 0.01%. Some elements (*eg.* silicon) are seemingly depleted from diffuse clouds and thought to comprise much of the dust particles within these regions.¹²⁶⁻¹²⁸

Dense interstellar clouds have gas densities greater than 10^4 particles cm^{-3} and temperatures that can be as low as 10 K.¹²⁵⁻¹²⁸ The density of the gas within dense interstellar clouds varies greatly, such that within some of the largest clouds, localised

regions of high relative density (*ca.* 10^6 cm^{-3}) undergo gravitational collapse. As the cloud collapses, the gaseous material becomes progressively more compressed and, as a consequence of the increase in pressure, the temperature within the collapsing region increases. This process may continue until finally the temperature and the pressure of the gas initiates nuclear fusion processes, and the birth of a newly formed star results. Accordingly, these regions are of particular interest to astronomers and other scientists alike.

In contrast to diffuse clouds which are completely permeated by ultraviolet-visible radiation, dense clouds are capable of providing shielding to their internal regions from ultraviolet-visible radiation.^{125,126,128} As a result, effectively all background starlight is either absorbed or scattered, hence such clouds are also referred to as *dark clouds*. Dust particles, typically $0.2 \mu\text{m}$ in diameter, are responsible for most of the extinction of background starlight.^{126,128} Such particles account for only 1% of the total interstellar matter, but despite their seemingly insignificant abundance, interstellar dust particles effectively absorb and scatter in the ultraviolet-visible region of the electromagnetic spectrum. It follows that dense (dark) clouds, unlike diffuse clouds, cannot be probed by optical absorption.

However, not all wavelengths are obscured by interstellar dust. Radio astronomy has been extensively used to probe these dense cold regions of the interstellar environment, with (radio) astronomical surveys collectively observing thousands of emission lines. These emission lines are the result of molecules in the gas phase relaxing from higher to lower rotational energy levels, the study of which allow for extremely accurate assignment of molecular structure.

Infrared astronomy has also been used to study dense interstellar clouds, though to a lesser extent than radio astronomy. In contrast to radio astronomy, which relies on molecules emitting radiation at radio wavelengths, infrared astronomy relies on absorption by molecules at infrared wavelengths. This is because dense clouds are too cool to emit radiation in the infrared. As a consequence, infrared astronomy of dense clouds requires a nearby background infrared source, which is typically in the form of a star, or even a star undergoing formation within the cloud itself.

Over 120 molecules have been identified in various interstellar and circumstellar environments, using microwave, infrared and ultraviolet spectroscopy.^{125,129-132} These are listed in Table 4.1. The list is surprisingly diverse and includes a number of common terrestrial chemicals, such as water, ethanol, ammonia and methane to name a few. Of greater interest, the list includes classes of molecules which are not common in the laboratory, for example, the highly unsaturated species; C_n ($n = 2, 3, 5$), C_nH ($1 \leq n \leq 8$), C_nCH_2 ($n = 1 - 3, 5$), and C_nO ($n = 1 - 3, 5$).^{125,129-136} By far the most dominant molecular species in dense interstellar clouds is molecular hydrogen, which is about 10^4 times more abundant than carbon monoxide, the next most abundant interstellar molecule.

TABLE 4.1 Species Detected in the Interstellar and Circumstellar Environments[#]

Number of atoms	Molecular Species
2	AlF, AlCl, C ₂ , CH, CH ⁺ , CN, CO, CO ⁺ , CP, CS, CSi, HCl, H ₂ , SiS, NH, NO, KCl, NS, NaCl, OH, PN, SO, SO ⁺ , SiN, SiO, HF, SH, FeO
3	C ₃ , C ₂ H, C ₂ O, C ₂ S, CH ₂ , HCN, HCO, HCO ⁺ , HCS ⁺ , HOC ⁺ , H ₂ O, H ₂ S, HNC, HNO, MgCN, MgNC, N ₂ H ⁺ , N ₂ O, NaCN, OCS, SO ₂ , c-SiC ₂ , CO ₂ , NH ₂ , H ₃ ⁺ , AINC
4	c-C ₃ H, I-C ₃ H, C ₃ N, C ₃ O, C ₃ S, C ₂ H ₂ , CH ₂ D ⁺ (?), HCCN, HCNH ⁺ , HNCO, HNCS, HOCO ⁺ , H ₂ CO, H ₂ CN, H ₂ CS, H ₃ O ⁺ , NH ₃ , SiC ₃
5	C ₅ , C ₄ H, C ₄ Si, I-C ₃ H ₂ , c-C ₃ H ₂ , CH ₂ CN, CH ₄ , HC ₃ N, HC ₂ NC, HCOOH, H ₂ CHN, H ₂ C ₂ O, H ₂ NCN, HNC ₃ , SiH ₄ , H ₂ COH ⁺
6	C ₅ H, C ₅ O, C ₂ H ₄ , CH ₃ CN, CH ₃ NC, CH ₃ OH, CH ₃ SH, HC ₃ NH ⁺ , HC ₂ CHO, HCONH ₂ , I-H ₂ C ₄ , C ₅ N
7	C ₆ H, CH ₂ CHCN, CH ₃ C ₂ H, HC ₅ N, HCOCH ₃ , NH ₂ CH ₃ , c-C ₂ H ₄ O
8	CH ₃ C ₃ N, HCOOCH ₃ , CH ₃ COOH(?), C ₇ H, H ₂ C ₆ , CH ₂ OHCHO
9	CH ₃ C ₄ H, CH ₃ CH ₂ CN, (CH ₃) ₂ O, CH ₃ CH ₂ OH, HC ₇ N, C ₈ H
10	CH ₃ C ₅ N(?), (CH ₃) ₂ CO, NH ₂ CH ₂ COOH(?)
11	HC ₉ N
13	HC ₁₁ N

[#] From National Radio Astronomy Observatory online database.¹³²

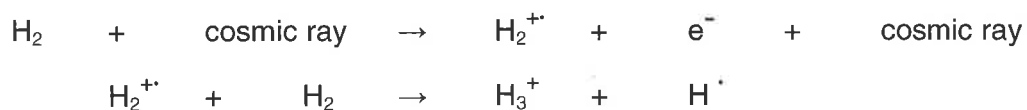
? Uncertain detection.

The molecular diversity within dense interstellar clouds is somewhat surprising given that the physical conditions present within them (*ie.* low densities and low temperatures) do not favour the occurrence of chemical reactions. Conversely, circumstellar envelopes have temperatures ranging from thousands of K in the innermost regions of the envelope down to 10 K at the outermost part of the envelope.¹²⁶ Moreover, the density within circumstellar envelopes is more conducive to chemical processes. This is reflected in the fact that over 50 of the molecules listed in Table 4.1 have been detected in such stellar regions, for example, in the circumstellar envelope of the carbon rich red giant star IRC+10216.¹³⁴ Strong stellar winds from such stars result in large amounts of matter reaching interstellar space. In addition, the enormous stellar explosions that occur during

supernovae events expel massive amounts of matter into interstellar space. It seems reasonable to suggest that many interstellar molecules are first formed within circumstellar envelopes and then transported to interstellar clouds. However, this is apparently not the case. Beyond stellar atmospheres there are vast regions of low-density space through which background interstellar radiation can readily penetrate. This ionising radiation effectively degrades all molecules present in these regions of interstellar space into atomic species. Thus the molecules found in interstellar clouds must be formed within those clouds.

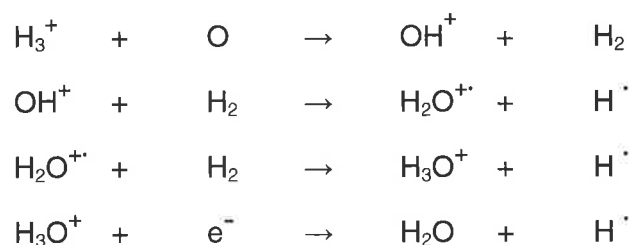
How then are molecules formed in the interstellar environment? Given that lifetimes of interstellar clouds can be greater than 10^6 years, then despite the seemingly low collision rates between atomic and molecular species, enough collisions can occur on the astronomical time scale to allow for the build up of molecules by collisional processes. Furthermore, many reactions between positive ions and neutral molecules are exothermic and have little or no energy barrier, and therefore can occur at the low temperatures observed in interstellar clouds.¹³⁷ Positive ions can easily be formed in diffuse clouds, since such environs are permeated by ultraviolet radiation. However, this same radiation is also able to disrupt chemical bonds resulting in photodissociation of molecular species. Consequently, large concentrations of molecules cannot be formed by ion-neutral reactions in diffuse regions of interstellar space, a result reflected in the composition of diffuse interstellar clouds (*ie.* dominated by atomic species). Conversely, dense interstellar clouds are overwhelmingly molecular in nature (as such these cloud-like structures are also referred to as *cold molecular clouds*) and provide effective shielding of their internal regions from external ultraviolet radiation. Such is the effectiveness of this shielding that

only cosmic rays,* can penetrate these dense clouds to effect ionisation. The unimolecular rate coefficient for cosmic ray ionisation of molecular hydrogen is estimated to be $\sim 10^{-17} \text{ s}^{-1}$.¹²⁶ Though seemingly low, the ionised dihydrogen formed is sufficient for ion-neutral chemistry to occur. Ionised dihydrogen readily reacts with the abundant molecular hydrogen forming H_3^+ ,^{125,126} an ionic species that has been detected in the interstellar environment (see Scheme 4.1).



SCHEME 4.1

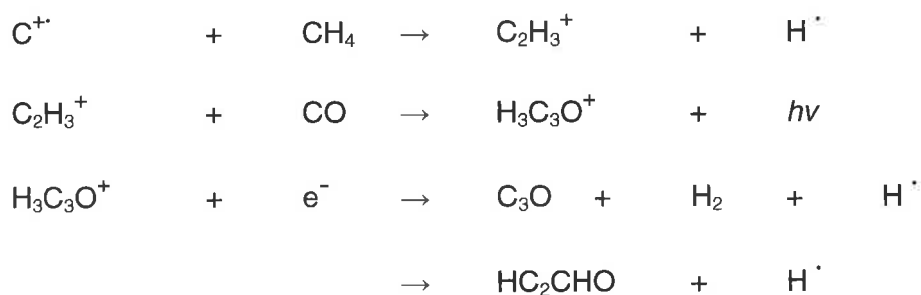
The ionic species H_3^+ can then react further to form small molecules such as water, as shown in Scheme 4.2.^{125,126}



SCHEME 4.2

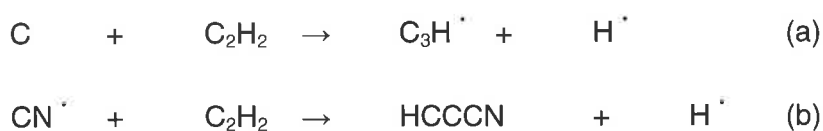
* Cosmic rays are nuclei travelling at near the speed of light. Consequently they have an extremely high penetrating power and are able to readily strip molecules of electrons.

Similarly, the ionic species CH_5^+ can be synthesised by the reaction of H_3^+ with atomic carbon followed by reactions with H_2 . Proton transfer from CH_5^+ to an abundant interstellar molecule such as CO produces the simple hydrocarbon methane.^{125,126} Small simple molecules such as methane can then react further to give larger and more complex interstellar molecules. For example, the synthesis of C_3O and HC_2CHO is initiated by C^+ insertion into methane (Scheme 4.3). Reaction of the resultant C_2H_3^+ with CO forms $\text{H}_3\text{C}_3\text{O}^+$, which may then capture an electron to form either C_3O or HC_2CHO .



SCHEME 4.3

Neutral-neutral reactions are also known to be efficient at low temperatures.¹³⁸⁻¹⁴⁰ For example low temperature reactions between atomic carbon and acetylene have been reported [Scheme 4.4 (a)].^{141,142} In addition, reactions of small radicals such as CN with acetylene have also been studied [Scheme 4.4 (b)].¹⁴³ It follows that larger interstellar molecules may also be synthesised by analogous neutral-neutral reactions.



SCHEME 4.4

B. Anion Formation in the Interstellar Medium

Discussions in the literature pertaining to the chemistry of the interstellar medium have primarily involved neutrals and cations to the virtual exclusion of anionic species. This is largely due to the fact that astronomical surveys to date have only unambiguously identified non-terrestrial neutral and cationic species.* Moreover, due to the abundance of radiation and the generally low energy required for electron detachment (typically 1 eV), it has long been considered that the interstellar and circumstellar environments are too hostile to enable anything but a transitory existence for any anionic species.¹⁴⁵⁻¹⁴⁷ More recently, the role of neutral-neutral reactions in the interstellar medium has been considered, and the inclusion of these reactions in chemical models has resulted in a greater understanding of interstellar clouds.^{139,148} The inclusion of negative ion chemistry into such models may result in further understanding of the chemical processes occurring in these environs.

Anion formation can occur by attachment of an electron to a neutral radical X initially resulting in an excited anion $[X^-]^\ddagger$ which can subsequently lose excess energy by emitting a photon; this process is known as *radiative attachment* [Scheme 4.5 (a)].^{145,149} Once formed, the excited species $[X^-]^\ddagger$ may undergo other chemical processes including; *electron detachment* [Scheme 4.5 (b)], *collisional stabilisation* [Scheme 4.5 (c)], and *decomposition* [Scheme 4.5 (d)].¹⁴⁵ The low density of the interstellar medium rules out collisional stabilisation. The rate of collision between the excited anion and a neutral molecule would be too low compared with the rates of competing processes, and

* A number of negative ions ($m/z < 50$) have been detected in the tail of Comet Halley using the on-board mass spectrometer of the space probe Giotto, however no unequivocal assignment was possible.¹⁴⁴

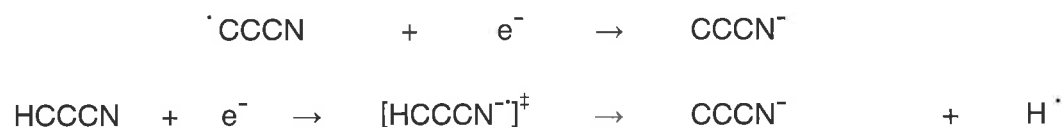
decomposition reactions forming smaller species are generally endothermic. It follows that radiative stabilisation and electron detachment are the only viable processes available energised anions occurring within interstellar clouds.*



SCHEME 4.5

The formation of anions by radiative electron attachment in dense interstellar clouds was first postulated by Herbst.¹⁴⁵ Using a statistical model, Herbst suggested that radiative attachment would be favourable for a radical neutral when a high vibrational density of states of the anion X^{-} existed at an internal energy equal to the electron affinity of the neutral X . Consequently, a number of interstellar molecules possessing large electron affinities may efficiently attach electrons with rate coefficients near the collision limit at cloud temperatures of 10 - 50 K (*eg.* Scheme 4.6).¹⁴⁵ Petrie and Herbst¹⁵⁰ calculated the abundance of C_3N^{-} in the dense interstellar cloud TMC-1 (Taurus Molecular Cloud-1) to be 1% relative to the observed abundance of the neutral. If present in this concentration, C_3N^{-} is a good candidate for future interstellar detection.

* A similar process where attachment of an electron to a neutral molecule occurs on the surface of an interstellar dust grain cannot be ruled out. However, chemistry on grain surfaces is not as well understood as gas phase processes, and is beyond the scope of the work presented here. Only gas phase anion formation will be discussed further.

**SCHEME 4.6**

Similarly, larger molecules with greater vibrational densities of states have been proposed to undergo radiative attachment.^{151,152} Examples of such molecules include carbon chains, which are known to have large electron affinities (> 2 eV), and polycyclic aromatic hydrocarbons (PAHs), which are known to have low electron affinities (< 1 eV) but have many degrees of freedom to disperse the excess energy of $[\text{X}^-]^\ddagger$. This stabilises the excited anion species with respect to electron detachment allowing for competitive emission of radiation to occur. However, electron attachment to neutrals under cold interstellar conditions is currently in question. This is a consequence of experimental investigations of electron attachment to anthracene and the fullerenes C_{60} and C_{70} , which indicate that there may be a barrier for the attachment process.¹⁵³⁻¹⁵⁵

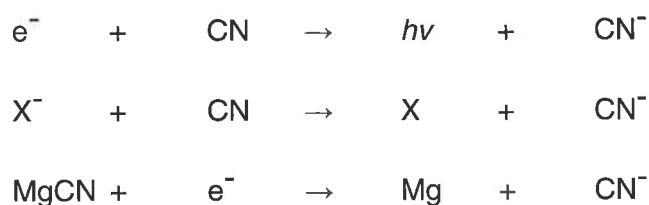
Small molecular species have few rotational and vibrational modes through which to disperse excess energy. Thus the lifetime of the excited anion is often too short for the radiative stabilisation process to effectively compete with the electron detachment process. A mechanism for the formation of small anions has been proposed, which involves a charge transfer from stable interstellar anions, such as anions of PAHs.¹⁵⁶ Collisions between PAH anions and small molecules of high electron affinity (*eg.* CN and CCH) may result in the formation of small anionic species with relatively low internal energies (Scheme 4.7). Thus a steady state of small anions may result by this mechanism. The

limiting factor of this charge transfer mechanism is the low number of anion-neutral collisions likely to occur within an interstellar cloud.



SCHEME 4.7

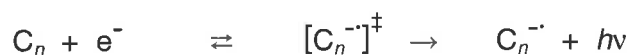
The contribution of negative ions to the chemistry within circumstellar envelopes has also been considered. Petrie¹⁵⁶ combined the anion formation processes of radiative electron attachment, charge transfer and dissociative electron attachment in an attempt to model the abundance of CN^{-} in the circumstellar envelope of the carbon-rich red giant IRC+10216 (see Scheme 4.8). With the inclusion of these processes the estimated abundance of CN^{-} was found to be sufficient for detection by radio astronomy.¹⁵⁶



SCHEME 4.8

More recently, Terzieva and Herbst¹²² modelled the efficiencies of radiative attachment to pure carbon chains C_n , where $n = 4 - 9$ (Scheme 4.9). They predict that for carbon chains of more than six carbon atoms, the rate coefficient for radiative stabilisation of the excited anion, $[C_n^{-}]^{\ddagger}$ is much greater than the rate coefficient for electron detachment. Therefore formation of a stable anion is predicted to occur for every collision that results in electron

capture. Flowing afterglow studies on C_n^- and C_nH^- anions carried by Barckholtz, Snow and Bierbaum¹²³ demonstrate that these anions react only very slowly with molecular hydrogen and, as such, their abundance is unlikely to be significantly depleted by reaction between the anionic species and the prevalent H_2 molecule.¹²³ In contrast, this study does suggest depletion of the anions by efficient processes with atomic hydrogen.



SCHEME 4.9

The proposal for large C_n^- anions within the interstellar medium has gained momentum by the recent tentative assignment of a number of thus far unassigned *diffuse interstellar bands* (DIBs) to the C_7^- anion.¹⁵⁷⁻¹⁶⁰ This was achieved by comparing a number of these DIBs with the optical transitions of the anions, C_6^- , C_7^- , C_8^- and C_9^- . While all of these anionic species are potential carriers of the DIBs, C_7^- was found to be the most likely candidate because it gives good agreement between the position of the bands, as well as the bandwidths, of four out of five DIBs. However the assignment is ambiguous, since many other candidates, including polyatomic aromatic hydrocarbons (PAHs), are also suggested to contribute to the diffuse interstellar bands.¹⁶¹⁻¹⁶³ An unequivocal assignment of such anions would result from studying the rotational transitions of such species using radio astronomy. A successful astronomical search for interstellar anions should therefore satisfy the following criteria: (i) the parent neutral should be a known interstellar species (or at least be part of an identified homologous series of molecules known to be abundant in interstellar sources); (ii) the parent neutral should have a large electron affinity and sufficient molecular size to efficiently undergo radiative electron attachment; and (iii) the

anion itself should be structurally simple and possess a high dipole moment to aid in its identification by radio astronomy.

The C_n series does not meet the final requirement outlined above and would therefore need to be identified by a spectroscopic method other than rotational spectroscopy. However it is envisaged that addition of a CH, CH_2 or CO moiety (among others) at the terminal position of a pure carbon chain, would be sufficient to meet all the requirements outlined above. A systematic theoretical investigation into the structures and properties of the C_nH , $C_{n-1}CH_2$ and C_nO neutrals and anions follows, with emphasis on those properties that are pertinent to their possible presence and detectability in the interstellar medium.

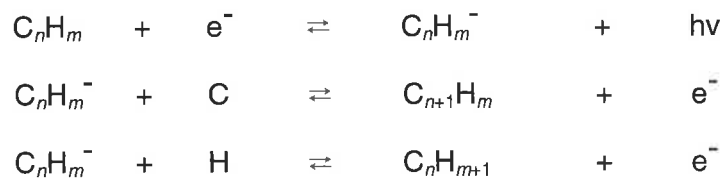
2. RESULTS AND DISCUSSION

A. The C_nH Series

i. Interstellar and Laboratory Detection of C_nH

The molecules CH, C_2H , *lin*- C_3H , *cyc*- C_3H , C_4H , C_5H , C_6H , C_7H and C_8H have all been detected in the interstellar environment.^{164,165} In each case, the linear carbon chain isomer with terminal hydrogen atom has been detected. A cyclic isomer of C_3H was observed in addition to the linear isomer. It has been suggested that *cyc*- C_3H is the lowest member of another series of interstellar molecules yet to be discovered, with *cyc*- C_3 -CCH and *cyc*- C_3 -(CC) $_2$ H being possible candidates for interstellar detection.^{166,167} We limit this investigation to only the linear isomers of the C_nH series.

The role of neutral-neutral reactions in the formation of the large interstellar molecules has been previously investigated.¹⁶⁸⁻¹⁷¹ For example, it has been shown that under interstellar conditions, CN and C_2H radicals readily add to unsaturated hydrocarbons forming larger cumulenes and heterocumulenes.^{170,172} Anion-neutral processes involving the large cumulenenic systems, C_nH_m ($10 \leq n \leq 23$, $m = 0, 1$) have been added to standard theoretical models of interstellar chemistry, these processes are shown in Scheme 4.10.¹⁷¹



SCHEME 4.10

The discovery of the C_nH series in the interstellar environment has challenged chemists to synthesise these unusual species in the laboratory. A variety of methods have been used to generate and detect these species; for example, the gas phase synthesis of C_3H by neutralisation of C_3H^+ in a $^+NR^+$ experiment has been reported.¹⁷³ An alternative experimental route to the C_3H neutral is by the reaction between C and C_2H_2 ; in this case the products were detected by angular distribution with a time-of-flight mass spectrometer.¹⁷⁴ A number of C_nH radicals are formed in the combustion of various fuels, which can be trapped by condensing the combustion gases at liquid nitrogen temperature along with excess radical scavenger (Me_2S_2); this method has successfully generated C_2H ,¹⁷⁵ C_3H ,¹⁷⁶ C_4H and C_6H .¹⁷⁵ Rotational spectroscopy has also been used to investigate a number of C_nH molecules *viz.*; C_2H ,¹⁷⁷ C_3H ,¹⁷⁸ C_5H ,¹⁷⁹ C_6H ,¹⁸⁰ C_7H ,^{181,182}, C_8H ,¹⁸² C_9H ,¹⁸² $C_{10}H$,¹⁸³ $C_{11}H$,^{182,183} and $C_{12}H$, $C_{13}H$, and $C_{14}H$.¹⁸³ In addition, studies involving electronic spectroscopy of a number of C_nH (neutrals and cations) have been reported.¹⁸⁴⁻¹⁸⁶

The corresponding anions have also attracted attention in recent years. For example, the photoelectron spectra of C_2H^- , C_3H^- , C_4H^- , C_6H^- and C_8H^- have been reported, thus providing accurate experimental values of the electron affinity of the corresponding neutrals.^{187,188} The C_nH^- anions, where n is even, were generated in a pulsed discharge of acetylene and carbon dioxide in neon,¹⁸⁷ while C_3H^- was generated by reaction of allene with molecular oxygen.¹⁸⁸ The electronic absorption spectra of $C_{2n}H^-$ ($n = 4 - 12$)^{189,190} and $C_{2n-1}H^-$ ($n = 5-8$)¹⁹¹ have also been reported. The generation of the anions; C_3H^- ,¹⁹² C_5H^- ^{193,194} and C_7H^- ¹⁹⁵ in a chemical ionisation source is particularly interesting. The anions were generated by the gas phase deprotonation of a polyacetylide precursor,

followed by decomposition to give the appropriate C_nH^- anion with known bond connectivity as illustrated in Scheme 4.11.



SCHEME 4.11

ii. C_nH and C_nH^- Ground State Geometries

The geometries of the neutrals C_nH ($2 \leq n \leq 10$) were optimised for this study at the B3LYP/6-31G(d) level of theory. The optimised geometries and energies are given in Figure 4.1 and Table 4.2 respectively. C_nH neutrals where n is an odd number have $^2\Pi$ ground states, with the exception of C_3H which is non-linear and has a $^2A'$ ground state. For even- n C_nH neutrals, a shift from $^2\Sigma$ to $^2\Pi$ ground states is observed with increasing chain length.¹⁹⁶ While it is clear that C_2H and C_6H have $^2\Sigma$ and $^2\Pi$ ground states respectively, C_4H has a small $^2\Sigma - ^2\Pi$ energy splitting resulting in some debate over its ground state.¹⁹⁶⁻¹⁹⁸ Woon¹⁹⁶ studied this quandary using the coupled cluster method. He found that for smaller basis sets the $^2\Pi$ state was favoured by 3.15 kJ mol^{-1} while, at the estimated basis set limit the $^2\Sigma$ state is favoured by 0.86 kJ mol^{-1} . In comparison, our modest B3LYP/aug-cc-pVDZ//B3LYP/6-31G(d) calculations predict a $^2\Pi$ ground state for C_4H .

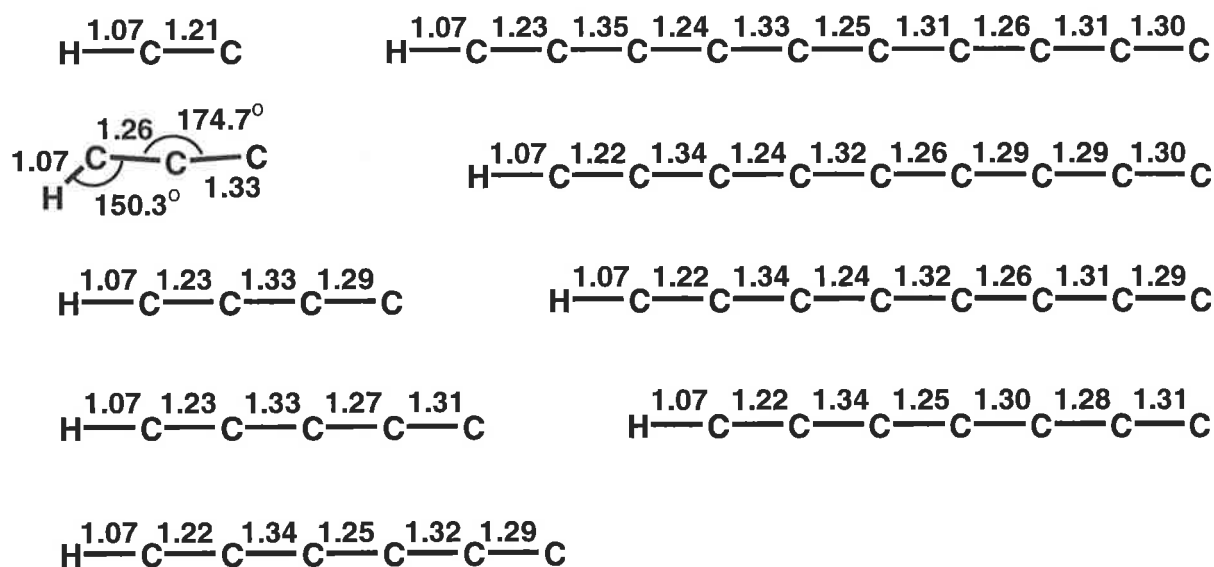


FIGURE 4.1 B3LYP/6-31G(d) geometries of neutrals C_nH . Bond lengths are given in Angstroms.

TABLE 4.2 Calculated properties of B3LYP/6-31G(d) neutrals C_nH ($n = 2 - 10$).^a

	C_2H	C_3H	C_4H	C_5H	C_6H
Ground Electronic State	$^2\Sigma$	$^2A'$	$^2\Pi$	$^2\Pi$	$^2\Pi$
Molecular Symmetry	$C_{\infty v}$	C_s	$C_{\infty v}$	$C_{\infty v}$	$C_{\infty v}$
B3LYP/aug-cc-pVDZ Energy (Hartrees)	-76.61569	-114.69372	-152.79048	-190.87133	-228.96308
CCSD(T)/aug-cc-pVDZ Energy (Hartrees)	-76.40782	-114.37133	-152.35716	-190.32642	-228.29568
Zero point energy (Hartrees)	0.01439	0.01733	0.02507	0.02996	0.03632
	C_7H	C_8H	C_9H	$C_{10}H$	
Ground Electronic State	$^2\Pi$	$^2\Pi$	$^2\Pi$	$^2\Pi$	
Molecular Symmetry	$C_{\infty v}$	C_s	$C_{\infty v}$	$C_{\infty v}$	
B3LYP/aug-cc-pVDZ Energy (Hartrees)	-267.04405	-305.13339	-343.21460	-381.30108	
Zero point energy (Hartrees)	0.04132	0.04752	0.05247	0.05868	

a. B3LYP/aug-cc-pVDZ and CCSD(T)/aug-cc-pVDZ single point energies include zero point correction (calculated from B3LYP/6-31G(d) vibrational frequencies).

The geometries of the C_nH^- anions were also calculated at the B3LYP/6-31G(d) level of theory. Geometries and energies are given in Figure 4.2 and Table 4.3, along with calculated dipole moments and rotational constants of the anions. Distinctions between C_nH^- anions with odd versus even number of carbon atoms are more apparent than those of the corresponding neutrals, especially at short chain lengths. For example, the structure of the C_4H^- anion is linear and can be considered to be essentially acetylenic in nature with alternating short (~ 1.24 Å) and long (~ 1.37 Å) carbon-carbon bonds, which may be considered to be triple and single bonds respectively. In contrast, the C_3H^- anion is bent and can be considered to be allene-like with equivalent carbon-carbon bonds (~ 1.31 Å) which are close to double-bond in character. As with the neutral C_nH series the structures of odd and even homologues appear to converge with increasing chain length, with C_9H^- only slightly deviating from linearity. The linear n -even anions have a (singlet) $^1\Sigma$ electronic ground state; this corresponds to the additional electron of the anion in a tightly bound σ -orbital on the terminal carbon. This electronic configuration would be expected to be very stable and hence give rise to large electron affinities of the corresponding neutrals. In contrast, the (triplet) $^3A''$ electronic configuration of the n -odd anions corresponds to two unpaired electrons occupying orthogonal π -orbitals. This would be expected to give rise to less strongly bound electrons and hence lower electron affinities for C_nH n -odd neutrals.

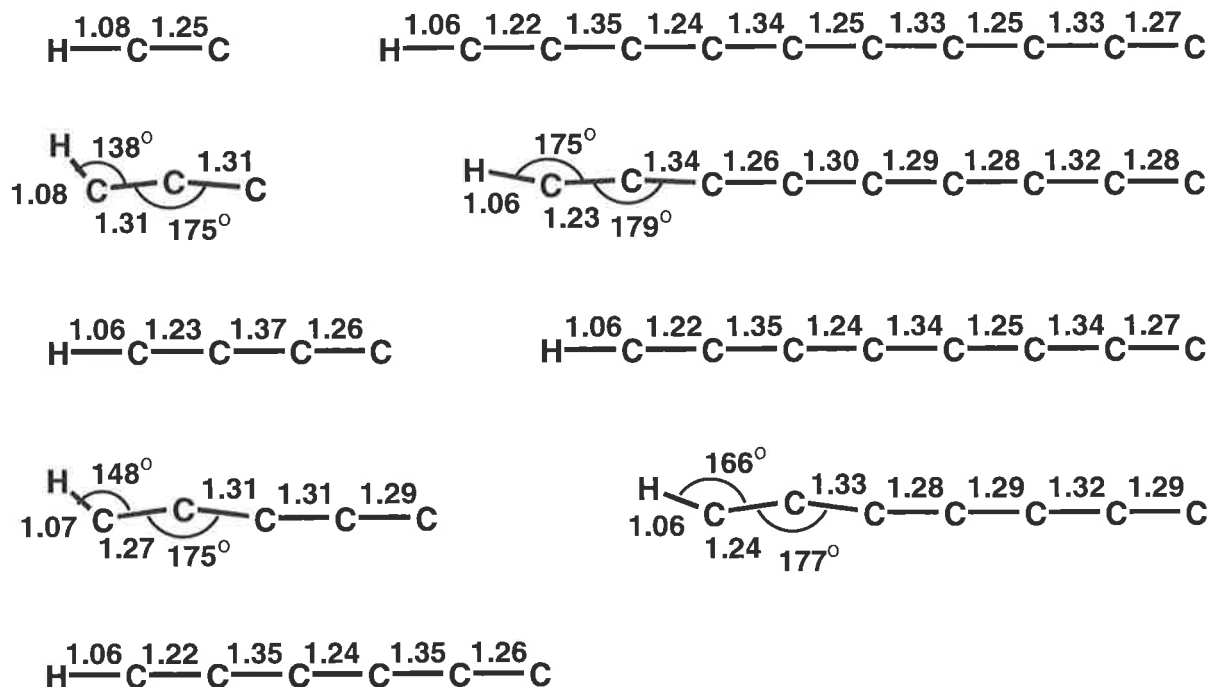


FIGURE 4.2 B3LYP/6-31G(d) geometries of anions C_nH^- . Bond lengths are given in Angstroms.

The C_3H^- anion has been the subject of a high-level theoretical study,¹⁹⁹ where the calculated geometries for the $^3A''$ state at the CASSCF/D95v** and QSCID(T)/D95** levels of theory agree with the B3LYP/6-31G(d) geometries presented here to within 0.02 Å and 3°. A recent large-scale theoretical study on the C_4H^- anion reports a ground state rotational constant of 4.658 GHz,²⁰⁰ in good agreement with a rotational constant of 4.639 GHz calculated using the B3LYP/6-31G(d) equilibrium geometry. The agreement between the theoretical data presented here and those calculated at higher levels of theory suggests that the B3LYP/6-31G(d) level of theory is a good approach to calculating geometries of cumulenonic anions at relatively low computational cost.

TABLE 4.3 Calculated properties of B3LYP/6-31G(d) anions C_nH^- ($n = 2 - 10$).^a

	C_2H^-	C_3H^-	C_4H^-	C_5H^-	C_6H^-
Ground Electronic State	$^1\Sigma$	$^3A''$	$^1\Sigma$	$^3A''$	$^1\Sigma$
Molecular Symmetry	$C_{\infty v}$	C_s	$C_{\infty v}$	C_s	$C_{\infty v}$
B3LYP/aug-cc-pVDZ Energy (Hartrees)	-76.73165	-114.76422	-152.91668	-190.96340	-229.09639
CCSD(T)/aug-cc-pVDZ Energy (Hartrees)	-76.51489	-114.43661	-152.48497	-190.41281	-228.44811
Zero point energy (Hartrees)	0.01459	0.01644	0.02415	0.02796	0.03549
Dipole Moment (Debye)	3.4	3.7	5.9	5.7	8.2
Rotational Constants (GHz)	41.531	1204.155 11.052 10.952	4.639	2026.106 2.359 2.356	1.371
	C_7H^-	C_8H^-	C_9H^-	$C_{10}H^-$	
Ground Electronic State	$^3A''$	$^1\Sigma$	$^3A''$	$^1\Sigma$	
Molecular Symmetry	C_s	$C_{\infty v}$	C_s	$C_{\infty v}$	
B3LYP/aug-cc-pVDZ Energy (Hartrees)	-267.15100	-305.27261	-343.33267	-381.44504	
Zero point energy (Hartrees)	0.03926	0.04786	0.05006	0.05956	
Dipole Moment (Debye)	8.2	10.4	10.3	12.7	
Rotational Constants (GHz)	10371.559 0.863 0.863	0.581	56776.098 0.408 0.408	0.299	

a. B3LYP/aug-cc-pVDZ and CCSD(T)/aug-cc-pVDZ single point energies include zero point correction (calculated from B3LYP/6-31G(d) vibrational frequencies).

iii. Calculated C_nH Electron Affinities

The adiabatic electron affinities of the C_nH neutrals have been determined by calculating the difference in energy between neutral and anionic ground states. In order to more accurately determine the electronic energies, and in turn the electron affinities, higher single point energy calculations were carried out on the B3LYP/6-31G(d) geometries. The calculated electron affinities obtained using the B3LYP/aug-cc-pVDZ//B3LYP/6-31G(d) method (Table 4.4) are in reasonable agreement with most known experimental values, differing by less than 0.2 eV. Electron affinities calculated at the CCSD(T)/aug-cc-pVDZ//B3LYP/6-31G(d) level are included in Table 4.4 for $n \leq 6$; for larger members of the series the CCSD(T) method is not feasible using our available computing resources. Experimental and theoretical results demonstrate a clear trend of increasing EA with increasing carbon chain length. The even- n homologues EAs rise more dramatically than their odd- n counterparts, resulting in an overall stepped increase in EA as the chain length increases. This is illustrated in the plot of EA versus carbon chain length n (Figure 4.3). This is consistent with the experimental electron affinities of carbon chains ($2 \leq n \leq 9$) which are plotted in Figure 4.3 for comparison.²⁰¹

TABLE 4.4 Adiabatic electron affinities (eV) of B3LYP/6-31G(d) optimised C_nH neutrals.

	C_2H	C_3H	C_4H	C_5H	C_6H	C_7H	C_8H	C_9H	$C_{10}H$
B3LYP/aug-cc-pVDZ	3.15	1.96	3.46	2.56	3.65	2.97	3.78	3.28	3.90
CCSD(T)/aug-cc-pVDZ	2.91	1.82	3.50	2.40	4.17	-	-	-	-
Experimental	2.956 ^a (0.020)	1.858 ^b (0.027)	3.558 ^a (0.015)	-	3.809 ^a (0.015)	-	3.966 ^a (0.010)	-	-

a. Taylor *et al.*¹⁸⁷ b. Oakes and Ellison¹⁸⁸

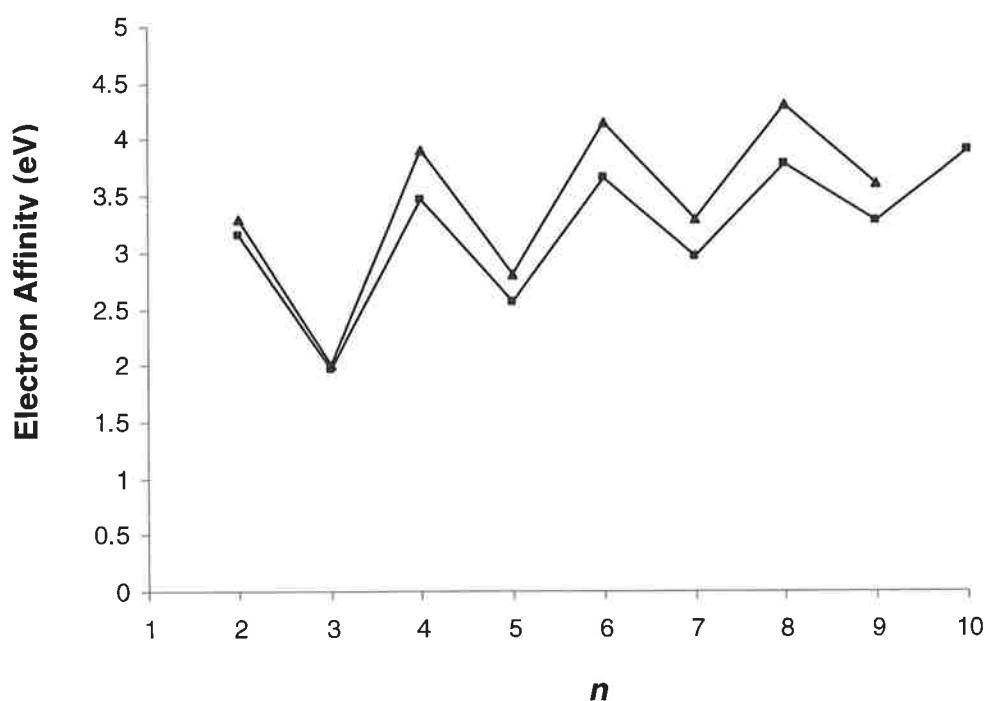


FIGURE 4.3 Plot of the calculated electron affinity in electron volts, $EA(C_nH)$, versus the number of carbons in the carbon chain, n (shown as squares). The experimentally determined $EA(C_n)$ values²⁰¹ are also included for comparison (shown as triangles).

B. The $C_{n-1}CH_2$ Series

i. Interstellar and Laboratory Detection of $C_{n-1}CH_2$

Another series of interstellar molecules is the $C_{n-1}CH_2$ series of which CH_2 , C_2H_2 , *lin*- C_3H_2 , *cyc*- C_3H_2 , C_4H_2 , C_6H_2 having been detected in the interstellar medium.^{129-131,134} Larger members of this homologous series are considered prime candidates for future detection. These cumulenenic species have been investigated extensively. Rotational contours of large members of the $C_{n-1}CH_2$ series, C_7H_2 to $C_{15}H_2$, have been compared with several diffuse interstellar bands and found to be consistent with a regularly spaced group of diffuse interstellar bands near 6850 Å.²⁰² The study could not rule out the contribution of any charged $C_{n-1}CH_2$ species to the group of bands considered. This is of particular interest to this investigation, with unequivocal identification of the corresponding anions likely to come from observation of their rotational transitions.

Laboratory detection and study of potential interstellar species is pivotal to the likelihood of their interstellar detection. For example, with experimental data from laboratory detection of $CCCH_2$ and $CCCCH_2$,^{203,204} these species were positively identified as interstellar species.^{205,206} The cyclic isomer of C_3H_2 was the first C_3H_2 isomer to be detected in interstellar space, and interestingly, it was also the first interstellar organic ring molecule to be detected.²⁰⁷ Photolysis of *cyc*- C_3H_2 results in the formation of the linear $CCCH_2$ isomer by a reversible process.²⁰⁸ The rotational spectra of C_5H_2 , C_6H_2 , C_7H_2 , C_8H_2 and C_9H_2 have been recorded in the laboratory using Fourier transform microwave spectroscopy^{182,209,210} but, with the exception of C_6H_2 await detection in the interstellar environment.

Neutralisation-reionisation (NR) mass spectrometry has been used to generate vinylidene²¹¹ (CCH_2). This was previously generated by photolysis and pyrolysis and thought to be an extremely short-lived species.²¹²⁻²¹⁴ Mass spectrometry has demonstrated the stabilities of the anion, the neutral (with a lifetime $\geq 0.4 \mu\text{s}$) and the cation.²¹¹ A subsequent experiment has reported detection of the CCH_2 neutral after $3.5 \mu\text{s}$.²¹⁵ Both the CCH_2 anion and neutral were predicted to be stable by *ab initio* calculations, with the implication that the actual neutral formed is the triplet species, since the singlet is predicted to rearrange to HCCH under NR conditions. Similar MS studies^{173,192,216-219} on the C_3H_2 , C_4H_2 , C_5H_2 and C_7H_2 molecular systems have generated the neutrals, anions and cations of a number of isomers including the cumulenic species considered in this investigation. The linear isomers C_3H_2^- , C_5H_2^- and C_7H_2^- were generated by chemical ionisation followed by decomposition of the parent anion to give anions with known bond connectivities as outlined in Scheme 4.12. The electron affinities of CCH_2 and C_2CH_2 have been determined experimentally by photoelectron spectroscopy of the corresponding anions,^{188,220} again allowing comparison with our theoretical data presented here. In these experiments CCH_2^- and C_2CH_2^- were generated by reaction of the oxygen radical anion with ethylene²²⁰ and allene,¹⁸⁸ respectively.



SCHEME 4.12

ii. $C_{n-1}CH_2$ and $C_{n-1}CH_2^-$ Ground State Geometries

The geometries of the neutrals $C_{n-1}CH_2$, where $2 \leq n \leq 10$, were optimised at the B3LYP/6-31G(d) level of theory, converging to the C_{2v} structure in each case. The optimised geometries and energies are shown in Figure 4.4 and Table 4.5. All $C_{n-1}CH_2$ neutrals were calculated to have a 1A_1 electronic ground electronic state with little structural change with increasing chain length.

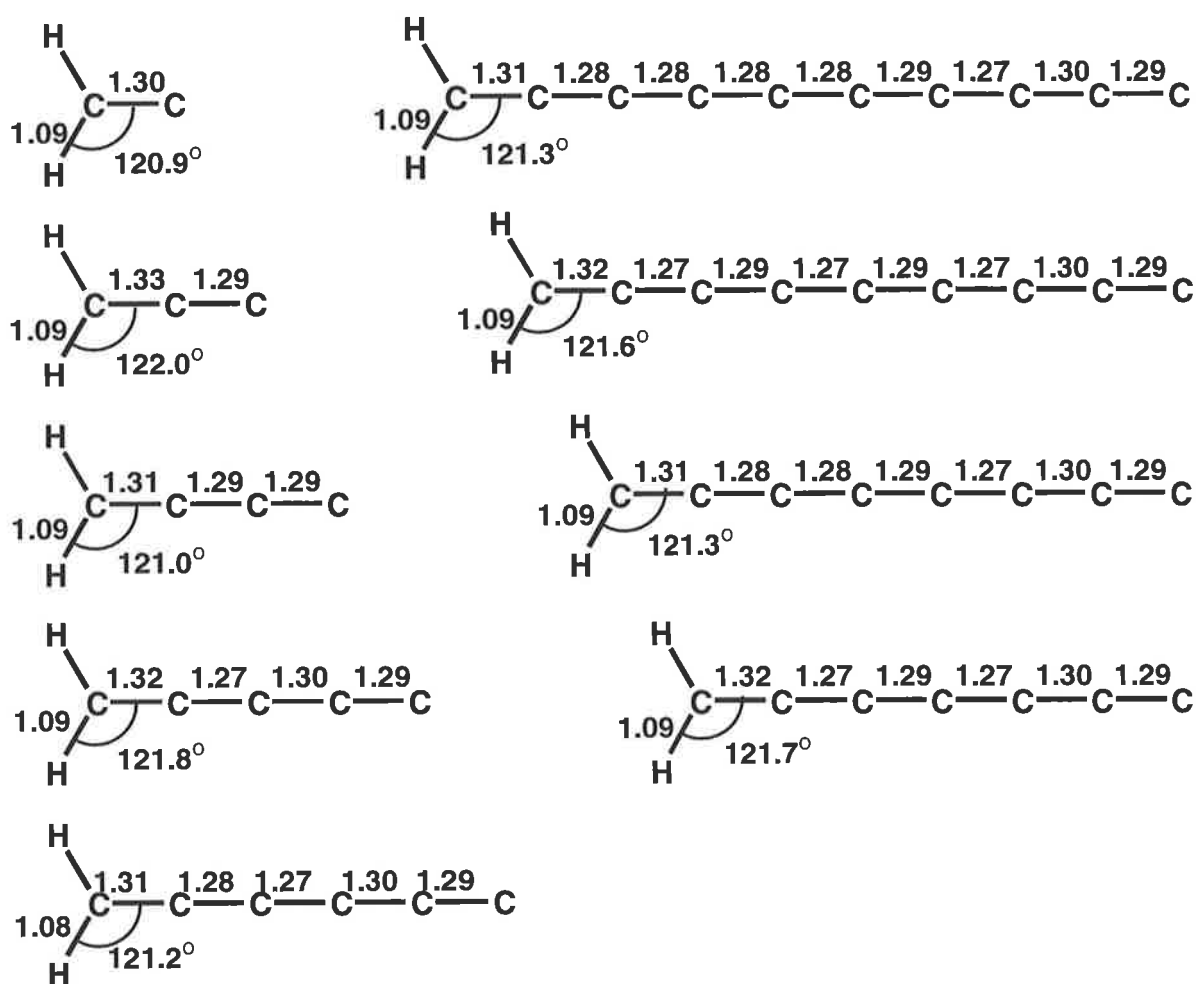


FIGURE 4.4 B3LYP/6-31G(d) geometries of neutrals $C_{n-1}CH_2$. Bond lengths are given in Angstroms.

TABLE 4.5 Calculated properties of B3LYP/6-31G(d) neutrals $C_{n-1}CH_2$ ($n = 2 - 10$).^a

	CCH₂	C₂CH₂	C₃CH₂	C₄CH₂	C₅CH₂
Ground Electronic State	¹ A ₁	¹ A ₁	¹ A ₁	¹ A ₁	¹ A ₁
Molecular Symmetry	C _{2v}	C _{2v}	C _{2v}	C _{2v}	C _{2v}
B3LYP/aug-cc-pVDZ Energy (Hartrees)	-77.27464	-115.34855	-153.43966	-191.51508	-229.60307
CCSD(T)/aug-cc-pVDZ Energy (Hartrees)	-77.05766	-115.02493	-153.00475	-190.97184	-228.94839
Zero point energy (Hartrees)	0.02387	0.03129	0.03620	0.04203	0.04723
	C₆CH₂	C₇CH₂	C₈CH₂	C₉CH₂	
Ground Electronic State	¹ A ₁	¹ A ₁	¹ A ₁	¹ A ₁	
Molecular Symmetry	C _{2v}	C _{2v}	C _{2v}	C _{2v}	
B3LYP/aug-cc-pVDZ Energy (Hartrees)	-267.68094	-305.76756	-343.84678	-381.93255	
Zero point energy (Hartrees)	0.05294	0.05826	0.06388	0.06915	

a. B3LYP/aug-cc-pVDZ and CCSD(T)/aug-cc-pVDZ single point energies include zero point correction (calculated from B3LYP/6-31G(d) vibrational frequencies).

The geometries of the $C_{n-1}CH_2^-$ anions were also calculated at the B3LYP/6-31G(d) level of theory. The geometries, energies, dipole moments and rotational constants are given in Figure 4.5 and Table 4.6. There is little variation in either bond length or angle with an increase in the carbon chain length. This may be expected to continue for even larger chain lengths and therefore allow sensible structural predictions to be made without further calculation. As mentioned above, the neutrals $C_{n-1}CH_2$ have ¹A₁ ground states. This corresponds to a singlet carbene with the lone pair on the terminal carbon atom. The radical anions $C_{n-1}CH_2^-$ can then be considered to be formed by adding an electron to a π -orbital. When n is even, the additional electron is in an orbital in the C-C-H plane resulting in ²B₂ anions, whereas when n is odd the additional electron is placed in an orbital orthogonal to the C-C-H plane.

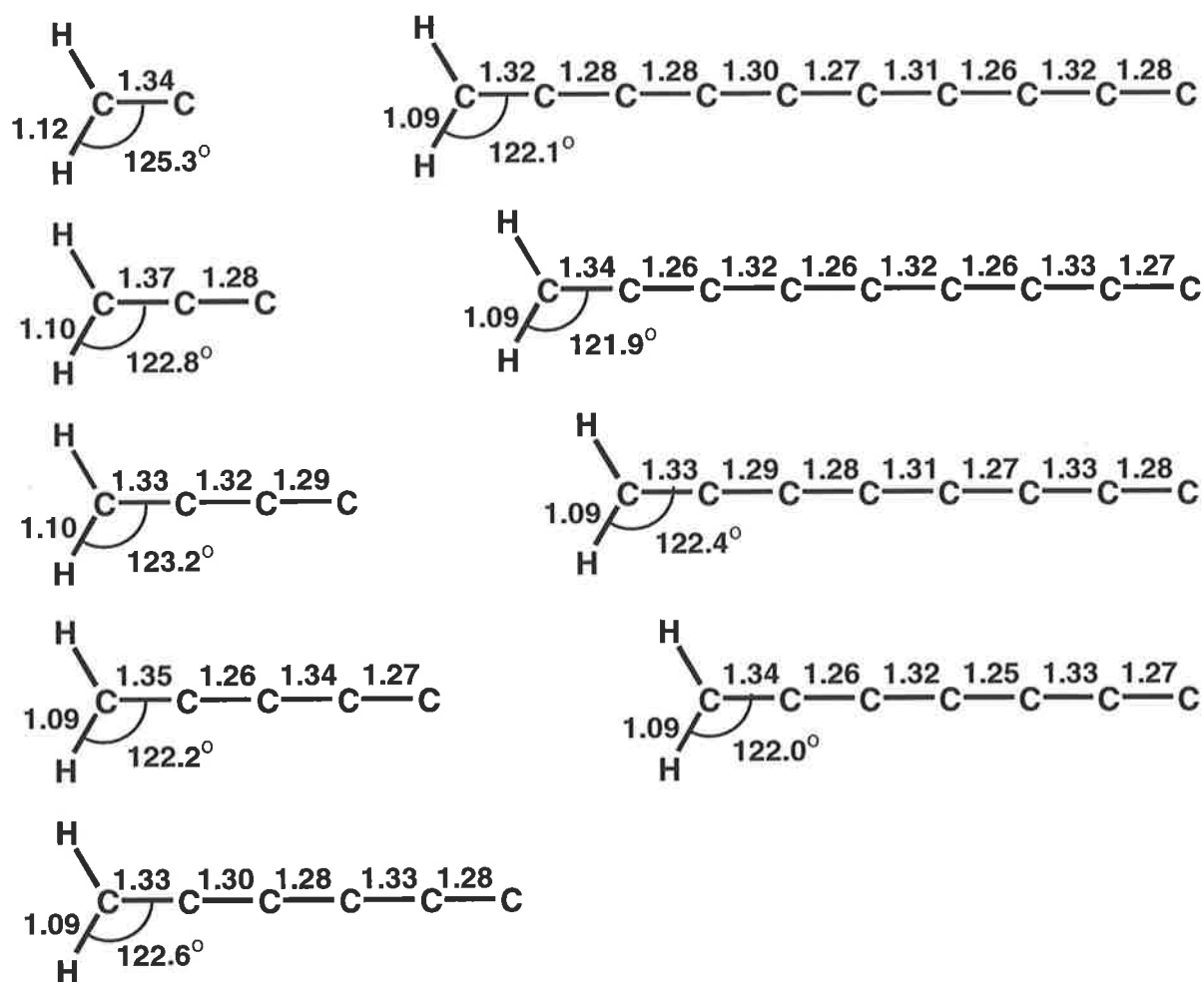


FIGURE 4.5 B3LYP/6-31G(d) geometries of anions $C_{n-1}CH_2^-$. Bond lengths are given in Angstroms.

TABLE 4.6 Calculated properties of B3LYP/6-31G(d) anions $C_{n-1}CH_2^-$ ($n = 2 - 10$).^a

	CCH_2^-	$C_2CH_2^-$	$C_3CH_2^-$	$C_4CH_2^-$	$C_5CH_2^-$
Ground Electronic State	2B_2	2B_1	2B_2	2B_1	2B_2
Molecular Symmetry	C_{2v}	C_{2v}	C_{2v}	C_{2v}	C_{2v}
B3LYP/aug-cc-pVDZ Energy (Hartrees)	-77.29935	-115.41823	-153.50611	-191.60927	-229.69468
CCSD(T)/aug-cc-pVDZ Energy (Hartrees)	-77.07395	-115.08511	-153.0618	-191.05643	-229.02804
Zero point energy (Hartrees)	0.02292	0.02959	0.03463	0.04079	0.04600
Dipole Moment (Debye)	3.5	5.0	5.7	7.0	7.7
Rotational Constants (GHz)	299.859 35.893 32.056	295.413 10.256 9.912	296.088 4.356 4.293	293.822 2.253 2.236	294.719 1.318 1.312
	$C_6CH_2^-$	$C_7CH_2^-$	$C_8CH_2^-$	$C_9CH_2^-$	
Ground Electronic State	2B_1	2B_2	2B_1	2B_2	
Molecular Symmetry	C_{2v}	C_{2v}	C_{2v}	C_{2v}	
B3LYP/aug-cc-pVDZ Energy (Hartrees)	-267.79109	-305.87546	-343.96830	-382.05079	
Zero point energy (Hartrees)	0.05212	0.05731	0.06336	0.06833	
Dipole Moment (Debye)	9.0	9.6	10.9	11.6	
Rotational Constants (GHz)	293.225 0.836 0.834	294.453 0.564 0.563	292.848 0.398 0.398	293.384 0.292 0.292	

a. B3LYP/aug-cc-pVDZ and CCSD(T)/aug-cc-pVDZ single point energies include zero point correction (calculated from B3LYP/6-31G(d) vibrational frequencies).

iii. Calculated $C_{n-1}CH_2$ Electron Affinities

In order to more accurately determine the electronic energies, and in turn the electron affinities, higher single point energy calculations were carried out on the B3LYP geometries. The calculated B3LYP/aug-cc-pVDZ//B3LYP/6-31G(d) electron affinities are given in Table 4.7; for comparison electron affinities for $n \leq 6$ obtained using CCSD(T)/aug-cc-pVDZ//B3LYP/6-31G(d) data are also included in Table 4.7. A plot of the B3LYP/aug-cc-pVDZ//B3LYP/6-31G(d) electron affinities is shown in Figure 4.6. Again a stepped increase in electron affinity is observed with increasing carbon chain

length (*cf.* C_nH neutrals), which may be the result of the relative stability of the 2B_1 and 2B_2 electronic states of the $C_{n-1}CH_2^-$ anions.

TABLE 4.7 Adiabatic electron affinities (eV) of B3LYP/6-31G(d) optimised $C_{n-1}H_2$ neutrals.

	CCH_2	C_2CH_2	C_3CH_2	C_4CH_2	C_5CH_2	C_6CH_2	C_7CH_2	C_8CH_2	C_9CH_2
B3LYP/ aug-cc-pVDZ	0.7	1.94	1.85	2.60	2.53	3.02	2.96	3.32	3.24
CCSD(T)/ aug-cc-pVDZ	0.47	1.68	1.59	2.33	1.99	-	-	-	-
Experimental	0.447 ^a (0.002)	1.794 ^b (0.008)	-	-	-	-	-	-	-

a. Ervin *et al.*²²⁰ b. Oakes and Ellison¹⁸⁸

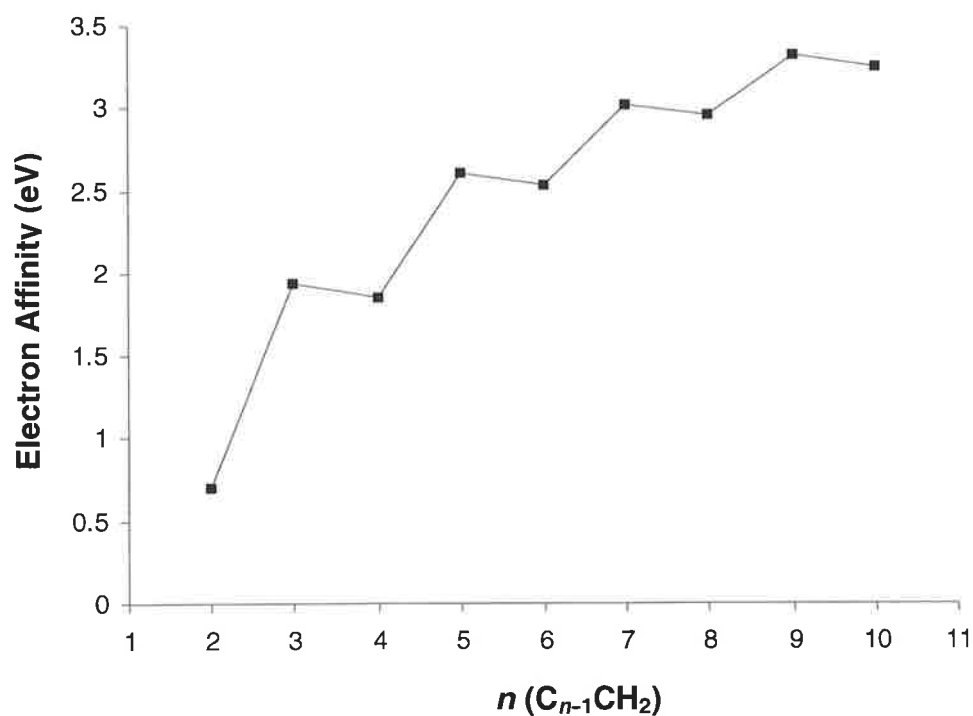


FIGURE 4.6 Plot of the calculated electron affinity in electron volts, $EA(C_{n-1}CH_2)$, versus the number of carbons in the carbon chain, n .

C. The C_nO Series

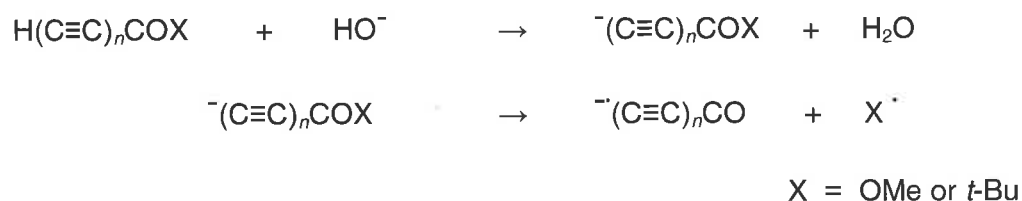
i. Interstellar and Laboratory Detection of C_nO

A number of polyatomic carbon monoxides, C_nO , have been detected in the interstellar medium *viz.*, CO, CO⁺, C₂O, C₃O and C₅O. The mechanism of their formation under such conditions has been debated in the literature. For example, it has been shown experimentally that CO reacts with polyatomic carbon ions C_n^{+} ($n = 1 - 6$) and C_nH^+ ($n = 2 - 5$) to form polyatomic carbon monoxides and dioxides under selected-flow tube conditions at 296K.²²¹ The rate for addition was observed to increase as the carbon chain length of the initial C_n^{+} cation increased, which was attributed to an increase in the lifetime of the intermediate addition complex (*cf.* increased lifetime of the anion species $[X^-]^{\ddagger}$ for radiative attachment). Neutral-neutral reactions involving O and C_n clusters have also been investigated.¹⁴⁸ In particular, quantum chemical and dynamical studies have been carried out on the prototypical neutral-neutral reaction between O and C₃; these studies predict that such reactions do not occur rapidly at low temperature.²²² However, excited C₃ has been implicated in the synthesis of C₄O and C₆O by photolysis of matrix (Ne and Ar at 4K) trapped C and CO.²²³ Recently, complexes of linear C_n ($n = 3-9$) clusters with H₂O (formed in Ar matrices) have been studied by FTIR. Photolysis of these $C_n \cdot (H_2O)_x$ clusters has led to the formation of a number of C_nO species.²²⁴⁻²²⁶ The synthesis of molecules on the surface of interstellar dust grains is an area of considerable interest: it may be that photolysis of these $C_n \cdot (H_2O)_x$ clusters on dust grains are significant processes in interstellar clouds.

Fourier-transform microwave spectroscopy has been used in the investigation of the C_nO ($2 \leq n \leq 9$) series.^{227,228} These species were generated by an electric discharge of carbon

suboxide (C_2O_3) diluted in Ar. The ground states were determined to be $^1\Sigma^+$ and $^3\Pi^-$ for $C_{2n}O$ ($n = 1 - 4$) and $C_{2n-1}O$ ($n = 2 - 5$), respectively.

Of the corresponding negative ions, C_2O^- , C_3O^- and C_4O^- have been generated from carbon suboxide (C_3O_2) and their photoelectron spectra^{188,229} recorded, giving electron affinities for comparison to those presented here. These ions were generated in either a pulsed discharge²²⁹ or in a Branscomb ion source.¹⁸⁸ Preparation of the gas phase anions C_3O^- , C_5O^- and C_7O^- by chemical ionisation of suitable precursors, followed by decomposition of the parent anion have also been reported and are outlined in Scheme 4.13.²³⁰⁻²³²



SCHEME 4.13

ii. C_nO and C_nO^- Ground State Geometries

The geometries of the neutrals C_nO , where $2 \leq n \leq 10$, were optimised at the B3LYP/6-31G(d) level of theory, converging to the linear structure in each case. The optimised geometries and energies are given in Figure 4.7 and Table 4.8. The electronic ground state of the C_nO neutrals were calculated to alternate between the triple $^3\Sigma$ and singlet $^1\Sigma$

electronic states. This is in agreement with experimental^{227,228} and previous theoretical²³³ studies.



FIGURE 4.7 Geometries of B3LYP/6-31G(d) neutrals C_nO . Bond lengths are given in Angstroms.

TABLE 4.8 Calculated properties of B3LYP/6-31G(d) neutrals C_nO ($n = 2 - 10$).^a

	C₂O	C₃O	C₄O	C₅O	C₆O
Ground Electronic State	³ Σ	¹ Σ	³ Σ	¹ Σ	³ Σ
Molecular Symmetry	C _{∞v}	C _{∞v}	C _{∞v}	C _{∞v}	C _{∞v}
B3LYP/aug-cc-pVDZ Energy (Hartrees)	-151.28352	-189.42021	-227.45440	-265.57425	-303.62606
CCSD(T)/aug-cc-pVDZ Energy (Hartrees)	-150.91100	-188.94169	-226.85508	-264.87128	-302.80342
Zero point energy (Hartrees)	0.00871	0.01574	0.01971	0.02654	0.03077
	C₇O	C₈O	C₉O	C₁₀O	
Ground Electronic State	¹ Σ	³ Σ	¹ Σ	³ Σ	
Molecular Symmetry	C _{∞v}	C _{∞v}	C _{∞v}	C _{∞v}	
B3LYP/aug-cc-pVDZ Energy (Hartrees)	-341.73506	-379.79535	-417.89795	-455.96179	
Zero point energy (Hartrees)	0.03789	0.04207	0.04910	0.05301	

a. B3LYP/aug-cc-pVDZ and CCSD(T)/aug-cc-pVDZ single point energies include zero point correction (calculated from B3LYP/6-31G(d) vibrational frequencies).

The structures of C_nO^- were optimised at the B3LYP/6-31G(d) level of theory. The structures, energies, dipole moments and rotational constants are given in Figure 4.8 and Table 4.9. With the exception of C_3O^- , all C_nO^- anions are linear with a $^2\Pi$ electronic ground state. As the chain length increases, CC bond lengths tend to approach a uniform bond length (~ 1.30 Å) and hence the C_nO^- anions appear to become more cumulene-like with increasing chain length. The C_3O^- anion is an exception to the linear $^2\Pi$ anionic series, displaying some Renner-Teller distortion giving it a $^2A'$ ground state.

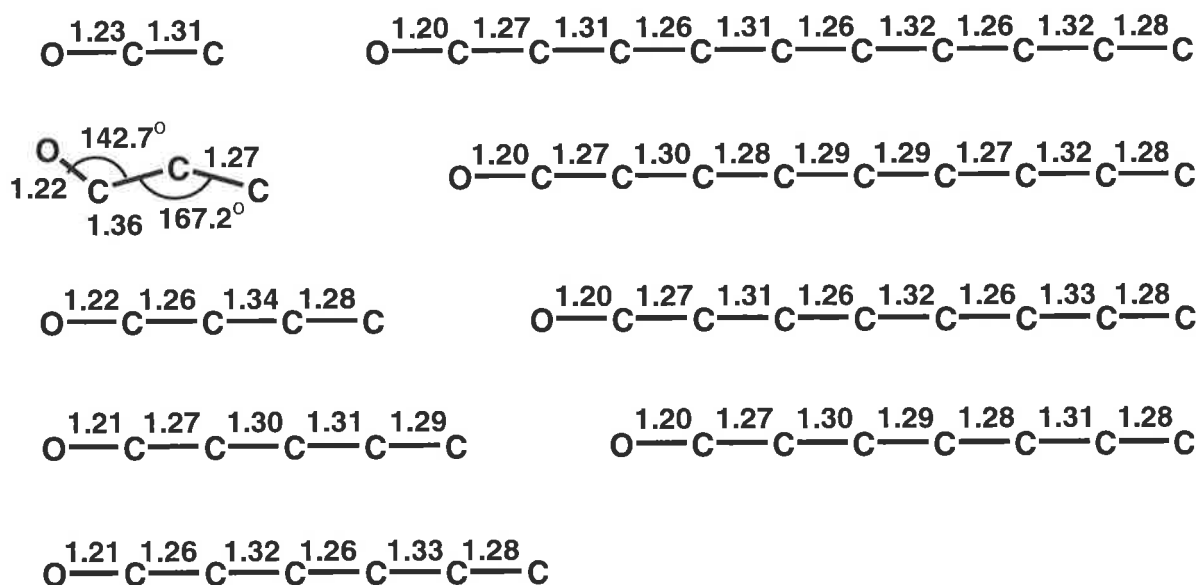


FIGURE 4.8 Geometries of B3LYP/6-31G(d) anions C_nO^- . Bond lengths are given in Angstroms.

TABLE 4.9 Calculated properties of B3LYP/6-31G(d) anions C_nO^- ($n = 2 - 10$).^a

	C_2O^-	C_3O^-	C_4O^-	C_5O^-	C_6O^-
Ground Electronic State	$^2\Pi$	$^2A'$	$^2\Pi$	$^2\Pi$	$^2\Pi$
Molecular Symmetry	$C_{\infty v}$	C_s	$C_{\infty v}$	$C_{\infty v}$	$C_{\infty v}$
B3LYP/aug-cc-pVDZ Energy (Hartrees)	-151.36797	-189.46344	-227.56168	-265.64989	-303.74712
CCSD(T)/aug-cc-pVDZ Energy (Hartrees)	-150.98663	-188.97702	-266.96041	-264.91427	-302.92665
Zero point energy (Hartrees)	0.00933	0.01286	0.02004	0.02453	0.03127
Dipole Moment (Debye)	3.6	3.8	4.9	5.5	6.0
Rotational Constants (GHz)	11.383	306.822 4.772 4.698	2.294	1.322	0.832
	C_7O^-	C_8O^-	C_9O^-	$C_{10}O^-$	
Ground Electronic State	$^2\Pi$	$^2\Pi$	$^2\Pi$	$^2\Pi$	
Molecular Symmetry	$C_{\infty v}$	$C_{\infty v}$	$C_{\infty v}$	$C_{\infty v}$	
B3LYP/aug-cc-pVDZ Energy (Hartrees)	-341.83290	-379.92604	-418.01054	-456.09974	
Zero point energy (Hartrees)	0.03608	0.04274	0.04729	0.05391	
Dipole Moment (Debye)	6.6	7.1	7.6	8.3	
Rotational Constants (GHz)	0.559	0.393	0.288	0.217	

a. B3LYP/aug-cc-pVDZ and CCSD(T)/aug-cc-pVDZ single point energies include zero point correction (calculated from B3LYP/6-31G(d) vibrational frequencies).

iii. Calculated C_nO Electron Affinities

Single point energy calculations at the B3LYP/aug-cc-pVDZ level of theory were carried out on the optimised C_nO and C_nO^- geometries to more accurately determine the electronic energies, and in turn the electron affinities. The calculated B3LYP/aug-cc-pVDZ//B3LYP/6-31G(d) electron affinities are given in Table 4.10; for comparison CCSD(T)/aug-cc-pVDZ//B3LYP/6-31G(d) electron affinities are also given for $n \leq 6$. A plot of B3LYP/aug-cc-pVDZ//B3LYP/6-31G(d) electron affinities versus the carbon chain

length is shown in Figure 4.9. Again the observed trend clearly indicates that electron affinities increase for the larger systems.

TABLE 4.10 Adiabatic electron affinities (eV) of B3LYP/6-31G(d) optimised C_nO neutrals.

	C_2O	C_3O	C_4O	C_5O	C_6O	C_7O	C_8O	C_9O	$C_{10}O$
B3LYP/aug-cc-pVDZ	2.28	1.25	2.91	2.11	3.28	2.71	3.54	3.11	3.73
CCSD(T)/aug-cc-pVDZ	2.04	1.04	2.86	1.88	3.34	-	-	-	-
Experimental	2.289 ^a (0.018)	1.34 ^b (0.15)	2.05 ^b (0.15)	-	-	-	-	-	-

a. Zengin *et al.*²²⁹ b. Oakes and Ellison¹⁸⁸

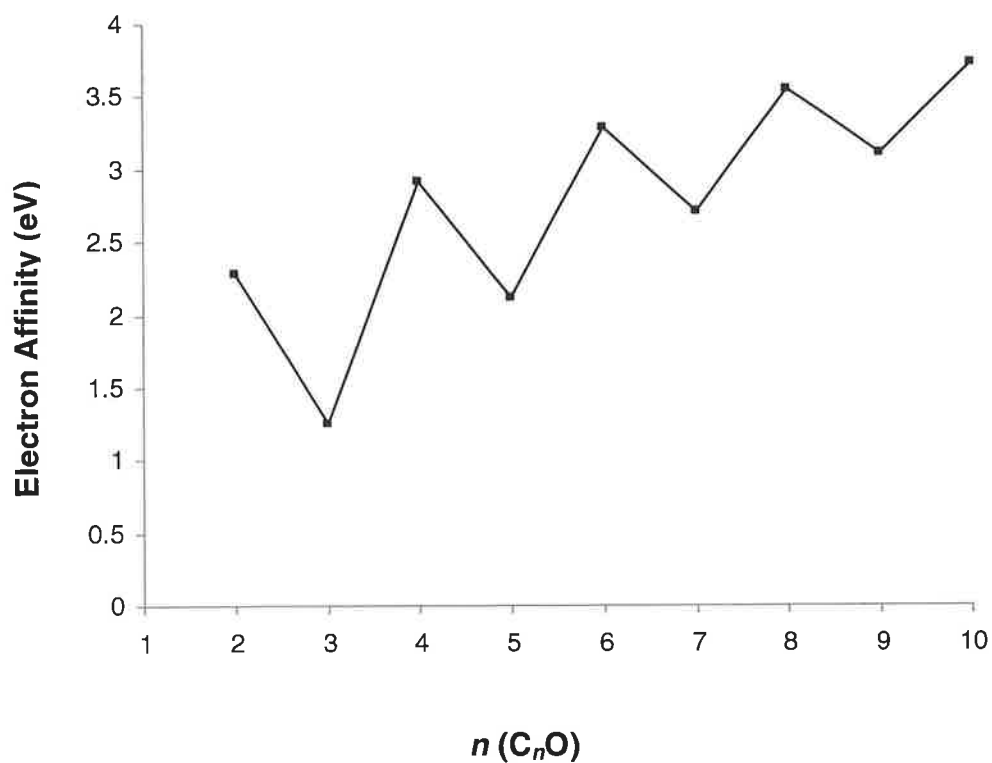


FIGURE 4.9 Plot of the calculated electron affinity in electron volts, $EA(C_nO)$, versus the number of carbons in the carbon chain, n .

The electron affinities of C₃O and C₄O have been the subject of recent high-level calculations by Riestra-Kiracofe *et al.*²³⁴ who calculate the electron affinities of C₃O and C₄O to be 0.93 ± 0.10 eV and 2.99 ± 0.10 eV respectively. They suggest that the experimental electron affinities (1.34 ± 0.15 and 2.05 ± 0.15 eV)¹⁸⁸ are erroneous. Their theoretical value for the electron affinity of C₄O is in close agreement (< 0.1 eV) to the B3LYP/aug-ccpVDZ//B3LYP/6-31G(d) value presented here (Table 4.10). However, our electron affinity of C₃O differs from that of Riestra-Kiracofe *et al.*²³⁴ by more than 0.3 eV. The CCSD(T)/aug-cc-pVDZ//B3LYP/6-31G(d) level of theory predicts an electron affinity of 1.03 eV (Table 4.10), which is in closer agreement to the Riestra-Kiracofe *et al.* value and thus closer to the true electron affinity.

D. The Possible Detection of C_nH^- , $C_{n-1}CH_2^-$, and C_nO^- as Interstellar Species

The anions, C_nH^- , $C_{n-1}CH_2^-$, and C_nO^- ($2 \leq n \leq 10$) represent the charged counterparts of either; (i) identified interstellar molecules or (ii) members of an homologous series of molecules of which several members have been identified. The calculations presented here demonstrate that the electron affinities of the parent neutrals, C_nH , $C_{n-1}CH_2$ and C_nO are quite large and increase up to nearly 4 eV with increasing length of the carbon chain. It seems possible also from the plots of n versus EA, that this trend may continue beyond the chain lengths investigated here, and that larger molecules have still larger EAs.

Terzieva and Herbst¹²² predict efficient radiative attachment of an electron to carbon chains when there are six or more carbons in the chain. The increase in efficiency of electron attachment with increasing carbon chain length may be considered the result of two effects. Increasing the carbon chain length; (i) increases the electron affinity, thus increasing the lifetime of the intermediate electron-neutral complex, $[C_n^-]^\ddagger$ against electron detachment and (ii) increases the degrees of freedom in the molecule providing for a greater density of states at the electron affinity threshold, and more effective distribution of the excess internal energy in the complex delaying electron detachment. In light of these considerations, it is expected that the neutrals C_nH , $C_{n-1}CH_2$ and C_nO should efficiently attach electrons in the interstellar environment. In previous sections it has been demonstrated that these systems have large electron affinities, which increase with increasing carbon chain length similar to the corresponding C_n molecules (Figure 4.3). Further, the additional hydrogen or oxygen atom in the C_nH , $C_{n-1}CH_2$ and C_nO species will provide additional degrees of freedom compared to the C_n analogues. In the case of the C_nH and $C_{n-1}CH_2$ series, the additional degrees of freedom will be made up (in part) of low

frequency C-H bending modes. These will further increase the density of states and thus the lifetime of the excited anion species, $[X^-]^\ddagger$. A qualitative analysis of the data presented here suggests that; (i) neutral C_nH , $C_{n-1}CH_2$ and C_nO are likely to efficiently attach electrons in interstellar clouds and (ii) once formed, C_nH^- , $C_{n-1}CH_2^-$ and C_nO^- anions are likely to have lifetimes in the interstellar medium comparable to those estimated for C_n^- anions (up to 2 weeks for C_9^-).¹²²

Barckholtz, Snow and Bierbaum¹²³ have examined experimentally the reactions of C_n^- ($n = 2, 4 - 10$) and C_nH^- anions (where $n = 2, 4, 6$ and 7) with molecular hydrogen (the most abundant interstellar gas) in a flowing afterglow-selected ion flow tube at room temperature and 0.5 torr helium pressure. Associative detachment of C_nH^- (and C_n^-) anions by reaction with H_2 (Scheme 4.14) occurred too slowly to be measured experimentally.* Therefore it seems unlikely that populations of these anions would be substantially depleted by reaction with molecular hydrogen in interstellar clouds

**SCHEME 4.14**

Barckholtz *et al.*¹²³ further demonstrated that poly-carbon anions (C_n^- , $n = 2 - 10$) react with atomic hydrogen in two ways depending on the chain length. For carbon chains where $n < 7$ the reaction proceeds exclusively by associative electron detachment [Scheme

* The occurrence of associative detachment was confirmed by addition of SF_6 to the reaction flow tube to scavenge electrons, which resulted in the detection of SF_6^- .

4.15 (a)], whereas for $n \geq 7$ both electron detachment and the association product anion [Scheme 4.15 (b)] are observed. The branching ratio between electron detachment and the association reaction increases to favour formation of the association product anion. These results suggest that if large poly-carbon anions (C_n^{--} , $n \geq 7$) are present in the interstellar environment, reactions with atomic hydrogen could provide a further pathway to the C_nH^- anions discussed here. However, C_nH^- anions ($n = 2, 4, 6, 7$) were also found to react with atomic hydrogen by associative electron detachment suggesting that these anions may be depleted in interstellar regions of high atomic hydrogen density.

**SCHEME 4.15**

Neutral C_nH and C_nO molecules have simple linear structures with significant permanent electric dipole moments. These properties have aided their characterisation by microwave spectroscopy in the laboratory and subsequent detection in astronomical sources. Similarly, the neutral $C_{n-1}CH_2$ cumulenes are simple symmetric tops with electric dipole moments increasing up to 10 Debye for $n = 10$. Electronic structure calculations described here predict similar properties for the corresponding anions. C_nH^- and C_nO^- anions are generally linear structures, while $C_{n-1}CH_2^-$ anions are all symmetric tops. The calculated electric dipole moments of these all the anions are listed in Tables 4.3, 4.6 and 4.9. These values are plotted in Figure 4.10 as a function of the number of carbon atoms n . This

figure clearly demonstrates the increasing dipole moment with increasing carbon chain length.

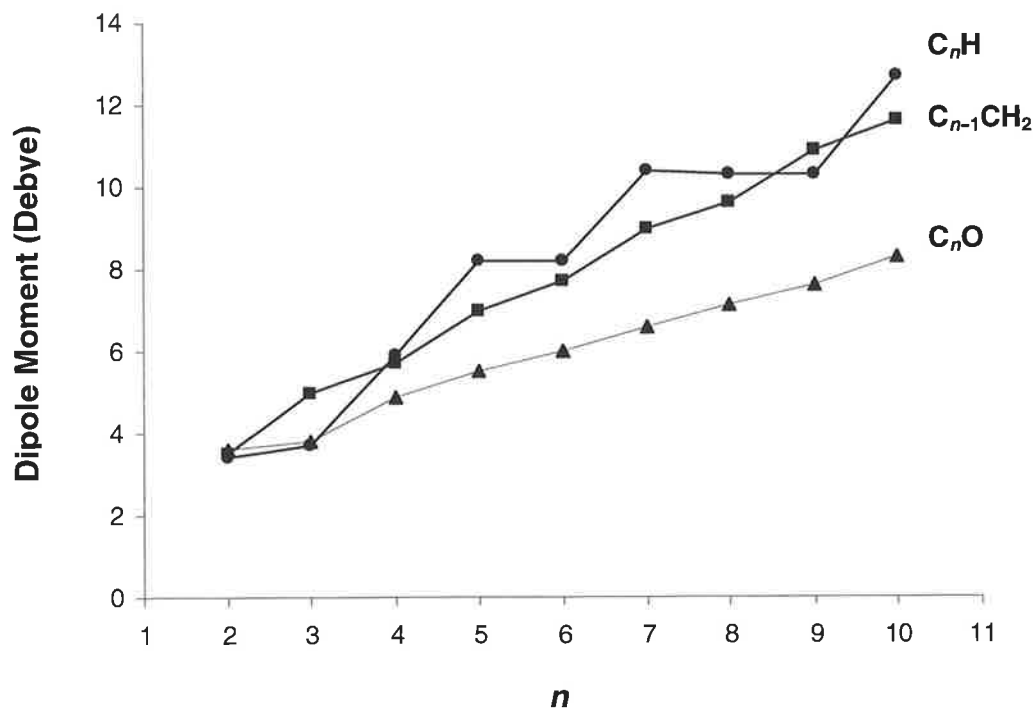


FIGURE 4.10 A plot of the dipole moments (debye) of the anions, C_nH^- , $C_{n-1}CH_2^-$ and C_nO^- versus the number of carbons in the carbon chain, n .

Theoretical calculation of the physical properties of molecules (*eg.* geometries, electron affinities, dipole moments and rotational constants), particularly at the relatively modest levels of theory used in this study, are most often of insufficient quality for use in direct astronomical searches. This is because rotational constants are dependent on the equilibrium internuclear distances squared. To obtain accurate rotational constants from theoretical geometries the internuclear distances require an accuracy of 10^{-8} Å. Despite this inadequacy of theoretical calculations in this context, the results presented here should

serve as a useful guide for laboratory experiments, which could produce data of the necessary precision.

E. Conclusions

Many of the neutral C_nH , $C_{n-1}CH_2$ and C_nO species investigated here have been detected in interstellar and circumstellar environments. It has been suggested that additional members of each series may also exist in space and await detection. The electronic structure calculations presented here predict that the cumulenes, C_nH and $C_{n-1}CH_2$, and heterocumulenes, C_nO have large electron affinities that increase with carbon chain length. Such properties suggest that members of these interstellar series of molecules may radiatively attach electrons in the interstellar environment, and that the corresponding anions are likely to be stable with respect to electron detachment. Sufficient populations of these anions in interstellar environs may result from this process allowing for their astronomical detection. The calculated properties for the C_nH^- , $C_{n-1}CH_2^-$ and C_nO^- anions presented here should serve as a useful guide to future laboratory experiments and astronomical surveys.

3. THEORETICAL METHODS

All anion and neutral geometries were optimised using the B3YLP theoretical method,^{83,84} with the relatively modest 6-31G(d) basis set. This approach allows the calculation of the increasingly large molecules investigated in this study (up to 11 heavy atoms). The B3LYP method has been shown previously to give molecular geometries that agree well with more computationally expensive approaches.^{235,236} Stationary points on the potential energy surface were characterised as minima (no imaginary frequencies) by calculation of the frequencies using analytical gradient procedures. Zero-point energies were determined using the calculated frequencies and were scaled by 0.9806.⁸⁹ Scaled zero-point energies were then used as a zero-point energy correction for the electronic energy at the B3LYP/6-31G(d) level of theory as well as the higher levels of theory used. In order to more accurately model the electron affinities and dipole moments, higher level single point energies were carried out using the larger correlation consistent Dunning basis set aug-cc-pVDZ^{237,238} which includes diffuse functions. The coupled cluster CCSD(T) method^{239,240} was employed as a further check of the calculated electronic energies for species where $n \leq 6$. All calculations were carried out using the Gaussian 98 suite of programs²⁴¹ using the Power Challenge supercomputer of the Australian National University Supercomputing Facility (Canberra).

CHAPTER 5

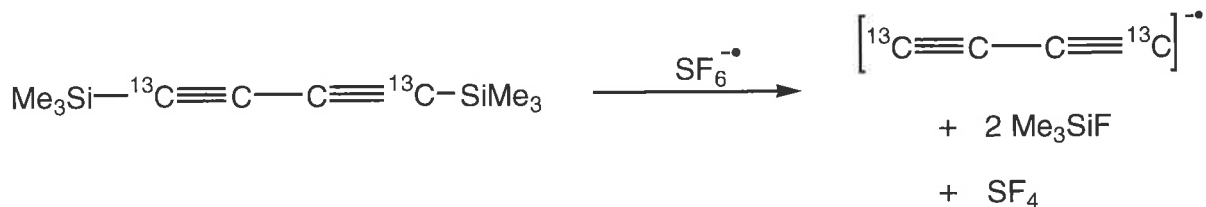
FORMATION OF C₃ FROM THE LINEAR [CCC]⁻ ANION IN THE GAS PHASE

1. INTRODUCTION

The chemistry of small carbon clusters has attracted significant interest in past years,^{242,243} due to their participation in circumstellar and interstellar chemistry,^{134,244,245} combustion processes,²⁴⁶ and material sciences.²⁴⁷ Understanding the precise role in each of these systems demands detailed knowledge of the structure and reactivity of such molecules. Small carbon clusters are present in stellar media^{134,244,245} and, while to date only C₂, C₃ and C₅ have been definitively identified in the stellar medium (*eg.* in the circumstellar envelope of IRC+10216¹³⁴), they are considered^{248,249} to be the precursors of large carbon molecules^{250,251} including aromatic species and fullerenes.²⁵² Long carbon chains have also been proposed to be possible carriers of the diffuse interstellar bands (see Chapter 4).

A number of linear and cyclic carbon clusters have been made by various techniques, and have been characterised.^{133,248,249,253-271} The most common method of generating carbon clusters is by laser ablation followed by supersonic expansion into an inert carrier gas, such as Ar or He.²⁵² More specific methods have been developed to give better control in the generation process allowing the generation of specific small carbon species. For example, the linear ¹³C labelled radical anions [¹³CCC¹³C]⁻ ²⁷⁰ and [CC¹³CCC]⁻ ²⁷¹ were formed by chemical ionisation to give anions of known connectivity; the synthesis of the [¹³CCC¹³C]⁻ radical anion is shown in Scheme 5.1. Conversion of these negatively

charged species into the corresponding neutrals was effected by collisional oxidation in a collision cell of a mass spectrometer, with the generated neutral species being probed by reionisation using the neutralisation-reionisation process ($^-NR^+$).



SCHEME 5.1

The energised neutrals $^{13}\text{CCC}^{13}\text{C}$ ²⁷⁰ and CC^{13}CCC ²⁷¹ were shown to undergo carbon scrambling within the timeframe of the $^-NR^+$ experiment (10^{-6} sec). Theoretical studies indicate that the scrambling mechanisms proceed through a rhombic C_4 intermediate and a carbon substituted rhombic intermediate respectively (see Scheme 5.2).^{270,271}



SCHEME 5.2

Earlier experimental studies of the C_4 system appeared to exclusively produce the linear isomer^{242,243} with evidence for the more stable rhombic structure only obtained through coulomb explosion imaging.^{272,273} In these experiments a cesium beam sputter source produced a fast beam of $[C_4]^-$ anions. These anions were mass selected and intersected

with a tuneable laser used to photodetach an electron from the anion. It was observed that electrons could be photodetached at an energy of 2.1 ± 0.1 eV. This is consistent with a rhombic C_4 structure since the electron affinity of the rhombic and linear isomers of C_4 are 2.24 eV (theoretical)²⁷⁴ and 3.88 eV (experimental)^{201,275} respectively. In addition, the coulomb explosion resulting from collision of the C_4 neutrals (formed by photodetachment at 2.1 eV) and a thin foil was consistent with modelling based on C_4 with a rhombic geometry.

Following on from the above studies into C_4 and C_5 carbon cumulenes, the present study is involved with the smaller polyatomic pure carbon cumulene C_3 . The aims of the project are to (i) make labelled linear neutral $CC^{13}C$ from an anion precursor of known connectivity, and (ii) determine whether the energised neutral $CC^{13}C$ equilibrates its carbons.

2. RESULTS AND DISCUSSION

i. Detection of C_3 in the Interstellar Medium and the Terrestrial Laboratory

The smallest polyatomic cumulene linear C_3 , has been detected in a number of non-terrestrial sources including comets,^{276,277} circumstellar envelopes,^{134,278} cold dense molecular clouds,²⁷⁹ and diffuse molecular clouds.²⁸⁰ Given that C_3 does not possess a permanent dipole moment it cannot be detected using the standard radio astronomical methods responsible for the initial detection of most known interstellar molecules. In 1951, Douglas²⁸¹ identified the $A^1\Pi_u - X^1\Sigma_g^+$ emission spectrum of C_3 near 4050 Å; these lines were in fact observed earlier by Huggins²⁷⁶ (1882) and Swings²⁷⁷ (1942) in the

emission spectra of comet tails. This makes CCC one of the earliest detected non-terrestrial molecules. Decades later, the anti-symmetric stretching mode ν_3 (2040 cm⁻¹) was detected (by infrared spectroscopy) in the circumstellar envelope around the evolved carbon rich star IRC+10216.¹³⁴ The C₃ molecule has also been detected in interstellar clouds, for example, in a dense interstellar cloud in the direction of Sagittarius B2. The absence of suitable infrared background sources for the dense cloud meant that searching for the ν_3 stretching mode was not feasible. However, recent laboratory measurements in the far infrared of the ν_2 bending mode (63.42 cm⁻¹) allowed for direct searching for its absorption line.²⁷⁹ Until recently, the only remaining non-terrestrial reservoir of molecules in which detection of C₃ had eluded astronomers was the diffuse interstellar clouds. However, neutral C₃ was detected (in 2001) in three diffuse interstellar clouds by Maier *et al.*²⁸⁰ using optical spectroscopy, identified by the emission line near 4052 Å. Observation of C₃ in diffuse regions of the interstellar environment support the suggestion that carbon chain species are good candidates as carriers of the uncharacterised spectral features between 4000 Å and 8500 Å (known as the diffuse interstellar bands). Furthermore, the discovery of the C₃ molecule in a number of interstellar and circumstellar environs demonstrates its importance in the chemistry of these various regions of the interstellar medium and explains its interest to many researchers from various scientific fields.

Linear C₃ has been formed using a variety of methods,²⁸² for example by infrared multiple photon photolysis of allene,²⁸³ and by fast electric discharge in the supersonic expansion of CO.²⁸⁴ In both cases the neutral was probed by laser induced fluorescence. Experimental measurements on linear CCC include the determination of electron affinity of the neutral (1.981eV) by photoelectron spectroscopy,¹⁸⁸ and other spectroscopic

measurements^{253,254,282,285} including the far infrared measurements²⁸⁵ which were subsequently used in the successful search for linear C_3 in cold molecular clouds.²⁷⁹ The stability of C_3 has been demonstrated by it being a dominant photofragment of $[C_n]^+$ cations ($4 < n < 20$), while in the particular case of $[C_3]^+$, no photofragment was observed.²⁸⁶ Laser ablation time-of-flight mass spectrometry has been used to generate $[C_3]^+$ radical cations,²⁸⁷ while the linear $[C_3]^-$ radical anion has been formed by laser ablation of graphite deposited in argon matrices and subsequently studied by infrared spectroscopy assigning a linear structure to the anion.²⁸⁸

Theoretical interest in this system has led to many studies on the neutral C_3 potential energy surface²⁸⁹⁻²⁹⁶ as well as the potential energy surfaces of the $[C_3]^-$ radical anion,^{266,291,295,297} and $[C_3]^+$ radical cation.^{291,298-302} The ground state of the neutral is the $^1\Sigma_g^+$ state with the possible cyclic structures highly energetic in comparison. The stationary point corresponding to a cyclic structure on the singlet neutral potential surface is a transition state (see later discussion) for the degenerate isomerisation of linear C_3 .²⁹⁰

ii. Stability and Possible Rearrangement of the $[CC^{13}C]^-$ Radical Anion

It has been shown previously that singlet CCC is the ground state on the C_3 neutral potential energy surface and that the corresponding singlet cyclic C_3 is not a local minimum on that surface.²⁹⁰ Triplet CCC neutral is also a stable species, with a singlet-triplet splitting of 201 kJ mol^{-1} .²⁸² The doublet $[CCC]^-$ anion should be a suitable precursor to effect a one-electron oxidation via a Franck Condon vertical process to yield the required linear species CCC. However, there is a complication, because two stable

$[C_3]^-$ radical anions exist. One is the required linear species $[CCC]^-$, the other is the $[cyc-C_3]^-$ radical anion. The B3LYP/6-311G(d) optimised geometries of these species are given in Table 5.1, together with their relative energies calculated at the CCSD(T)/aug-cc-pVTZ//B3LYP/6-311G(d) level of theory. The highest level theoretical approach to the $[C_3]^-$ radical anion reported to date has been carried out by Schmatz and Botschwina.²⁶⁴ Using the coupled cluster approach CCSD(T) together with a basis set containing 255 contracted GTOs (gaussian-type orbitals) they predict a CC bond length of 1.307 Å for $[CCC]^-$: this is in excellent agreement with the B3LYP/6-311G(d) value of 1.306 Å presented here (Table 5.1). While the linear $[CCC]^-$ radical anion is the lower in energy of the two anions, the cyclic radical anion is only higher in energy by 42 kJ mol⁻¹ at our chosen level of theory. Based on this small difference in energy, the possibility must be considered that both anion radicals might be formed in the ion source of the mass spectrometer from a neutral precursor with linear CCC connectivity.

TABLE 5.1 Calculated properties of the $[C_3]^-$ radical anion.

	Linear	Cyclic	TS
State	$^2\Pi_g$	2A_1	$^2A'$
Energy (Hartrees) ^a	-113.9016615	-113.8851092	-113.842067
Relative Energy (kJ mol ⁻¹)	0	43	156
C_1C_2 (Å) ^b	1.306	1.363	1.287
C_2C_3	1.306	1.363	1.434
C_1C_3	2.612	1.545	2.179
$C_1C_2C_3$ (°)	180.0	69.0	106.3

a. Energies calculated at the CCSD(T)/aug-cc-pVTZ level of theory and include zero point correction (calculated from B3LYP/6-311G(d) vibrational frequencies). b. Geometries optimised at the B3LYP/6-311G(d) level of theory.

The rearrangement of linear $[CCC]^-$ to $[cyc-C_3]^-$ has been computed at the CCSD(T)/aug-cc-pVTZ//B3LYP/6-311G(d) level of theory and is illustrated in Figure 5.1, with full geometries and energies recorded in Table 5.1. There is a barrier of 156 kJ mol^{-1} for the conversion of the linear to the cyclic anion; the reaction is endothermic by 43 kJ mol^{-1} . Negative ion chemical ionisation is generally regarded as a soft ionisation method, and therefore it is unlikely that sufficient energy is imparted to the $[CCC]^-$ radical anion for such a rearrangement to occur in the ion source of the mass spectrometer. In an earlier study,²⁷⁰ the barrier for rearrangement of $[CCCC]^-$ to rhombic $[C_4]^-$ was calculated to be 132 kJ mol^{-1} at the CCSD(T)/aug-cc-pVDZ//B3LYP/6-31(d) level of theory; this rearrangement does not occur experimentally. Similarly, no rearrangement was noted for the $[CCCCC]^-$ radical anion.²⁷¹

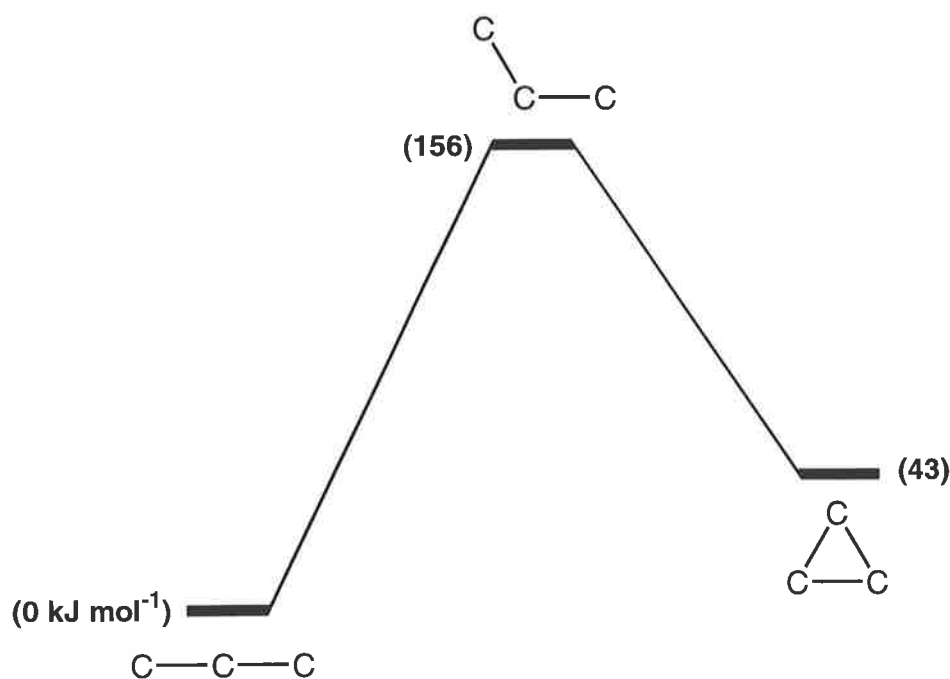
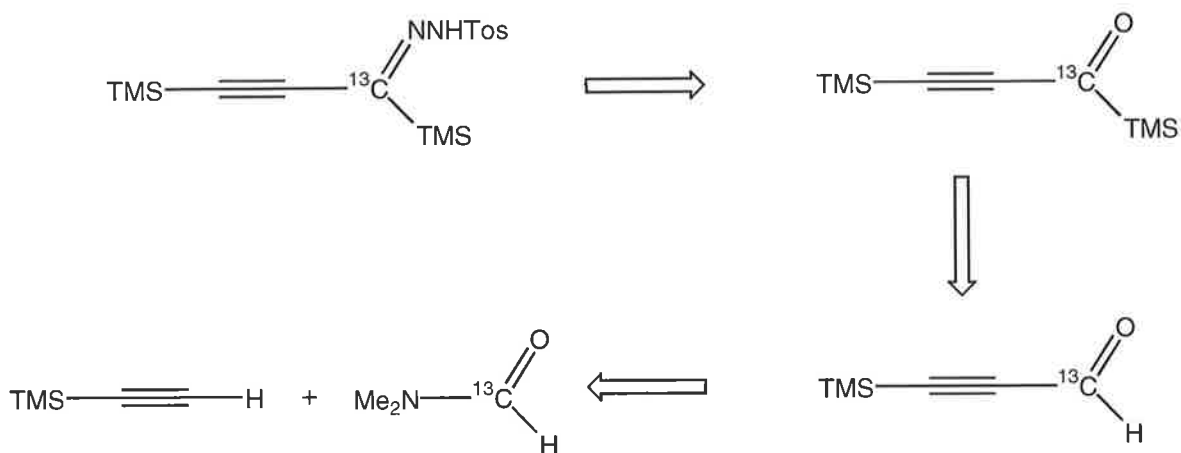


FIGURE 5.1 Calculated reaction coordinates for the interconversion of $[CCC]^-$ to $[cyc-C_3]^-$. Full details are given in Table 5.1.

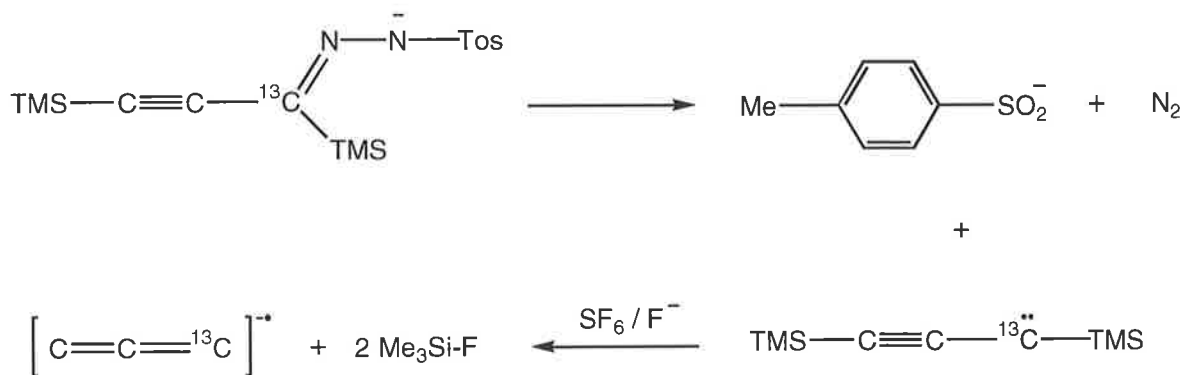
iii. Generation of the Linear $[CC^{13}C]^-$ Radical Anion

The introduction of a ^{13}C atom into the carbon chain of C_3 requires synthesis of a suitable precursor designed to liberate the labelled linear radical anion $[CCC]^-$ with known connectivity. The labelled carbon can be at either the central carbon or a terminal carbon. The labelling of the central carbon appears desirable since any loss of ^{13}C is evidence for rearrangement, however a ^{13}C at a terminal position will give a 1 : 1 ratio of the losses of $^{12}C : ^{13}C$ in the event of no rearrangement and 2 : 1 for complete statistical rearrangement. It turns out that a precursor designed to liberate linear $[CC^{13}C]^-$ radical anion is synthetically accessible using known procedures and commercially available reagents. The major steps of the retro-synthesis of the precursor, 1,3-bis(trimethylsilyl)-1- ^{13}C -prop-2-yne-1-*p*-tosylhydrazone are shown in Scheme 5.3. This compound may be synthesised starting with trimethylsilyl acetylene and ^{13}C labelled dimethyl formamide.



SCHEME 5.3

The radical anion $[CC^{13}C]^-$ was generated from the ^{13}C labelled tosylhydrazone, $Me_3Si-C\equiv C-^{13}C(NNHTos)(SiMe_3)$. Ionisation was effected using the SF_6 modification of the Squires double desilylation procedure²² (which uses F^-/NF_3), together with deprotonation of the tosylhydrazone to effect formation of a carbene intermediate.³⁰³ The precise sequence for this procedure is not known (just as the intimate mechanism of the Squires double desilylation is not known²²). This procedure is analogous to that used previously for the synthesis of $[CC^{13}CCC]^-$.²⁷⁰ A possible rationale for the overall reaction is given Scheme 5.4. Formation of $[M - H]^-$, $p-CH_3-C_6H_4-SO_2^-$ and $[CC^{13}C]^-$ anions in the ion source of the mass spectrometer are consistent with the proposed process shown in Scheme 5.4.



SCHEME 5.4

The collision induced mass spectrum (MS/MS) of $[CC^{13}C]^-$ shows a pronounced peak due to the parent radical anion together with two weak peaks corresponding to losses of ^{12}C and ^{13}C . The spectrum was scanned at maximum sensitivity over the region containing m/z 24 and 25 ($[CC]^-$ and $[C^{13}C]^-$) giving a peak area ratio (m/z 24 to m/z 25) of 1 : 1. This result demonstrates that the carbons of $[CC^{13}C]^-$ are not scrambling prior to, or during the

losses of ^{12}C and ^{13}C . This is interesting, since the dissociation process $[C_3]^- \rightarrow [C_2]^- + C$, has $\Delta H = +603 \text{ kJ mol}^{-1}$; * similar results were obtained for linear C_4 and C_5 .^{270,271}

In view of the experimental observation that $[CC^{13}C]^-$ may decompose (by loss of ^{12}C and ^{13}C) without prior or accompanying rearrangement of the carbon skeleton, is it possible that the transition state for this process is inaccessible? We have calculated bending potentials for several low lying electronic states of $[C_3]^-$ at the B3LYP/6-311G(d) level of theory, these curves are shown in Figure 5.2. Renner-Teller splitting of the $^2\Pi_g$ ground state occurs upon symmetrical bending of $[CCC]^-$ as studied previously using a number of high-level procedures.^{261,295} The two Renner-Teller bending potentials (2B_2 and 2A_2) increase dramatically in energy upon symmetrical bending of the anion radical. In contrast, the cyclic anion is a local minimum on the 2A_1 surface, and this increases in energy with increasing CCC bond angle. The $^2\Pi_g$ excited state is attained some 343 kJ mol^{-1} higher in energy than the $^2\Pi_u$ ground state (calculated at the MRD-CI/6-311+G(d)//CASSCF/6-31G(d) level of theory).²⁹³ Thus, if only symmetrical bending is considered, theory suggests that neither ring opening nor ring closing processes are energetically viable. At first sight this appears to be at variance with the transition state detailed in Table 5.1. However the transition state is not symmetrical and lies on the $^2A'$ surface near the crossing point of the 2A_1 and 2B_2 surfaces. Therefore the anion rearrangement not only has a barrier, but it is also dependent on accessing the transition

* <http://webook.nist.gov/> - C_3^- 638; C_3 , 820; C_2^- , 525; C_2 , 838; C, 717 kJ mol^{-1} . In addition, EA C_2 , $3.273 \pm 0.008 \text{ eV}$ ²⁹³ and C, 1.262 eV .³⁰³

state on the $^2A'$ potential energy surface. In addition, rearrangement of energised $[CCC]^-$ has to compete with collision induced electron detachment.

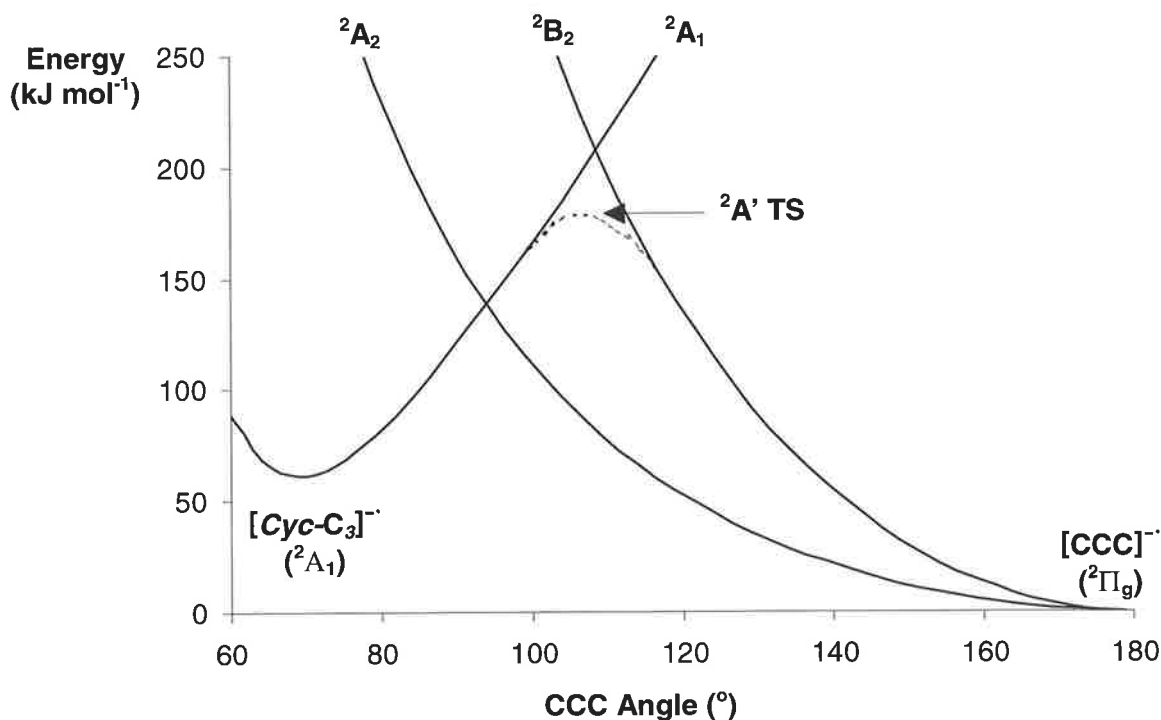


FIGURE 5.2 B3LYP/6-311G(d) bending potential energy surface of low lying electronic states of the $[C_3]^-$ radical anion.

iv. The $^-CR^+$ and $^-NR^+$ Mass Spectra of $[CC^{13}C]^-$

The $^-CR^+$ and $^-NR^+$ mass spectra of $[CC^{13}C]^-$ are shown in Figure 5.3. The spectra are simple, showing recovery signals and fragment peaks corresponding to losses of ^{12}C and ^{13}C together with $^{12}C_2$ and $^{12}C^{13}C$. The spectra are very similar to each other except for the peak at m/z 18.5 in the $^-CR^+$ spectrum which is due to doubly-charged $[CC^{13}C]^{++}$. The peaks due to losses of ^{12}C and ^{13}C (m/z 25 and 24) have an area ratio of 2 : 1, while those corresponding to losses of $^{12}C_2$ and $^{12}C^{13}C$ (m/z 13 and 12) have an area ratio of 1 : 2.

These ratios indicate that the carbon chain scrambles statistically either during the formation of [¹²C₂¹³C]⁺, or accompanying decomposition of the parent radical cation.

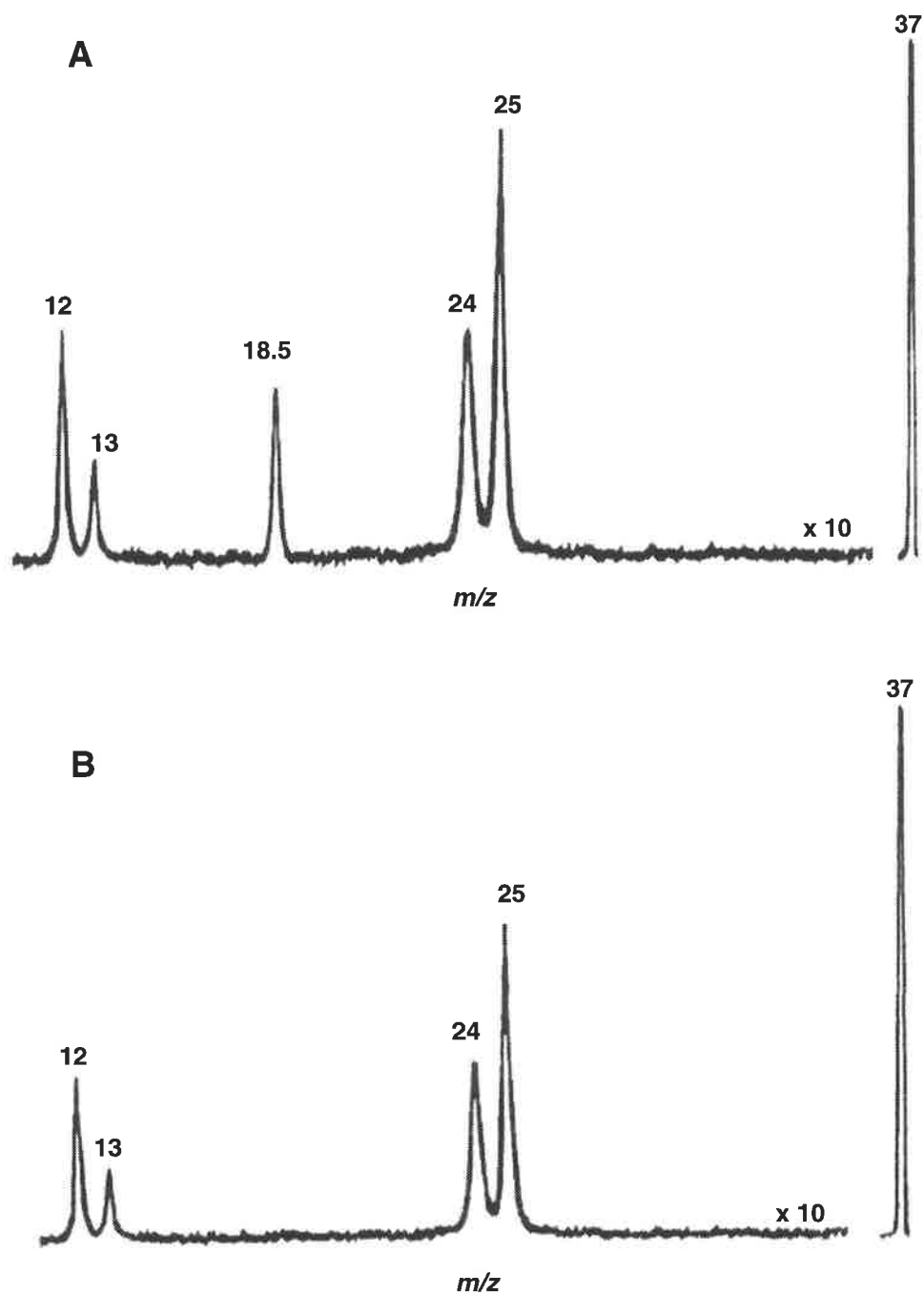


FIGURE 5.3 (A) ⁻CR⁺ and (B) ⁻NR⁺ mass spectra of the [C₃]⁻ radical anion. For experimental conditions see Experimental Section.

v. The Rearrangement of Linear [CC¹³C]⁺ to the Cyclic Isomer

The [C₃]⁺ potential energy surface has been investigated at the CCSD(T)/aug-cc-pVTZ//B3LYP/6-311G(d) level of theory. The results are shown in Figure 5.4 with full details of geometries and energies given in Table 5.2. There has been debate as to whether the linear ²Σ_u or the cyclic ²B₂ structure is the ground state.^{291,292,298,300-302} Our calculations predict that the cyclic ²B₂ radical cation corresponds to the global minimum on the cation potential energy surface, with the linear ²Σ_u state lying 24 kJ mol⁻¹ above the ground state. This is in agreement with higher level calculations, for example, the complete active space (CASSCF) method favours the cyclic isomer by 22 kJ mol⁻¹.³⁰¹ The energy required to convert the linear to the cyclic cation is calculated to be less than 12 kJ mol⁻¹. When the radical anion [CCC]⁻ undergoes vertical two-electron oxidation to the linear cation, the excess Franck-Condon energy is only 2 kJ mol⁻¹ at the B3LYP/6-311G(d) level of theory. This small energy difference can be attributed to the similar geometries of the anion and cation (*cf.* data in Tables 5.1 and 5.2). This Franck-Condon excess energy of 2 kJ mol⁻¹ is not sufficient to surmount the 12 kJ mol⁻¹ barrier between the linear and cyclic [C₃]⁺ cation radicals. However, the actual excess energy of the cation formed will be more than the excess Franck-Condon energy, either as a consequence of some formation energy of the anion radical being carried through to the cation, or by some subsequent collision process of the cation. Thus it is expected that the majority of the initially formed [CC¹³C]⁺ radical cations in the ⁻CR⁺ process will rearrange over the 12 kJ mol⁻¹ barrier to yield the [cyc-C₃]⁺ radical cation, a process which essentially scrambles the carbon atoms.

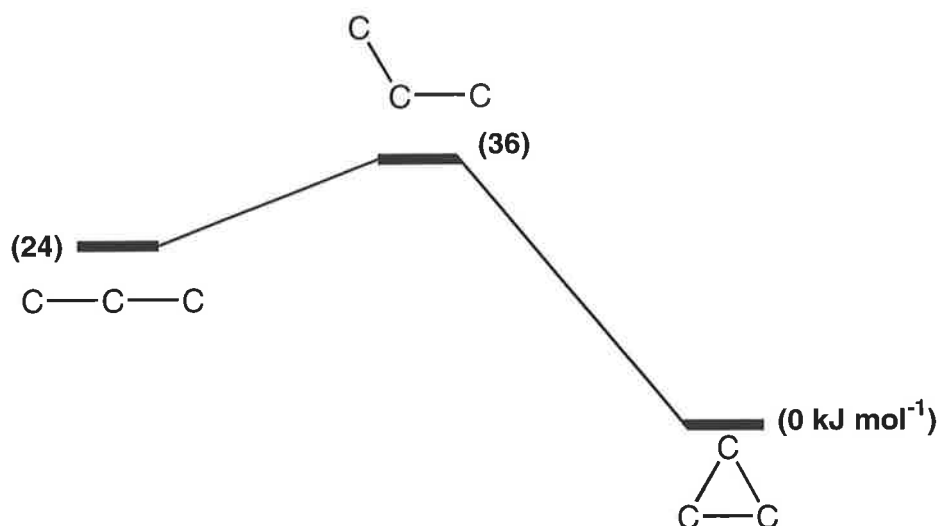


FIGURE 5.4 Calculated reaction coordinates for the interconversion of [CCC]⁺ to [cyc-C₃]⁺. Full details are given in Table 5.2.

TABLE 5.2 Calculated properties of the [C₃]⁺ radical cation.

	Linear	Cyclic	TS
State	² Σ _u	² B ₂	² B ₂
Energy (Hartrees) ^a	-113.389070	-113.398386	-113.384757
Relative Energy (kJ mol ⁻¹)	24	0	36
C ₁ C ₂ , C ₂ C ₃ (Å) ^b	1.290	1.316	1.293
C ₁ C ₃	2.580	1.446	2.333
C ₁ C ₂ C ₃ (°)	180.0	66.6	128.9

a. Energies calculated at the CCSD(T)/aug-cc-pVTZ level of theory and include zero point correction (calculated from B3LYP/6-311G(d) vibrational frequencies). b. Geometries optimised at the B3LYP/6-311G(d) level of theory.

vi. The Conversion of [CC¹³C]⁻ to Neutral CC¹³C

The ⁻CR⁺ and ⁻NR⁺ spectra of [CC¹³C]⁻ show the same fragment peaks in the same ratio.

The ⁻NR⁺ spectrum shows the presence of a pronounced recovery signal confirming that a neutral C₃ is stable for the microsecond duration of the ⁻NR⁺ experiment. The similarity of the ⁻NR⁺ and ⁻CR⁺ spectra of [CC¹³C]⁻ suggests that no major decomposition of the

neutral occurs on the microsecond time scale (for $\text{CCC} \rightarrow \text{CC} + \text{C}$, $\Delta H = 734 \text{ kJ mol}^{-1}$). Since complete ¹³C scrambling is noted for both ⁻CR⁺ and ⁻NR⁺ spectra, this means that the ⁻NR⁺ spectrum (Figure 5.3) provides no information concerning the question of carbon scrambling of the neutral. In this context, it has been recently reported that carbon scrambling within the ¹³C labelled [C₃]⁺ species produced by dissociative ionisation of [CH₃-¹³C=CH₂]⁺ precedes formation of a labelled neutral C₃ by one-electron vertical reduction in a ⁺NR⁺ experiment.³⁰⁴

Since the ⁻NR⁺ spectrum of [CC¹³C]⁻ gives no data concerning the possibility of carbon scrambling occurring during or subsequent to the vertical one-electron oxidation of the anion to the neutral, the next obvious experiment is to measure the ⁻NR⁻ spectrum. Since the CID mass spectrum of [CC¹³C]⁻ shows no carbon scrambling in the anion, rearrangement of the carbon skeleton of the neutral CC¹³C should be readily identifiable in the ⁻NR⁻ spectrum of [CC¹³C]⁻. Unfortunately, the fragmentations of the anion are highly energetic and compete with the simple electron detachment process; the fragment peaks in the resultant CID spectrum of [CC¹³C]⁻ are very weak (see earlier). A peak corresponding to the [C₃]⁻ parent anion radical is observed in the ⁻NR⁻ spectrum, however no fragment anions were detected using the maximum sensitivity of the instrument.

The geometry of the neutral ¹Σ_g ground state of CCC has been calculated at the B3LYP/6-311G(d) level of theory. Results are recorded in Table 5.3, together with data obtained from previous studies. We obtain a value of 1.291 Å for the CC bond length; this should be compared with the experimental value of 1.297 Å,²⁷⁸ and a 'best' theoretical value of 1.295 Å obtained previously.²⁹²

TABLE 5.3 Calculated properties of C₃ neutrals.

	Singlet linear	Singlet TS	Triplet linear	Triplet cyclic	Triplet TS
State	¹ Σ _g	¹ A ₁	³ Π _u	³ A ₁ '	³ A'
Energy (Hartrees)	-113.83020	-113.79769	-113.75265	-113.79767	-113.69263
Relative Energy (kJ mol ⁻¹)	0	104	204	85	361
C ₁ C ₂ (Å)	1.291	1.260	1.294	1.370	1.376
C ₂ C ₃	1.291	1.471	1.294	1.370	1.301
C ₁ C ₃	2.582	1.471	2.588	1.370	2.146
C ₁ C ₂ C ₃ (°)	180.0	64.7	180.0	60.0	106.5

a. Energies calculated at the CCSD(T)/aug-cc-pVTZ level of theory and include zero point correction (calculated from B3LYP/6-311G(d) vibrational frequencies). b. Geometries optimised at the B3LYP/6-311G(d) level of theory.

Our CCSD(T)/aug-cc-pVTZ//B3LYP/6-311(d) theoretical study of the triplet C₃ neutral potential energy surface predicts the linear ³Π_u state to be 204 kJ mol⁻¹ higher in energy than the ¹Σ_g ground state, is in agreement with the experimental value of 201 kJ mol⁻¹.²⁸² There is also a cyclic neutral of D_{3h} symmetry on the triplet potential energy surface.^{288,293} At the CCSD(T)/aug-cc-pVTZ//B3LYP/6-311(d) level of theory, the cyclic neutral is 85 kJ mol⁻¹ higher in energy than the ground state singlet (Table 5.3).

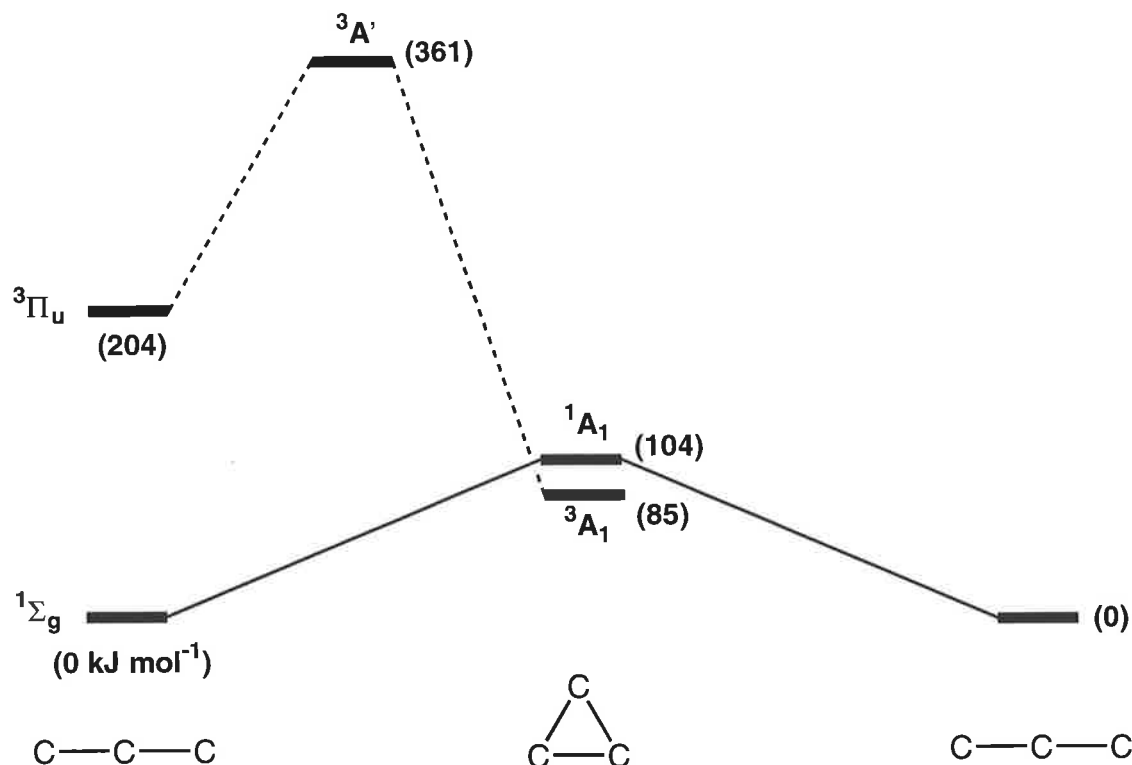


FIGURE 5.5 Isomerisation processes of singlet (solid line) and triplet (dashed line) neutral C_3 . Full details are given in Table 5.3.

The degenerate rearrangement of neutral $^1\Sigma_g$ CCC via the 1A_1 cyclic transition state is calculated to require 104 kJ mol^{-1} (Table 5.3). This is shown in Figure 5.5 along with the conversion of the $^3\Pi_u$ state to the more stable 3A_1 on the triplet potential energy surface, a process which has a barrier of 157 kJ mol^{-1} . Since the energy of the $^-NR^+$ procedure cannot be controlled, both the $^1\Sigma_g$ and $^3\Pi_u$ CCC neutrals could be accessible in the one-electron vertical oxidation from $[CCC]^-$, however rearrangement is more likely to occur via the degenerate rearrangement of the singlet neutral. In previous studies of the carbon scrambling observed for singlet forms of neutral CCCC²⁷⁰ and CCCCC²⁷¹ the respective barriers for the scrambling processes were calculated to be 120 and 224 kJ mol^{-1} at the CCSD(T)/aug-cc-pVDZ//B3LYP/6-31(d) level of theory. These energies are significantly

higher than the Franck-Condon excess energies imparted to those neutrals during the one-electron oxidation processes. Both of those barriers are greater than that required for the degenerate rearrangement of singlet CCC. It therefore seems likely that at least a proportion of the CC¹³C neutrals formed from [CC¹³C]⁻ will undergo the degenerate rearrangement (Table 5.3), with consequent randomisation of the carbons. Unfortunately we have no experimental probe to substantiate this proposal.

vii. Conclusions

The radical anion [CC¹³C]⁻ has been prepared by an unequivocal gas-phase synthesis, and this anion retains its skeletal integrity under the collision conditions necessary to effect one-electron vertical oxidation to the corresponding CCC neutral molecule. The radical anion [CC¹³C]⁻ is converted by two-electron vertical oxidation to [CC¹³C]^{+•} which requires an excess energy of only 12 kJ mol⁻¹ to interconvert to the more stable [cyc-C₂¹³C]^{+•}. The radical anion [CC¹³C]⁻ was converted, by collisional one-electron oxidation, to corresponding neutral, which was found to be stable for microsecond duration of the experiment. Theoretical calculations indicate that the singlet neutral requires an excess energy of 104 kJ mol⁻¹ in order to effect a degenerate rearrangement through a cyclic C₂¹³C transition state; a process which essentially randomises the three carbon atoms. It is likely that some neutrals will equilibrate the carbons by this process, but no experimental probe was available to substantiate this proposal.

3. EXPERIMENTAL

A. Mass Spectrometric Methods

The experiments were performed using a four-sector modified ZAB/AMD 604 mass spectrometer with BEBE configuration, where B and E represent magnetic and electric sectors respectively. The [CC¹³C]⁻ radical anion was generated by chemical ionisation (CI) in the negative ion mode, with typical source conditions as follows: source temperature 200 °C, repeller voltage -0.5 V, ion extraction voltage 8 kV, mass resolution $m/\Delta m \geq 1500$. The precursor 1,3-bis(trimethylsilyl)-1-¹³C-prop-2-yne-1-p-tosylhydrazone, was placed in a small glass capillary tube which was then inserted into the CI source via the direct probe. The probe tip was heated to 60 - 80 °C to generate a background pressure of *ca.* 10⁻⁵ Torr inside the source housing. The [CC¹³C]⁻ radical anion was formed (see Scheme 5.4), utilising a 1:1 mixture of H₂O and SF₆ as CI reagent gases (to liberate the reagent ions HO⁻ and F⁻ respectively: the latter is a modification²⁷⁰ of the Squires *bis* S_N2(Si) reaction with F⁻/NF₃²²) at a measured pressure of *ca.* 10⁻⁴ Torr inside the source housing.

Collisional induced dissociation (CID) of B mass selected ions was effected in the second of the tandem collision cells positioned between B and E. Helium was used as a target gas. The pressure of the collision gas in the cell was maintained such that 80% of the parent ion beam was transmitted through the cell. This corresponds to essential single collision conditions.³⁰ Product ions resulting from CID were recorded by scanning E.

Neutralisation-reionisation^{40,41,305-307} (⁻NR⁺ and ⁻NR⁻) experiments were performed for B mass-selected [CC¹³C]⁻ utilising the dual collision cells located between sectors B and

E. Neutralisation of the anions was achieved by collisional electron detachment using O₂ (80% transmittance of the main beam) as collision gas, while reionisation of neutrals to cations was also achieved by collision of the neutrals with O₂, again at 80% transmittance of the main beam. Reionisation to anions was effected using xenon (80% transmittance of the main beam). Any ions remaining after the first collision event were deflected from the primary neutral beam using an electrode maintained at a high voltage (1.0 kV) positioned before the second collision cell. In order to detect a reionisation signal due to the parent, the neutral species must be stable for approximately one microsecond.

Charge reversal (⁻CR⁺) spectra^{31,34,35} were recorded using single collision conditions in collision cell 1 (O₂, 80% transmission of main beam). ⁻CR⁺ spectra were then recorded as for the CID experiment except that the polarity of the electric sector was reversed to allow detection of positive ions.

B. Synthetic Procedures

The labelled precursor was prepared by known procedures (¹³C = 99.5%).^{308,309}

C. Theoretical Methods

Geometry optimisations were carried out with the B3LYP method^{83,84} using the 6-311G(d) basis set within the GAUSSIAN 98 suite of programs.²⁴¹ Stationary points were characterised as either minima (no imaginary frequencies) or transition structures (one imaginary frequency) by calculation of the frequencies using analytical gradient procedures. Intrinsic reaction coordinate (IRC) calculations were used to examine the

reaction path on the potential energy surface leading away from a given transition state, thus confirming connection between minima and the transition state. The calculated frequencies were also used to determine zero-point vibrational energies, which were used as a zero-point correction for the electronic energies. Some problems have been highlighted in the literature regarding the use of the B3LYP method for the accurate prediction of molecular energies for carbon clusters,³¹⁰ even though the method continues to be used with success.^{293,311-313} More accurate energies for the B3LYP geometries were determined using the CCSD(T) method^{76,239,314} together with the Dunning aug-cc-pVTZ basis set.^{237,238} The CCSD(T)/aug-cc-pVTZ//B3LYP/6-311G(d) approach used in this study computes the adiabatic electron affinity of linear C_3 to be 1.945 eV in good agreement with the experimentally measured value of 1.981 eV.¹⁸⁸ All calculations were carried out on the Alpha Server at the Australian Partnership for Advanced Computing (APAC) National Facility (Canberra).

CHAPTER 6

GENERATION OF BOROCUMULENIC SYSTEMS IN THE GAS PHASE

1. INTRODUCTION

Carbon clusters (cumulenes) have been studied in great detail due to their importance in astrochemistry,^{242,243} as discussed in the preceding chapters. In contrast, studies on similar compounds containing boron and carbon have concentrated mainly on borocumulenes with boron occupying a terminal position in such molecules. A number of studies have involved heating boron/carbon mixtures at high temperatures, while the use of lasers to ablate boron/carbon mixtures have also been employed. A number of products resulting from these processes have been trapped in low temperatures matrices (*eg.* solid argon), and the structures of the major products determined using various spectroscopic methods including infrared spectroscopy and electron spin resonance spectroscopy. The following species have been reported: (i) the anion, neutral and cation of BC,³¹⁵⁻³²¹ (ii) neutral BC₂ of which the cyclic form is some 25 kJ mol⁻¹ more negative in energy than the linear structure,³²²⁻³²⁴ linear [BC₂]⁻,^{321,325-327} and [cyc-BC₂]⁺,³²⁸ (iii) linear [BC₃]⁻ and linear BC₃,³²⁹ rhombic [BC₃]⁺,³²⁸ (iv) linear [BC₄]⁻,³²⁵ and [cyc-BC₄]⁺,³²⁸ (v) bent (distorted 'linear') [BC_n]⁻ (*n* = 5 - 13),³²⁵ (vi) linear BCCB,³²⁹ and complexes of B and CO, for example BCO, B(CO)₂, (CBO)₂.^{325,326,330,331} The OCBBCO neutral has been reported, this interesting molecule exhibits some boron-boron triple bond character.³³² The anions [CH₂=B=CH₂]⁻ and [CH₂=B=O]⁻ have also been reported,³³³ these anions were generated by collision induced dissociation using a VG ZAB 2HF mass spectrometer.

As part of their studies into borocumulene anions Zhan and Iwata³²⁶ observed a number of (minor) peaks in a time-of-flight mass spectrum with m/z values corresponding to borocumulene oxides anions of general formula $[C_{2n}BO]^-$ (where $n = 1 - 5$). These anions were generated by focusing a laser (Nd:YAG, 532 nm, 7 ns) on the sample (graphite doped with $Na_2B_7O_4$ solution) under vacuum. Anions within the resulting plasma diffused into a pulsed acceleration zone and were then accelerated along a flight tube to a detector by a voltage of 1 kV. The $[C_{2n}BO]^-$ anions were observed along with the more abundant $[C_nB]^-$ anions. The nature of this experiment meant that no structural data could be determined experimentally, however the authors did suggest that these anions may have $(C=C)_n=B=O$ structure.

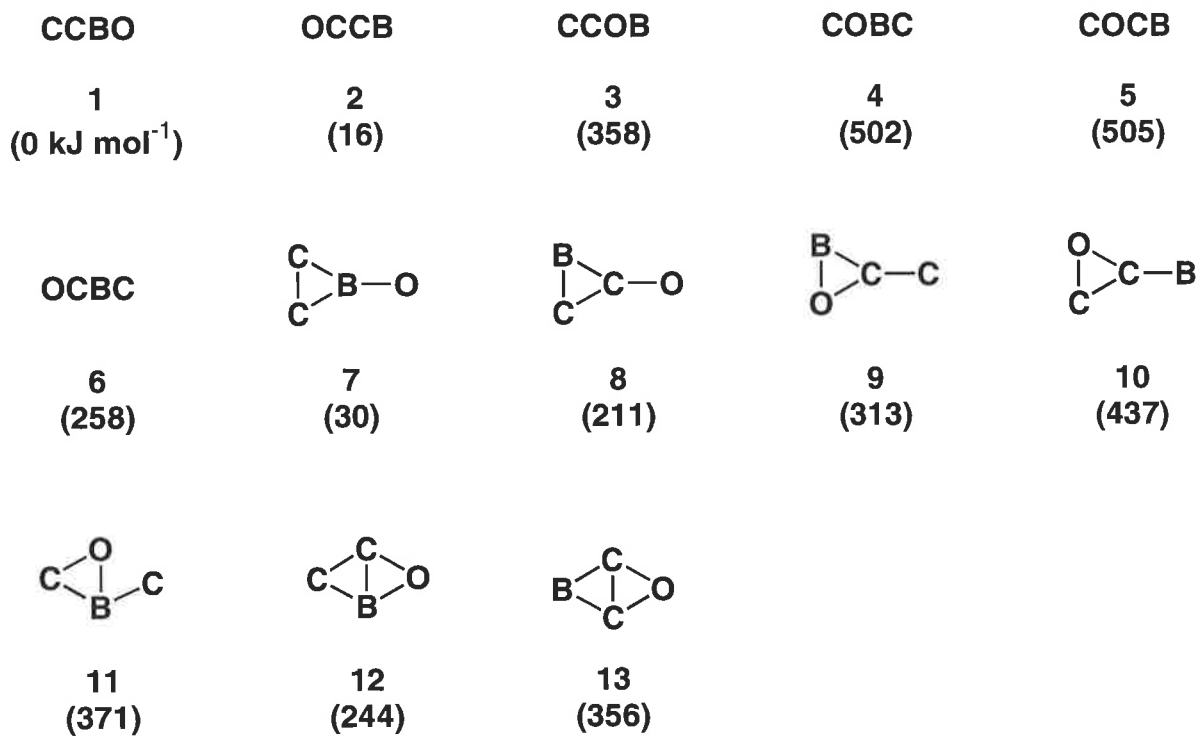
It would be of interest to produce transient neutral borocumulenes in the mass spectrometer. Collision induced vertical oxidation from an anion of known bond connectivity would result in the generation of such unusual species. Borocumulenes in which the boron occupies a terminal position would be difficult to make by such synthetic techniques. However, it might be possible to make borocumulenes and borocumulene oxides possessing a non-terminating boron atom. This chapter describes studies into the generation of three such neutral species with the following bond connectivities; CCBO, CCCCBO and CCBCC.

2. RESULTS AND DISCUSSION

A. Formation of CCBO and [CCBO]⁺ from [CCBO]⁻ in the Gas Phase

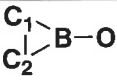
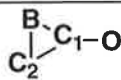
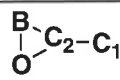
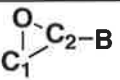
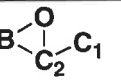
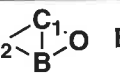
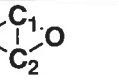
The aim of this study is to generate the neutral borocumulene oxide with CCBO bond connectivity and investigate its stability to rearrangement and dissociation. Specifically, this part addresses two questions, namely (i) can the CCBO neutral be formed from linear [CCBO]⁻ by the neutralisation-reionisation (⁻NR⁺) process? and (ii) does neutral CCBO rearrange under the conditions of the ⁻NR⁺ experiment, and if so, what is the product and what is the mechanism involved in the rearrangement?

Since little is known on the C₂BO system, the first step is to ascertain whether or not the neutral is stable from a theoretical viewpoint before embarking on any experimentation. Thirteen isomers of C₂BO were found to be stable on the MP2(full)/6-31G(d) neutral potential energy surface. The bond connectivities and relative energies [MP4SDTQ/aug-cc-pVTZ//MP2(full)/6-31G(d)] of these radical species and are illustrated in Scheme 6.1 with full details of geometries given in Table 6.1. The target neutral CCBO is the global minimum on the neutral surface. There are two other isomers, OCCB (**2**) and *cyc*-CCB-O (**7**), which are within 30 kJ mol⁻¹ of CCBO, while the remaining ten isomers are 211 to 505 kJ mol⁻¹ higher in energy than CCBO.



SCHEME 6.1

TABLE 6.1 Calculated properties of C₂BO neutrals.

	C ₁ C ₂ BO	OC ₁ C ₂ B	C ₁ C ₂ OB	C ₁ OBC ₂	C ₁ OC ₂ B	OC ₁ BC ₂	
	1	2	3	4	5	6	7
State	² Σ	² Σ	² A'	² Σ	² Σ	² Σ	² A ₁
Symmetry	C _{∞v}	C _{∞v}	C _s	C _{∞v}	C _{∞v}	C _{∞v}	C _{2v}
Relative Energy (kJ mol ⁻¹) ^a	0	16	358	502	505	258	30
Electron Affinity (eV)	4.8	2.6	4.4			4.4	-0.9
Ionisation Energy (eV)	12.6	12.9					14.4
C ₁ C ₂ (Å) ^b	1.182	1.293	1.179				1.291
C ₂ B	1.491	1.340		1.292	1.304	1.346	1.684
C ₁ B						1.433	
BO	1.217		1.314	1.399			1.217
C ₁ O		1.173		1.175	1.165	1.163	
C ₂ O			1.302		1.328		
C ₁ C ₂ O (°)			178.7				
C ₂ OB			155.0				
C ₁ C ₂ B							67.5
C ₂ BO							157.5
							
	8	9	10	11	12	13	
State	² A'	² A'	² A'	n/a	² A'	² A ₁	
Symmetry	C _s	C _s	C _s	C ₁	C _s	C _{2v}	
Relative Energy (kJ mol ⁻¹)	211	313	437	371	244	356	
Electron Affinity (eV)	3.4	3.7	3.0		2.7		
Ionisation Energy (eV)					14.8		
C ₁ C ₂ (Å)	1.568	1.303	1.460	1.355	1.322	1.505	
C ₂ B	1.401	1.510	1.344	1.525	1.454	1.458	
C ₁ B					1.643		
BO		1.332		1.375	1.402		
C ₁ O	1.185		1.298		1.453	1.413	
C ₂ O							
C ₁ C ₂ B (°)	61.0	163.3	164.7	90.5	72.4		
C ₂ BO		63.3		74.3	106.4		
C ₂ C ₁ O	138.8		65.6	70.6	111.0		
BOC ₁				84.6	70.2		
BC ₁ O						116.8	
C ₁ OC ₂						64.4	
C ₁ BC ₂						62.2	
OBC ₂ C ₁				-51.9			

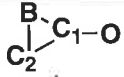
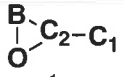
a. Energies are calculated at the MP4/aug-cc-pVTZ//MP2(full)/6-31G(d) level of theory and are relative to **1** (-175.904292 Hartrees). b. MP2(full)/6-31G(d) geometries.

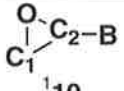
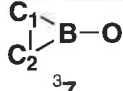
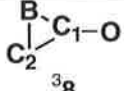
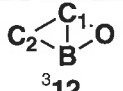
i. The Formation of the Linear $[\text{CCBO}]^-$ Anion

In order to generate the CCBO radical neutral using the neutralisation-reionisation method, the linear $[\text{CCBO}]^-$ anion must be easily formed from a suitable precursor, and it must retain its linear structure under the experimental conditions. If the $[\text{CCBO}]^-$ anion readily rearranges, then it is not suitable for generation of CCBO neutral by vertical oxidation. The results of theoretical calculations on the $[\text{CCBO}]^-$ anion are summarised in Table 6.2, along with other possible isomers of the $[\text{C}_2\text{BO}]^-$ anionic system. There are twelve minima on the $[\text{C}_2\text{BO}]^-$ anion potential energy surface with the global minimum corresponding to the singlet $[\text{CCBO}]^-$ species. There does exist a triplet form of $[\text{CCBO}]^-$, but it is 467 kJ mol^{-1} higher in energy than singlet $[\text{CCBO}]^-$. Of the remaining ten anionic species, six are singlets with energies ranging between $224 - 612 \text{ kJ mol}^{-1}$ higher in energy than the singlet $[\text{CCBO}]^-$ ground state, and four are high energy triplets ($> 447 \text{ kJ mol}^{-1}$).

Singlet $[\text{CCBO}]^-$ is linear and can be represented by the valence bond structure $[:\text{C}=\text{C}=\text{B}=\text{O}]^-$. The extra electron is involved in the multiple bonding around boron. The effect of electron delocalisation is evident by the C-C bond distance, which increases from 1.18 \AA in the neutral (*cf.* 1.18 \AA in acetylene) to 1.27 \AA in the anion. Further, the C-B bond distance decreases from 1.49 \AA to 1.45 \AA upon addition of the extra electron to form the anion from the neutral. The ground states of both the neutral and the singlet anion of CCBO are linear suggesting that the anion is a suitable precursor to the neutral.

TABLE 6.2 Calculated properties of $[\text{C}_2\text{BO}]^-$ anions.

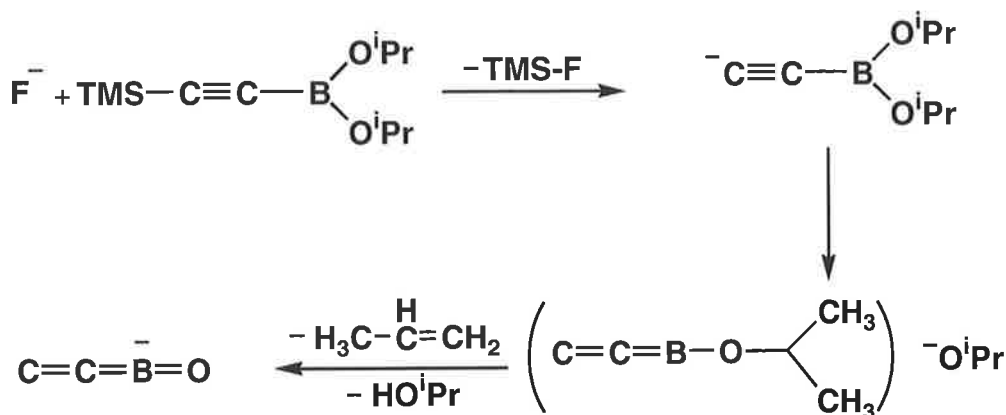
	$\text{C}_1\text{C}_2\text{BO}$ 1_1	$\text{OC}_1\text{C}_2\text{B}$ 1_2	$\text{C}_1\text{C}_2\text{OB}$ 1_3	OC_1BC_2 1_6	 1_8	 1_9
State	$^2\Sigma$	$^2\Sigma$	$^2A'$	$^2\Sigma$	$^2\Sigma$	$^2\Sigma$
Symmetry	$C_{\infty v}$	$C_{\infty v}$	$C_{\infty v}$	$C_{\infty v}$	C_s	C_s
Relative Energy (kJ mol^{-1}) ^a	0	224	399	297	340	419
C_1C_2 (Å) ^b	1.269	1.279	1.266		1.595	1.269
C_2B	1.447	1.437		1.409	1.425	
C_1B				1.406	1.454	1.857
BO	1.242		1.275			1.347
C_1O		1.215	1.354	1.209	1.214	1.426
C_2O						
$\text{C}_1\text{C}_2\text{O}$ (°)					133.9	179.0
BC_2C_1					57.3	
C_2BO						
C_2OB						84.0

	 $^1_{10}$	$\text{C}_1\text{C}_2\text{BO}$ 3_1	$\text{OC}_1\text{C}_2\text{B}$ 3_2	 3_7	 3_8	 $^3_{12}$
State	$^1A'$	$^3A'$	$^3A'$	3B_2	$^3A'$	$^3A''$
Symmetry	C_s	C_s	C_s	C_{2v}	C_s	C_s
Relative Energy	612	467	456	579	447	726
C_1C_2 (Å)	1.382	1.255	1.261	1.271	1.406	1.423
C_2B	1.464	1.444	1.416	1.598	1.490	1.620
C_1B				1.598	1.595	1.620
BO		1.261				1.458
C_1O	1.377		1.227		1.238	1.721
C_2O	1.56					1.721
$\text{C}_1\text{C}_2\text{O}$ (°)	69.0		179.9		153.0	65.6
BC_2C_1	167.8	168.5	170.0	64.3	66.8	63.9
C_2BO		168.4		154.3		67.7
C_2OB						
$\text{C}_1\text{C}_2\text{BO}$						78.4

a. Energies are calculated at the MP4/aug-cc-pVTZ//MP2(full)/6-31G(d) level of theory and are relative to 1_1 (-176.079751 Hartrees). b. MP2(full)/6-31G(d) geometries.

Generation of the $[\text{CCBO}]^-$ anion in the chemical ionisation source of the mass spectrometer was effected as shown in Scheme 6.2. The first step involves a $\text{S}_{\text{N}}2(\text{Si})$ reaction between the trimethylsilyl protected ethynyl borate to form the acetylide anion $[\text{CCB}(\text{O}^i\text{Pr})_2]^-$. The overall sequence of $[\text{CCBO}]^-$ formation may be rationalised as shown

in Scheme 6.2 where the desilylated anion forms the ion-neutral complex $[(\text{CCBO})^i\text{Pr}]^- \text{O}^i\text{Pr}$. This is followed by the *iso*-propoxide anion effecting an elimination reaction on the neutral to give $\text{CH}_3\text{CH}=\text{CH}_2$, $^i\text{PrOH}$ and the required anion $[\text{CCBO}]^-$ with known bond connectivity.



SCHEME 6.2

If the anion does rearrange to $[\text{OCCB}]^-$ (*ie.* the other low energy isomer) then loss of CO should be observed under CID conditions. The collision induced mass spectrum (MS/MS) of $[\text{CCBO}]^-$ shows minimal fragmentation, however no loss of CO is observed. The only fragment peaks observed in the CID spectrum are due to loss of C and C_2 from the parent anion. This is a wholly unexpected result given that the electron affinity of CC is known to be greater than that of BO, yet no loss of BO is observable. The thermochemistry of a number of anionic decompositions were calculated at the MP4SDTQ/aug-cc-pVDZ//MP2(full)/6-31G(d) level of theory are given in Table 6.3. Both losses of CC and BO from the $[\text{CCBO}]^-$ anion are endothermic by 674 and 633 kJ mol^{-1} respectively. The difference in the thermochemistry of the two processes is comparatively small and therefore factors other than thermochemistry may be significant. For example, there may be a barrier to

and/or lower probability for the dissociation to CC^- and BO as compared to the formation of BO^- .

TABLE 6.3 Selected $[\text{C}_2\text{BO}]^-$ dissociations energies. ^a *

Parent Anion	Fragment Species ^b	Energy (kJmol^{-1}) ^c
[CCBO] ⁻	⁴ C ⁻ + ⁴ CBO	1088
	C + ³ CBO ⁻	928
	O ⁻ + CCB	1024
	O + CCB ⁻	884
	CC + BO ⁻	674
	CC ⁻ + BO	633
[OCCB] ⁻	BC ⁻ + ¹ CO	519
	⁴ BC + ² CO ⁻	823

a. Calculated at the MP4/aug-cc-pVTZ//MP2(full)/6-31G(d) level of theory.

b. Full details given in Table 6.15. c. Relative to ¹[CCBO]⁻ (-176.079751 Hartrees) and ¹[OCCB]⁻ (-175.994556 Hartrees).

Other dissociations of $[\text{CCBO}]^-$ are also listed in Table 6.3. Loss of CO from $[\text{OCCB}]^-$ is the least endothermic dissociative process calculated and therefore should be observed if $[\text{CCBO}]^-$ rearranges. No loss of CO is observed in the CID mass spectrum of the $[\text{CCBO}]^-$ anion indicating that it does not rearrange under CID conditions.

ii. Conversion of $[\text{CCBO}]^-$ to Neutral CCBO

The next stage in the experimental investigation of this system is the conversion of $[\text{CCBO}]^-$ to the corresponding neutral. Therefore the radical neutral CCBO needs to be stable to rearrangement and/or dissociation under the conditions of Franck-Condon vertical oxidation. This is examined theoretically by considering which of the isomers listed in

* An examiner has indicated that it is important to include available experimental values for C and BO. There are $EA(\text{C}) = 3.272 \text{ eV}$, $IE(\text{C}) = 11.41 \text{ eV}$, $EA(\text{BO}) = 2.50 \text{ eV}$, $IE(\text{BO}) = 13.3 \text{ eV}$.

Scheme 6.1 could be accessible from $[\text{CCBO}]^-$ following vertical Franck-Condon oxidation to form CCBO.

The minimum excess (Franck-Condon) energy imparted to the system upon formation of the neutral can be calculated by comparison of the energy of the CCBO ground state neutral with that of the neutral initially formed in the oxidation process (*ie.* the neutral with geometry corresponding to the ground state $[\text{CCBO}]^-$). This predicts the Franck-Condon excess energy to be 45 kJ mol^{-1} . This is regarded as a minimum energy since there are other means to impart excess energy to the neutral, including (i) transfer of excess energy of the anion from its formation to the neutral, and (ii) as a consequence of keV collisions of the initially-formed neutral in the collision cell. The Franck-Condon excess energy (45 kJ mol^{-1}) is greater than the relative energy differences of two low-energy isomers in Scheme 6.2 namely, OCCB (**2**, $+16 \text{ kJ mol}^{-1}$) and *cyc*-CCB-O (**7**, $+30 \text{ kJ mol}^{-1}$). In principle these structures could be accessible provided the barriers to their formation can be surmounted.

The interconversion of CCBO (**1**) to OCCB (**2**) and *cyc*-CCB-O (**7**) was studied using *ab initio* calculations as summarised in Figure 6.1. Full details of geometries and energies of neutrals and transition states are listed in Table 6.1 and 6.4 respectively. The reaction path proceeds via *cyc*-CCB-O (**7**, $+30 \text{ kJ mol}^{-1}$) and another cyclic intermediate (**12**, $+244 \text{ kJ mol}^{-1}$). While the rearrangement to OCCB is endothermic by only 16 kJ mol^{-1} , the overall energy required is at least 267 kJ mol^{-1} . The Franck-Condon energy is only 45 kJ mol^{-1} and therefore an additional 222 kJ mol^{-1} of excess energy is required for the rearrangement to proceed. Based on the theoretical data, oxygen migration upon neutralisation seems unlikely. In contrast, the interconversion of CCBO to *cyc*-CCB-O (**7**) has a barrier of 77 kJ mol^{-1} . Therefore only 32 kJ mol^{-1} of excess energy above that of the Franck-Condon energy need be imparted into the system for this interconversion to occur.

If *cyc*-CCB-O (7) is formed initially in reasonable yield, it will be in equilibrium with CCBO within the timeframe of the NR procedure (*ca.* 10^{-6} sec.). This equilibrium will favour CCBO, since it is lower in energy by 30 kJ mol^{-1} and, thus the proportion of *cyc*-CCB-O (7) in an equilibrium mixture will be very small.

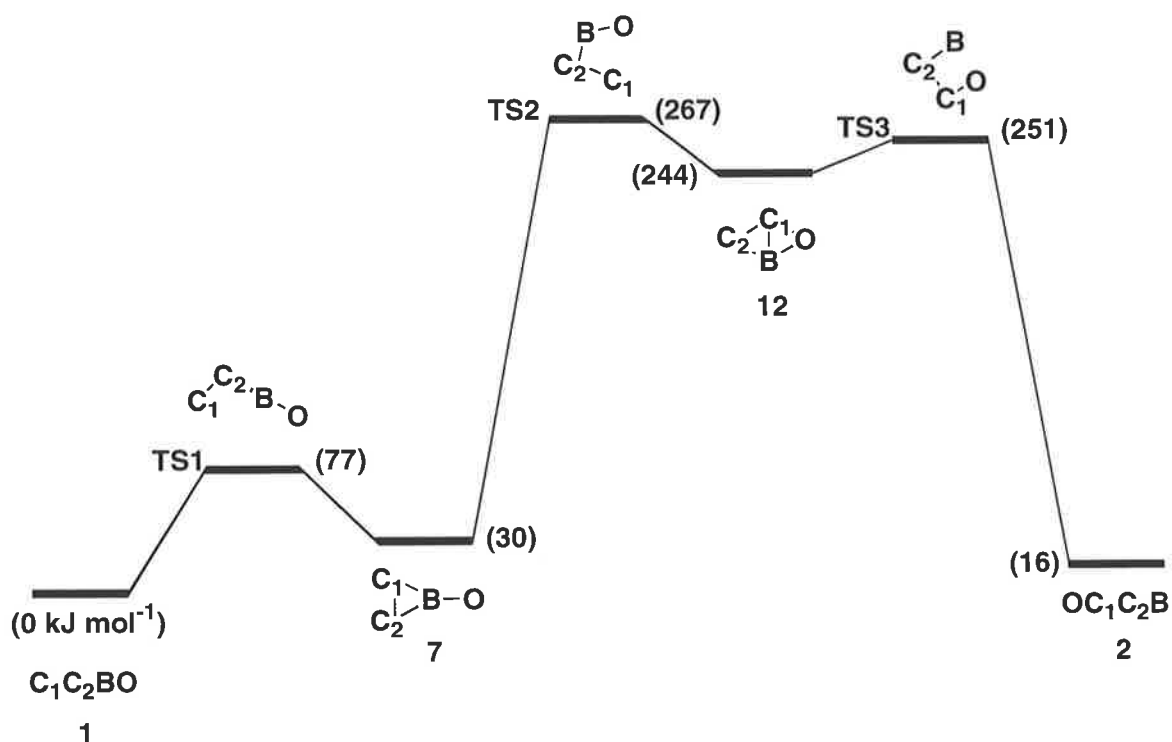


FIGURE 6.1 Calculated pathway for the interconversion of CCBO (1) to OCCB (2) and *cyc*-C₂BO (7). For full details see Tables 6.1 and 6.4.

TABLE 6.4 Calculated properties of transition states for the interconversion of neutral CCBO to OCCB as shown in Figure 6.1.

	TS1	TS2	TS3
State	$^2A'$	$^2A'$	$^2A'$
Symmetry	C_s	C_s	C_s
Relative Energy (kJ mol ⁻¹) ^a	77	267	252
C ₁ C ₂ (Å) ^b	1.206	1.338	1.281
C ₂ B	1.505	1.433	1.464
C ₁ B	2.092	1.754	1.519
BO	1.222	1.247	
C ₂ O			1.350
C ₁ C ₂ B (°)	100.5	78.5	66.9
C ₂ BO	175.1	121.3	
C ₂ C ₁ O			127.6

a. Energies are calculated at the MP4/aug-cc-pVTZ//MP2(full)/6-31G(d) level of theory and are relative to **1** (-175.904292 Hartrees). b. MP2(full)/6-31G(d) geometries.

The $\bar{C}R^+$ and $\bar{N}R^+$ spectra of the $[CCBO]^-$ anion are shown in Figure 6.2. The $\bar{N}R^+$ spectrum is dominated by the recovery signal at m/z 51, indicating that the parent neutral(s) is stable on the microsecond time scale of the experiment. Fragment peaks observed in the $\bar{N}R^+$ spectrum arise from the competitive losses of O, C₂ and BO. These losses are consistent with a species of CCBO connectivity. Interestingly, there is a peak at m/z 23, corresponding to the loss of CO, as well as a smaller peak corresponding to loss of BC at m/z 28. These peaks are inconsistent with the CCBO connectivity and therefore indicate that a rearrangement occurs during the $\bar{N}R^+$ process. It is unclear whether the rearrangement is a process of the neutral or cationic C₂BO species using the $\bar{N}R^+$ data alone. In the $\bar{C}R^+$ process, it is likely that $[CCBO]^-$ undergoes a two-electron oxidation to form the cation directly.⁵⁰ The $\bar{C}R^+$ and $\bar{N}R^+$ spectra are very similar to each other suggesting that the observed fragment peaks in both spectra arise due to decompositions occurring upon cation formation. The similarity in the $\bar{C}R^+$ and $\bar{N}R^+$ spectra may be due

to auto electron detachment from B-mass selected $[\text{CCBO}]^-$ before entering the first collision cell; the $^- \text{CR}^+$ would be indistinguishable from $^- \text{NR}^+$ in such a case. The high electron affinity of the CCBO neutral (calculated to be 4.8 eV, Table 6.1) suggests that $[\text{CCBO}]^-$ should not undergo electron detachment under the experimental conditions. This supposition was supported experimentally as follows; under ideal $^- \text{CR}^+$ conditions (collision gas in cell two only) two MS/MS experiments were carried out. The first was a normal $^- \text{CR}^+$ experiment, while the second was conducted with the NR voltage turned on (a so-called $^- \text{N}_{\text{metastable}} \text{R}^+$ experiment). No recovery signal is observed in the $^- \text{N}_{\text{metastable}} \text{R}^+$ experiment and so the $[\text{CCBO}]^-$ anion does not appear to undergo auto electron detachment.

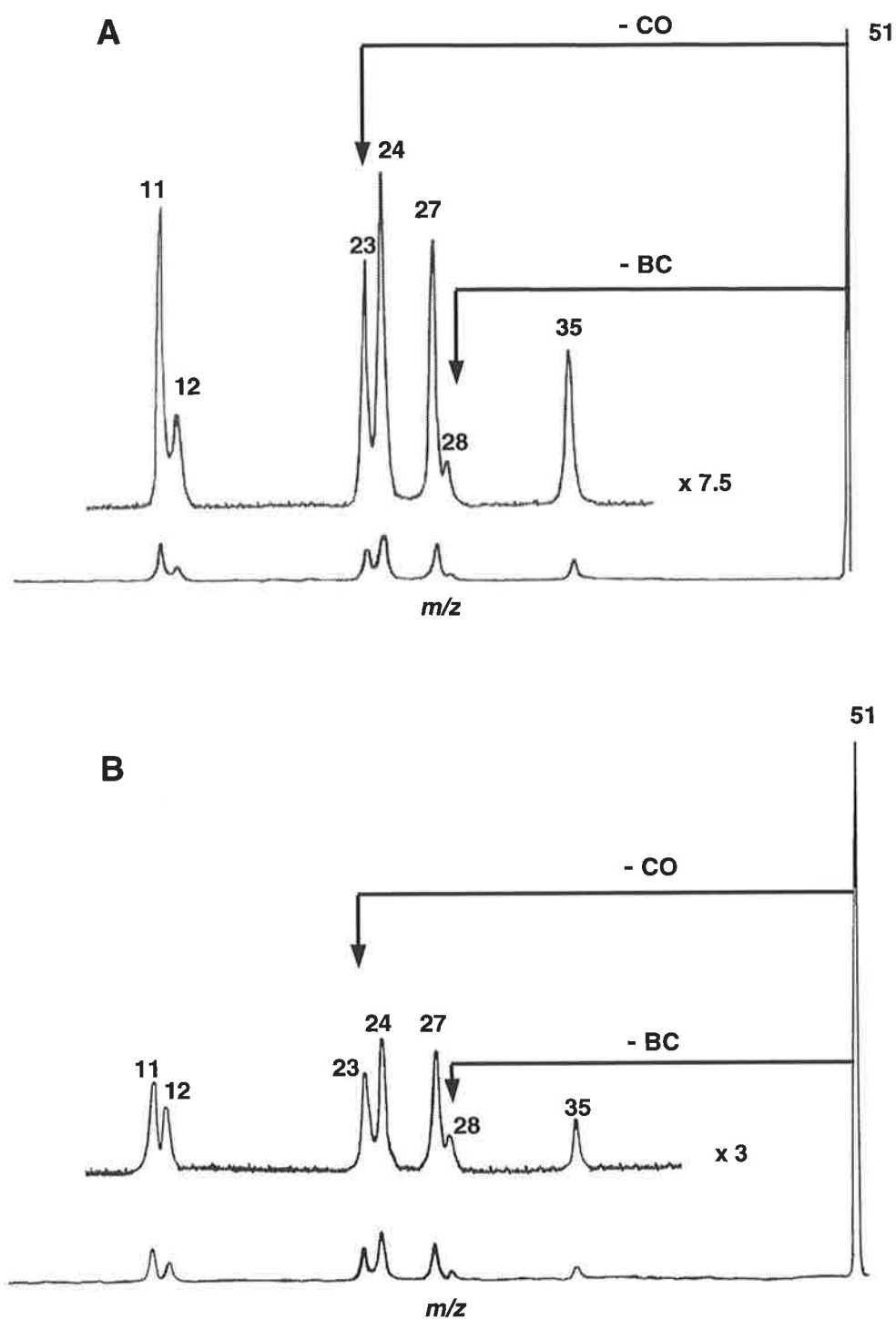


FIGURE 6.2 (A) ⁻CR⁺ and (B) ⁻NR⁺ mass spectra of the [CCBO]⁻ anion. For experimental conditions see Experimental Section.

Decomposition energies were calculated to provide additional insight into possible processes which may occur at the neutral and cation stages of the $\bar{\text{N}}\text{R}^+$ experiment, the results are listed in Tables 6.5 and 6.6 respectively. The loss of CO is endothermic from both neutral and cationic OCCB, however, it is more energetically favourable to occur from the neutral by 220 kJ mol^{-1} . Therefore an increased loss of CO in the $\bar{\text{N}}\text{R}^+$ spectrum (as compared to $\bar{\text{C}}\text{R}^+$) should be observed if the neutral rearranges to OCCB. Since the abundance of the peaks at m/z 23 and m/z 28 are similar in each spectrum, the loss of CO occurs from the cation, thus the vertical oxidation of the $[\text{CCBO}]^-$ anion yields the stable CCBO neutral.

TABLE 6.5 Energies of selected neutral $[\text{C}_2\text{BO}]$ dissociations. ^a

Parent Radical Connectivity	Fragment Species ^b			Energy (kJ mol^{-1}) ^c
CCBO	C	+	⁴ CBO	749
	O	+	CCB	698
	CC	+	BO	459
OCCB	O	+	CCB	682
	B	+	CCO	601
	⁴ BC	+	CO	409

a. Calculated at the MP4/aug-cc-pVTZ//MP2(full)/6-31G(d) level of theory. b. Full details given in Table 6.15. c. Relative to ²CCBO (-175.904292 Hartrees) and ²OCCB (-175.898210 Hartrees).

TABLE 6.6 Energies of selected $[\text{C}_2\text{BO}]^+$ dissociations. ^a

Parent Cation Connectivity	Fragment Species ^b			Energy (kJ mol^{-1}) ^c	
				from singlet	from triplet
[CCBO] ⁺	⁴ CC ⁺	+	BO	404	426
	CC	+	BO ⁺	437	459
	C ⁺	+	⁴ CBO	595	617
	O	+	³ CCB ⁺	574	597
[OCCB] ⁺	BC ⁺	+	CO	629	652
	⁴ BC	+	CO ⁺	762	786
	B ⁺	+	³ CCO	370	393
	O	+	³ CCB ⁺	769	792

a. Calculated at the MP4/aug-cc-pVTZ//MP2(full)/6-31G(d) level of theory. b. Full details given in Table 6.15. c. Relative to ¹CCBO⁺ (-175.432210 Hartrees), ³CCBO⁺ (-175.440459 Hartrees), ¹[OCCB]⁺ (-175.506080 Hartrees) and ³[OCCB]⁺ (-175.515076 Hartrees).

iii. Rearrangement of $[\text{CCBO}]^+$

It is proposed that the losses of CO and BC shown in Figure 6.2 are fragmentations of a decomposing cation, likely to have OCCB connectivity. The $[\text{CCBO}]^+$ cation is isoelectronic with CCCC, which is known to equilibrate its carbon atoms via the elusive rhombic C_4 intermediate. Does $[\text{CCBO}]^+$ undergo a similar conversion to $[\text{OCCB}]^+$ via the intermediacy of a rhombic structure? This was addressed theoretically using *ab initio* calculations. Geometries and energies of optimised $[\text{C}_2\text{BO}]^+$ cations are listed in Table 6.7. The triplet form of $[\text{CCBO}]^+$ is only 22 kJ mol^{-1} lower in energy than the corresponding singlet, and their structures are similar. Both the triplet and singlet forms of $[\text{CCBO}]^+$ will be accessible following Franck-Condon oxidation from the doublet neutral CCBO. The excess energy that the triplet cation has as a consequence of vertical Franck-Condon oxidation is calculated to be 20 kJ mol^{-1} [MP4SDTQ/aug-cc-pVTZ//MP2(full)/6-31G(d)], whereas singlet $[\text{CCBO}]^+$ has an excess Franck Condon energy of 34 kJ mol^{-1} .

The interconversions of triplet and singlet $[\text{CCBO}]^+$ to triplet and singlet $[\text{OCCB}]^+$ are shown in Figures 6.3 and 6.4 respectively. Details of geometries and energies of stable species are shown in Table 6.7, and of transition states in Table 6.8. Triplet and singlet $[\text{OCCB}]^+$ are global minima on their respective potential energy surfaces. The $^3[\text{OCCB}]^+$ cation is 196 kJ mol^{-1} lower in energy than $^3[\text{CCBO}]^+$, similarly $^1[\text{OCCB}]^+$ is 194 kJ mol^{-1} lower in energy than $^1[\text{CCBO}]^+$. Both rearrangement processes are therefore significantly exothermic. The triplet and singlet rearrangements are stepwise with the largest barriers in each being 88 and 116 kJ mol^{-1} respectively. The triplet and singlet processes can only proceed if additional excess energy (69 and 82 kJ mol^{-1} respectively) is available. Experimentally, the parent cation(s) produces the base peak of the $^-\text{CR}^+$ spectrum, with all

peaks due to fragment ions being of small abundance. The rearrangement peaks (formed by loss of CO and BC) are minor, suggesting that there must still be unrearranged $[\text{CCBO}]^+$ in this system. This is a consequence of the cation rearrangement being a slower reaction than the simple cleavage processes shown in the $^-\text{CR}^+$ spectrum, and the small time available between formation and fragmentation of the parent cations in the second collision cell. The thermochemistry of the observed dissociations (Table 6.6) show much higher energies required to effect simple cleavage compared with the rearrangements shown in Figures 6.3 and 6.4.

TABLE 6.7 Calculated properties of stable $[C_2BO]^+$ cations.

	C_1C_2BO 3_1	$\begin{array}{c} C_1 \\ \\ C_2 \end{array} B-O$ 3_7	$\begin{array}{c} C_1 \\ \\ C_2 \end{array} \begin{array}{c} C_1 \\ \\ B \end{array} O$ ${}^3_{12}$	OC_1C_2B 3_2
State	${}^3\Pi$	3B_2	${}^3A'$	${}^3A'$
Symmetry	$C_{\infty v}$	C_s	C_s	C_s
Relative Energy (kJ mol ⁻¹) ^a	0	0	72	-196
C_1C_2 (Å) ^b	1.208	1.282	1.317	1.351
C_2B	1.430	1.576	1.533	1.396
C_1B		1.576	1.696	
BO	1.292	1.312	1.291	
C_1O			1.649	1.132
C_1C_2B (°)	180.0	66.0	72.6	179.9
C_2BO	180.0	156.0	113.2	
C_2C_1O			105.0	180.0
C_1OB			69.3	

	C_1C_2BO 1_1	$\begin{array}{c} C_1 \\ \\ C_2 \end{array} B-O$ 1_7	$\begin{array}{c} C_1 \\ \\ C_2 \end{array} \begin{array}{c} C_1 \\ \\ B \end{array} O$ ${}^1_{12}$	OC_1C_2B 1_2
State	${}^1A'$	${}^1A'$	${}^1A'$	${}^1A'$
Symmetry	C_s	C_s	C_s	C_s
Relative Energy (kJ mol ⁻¹) ^a	22 (0)	35 (13)	75 (53)	-172 (-194)
C_1C_2 (Å) ^b	1.1918	1.220	1.29	1.342
C_2B	1.4292	1.418	1.47	1.394
C_1B		2.025	1.56	
BO	1.3168	1.315	1.45	
C_1O			1.36	1.134
C_1C_2B (°)	180.0	100.0	68.5	180.0
C_2BO	180.0	175.3	103.9	180.0
C_2C_1O			120.4	
C_1OB			67.2	

a. Energies are calculated at the MP4/aug-cc-pVTZ//MP2(full)/6-31G(d) level of theory and are relative to 3_1 (-175.440459 Hartrees). Relative energies given in parenthesis are relative to 1_1 (-175.432210 Hartrees). b. MP2(full)/6-31G(d) geometries.

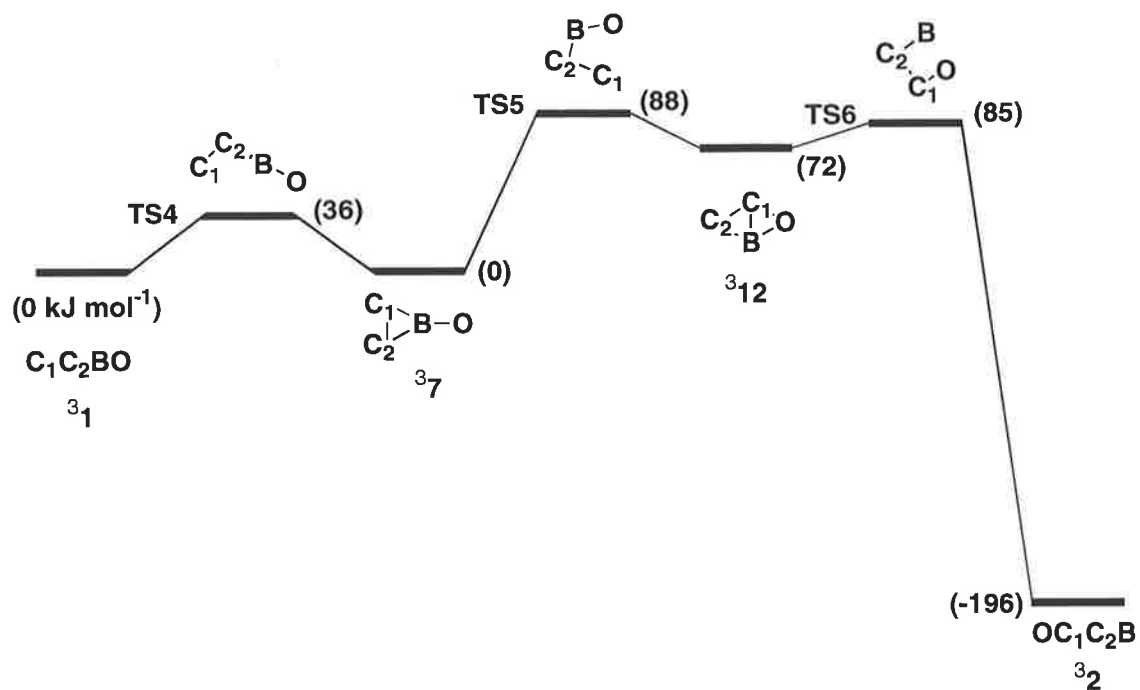


FIGURE 6.3 Calculated pathway for the rearrangement of ${}^3[\text{CCBO}]^+$ to ${}^3[\text{OCCB}]^+$. For full details see Tables 6.7 and 6.8.

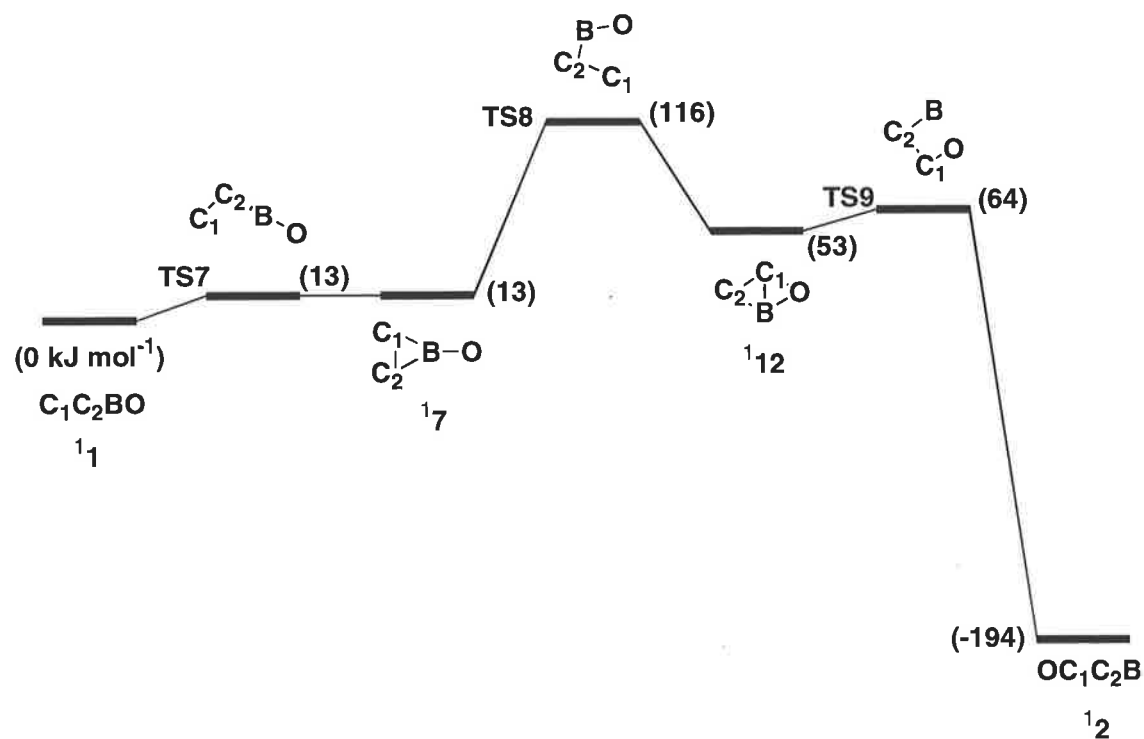
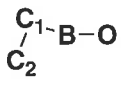
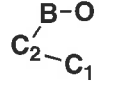
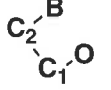
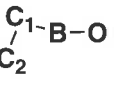
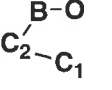
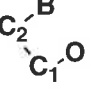


FIGURE 6.4 Calculated pathway for the rearrangement of ${}^1[\text{CCBO}]^+$ to ${}^1[\text{OCCB}]^+$. For full details see Tables 6.7 and 6.8.

TABLE 6.8 Calculated properties of transition states shown in Figures 6.3 and 6.4.

						
	TS4	TS5	TS6	TS7	TS8	TS9
State	$^3A'$	$^3A'$	$^3A'$	$^1A'$	$^1A'$	$^1A'$
Symmetry	C_s	C_s	C_s	C_s	C_s	C_s
Relative Energy (kJ mol $^{-1}$) ^a	36	89	85	35	138	86
				(13) ^b	(116) ^b	(64) ^b
C ₁ C ₂ (Å) ^c	1.206	1.284	1.327	1.210	1.269	1.320
C ₂ B	1.410	1.518	1.491	1.412	1.474	1.476
C ₁ B	2.152	1.760	1.617	2.204	1.723	1.648
BO	1.313	1.234		1.313	1.256	
C ₁ O			1.258			1.204
C ₁ C ₂ B (°)	110.4	77.3	69.8	114.2	77.5	72.0
C ₂ BO	178.3	129.0		178.7	129.4	
C ₂ C ₁ O			129.1			135.6

a. Energies are calculated at the MP4/aug-cc-pVTZ//MP2(full)/6-31G(d) level of theory and are relative to $^3\mathbf{1}$ (-175.440459 Hartrees). Relative energies given in parenthesis are relative to $^1\mathbf{1}$ (-175.432210 Hartrees). b. MP2(full)/6-31G(d) geometries.

iv. Conclusions

The neutral CCBO was formed by vertical one-electron oxidation of the corresponding anion [CCBO] $^-$. Collisional ionisation of the transient neutral gives rise to the [CCBO] $^+$ cation and more interesting loss of CO. Comparison of $^-NR^+$ and $^-CR^+$ data gives no insight to the behaviour of the neutral and indicates that the CCBO species is stable on the microsecond time scale of the experiment. Therefore the observed fragmentations in both spectra are cationic processes. In turn, this means that some of the [CCBO] $^+$ cations are energised and undergo a rearrangement process. Theoretical calculations employed to investigate the rearrangement found that the [CCBO] $^+$ cation may rearrange via a distorted rhombic intermediate to the more stable [OCCB] $^+$ cation. The analogous process for the neutral was also investigated but it required 150 kJ mol $^{-1}$ more than the energy required to effect the cationic rearrangement. Thus the CCBO neutral remains stable for the microsecond time scale of the $^-NR^+$ experiment.

B. Formation of CCCCBO in the Gas Phase

It has been shown that the linear borocumulene oxide with CCBO bond connectivity can be generated in the gas phase using the neutralisation-reionisation ($\bar{\text{NR}}^+$) technique. The CCBO neutral was determined to be stable to rearrangement under $\bar{\text{NR}}^+$ conditions. It would be interesting to generate larger members of the C_nBO series and investigate their behaviour under the same experimental conditions. The CCCCBO neutral is an ideal target for such a study since the known chemistry described in the previous section may easily be extended. This study addresses two questions, (i) can the CCCCBO neutral be formed from the corresponding anion in a $\bar{\text{NR}}^+$ experiment? and (ii) is the CCCCBO neutral stable to rearrangement under $\bar{\text{NR}}^+$ conditions?

i. The [CCCCBO] $^-$ Anion

The required [CCCCBO] $^-$ anion was generated in the chemical ionisation source by an analogous process to that used to generate the [CCBO] $^-$ anion. The collision induced mass spectrum (MS/MS) of this anion is dominated by the parent anion with any fragmentations being lost in the noise of the spectrum.* In analogy to the [CCBO] $^-$ anion, theory does predict a linear species of [CCCCBO] $^-$ connectivity. The electron affinity of the corresponding neutral CCCCBO is calculated † to be 5.8 eV. This value is 1.0 eV larger

* Preliminary CID measurements suggest that loss of BO occurs from this anion, however the fragment peak is extremely weak and we have experienced difficulties in confirming this result.

† Determined using the MP4STDQ/aug-cc-pVDZ//MP2(full)/6-31G(d) energies of -251.825142 and -251.611593 Hartrees for CCCCBO $^-$ and CCCCBO respectively.

neutralisation-reionisation process. The question remains whether enough energy is imparted into the system to effect any rearrangement of the system.

ii. The $\bar{\text{C}}\text{R}^+$ and $\bar{\text{N}}\text{R}^+$ Mass Spectra of $[\text{CCCCBO}]^-$

The $\bar{\text{C}}\text{R}^+$ and $\bar{\text{N}}\text{R}^+$ mass spectra of the $[\text{CCCCBO}]^-$ anion are shown in Figure 6.5. The $\bar{\text{N}}\text{R}^+$ spectrum is dominated by the recovery signal at m/z 75, indicating that the parent neutral(s) is stable on the time scale of the experiment. A number of the fragment ions observed in the $\bar{\text{N}}\text{R}^+$ spectrum are consistent with a species of CCCCBO connectivity: these are the losses of C, O, C_2 , BO, CBO, C_4 , C_2BO and C_3BO . However, there are a number of peaks that are not consistent with the CCCCBO connectivity: these are the losses of CO, C_2O , C_3O and C_4O . On inspection of the $\bar{\text{N}}\text{R}^+$ and $\bar{\text{C}}\text{R}^+$ spectra (Figure 6.5) it can be seen that the loss of CO and CBO are greater in the $\bar{\text{N}}\text{R}^+$ case. The increase in loss of CO is indicative of the partial rearrangement of the parent neutral prior to the decomposition that occurs upon ionisation to the cation. This is in contrast to the previous study of the CCBO system where no substantial difference between the $\bar{\text{N}}\text{R}^+$ and $\bar{\text{C}}\text{R}^+$ spectra was observed; this was attributed to the stability of the CCBO species and rearrangement of the cation $[\text{CCCBO}]^+$.

The calculated thermochemistry for selected dissociations of the C_4BO and $[\text{C}_4\text{BO}]^+$ systems are listed in Table 6.9 and 6.10 respectively. Decompositions involving loss of CO or BO are the least energetic for both neutral and cation, with those occurring from neutral C_4BO being more energetically favourable than the corresponding losses from the cation.

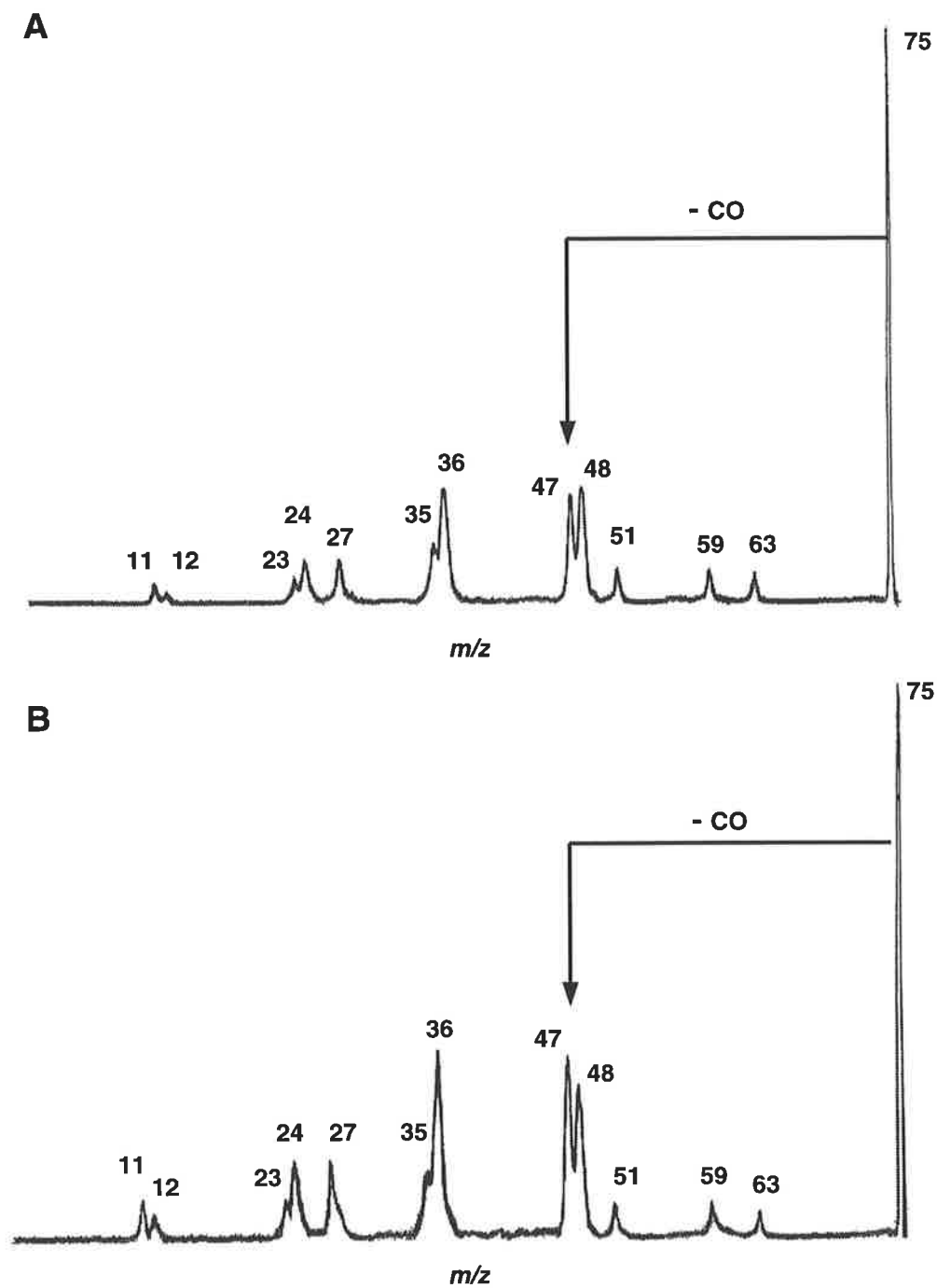


FIGURE 6.5 (A) CR^+ and (B) NR^+ mass spectra of the $[\text{CCCCBO}]^-$ anion. For experimental conditions see Experimental Section.

TABLE 6.9 Energies of selected neutral C_4BO dissociations. ^a

Parent Radical Connectivity	Fragment Species ^b			Energy (kJ mol ⁻¹)
CCCCBO	CCCC	+	BO	125
	CCC	+	CBO	464
OCCCCB	BCCC	+	CO	228
	BCC	+	CCO	462

a. Calculated at the MP4/aug-cc-pVDZ//MP2(full)/6-31G(d) level of theory. b. Full details given in Table 6.16.

TABLE 6.10 Energies of selected ^{cationic} neutral $[C_4BO]^+$ dissociations. ^a

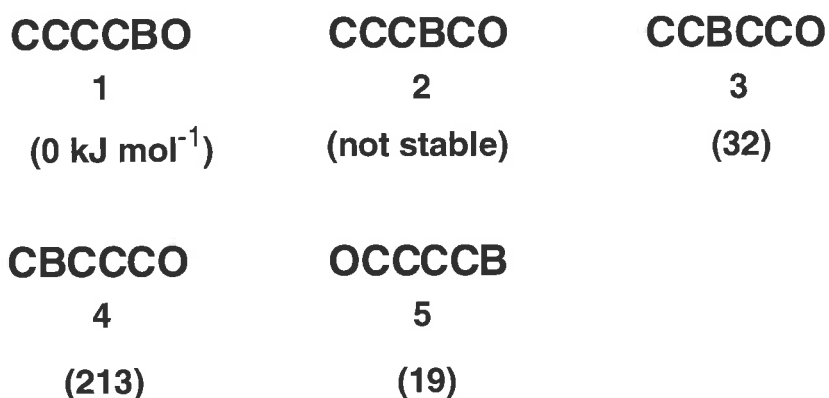
Parent Radical Connectivity	Fragment Species ^b			Energy (kJ mol ⁻¹)
$[CCCCBO]^+$	CCCC ⁺	+	BO	415
	CCCC	+	BO ⁺	340
	CCC ⁺	+	CBO	510
	CCC	+	CBO ⁺	509
$[OCCCCB]^+$	BCCC ⁺	+	CO	417
	BCCC	+	CO ⁺	953
	BCC ⁺	+	CCO	1067
	BCC	+	CCO ⁺	623

a. Calculated at the MP4/aug-cc-pVDZ//MP2(full)/6-31G(d) level of theory. b. Full details given in Table 6.16.

iii. Rearrangement of the C_4BO Neutral

As the carbon chain increases in the C_nBO series the possible number of distinct structural isomers increases dramatically. It is well beyond the scope and time constraints of this study to investigate all possible connectivities of a molecule containing one B atom, one O atom and four C atoms. Therefore we must limit our investigation to a few reasonable structures. Linear isomers are simple and as such are a good starting point for our theoretical investigation. This seems reasonable in light of the C_2BO system in which linear CCBO and OCCB neutrals were found to be significantly lower in energy than ten out of the remaining eleven stable isomers (Scheme 6.1). Also from the C_2BO study it was

observed that linear connectivities with a terminal O atom are more stable than those with a bridging O atom by between 244 and 489 kJ mol⁻¹. We limit the linear structures of interest initially to the five species shown in Scheme 6.4. Apart from CCCBCO (2)* all of the species shown are stable with linear geometries and have a ²Σ electronic state.

**SCHEME 6.4**

The geometries and energies of the optimised linear C₄BO neutrals are given in Table 6.11. Three of the four stable linear isomers are within 32 kJ mol⁻¹ of each other, while the CCCCBO neutral is the lowest in energy. Both OCCCCB and CCBCCO are low energy isomers that may contribute to the loss CO. The OCCCCB neutral is of particular interest since it may fragment to produce all losses in the ⁻NR⁺ spectrum unaccounted for by the CCCCBO connectivity. The OCCCCB neutral is just 19 kJ mol⁻¹ higher in energy than CCCCBO. This is comparable to the OCCB isomer of the C₂BO system, which was 16 kJ mol⁻¹ above the CCBO ground state. Rearrangement of the CCBO to OCCB via a rhombic

* The CCCBCO species could not be optimised due to the failure of the wavefunction to converge. It is therefore likely that such a species would not be stable.

intermediate was calculated to have a barrier of 267 kJ mol⁻¹. Does there exist a rearrangement of CCCCBO to OCCCCB? What is the energy required for the rearrangement to occur?

TABLE 6.11 Calculated properties of stable C₄BO neutrals shown in Scheme 6.4.

	C ₁ C ₂ C ₃ C ₄ BO 1	C ₁ C ₂ BC ₃ C ₄ O 3	C ₁ BC ₂ C ₃ C ₄ O 4	OC ₁ C ₂ C ₃ C ₄ B 5
State	² Σ	² Σ	² Σ	² Σ
Symmetry	C _{∞v}	C _{∞v}	C _{∞v}	C _{∞v}
Relative Energy (kJ mol ⁻¹) ^a	0	32	213	19
C ₁ C ₂ (Å) ^b	1.173	1.183		1.283
C ₂ C ₃	1.408		1.273	1.278
C ₃ C ₄	1.173	1.293	1.295	1.288
C ₄ B	1.491			1.354
C ₁ B			1.382	
C ₂ B		1.493	1.411	
C ₃ B		1.338		
BO	1.218			
CO		1.176	1.177	1.175

a. Energies are calculated at the MP4/aug-cc-pVTZ//MP2(full)/6-31G(d) level of theory and are relative to **1** (-251.6115927 Hartrees). b. MP2(full)/6-31G(d) geometries.

The simplest scenario to investigate is the formation of a six-membered intermediate from CCCCBO, which may then ring-open to form OCCCCB. This rearrangement was investigated at the MP4SDTQ/aug-cc-pVDZ//MP2(full)/6-31G(d) level of theory and is shown in Figure 6.6. Full details of transition states are given in Table 6.12. The cyclic intermediate (**6**) has a relative energy of 167 kJ mol⁻¹ and a barrier to its formation of 224 kJ mol⁻¹ (via **TS1**). If formed, it has sufficient excess energy to ring-open via **TS2** to form the OCCCCB species.

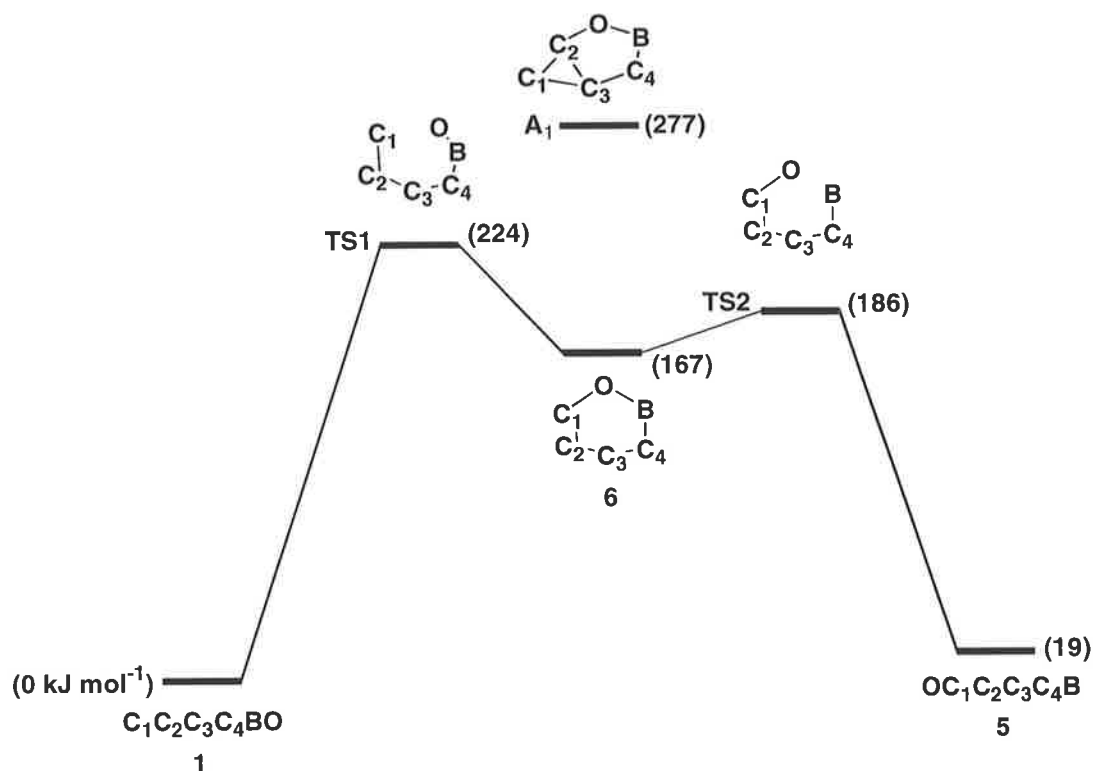
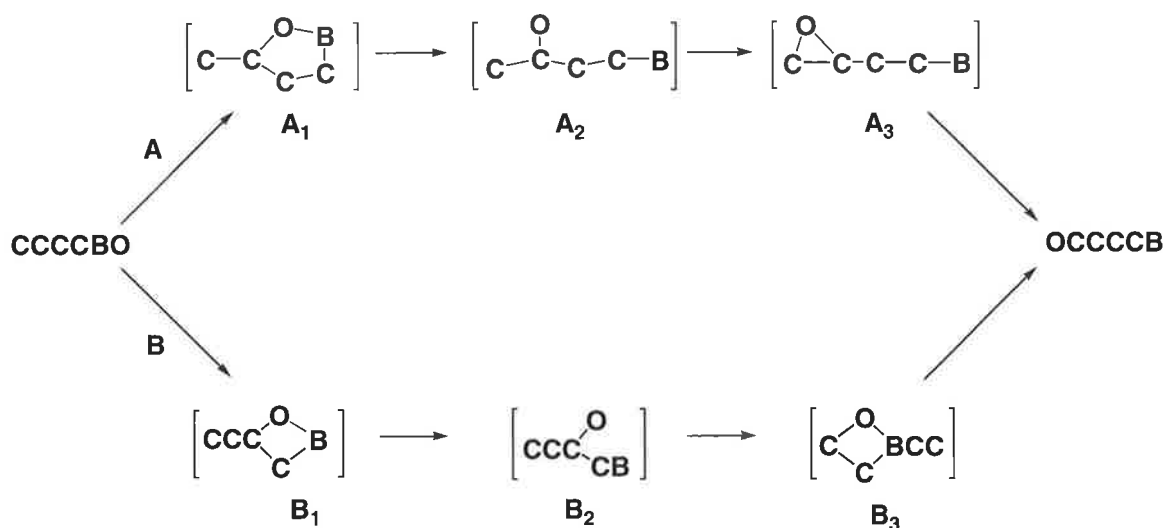


FIGURE 6.6 Calculated rearrangement of CCCCBO to OCCCCB via cyclic intermediate. For full details see Tables 6.11 and 6.12.

Two other pathways for the rearrangement of CCCCBO to OCCCCB are outlined in Scheme 6.6. The two processes involve the initial formation of either a five (**A**) or four (**B**) centred species. The intermediate **A**₁ is detailed in Table 6.12. It is slightly distorted with the branching carbon atom forming a C₃ ring system. Intermediate **A**₁ has a relative energy of 277 kJ mol⁻¹ compared to CCCCBO and is 53 kJ mol⁻¹ more energetic than **TS1** (see Figure 6.6). Therefore rearrangement via the six-membered intermediate is more energetically favourable than via the five-membered intermediate. Similarly, process **B** as shown in Scheme 6.5 may be ruled out in favour of the proposed six-centred mechanism. No intermediate corresponding to **B**₁ could be found, but **B**₂ (Table 6.12) lies 583 kJ mol⁻¹ higher in energy than the CCCCBO neutral.



SCHEME 6.5

TABLE 6.12 Calculated properties of intermediates and transition states for the rearrangement of CCCCBO as shown in Figure 6.6 and Scheme 6.5.

	6	TS1	TS2	A ₁	B ₂
State	² A'	² A'	² A'	² A'	² A'
Symmetry	C _s	C _s	C _s	C _s	C _s
Relative Energy (kJ mol ⁻¹) ^a	167	224	186	277	583
C ₁ C ₂ (Å) ^b	1.300	1.212	1.302	1.358	1.178
C ₂ C ₃	1.360	1.402	1.379	1.478	1.501
C ₃ C ₄	1.305	1.237	1.304	1.266	1.446
C ₄ B	1.415	1.487	1.448	1.495	1.333
C ₁ O	1.393		1.235		
C ₃ O					1.175
BO	1.362	1.245		1.441	
C ₂ O				1.341	
C ₁ C ₂ C ₃ (°)	94.8	106.5	82.3	63.4	179.3
C ₂ C ₃ C ₄	164.4	170.0	168.1	88.9	107.1
C ₃ C ₄ B	78.2	84.7	92.5	126.1	177.2
C ₄ BO	149.9	162.9		99.3	
C ₂ C ₁ O	133.7		160.8		
C ₂ C ₃ O					124.4
C ₁ OB	99.1				
C ₂ OB				100.3	

a. Energies are calculated at the MP4/aug-cc-pVDZ//MP2(full)/6-31G(d) level of theory and are relative to CCCCBO (-251.6115927 Hartrees). b. MP2(full)/6-31G(d) geometries.

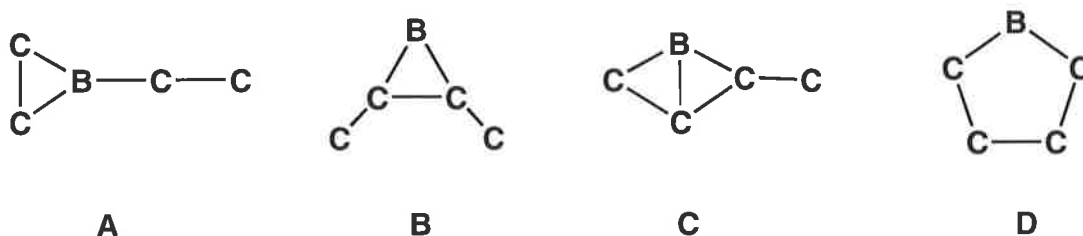
iii. Conclusions

The neutral CCCCBO may be formed by vertical one-electron oxidation of the corresponding anion [CCCCBO]⁻. Collisional ionisation of the transient neutral gives rise to recovery signal indicating that the parent neutral(s) is stable for the microsecond time scale of the experiment. More interesting is the loss of CO observed in the ⁻NR⁺ spectrum. Comparison of ⁻NR⁺ and ⁻CR⁺ data show that neutral CCCCBO rearranges (possibly to OCCCCB) on the microsecond time scale of the ⁻NR⁺ experiment. This should be contrasted with neutral CCBO which does not rearrange under ⁻NR⁺ conditions. Theory suggests that the CCCCBO system rearranges through a six-membered intermediate to form the OCCCCB neutral, a mechanism not available to CCBO.

C. Borocumulenes of CCBCC Connectivity

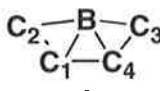
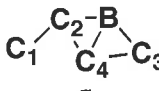
i. The CCBCC Species

We now turn our attention to the investigation of borocumulenes with CCBCC connectivity. The symmetrical nature of CCBCC should simplify the synthesis of suitable precursors as well as any theoretical studies into the system. Since studies on borocumulenes have concentrated on those possessing a terminal B atom we must first ascertain whether the target CCBCC neutral is stable from a theoretical viewpoint. There are three distinct linear connectivities of the C_4B system; CCBCC (1), BCCCC (2) and CBCCC (3). Both BCCCC and CBCCC optimise at the B3LYP/6-31G(d) level of theory to linear species with $^2\Sigma$ electronic states, while CCBCC optimises to a slightly bent geometry with C_{2v} symmetry and a 2B_2 electronic state (see Table 6.13). The lowest energy isomer is BCCCC, which is 178 kJ mol^{-1} lower in energy than the most energetic isomer CBCCC. The target of this study CCBCC is only 19 kJ mol^{-1} higher in energy than BCCCC. It should be possible to generate the CCBCC neutral by a $\bar{N}R^+$ process provided that a suitable precursor anion may be generated. It is possible that the CCBCC neutral could rearrange during the $\bar{N}R^+$ process. Any rearrangement of CCBCC would involve the initial formation of one or more of the cyclic structures shown in Scheme 6.6.



SCHEME 6.6

TABLE 6.13 Calculated properties of stable C₄B neutrals.

	C ₁ C ₂ BC ₃ C ₄	BC ₁ C ₂ C ₃ C ₄	C ₁ BC ₂ C ₃ C ₄		
	1	2	3	4	5
State	² B ₂	² Σ	² Σ	² A ₂	² A'
Symmetry	C _{2v}	C _{∞v}	C _{∞v}	C _s	C _s
Relative Energy (kJ mol ⁻¹) ^a	0	-19	159	16	80
C ₁ C ₂ (Å) ^b	1.277	1.276		1.301	1.307
C ₂ C ₃		1.297	1.282		
C ₃ C ₄	1.277	1.285	1.306	1.301	1.333
C ₁ C ₄				1.412	1.656
C ₁ B	1.413	1.367	1.373	1.576	
C ₂ B	1.413		1.405	1.606	1.481
C ₃ B					1.481
C ₄ B					1.580
C ₁ C ₂ B, C ₄ C ₃ B	158.4				
C ₂ BC ₃	179.2				
C ₂ C ₁ C ₄				130.5	61.1
C ₁ C ₄ C ₃				130.5	166.8
C ₄ C ₃ B				65.7	68.1
C ₂ BC ₃				149.7	110.9

a. Energies are calculated at the CCSD(T)/aug-cc-pVDZ//B3LYP/6-31G(d) level of theory and are relative to **1** (-176.453758 Hartrees). b. B3LYP/6-31G(d) geometries.

Isomer **A** (Cyc-C₂B-CC) optimises to a transition state with C_{2v} symmetry (Table 6.14) and involves the degenerate rearrangement of carbons 1 and 2. There is no probe for monitoring this process and so if it does occur under ⁻NR⁺ conditions it will not be observed. Cyclic isomers **B** and **D** both collapse to form a five-centred cyclic isomer (**4**), the geometry of which is detailed in Table 6.13. The five-centred species **4** has an energy just 16 kJ mol⁻¹ above that of the CCBCC isomer. The remaining isomer **C** optimises to either intermediate **4** or **5** (Table 6.13) depending on the initial C₁-C₂-C₄ angle. This indicates that isomer **C** lies close to a transition state linking intermediates **4** and **5** (see discussion below).

Using theoretical methods, we have investigated the reaction coordinate for the possible rearrangement of the C₄B neutral. The results are summarised in Figure 6.7 with full

details of minima and transition states given in Tables 6.13 and 6.14. The barrier for rearrangement of CCBCC through **TS1** to the cyclic isomer is 79 kJ mol^{-1} . Two other transition states were located on the potential energy surface and are included in Figure 6.7. Both essentially involve the interconversion of intermediates **5** and **6**, however when followed sequentially also provide a mechanism for the scrambling of the carbon atoms.

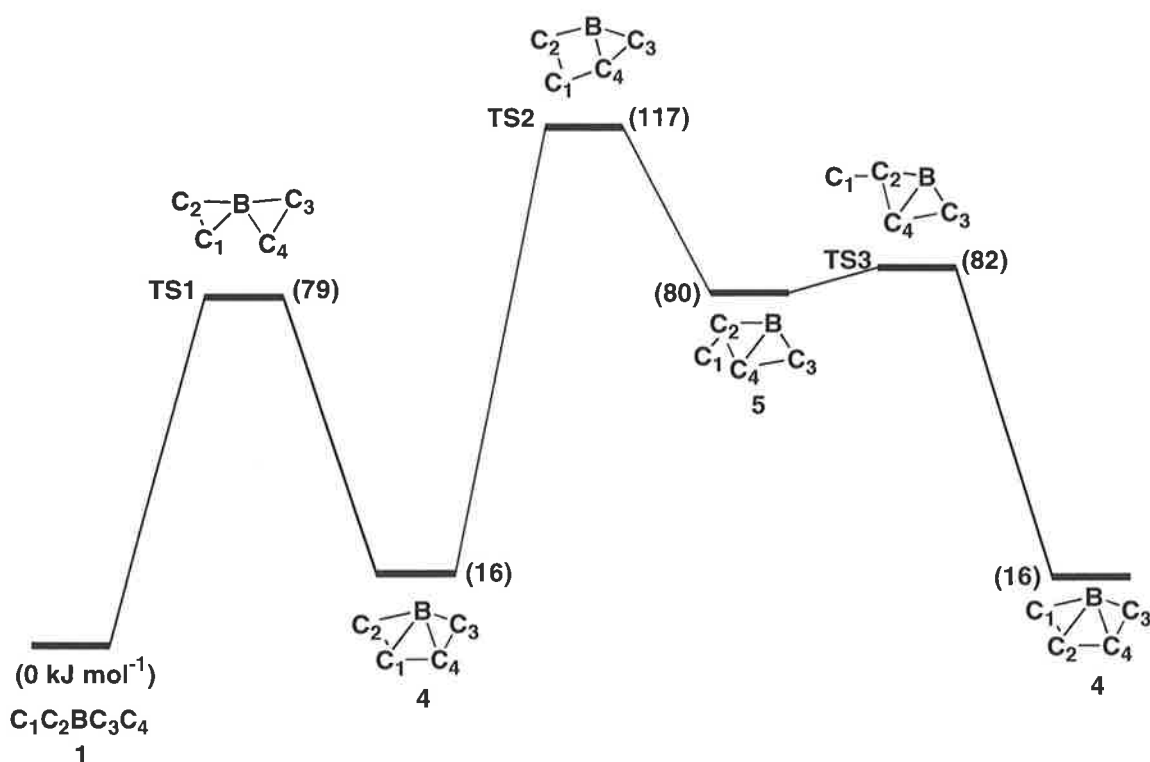
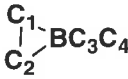
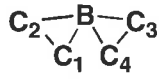
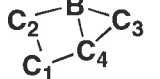
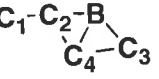


FIGURE 6.7 Calculated reaction coordinates for the rearrangement of CCBCC to the cyclic C_4B isomers.

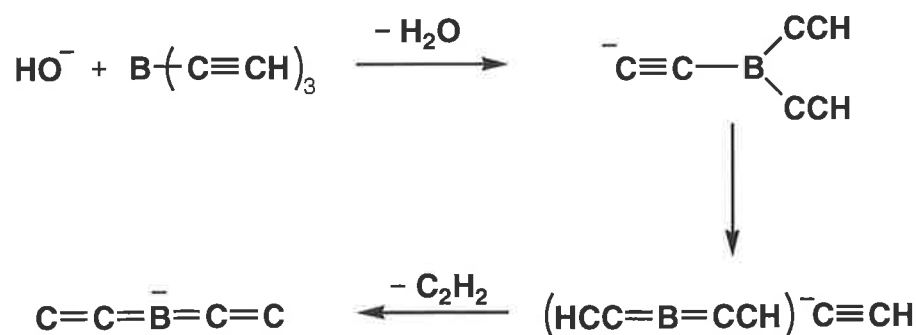
TABLE 6.14 Calculated properties of transition states shown in Figure 6.7.

				
		TS1	TS2	TS3
State	2A_1	–	${}^2A'$	${}^2A'$
Symmetry	C_{2v}	C_1	C_s	C_s
Relative Energy (kJ mol $^{-1}$) ^a	97	79	117	82
C ₁ C ₂ (Å)	1.275	1.287	1.320	1.304
C ₃ C ₄	1.224	1.330	1.330	1.319
C ₁ B		1.647		
C ₂ B	1.518	1.509	1.503	1.506
C ₃ B	1.476	1.453	1.460	1.488
C ₄ B		1.741		1.576
C ₁ C ₂ B	65.2	71.7	108.8	155.0
C ₂ BC ₃	155.2	148.6	126.9	109.8
C ₄ C ₃ B	180.0	77.3	68.0	68.0
C ₁ C ₂ BC ₃		-17.6		
C ₂ BC ₃ C ₄		-4.0		

a. Energies are calculated at the CCSD(T)/aug-cc-pVDZ//B3LYP/6-31G(d) level of theory and are relative to **1** (-176.453758 Hartrees). b. B3LYP/6-31G(d) geometries.

ii. The $[B(CCH)_3]^-$ Radical Anion as Precursor to the $[CCBCC]^-$ Anion

The next stage of the investigation is the attempted generation of an anionic species with the required bond connectivity. Boron triacetylide adducts are easily synthesised by the reaction between boron trifluoride and sodium acetylides.^{334,335} The $B(CCH)_3$ ·pyridine adduct was introduced into the source of the mass spectrometer liberating neutral $B(CCH)_3$ as a useful precursor for borocumulenic species. The expected reaction sequence is outlined in Scheme 6.7. Deprotonation effected by reaction with HO^- followed by loss of C_2H_2 should give result in the target precursor anion $[CCBCC]^-$.



SCHEME 6.7

The key to the above synthesis is the deprotonation reaction which, unfortunately, is not observed. Electron capture of the precursor is favoured over deprotonation and formation of the molecular radical anion $[\text{B}(\text{CCH})_3]^-$ occurs. The collision induced mass spectrum (MS/MS) of the $[\text{B}(\text{CCH})_3]^-$ radical anion is shown in Figure 6.8. The major processes that occur upon collision are those involving sequential H loss and loss of the $\cdot\text{CH}$ radical to produce m/z 85, 84, 83 and 73 respectively. Loss of the $\cdot\text{CCH}$ radical from $[\text{B}(\text{CCH})_3]^-$ gives a peak at m/z 61 corresponding to $[\text{HCCBCCH}]^-$. A peak due to the target anion $[\text{CCBCC}]^-$ is observed at m/z 59 but it is only a minor peak. Unfortunately this species is not produced in the ion source of the mass spectrometer and thus cannot be used as a precursor to CCBCC in a ${}^-\text{NR}^+$ experiment.

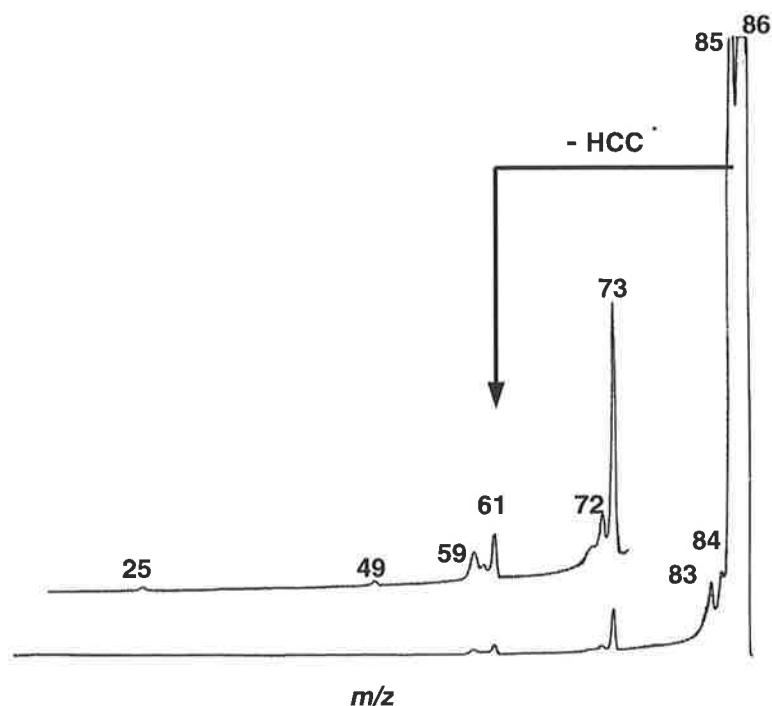


FIGURE 6.8 Collision induced mass spectrum (MS/MS) of the $[B(CCH)_3]^-$ anion. For experimental conditions see Experimental Section.

ii. Formation of HCCBCCH from $[HCCBCCH]^+$

The ${}^-\text{CR}^+$ mass spectrum of the $[B(CCH)_3]^-$ radical anion is shown in Figure 6.9. It shows more pronounced fragmentations than the CID mass spectrum (Figure 6.8). Major peaks are formed by losses of H^\cdot , ${}^-\text{CCH}$ and C_2H_2 . The fragment cation at m/z 61 corresponding to the $[HCCBCCH]^+$ cation is the second largest peak in the spectrum. This is of much greater intensity than the corresponding anion in the CID mass spectrum (Figure 6.8). This suggests the possibility that the $[HCCBCCH]^+$ cation may be formed in the ion source of the mass spectrometer from the precursor cation $[B(CCH)_3]^+$.

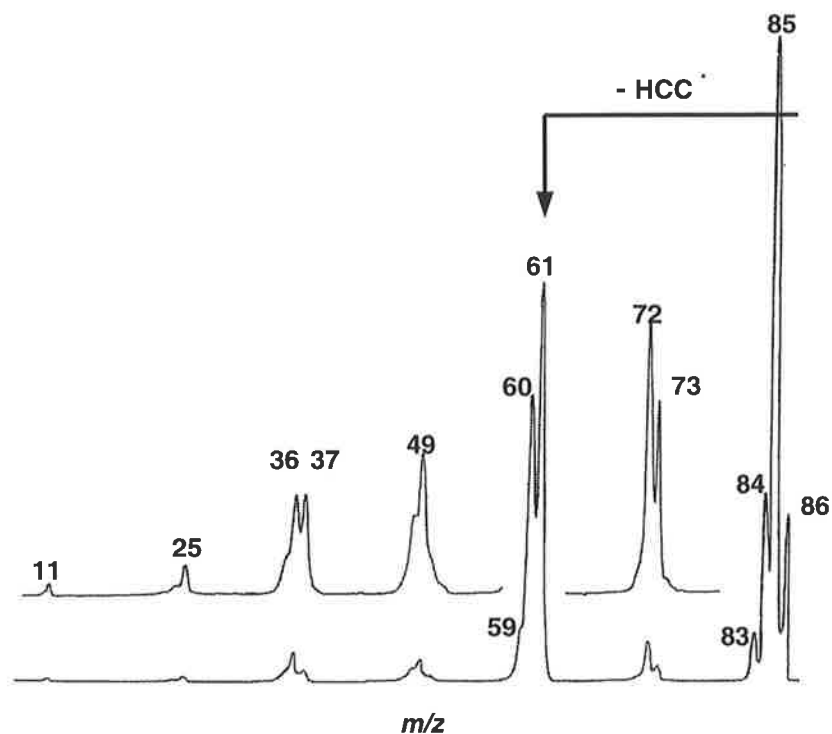


FIGURE 6.9 Charge reversal ($^{-}CR^{+}$) mass spectra of the $[B(CCH)_3]^{-}$ Anion. For experimental conditions see Experimental Section.

As anticipated, the $[HCCBCCH]^{+}$ cation (m/z 61) is a major peak formed by dissociative ionisation of $[B(CCH)_3]^{+}$ in the ion source of the mass spectrometer. Both CID and $^{+}NR^{+}$ experiments were carried on the B-mass selected cation at m/z 61: these spectra are shown in Figure 6.10. Under CID conditions the expected losses of H \cdot , \cdot CH and \cdot CCH are observed, forming m/z 60, 48 and 36 respectively. Loss of 12 Da., which is either loss of C or BH, indicates that hydrogen transfer is occurring. Of greater interest is the loss of B (11 Da.). These data indicate that some rearrangement of the carbon/boron framework is occurring for energised $[HCCBCCH]^{+}$.

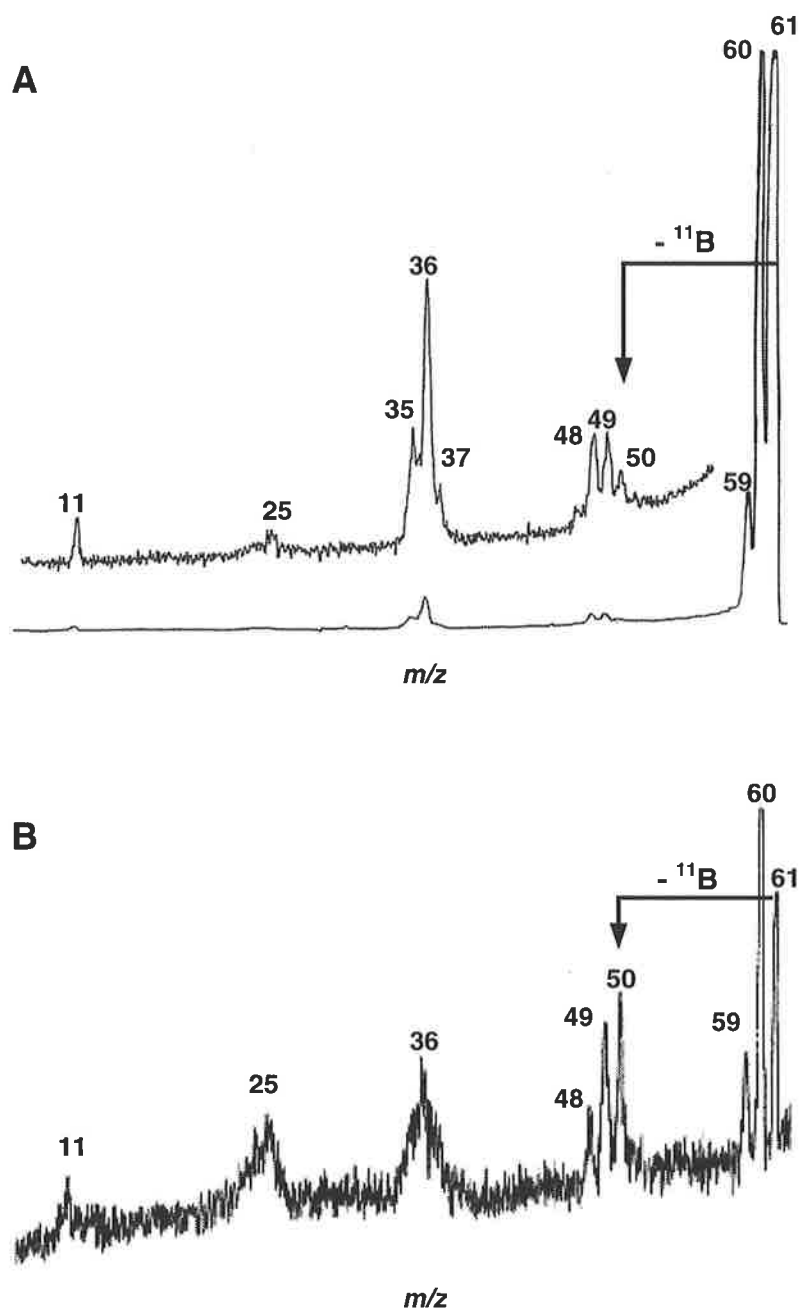


FIGURE 6.10 (A) Collision induced (MS/MS) and (B) $^{+}\text{NR}^{+}$ mass spectra of $[\text{HCCBCCH}]^{+}$. For experimental conditions see Experimental Section.

The $^{+}\text{NR}^{+}$ spectrum of the m/z 61 cation is much weaker in intensity than the CID mass spectrum but it does show similar fragment peaks. The recovery signal at m/z 61 indicates that the neutral(s) is stable for the microsecond time scale of the experiment. It is

interesting that the loss of B in the $^+NR^+$ spectrum is greater than the analogous loss in the CID mass spectrum, indicating that the transient neutral formed by electron addition to the cation is rearranging the carbon/boron framework within its lifetime. Theoretical investigations into the non-hydrogenated system C_4B suggested that the neutral with CCBCC connectivity might rearrange to the more stable BCCCC species via a five-membered cyclic intermediate (*cyc*- C_4B , Table 6.13). It is possible that an analogous process may occur for the HCCBCCH species. This is currently under investigation and due to time constraints no results are currently available.

iv. Conclusions

Investigations into the possible substitution of boron into the central position of a cumulenic molecule have been described. The pure borocumulene target CCBCC was observed as either a fragment anion or cation under CID or $^+CR^+$ conditions respectively. Theoretical data indicated that the CCBCC neutral may rearrange upon formation to the more stable BCCCC neutral. No such CCBCC ionic species can be generated in the ion source of the mass spectrometer to allow for its oxidation/reduction to the corresponding CCBCC neutral. The $[HCCBCCH]^+$ cation may be formed by dissociation of $[B(CCH)_3]^+$ in the ion source of the mass spectrometer. Successful neutralisation of this cationic species is indicated by the recovery signal in a $^+NR^+$ experiment. The loss of B from the neutral under $^+NR^+$ conditions provides direct evidence for backbone rearrangement of the transient HCCBCCH neutral.

3. EXPERIMENTAL

A. Mass Spectrometric Methods

All mass spectra were recorded using a modified VG ZAB 2HF mass spectrometer with BE configuration, where B and E represent magnetic and electric sectors, respectively. The $[\text{CCBO}]^-$ and $[\text{CCCCBO}]^-$ anions were generated by chemical ionisation (CI). The precursor in each case was placed in a small glass capillary tube which was then drawn out in a flame to create a very fine aperture, allowing for a slow steady release of sample vapour upon heating. The capillary was inserted into the CI source via the direct probe; the probe tip was heated to 60 - 80 °C to generate a background pressure of *ca.* 10^{-5} Torr inside the source housing. CI was effected using SF_6 as a reagent gas (to liberate the reagent ions F^- : this is a modification²⁷⁰ of the Squires *bis* $\text{S}_{\text{N}}2(\text{Si})$ reaction with F^-/NF_3 ²²) at a measured pressure of *ca.* 10^{-4} Torr inside the source housing. The $[\text{B}(\text{CCH})_3]^-$ radical anion was formed by electron capture of $\text{B}(\text{CCH})_3$. The instrument was operating in negative ion chemical ionisation mode. The $[\text{HCCBCCH}]^+$ cations were generated by dissociative electron impact (EI) ionisation of $\text{B}(\text{CCH})_3$ with the instrument operating in positive ionisation mode. Typical ion source conditions (negative ion) were as follows: source temperature 200 °C, repeller voltage -0.5 V, ion extraction voltage 7 kV, mass resolution $m/\Delta m \geq 1500$.

Collision induced dissociation (CID) of B-mass selected ions was effected in collision cells positioned between B and E. Argon was used as a target gas. The pressure of the collision gas in the cell was maintained such that 80% of the parent ion beam was transmitted through the cell, producing essentially single collision conditions.³⁰ Product ions resulting from CID were recorded by scanning the electric sector E.

Neutralisation-reionisation^{40,41,305-307} ($\bar{\text{NR}}^+$) experiments were performed for B-mass selected anions utilising the dual collision cells located between sectors B and E. Neutralisation of the anions was achieved by collisional electron detachment using O_2 at 80% transmittance as collision gas, while reionisation to cations was achieved by collision of the neutrals with O_2 , again at 80% transmittance. Any ions remaining after the first collision event were deflected from the primary neutral beam using an electrode maintained at a high voltage (1.5 kV) positioned before the second collision cell. In order to detect a reionisation signal due to the parent, the neutral species must be stable for approximately one microsecond. $^+\text{NR}^+$ experiments were carried out under using similar conditions as for $\bar{\text{NR}}^+$ with the following exceptions: instrument operated in positive ionisation mode, while xenon (collision cell 1) and oxygen (collision cell 2) were used as collision gases.

Charge reversal ($\bar{\text{CR}}^+$)^{31,35,110} of B-mass selected anions was effected by collision with oxygen in one of the collision cells, allowing 80% transmittance of the main beam and thus producing essentially single collision conditions.³⁰ $\bar{\text{CR}}^+$ spectra were then recorded as for the CID experiment except that the voltage of the electric sector was reversed in order to allow the passage of positive ions.

B. Synthetic Methods

$\text{B}(\text{CCH})_3 \cdot \text{pyridine}$ was prepared by a known synthetic procedure.³³⁵

(1-Trimethylsilylethynyl)diisopropoxyborane was prepared using a modified reported procedure.^{336,337} Trimethylsilylacetylene (4.2 cm^3 , 29.7 mmol) in anhydrous diethyl ether

(30 cm³) was cooled to -78°C under nitrogen, and *n*-butyllithium in hexane (2.4M, 12.5 cm³, 30.0 mmol) added over a period of 30 min. The organolithium reagent was then slowly added at -78°C to tri-*isopropyl* borate (7.0 cm³, 29.7 mmol) in diethyl ether (15.0 cm³) and the reaction maintained at -78°C for 2 hr. Anhydrous hydrogen chloride in diethyl ether (2.0M, 15.0 cm³, 30.0 mmol) was added and the mixture allowed to warm to 20°C. The lithium chloride was removed and the remaining solvent removed *in vacuo*. Distillation of the residue at 80°C/7mm Hg, gave the title compound (4.8g, 70% yield). ¹H nmr (200 MHz, in CDCl₃): δ 0.19 (s, 9H), 1.16 (d, 2x 6H, J = 6.1), 4.56 (septet, 2x 1H, J = 6.1).

(1-Trimethylsilylbutadiynyl)diisopropoxyborane was prepared as follows.

To bis(trimethylsilyl)butadiyne (1.0 g, 5.2 mmol) in anhydrous diethyl ether (30 cm³) at 20°C under nitrogen was added, methyl lithium lithium bromide complex in diethyl ether (1.5M, 4.0 cm³, 6.0 mmol) and the mixture allowed to stir for 16hr at 20°C. This organolithium reagent was then slowly added to tri-*isopropyl* borate (1.4 cm³, 6.1 mmol) in diethyl ether (20 cm³) at -78°C and the reaction maintained at -78°C for 4 hr. Anhydrous hydrogen chloride in diethyl ether (2.0M, 3.0 cm³, 6.0 mmol) was added and the mixture allowed to warm to 20°C. The precipitate was removed and the remaining solvent removed *in vacuo*. Any remaining tri-*isopropyl* borate and tri-*isopropyl* alcohol was removed by distillation at 90°C/10mm Hg to give product (0.6 g, 46 % yield).* ¹H nmr

* Attempts to further purify the compound led to decomposition. Mass spectrometric experiments were therefore carried out on samples which were >95% pure by nmr.

(200 MHz, in CDCl₃): δ 0.20 (s, 9H), 1.12 (d, 2x 6H, J = 6.2), 4.55 (septet, 2x 1H, J = 6.2).

C. Theoretical Methods

Geometry optimisations were carried using either the MP2(full) or B3LYP theoretical methods^{83,84} combined with the modest 6-31G(d) basis set. Stationary points on the potential energy surface were characterised as either minima (no imaginary frequencies) or transition structures (one imaginary frequency) by calculation of the frequencies using analytical gradient procedures. Intrinsic reaction coordinate (IRC) calculations were used to examine the reaction path on the potential energy surface leading away from a given transition state, thus confirming connection between minima and the transition state. The calculated frequencies were also used to determine zero-point vibrational energies which were then scaled⁸⁹ by 0.9661 [MP2(full)/6-31G(d)] or 0.9806 [B3LYP/6-31G(d)] and used as a zero-point correction for the electronic energies calculated at the respective levels of theory as well as at higher levels of theory. Higher level single point energies were carried out using the MP4 or CCSD(T) methods^{239,240} with the Dunning's aug-cc-pVDZ basis set.^{237,238} All calculations were carried out using the Gaussian 98 suite of programs²⁴¹ using the alpha server at the Australian Partnership for Advanced Computing National Facility (Canberra).

5. APPENDIX

TABLE 6.15 Properties of fragments used for the C₂BO dissociation energies.

	C ₁ C ₂ B ₃	C ₁ B ₂ O ₃	C ₁ C ₂ O ₃	CC	BO
Anion					
State	¹ Σ	³ Σ	² Π	² Σ _g	¹ Σ
Energy ^a	-100.753722	-137.937762	-151.150947	-75.934814	-99.997781
Bond (1-2) ^b	1.2809	1.5124	1.3103	1.2831	1.2547
Bond (2-3)	1.4583	1.2534	1.2338		
Neutral					
State	² A ₁	⁴ Σ	³ Σ	¹ Σ _g	² Σ
Energy	-100.649083	-137.830466	-151.066900	-75.825448	-99.903830
Bond (1-2)	1.2885	1.4863	1.3760	1.2638 *	1.2164 †
Bond (2-3)	1.5027	1.2232	1.1718		
Cation					
State	³ Σ	¹ Σ	² Π	⁴ Σ _g	¹ Σ
Energy	-100.223930	-137.431504	-150.663097	-75.374512	-99.440323
Bond (1-2)	1.1942	1.5618	1.5791	1.4029	1.2810
Bond (2-3)	1.4321	1.2341	1.1282		
	BC	CO	O	C	B
Anion					
State	¹ Σ	² Π	doublet	quartet	triplet
Energy	-62.603966	-113.13182	-75.040595	-37.834904	-24.612164
Bond	1.3794	1.2483			
Neutral					
State	⁴ Σ	¹ Σ	triplet	triplet	doublet
Energy	-62.549314	-113.193005	-74.989324	-37.788367	-24.602338
Bond	1.4853	1.1502			
Cation					
State	³ Π	² Σ	doublet	doublet	Singlet
Energy	-62.073525	-112.666334	-74.339305	-37.374964	-24.298274
Bond	1.3119	1.3173			

a. Energies calculated at the MP4/aug-cc-pVTZ//MP2(full)/6-31G(d) level of theory. b. MP2(full)/6-31G(d) geometries.

TABLE 6.16 Properties of fragments used for the C₄BO dissociation energies.

	C ₁ C ₂ C ₃ C ₄	B ₁ C ₂ C ₃ C ₄	CCC	BCC
Neutral				
State	¹ Σ _g	⁴ Σ	¹ Σ _g	² A ₁
Energy	-151.769941	-138.443109	-113.753838	-100.524051
Cation				
State	² Π	³ Σ	² Σ _u	³ Σ
Energy	-151.283182	-138.038754	-113.360056	-99.961432
	CCO	CBO	CO	BO
Neutral				
State	³ Σ	⁴ Σ	¹ Σ	² Σ
Energy	-150.904102	-137.681137	-113.074273	-99.794098
Cation				
State	² Π	¹ Σ	² Σ	¹ Σ
Energy	-150.510546	-137.287542	-112.465744	-99.335796

a. Energies calculated at the MP4/aug-cc-pVDZ//MP2(full)/6-31G(d) level of theory. b. MP2(full)/6-31G(d) bond lengths (Å): C₁C₂C₃C₄, neutral: C₁C₂, 1.250, C₂C₃, 1.272, C₃C₄, 1.250, cation: C₁C₂, 1.230, C₂C₃, 1.284, C₃C₄, 1.230. BC₁C₂C₃, neutral: BC₁, 1.390, C₁C₂, 1.294, C₂C₃, 1.304, cation, BC₁, 1.420, C₁C₂, 1.369, C₂C₃, 1.196. All other geometries are listed in Table 6.15.

* See 960 NIST database, CC = 1.2095 Å and BO = 1.2925 Å.

CHAPTER 7

SUMMARY AND CONCLUSIONS

1. EXPERIMENTAL STUDIES

Throughout this work anions have been generated by chemical ionisation or resonance capture of precursor molecules. Chemical ionisation was effected by either deprotonation of a neutral organic substrate or by the DePuy desilylation method. The desilylation method was employed for the generation of anions where either site specific charged centres or specific bond connectivities were required. For example, in the study of selected organic anions the *ortho*, *meta* and *para* isomers of $(\text{C}_6\text{H}_4)^-\text{CO}_2\text{Me}$ and $(\text{C}_6\text{H}_4)^-\text{OCO}_2\text{Me}$ were unequivocally generated. Syntheses of cumulenenic systems with known bond connectivity were also generated by the desilylation technique. These syntheses involved the initial removal of one or two trimethylsilyl groups by reaction of a suitably synthesised precursor with either HO^- (from H_2O) or F^- (from SF_6), followed by subsequent neutral losses to form the required anion. In addition, the generation of the linear $[\text{CCC}]^-$ radical anion involved *in situ* formation of a carbene by deprotonation of a tosyl hydrazone functionality. In one study, positive ions were generated in the source of the mass spectrometer by dissociative electron impact ionisation. Once the ions were formed, mass spectrometry was used as a tool for (i) the investigation of rearrangement reactions, (ii) the assignment of bond connectivities and (iii) the generation of interesting cumulenenic neutral species. These experimental studies were complemented by the use of various theoretical calculations.

MS/MS data of *ortho*, *meta* and *para* isomers of $[\text{M} - \text{H}]^-$ anion of methyl benzoate $[(\text{C}_6\text{H}_4)^-\text{CO}_2\text{Me}]$ indicate that the loss of CO is charge-induced with the charged centre

required to be on the phenyl ring at the *ortho* position. *Meta* and *para* $(\text{C}_6\text{H}_4)^-\text{CO}_2\text{Me}$ anions also undergo loss of CO, but first interconvert to the *ortho* isomer. Theoretical calculations indicate that this occurs by a H transfer process requiring an energy of 280 kJ mol^{-1} . Comparison of MS/MS data of the source formed $[\text{M} - \text{H} - \text{CO}]^-$ anion from methyl benzoate with the $[\text{M} - \text{H}]^-$ anion from anisole confirms that the product anion upon loss of CO is the *ortho* deprotonated anisole anion. Two possible mechanisms (Scheme 3.5, A and B) were proposed and investigated theoretically. The barrier the cyclisation process (mechanism A) is 87 kJ mol^{-1} lower in energy than that of the benzyne process (mechanism B), however the Arrhenius factor of B is significantly larger than that of A. Therefore, we cannot distinguish between the two given the available data.

Another organic system studied was deprotonated methyl phenyl carbonate $[(\text{C}_6\text{H}_4)^-\text{OCO}_2\text{Me}]$. This was chosen since a rearrangement reaction analogous to the loss of CO from deprotonated methyl benzoate may occur and result in loss of CO_2 from this system. Loss of CO_2 was only found to be significant from the *ortho* isomer of $(\text{C}_6\text{H}_4)^-\text{OCO}_2\text{Me}$. MS/MS data of the source formed product anion $[\text{M} - \text{H} - \text{CO}_2]^-$ from methyl phenyl carbonate showed that the anion was not the expected deprotonated anisole anion. Charge reversal experiments identified the $[\text{M} - \text{H} - \text{CO}_2]^-$ product anion to be the *ortho* cresol anion. Therefore the loss of CO_2 from $(\text{C}_6\text{H}_4)^-\text{OCO}_2\text{Me}$ is not analogous to the loss of CO from $(\text{C}_6\text{H}_4)^-\text{CO}_2\text{Me}$, but instead involves a methyl migration to give the *ortho* cresol anion and CO_2 . This process occurs via a concerted six-membered transition state, a process calculated to have a barrier of 191 kJ mol^{-1} .

Other mass spectrometric investigations described in this work involved the generation of cumulenenic species incorporating (i) ^{13}C and (ii) B and O atoms, such that bond connectivities were known.

Neutral losses of both C and C_2 are observed upon CR^+ and NR^+ of the $[\text{CCC}]^-$ radical anion. Theoretical calculations suggest the CCC neutral may rearrange provided that it has an energy of 104 kJ mol^{-1} . This requirement suggests that some of the CCC neutrals initially formed in a NR^+ experiment should undergo carbon scrambling. Labelling of the terminal carbon was carried out and showed that under both CR^+ and NR^+ experimental conditions the carbons become completely randomised. Since both spectra are essentially identical it is unclear whether the neutral undergoes any rearrangement. Theory provides insight here in that the cation upon formation requires only 12 kJ mol^{-1} to interconvert to its more stable cyclic isomer. This effectively scrambles the three carbons of the cation and masks any rearrangement of the neutral. Since the anion is known not to rearrange we attempted to circumvent the cation by ionising the neutral to the anion. This experiment was successful in reducing the CCC neutral to the corresponding $[\text{CCC}]^-$ radical anion, however the any loss of C in the NR^+ spectra is lost in baseline noise.

The CCBO system was also found to, at least partially, rearrange under both CR^+ and NR^+ conditions to form a species consistent with OCCB connectivity. Given that the rearrangement is not complete some species of CCBO connectivity must survive both experiments. Moreover, since NR^+ and CR^+ data of CCBO are identical no significant rearrangement or fragmentation is occurring during the lifetime of the neutral. Therefore CCBO is stable on the time scale of the experiment. This is the first reported synthesis of neutral CCBO. Theoretical investigations into the cationic system indicate that the

[OCCB]⁺ isomer is formed from [CCBO]⁺ in an exothermic reaction. The process occurs via a distorted rhombic intermediate requiring 88 kJ mol⁻¹ in the case of the triplet cation. The similar process on the neutral CCBO potential energy surface requires in excess of 267 kJ mol⁻¹. Theoretical data therefore supports the fact that the CCBO is formed and is stable for the lifetime of the experiment.

An extension of the chemistry involved in the CCBO study led to the generation of the CCCCBO species. Unlike the smaller system, the CCCCBO neutral was found to undergo a rearrangement process (possibly to OCCCCB) as indicated by the increased loss of CO during the ⁻NR⁺ experiment. Theoretical methods suggests that the CCCCBO system may rearrange through a six centred intermediate to the OCCCCB neutral.

Another aim of our studies into borocumulenes was the generation of a species with CCBCC connectivity. Theory indicates that this species may undergo rearrangement to the more stable BCCCC neutral. The target CCBCC was observed as either a fragment anion or cation under CID or ⁻CR⁺ conditions respectively. Unfortunately, no such CCBCC ionic species was formed in the ion source of the mass spectrometer to allow for its oxidation/reduction to the target CCBCC neutral. The [HCCBCCH]⁺ cation was formed by dissociative ionisation of [B(CCH)₃]⁺. Neutralisation of this cationic species was successful as indicated by a recovery signal in a ⁺NR⁺ experiment. Loss of B was observed to occur from the neutralised species indicating backbone rearrangement of the transient HCCBCCH neutral was occurring within the microsecond of the experiment.

The use of CID, ⁻CR⁺ and ⁻NR⁺ mass spectrometry throughout this thesis has demonstrated the ability to successfully investigate rearrangement reactions, and stabilities, of anions, neutrals and cations in the gas phase.

2. THEORETICAL STUDIES

Theoretical calculations complement experimental findings throughout this thesis.

A theoretical study examining possible anionic candidates for detection in interstellar space is described in Chapter 4. This follows known observations that (i) many cumulenic molecules are observed in the interstellar environment, (ii) these interstellar species were primarily identified by rotational spectroscopy and (iii) cumulenes typically have large electron affinities. The series of interstellar molecules C_nH , $C_{n-1}CH_2$ and C_nO ($n = 2 - 10$) were investigated using the B3LYP/aug-cc-pVDZ//B3LYP/6-31G(d) level of theory which gives good agreement with experimental data, and allows for the same method to be used for the larger members of each series. Two aspects were concentrated on (i) the adiabatic electron affinity of the (interstellar) neutral and (ii) the dipole moment of the corresponding anion. The results presented show large values for the electron affinities of the neutral, which increase with increased chain length. This suggests that they may undergo efficient attachment of an electron in the interstellar medium. The increasingly large dipole moments of the resulting stable cumulenic anions further indicate that the larger members of each series should be detectable by radio astronomical methods. The data obtained here provides a useful guide for future experimental work and astronomical searches for these and other analogous cumulenic anions, which may result in the identification of the first interstellar anions.

REFERENCES

- 1 Chapman, J. R. *Practical Organic Mass Spectrometry*; 2nd ed.; John Wiley & Sons: Chichester, **1993**.
- 2 Dempster *J. Phys. Rev.* **1918**, *18*, 415.
- 3 Rose, M. E.; Johnstone, R. A. W. *Mass Spectrometry for Chemists and Biochemists*; Cambridge University Press: Cambridge, **1982**.
- 4 Harrison, A. G. *Chemical Ionisation Mass Spectrometry*; CRC Press: Boca Raton, **1983**.
- 5 DePuy, C. H.; Bierbaum, V. M.; Flippin, L. A.; Grabowski, J. J.; King, G. K.; Schmitt, R. J.; Sullivan, S. A. *J. Am. Chem. Soc.* **1980**, *102*, 5012.
- 6 Klass, G.; Trenerry, C.; Sheldon, J. C.; Bowie, J. H. *Aust. J. Chem.* **1981**, *34*, 519.
- 7 Froelicher, S. W.; Freiser, B. S.; Squires, R. R. *J. Am. Chem. Soc.* **1986**, *108*, 2853.
- 8 Eichinger, P. C. H.; Bowie, J. H. *J. Org. Chem.* **1986**, *51*, 5078.
- 9 Dua, S.; Blanksby, S. J.; Bowie, J. H. *Int. J. Mass Spectrom.* **1999**, *196*, 45.
- 10 McDonald, R. N.; Chowdhury, A. K.; Sester, D. W. *J. Am. Chem. Soc.* **1980**, *102*, 6491.
- 11 Schalley, C. A.; Blanksby, S. J.; Harvey, J. N.; Schröder, D.; Zummack, W.; Bowie, J. H.; Schwarz, H. *Eur. J. Org. Chem.* **1998**, 987.
- 12 Chantry, P. J. *J. Chem. Phys.* **1969**, *51*, 3369.
- 13 Chantry, P. J. *J. Chem. Phys.* **1969**, *51*, 3380.
- 14 Lee, J.; Grabowski, J. J. *Chem. Rev.* **1992**, *92*, 1611.
- 15 Dawson, J. H. J.; Jennings, K. R. *J. Chem. Soc. Faraday Trans. 2* **1976**, *72*, 700.
- 16 Grabowski, J. J.; Mely, S. J. *Int. J. Mass Spectrom. Ion Processes* **1987**, *81*, 147.
- 17 Goode, G. C.; Jennings, K. R. *Adv. Mass Spectrom.* **1974**, *6*, 797.
- 18 Nibbering, N. M. M. *Recl. Trav. Chim. Pays-Bas.* **1981**, *100*, 297.
- 19 Budzikiewicz, H. *Angew. Chem., Int. Ed. Engl.* **1981**, *20*, 624.
- 20 Yates, B. F.; Bouma, W. J.; Radom, L. *J. Am. Chem. Soc.* **1984**, *106*, 5805.
- 21 Wenthold, P. G.; Hu, J.; Squires, R. R. *J. Am. Chem. Soc.* **1996**, *118*, 11865.
- 22 Wenthold, P. G.; Hu, J.; Squires, R. R. *J. Am. Chem. Soc.* **1994**, *116*, 6961.

- 23 Beynon, J. H.; Caprioli, R. M.; Ast, T. *Org. Mass Spectrom.* **1971**, *5*, 229.
- 24 Johnson, E. G.; Nier, A. O. *Phys. Rev.* **1953**, *91*, 10.
- 25 Cooks, R. G.; Beynon, J. H.; Caprioli, R. M.; Lester, G. R. *Metastable Ions*; Elsevier: Amsterdam, **1973**.
- 26 Haddon, W. F.; McLafferty, F. W. *J. Am. Chem. Soc.* **1968**, *90*, 4745.
- 27 Kim, M. S.; McLafferty, F. W. *J. Am. Chem. Soc.* **1978**, *100*, 3279.
- 28 Todd, P. J.; McLafferty, F. W. 'Collisionally Activated Dissociation of High Kinetic Energy Ions.' in *Tandem Mass Spectrometry*; McLafferty, F. W., Ed.; John Wiley & Sons: New York, **1983**.
- 29 Laramee, J. A.; Cameron, D.; Cooks, R. G. *J. Am. Chem. Soc.* **1981**, *103*, 12.
- 30 Holmes, J. L. *Org. Mass Spectrom.* **1985**, *20*, 169.
- 31 Bowie, J. H.; Blumenthal, T. *J. Am. Chem. Soc.* **1975**, *97*, 2959.
- 32 Bowie, J. H.; Blumenthal, T. *Aust. J. Chem.* **1976**, *29*, 115.
- 33 Howe, I.; Bowie, J. H.; Szulejko, J. E.; Beynon, J. H. *J. Chem. Soc. Chem. Commun.* **1979**, 983.
- 34 Szulejko, J. E.; Bowie, J. H.; Howe, I.; Beynon, J. H. *Int. J. Mass Spectrom. Ion Phys.* **1980**, *13*, 76.
- 35 Bursey, M. M. *Mass Spectrom. Rev.* **1990**, *9*, 555.
- 36 Danis, P. O.; Feng, R.; McLafferty, F. W. *Anal. Chem.* **1986**, *58*, 355.
- 37 Burgers, P. C.; Holmes, J. L.; Mommers, A. A.; Szulejko, J. E. *J. Am. Chem. Soc.* **1984**, *106*, 521.
- 38 Keough, T.; Beynon, J. H.; Cooks, R. G. *J. Am. Chem. Soc.* **1973**, *95*, 1695.
- 39 McLafferty, F. W.; Todd, P. J.; McGilvery, D. C.; Baldwin, M. A. *J. Am. Chem. Soc.* **1980**, *102*, 3360.
- 40 Goldberg, N.; Schwarz, H. *Acc. Chem. Res.* **1994**, *27*, 347.
- 41 Zagorevskii, D. V.; Holmes, J. H. *Mass Spectrom. Rev.* **1994**, *13*, 133.
- 42 McLafferty, F. W. *Science* **1990**, *247*, 925.
- 43 Terlouw, J. K.; Schwarz, H. *Angew. Chem. Int. Ed. Engl.* **1987**, *26*, 805.
- 44 McMahan, A. W.; Chowdhury, S. K.; Harrison, A. G. *Org. Mass. Spectrom.* **1989**, *24*, 620.
- 45 Villeneuve, S.; Burgers, P. C. *Org. Mass Spectrom.* **1986**, *21*, 733.

- 46 Danis, P. O.; Feng, R.; McLafferty, F. W. *Anal. Chem.* **1986**, *56*, 348.
- 47 Lorquet, J. C.; Leyh-Nihaut, B.; McLafferty, F. W. *Int. J. Mass Spectrom. Ion Processes* **1990**, *100*, 465.
- 48 Nguyen, V. G.; Turecek, F. *J. Mass Spectrom.* **1996**, *31*, 842.
- 49 Schalley, C. A.; Hornung, G.; Schröder, D.; Schwarz, H. *Chem. Soc. Rev.* **1998**, *27*, 91.
- 50 Schalley, C. A.; Hornung, G.; Schröder, D.; Schwarz, H. *Int. J. Mass Spectrom. Ion Processes* **1998**, *172*, 181.
- 51 Feng, R.; Wesdemiotis, C.; Baldwin, M. A.; McLafferty, F. W. *Int. J. Mass Spectrom. Ion Processes* **1988**, *86*, 95.
- 52 Wesdemiotis, C.; Feng, R.; Danis, P. O.; Williams, E. R.; McLafferty, F. W. *J. Am. Chem. Soc.* **1986**, *108*, 5847.
- 53 Wesdemiotis, C. *Org. Mass Spectrom.* **1988**, *23*, 155.
- 54 Hop, C. E. C. A.; Bordas-Nagy, J.; Holmes, J. L.; Terlouw, J. K. *Org. Mass Spectrom.* **1988**, *23*, 155.
- 55 Wesdemiotis, C.; Leyh, B.; Fura, A.; McLafferty, F. W. *J. Am. Chem. Soc.* **1990**, *112*, 8655.
- 56 McLafferty, F. W. 'Decompositions and Rearrangements of Organic Ions' in *Mass Spectrometry of Organic Ions*; McLafferty, F. W., Ed.; Academic Press: New York, **1963**.
- 57 Budzikiewicz, H.; Djerassi, C.; Williams, D. H. *Mass Spectrometry of Organic Compounds*; Holden-Day: San Francisco, **1967**.
- 58 Williams, D. H.; Howe, I. *Principles of Organic Mass Spectrometry*; McGraw Hill: London, **1972**.
- 59 Williams, D. H.; Fleming, I. *Spectroscopic Methods in Organic Chemistry, 4th ed.*; McGraw-Hill: London, **1989**.
- 60 Bowie, J. H. *Mass Spectrom. Rev.* **1990**, *9*, 349.
- 61 Bowie, J. H. 'The Fragmentations of (M-H)⁻ Ions Derived from Organic Compounds' in *Experimental Mass Spectrometry*; Russell, D. H., Ed.; Plenum Press: New York, **1994**.
- 62 Longevialle, P. *Mass Spectrom. Rev.* **1992**, *11*, 157.
- 63 Adams, J. *Mass Spectrom. Rev.* **1990**, *9*, 141.
- 64 Gross, M. L. *Int. J. Mass Spectrom. Ion Processes* **1992**, *118/119*, 137.

- 65 Levine, I. N. *Quantum Chemistry*; 4th ed.; Prentice Hall: London, **1991**.
- 66 Atkins, P. W. *Molecular Quantum Mechanics*; 2nd ed.; Oxford University Press: New York, **1983**.
- 67 Foresman, J. B.; Frisch, Æ. *Exploring Chemistry with Electronic Structure Methods*; 2nd ed.; Gaussian Inc.: Pittsburgh, **1993**.
- 68 Richards, W. G.; Cooper, D. L. *Ab Initio Molecular Orbital Calculations For Chemists*; Oxford University Press: Oxford, **1983**.
- 69 Hehre, W. J.; Radom, L.; Schleyer, P. v. R.; Pople, J. A. *Ab Initio Molecular Orbital Theory*; Wiley-Interscience: New York, **1986**.
- 70 Born, M.; Oppenheimer, J. R. *Ann. Phys.* **1927**, *84*, 457.
- 71 Hartree, D. R. *Proceedings of the Cambridge Philosophical Society* **1928**, *24*, 426.
- 72 Fock, V. *Z. Physik* **1930**, *61*, 126.
- 73 Mølllet, C.; Plesset, M. S. *Phys. Rev.* **1934**, *46*, 618.
- 74 Lee, T. J.; Scuseria, S. G. *J. Phys. Chem.* **1990**, *93*, 489.
- 75 Scuseria, G. E.; Lee, T. J. *J. Phys. Chem.* **1990**, *93*, 5851.
- 76 Raghavachari, K.; Trucks, G. W.; Pople, J. A.; Head-Gordon, M. *Chem. Phys. Lett* **1989**, *157*, 479.
- 77 Parr, R. G.; Yang, W. *Density-Functional Theory of Atoms and Molecules*; Oxford University Press: New York, **1989**.
- 78 Hohenberg, P.; Kohn, W. *Phys. Rev.* **1964**, *B 136*, 864.
- 79 Kohn, W.; Sham, L. *Phys. Rev.* **1965**, *140*, A1133.
- 80 Becke, A. D. *Phys. Rev. A* **1988**, *38*, 3098.
- 81 Perdew, J. P. *Phys. Rev. B* **1986**, *36*, 8822.
- 82 Lee, C.; Yang, W.; Parr, R. G. *Phys. Rev. B* **1988**, *37*, 785.
- 83 Becke, A. D. *J. Phys. Chem.* **1993**, *98*, 5648.
- 84 Stevens, P. J.; Devlin, F. J.; Chablowski, F.; Frisch, M. J. *J. Phys. Chem.* **1994**, *98*, 11623.
- 85 Andzelm, J.; Wimmer, E. *J. Chem. Phys.* **1992**, *96*, 1280.
- 86 Wong, M. W. *Chem. Phys. Lett.* **1996**, *256*, 391.
- 87 Hevko, J. H.; Dua, S.; Bowie, J. H.; Taylor, M. S. *J. Chem. Soc. Perkin Trans. 2* **1999**, 457.

- 88 Gilbert, R. C.; Smith, S. C. *Theory of Unimolecular and Recombination Reactions*; Blackwell Scientific Publications: Oxford, **1990**.
- 89 Scott, A. P.; Radom, L. *J. Phys. Chem.* **1996**, *100*, 16502.
- 90 Raftery, M. J.; Bowie, J. H.; Sheldon, J. C. *J. Chem. Soc. Perkin Trans. 2* **1988**, 563.
- 91 Reeks, L. B.; Eichinger, P. C. H.; Bowie, J. H. *Rapid Commun. Mass Spectrom.* **1993**, *7*, 286.
- 92 McAnoy, A. M. *Honours Thesis*; University of Adelaide: Adelaide, **1999**.
- 93 Raftery, M. J.; Bowie, J. H. *Aust. J. Chem.* **1987**, *47*, 711.
- 94 Eichinger, P. H.; Hayes, R. N.; Bowie, J. H. *J. Am. Chem. Soc.* **1991**, *113*, 1949.
- 95 Ho, A. C.; Bowie, J. H.; Fry, A. *J. Chem. Soc. B* **1971**, *1971*, 530.
- 96 Dua, S.; Bowie, J. H.; Cerda, B. A.; Wesdemiotis, C. *J. Chem. Soc. Perkin Trans. 2* **1998**, 1443.
- 97 Kleingeld, T. C.; Nibbering, N. M. M. *Tetrahedron* **1983**, *39*, 4193.
- 98 Eichinger, P. C. H.; Bowie, J. H.; Hayes, R. N. *Aust. J. Chem.* **1989**, *42*, 865.
- 99 Schulman, J. M.; Disch, R. L. *J. Am. Chem. Soc.* **1985**, *107*, 5059.
- 100 Wilzbach, K. E.; Ritcher, J. S.; Kaplan, J. L. *J. Am. Chem. Soc.* **1971**, *93*, 3782.
- 101 Dewar, M. J. S.; Krischner, S. J. *J. Am. Chem. Soc.* **1975**, *97*, 2932.
- 102 Bettinger, H. F.; Schriener, P. R.; Schaefer, H. F.; Schleyer, P. v. R. *J. Am. Chem. Soc.* **1998**, *120*, 5741.
- 103 Turro, N. J.; Renner, C. A.; Katz, T. J. *Tetrahedron Lett.* **1976**, 4133.
- 104 Gilbert, R. G.; Smith, S. C. *Theory of Unimolecular and Recombination Reactions*; Blackwell Scientific: Cambridge, **1990**.
- 105 Scott, A. P.; Radom, L. *J. Phys. Chem.* **1996**, *100*, 16502.
- 106 Heuts, J. P. A.; Gilbert, R. G.; Radom, L. *Macromolecules* **1995**, *28*, 8771.
- 107 Heuts, J. P. A.; Gilbert, R. G.; Radom, L. *J. Phys. Chem.* **1996**, *100*, 18997.
- 108 Dua, S.; Hevko, J. M.; Bowie, J. H., unpublished data.
- 109 Eichinger, P. C. H.; Bowie, J. H.; Hayes, R. H. *Aust. J. Chem.* **1989**, *42*, 865.
- 110 Szulejko, J. E.; Bowie, J. H.; Howe, I.; Beynon, J. H. *Int. J. Mass Spectrom. Ion Phys.* **1980**, *34*, 99.

- 111 Schultz, A. G.; Antoulinakis, E. G. *J. Org. Chem.* **1996**, *61*, 4555.
- 112 Earborn, C.; Jackson, P. M. *J. Chem. Soc. B* **1969**, 21.
- 113 Amedio, J. C.; Lee, G. T.; Prasad, K.; Repic, O. *Synth. Commun.* **1995**, *25*, 2599.
- 114 Wilbur, D. S.; Stone, W. E.; Anderson, K. W. *J. Org. Chem.* **1983**, *48*, 1542.
- 115 Neville, R. G. *J. Org. Chem.* **1960**, *25*, 1063.
- 116 Speier, J. C. *J. Am. Chem. Soc.* **1952**, *74*, 1063.
- 117 Oki, M.; Nakanishi, H. *Bull. Chem. Soc. Jpn.* **1971**, *44*, 3419.
- 118 Wilbur, D. S.; Stone, W. E.; Aderson, W. S. *J. Org. Chem.* **1983**, *48*, 1544.
- 119 Grunewald, G. N.; Davis, D. P. *J. Org. Chem.* **1978**, *43*, 3075.
- 120 McClelland, R. A.; Patel, G. *J. Am. Chem. Soc.* **1981**, *103*, 6912.
- 121 Frisch, M. J.; Trucks, G. W.; Schlegel, H. B.; Gill, P. M. W.; Johnson, B. G.; Robb, M. A.; Cheeseman, J. R.; Keith, T.; Peterson, G. A.; Montgomery, J. A.; Raghavachari, K.; Al-Laham, M. A.; Zakrzewski, V. G.; Ortiz, J. V.; Foresman, J. B.; Peng, C. Y.; Ayala, P. Y.; Chen, W.; Wong, M. W.; Andres, J. L.; Replogle, E. S.; Gomperts, R.; Martin, R. L.; Fox, D. J.; Binkley, J. S.; Defrees, D. J.; Baker, J.; Stewart, J. P.; Head-Gordon, M.; Gonzales, C.; Pople, J. A. *GAUSSIAN94*; Revision B 3 ed. ed.; GAUSSIAN Inc.: Pittsburgh PA, **1995**.
- 122 Terzieva, R.; Herbst, E. *Int. J. Mass Spectrom.* **2000**, *201*, 135.
- 123 Barckholtz, C.; Snow, T. P.; Bierbaum, V. M. *Astrophys. J.* **2001**, *547*, L171.
- 124 Blanksby, S. J.; McAnoy, A. M.; Dua, S.; Bowie, J. H. *Mon. Not. R. Astron. Soc.* **2001**, *328*, 89.
- 125 Smith, D.; Spanel, P. *Mass Spectrom. Rev.* **1995**, *14*, 255, and refs cited therein.
- 126 Herbst, E. *Chem. Soc. Rev.* **2001**, *30*, 168, and refs cited therein.
- 127 Herbst, E. *Angew. Chem. Int. Ed. Engl.* **1990**, *29*, 595.
- 128 Lequeux, J.; Roueff, E. *Phys. Rep.* **1991**, *200*, 241.
- 129 Olofsson, H. 'Molecules in the Stellar Environment, Lecture Notes in Physics' in *Molecules in the Stellar Environment, Lecture Notes in Physics*; Jorgenson, O. G., Ed.; Springer: Heidelberg, **1994**, pp 114 - 133, and references cited therein.
- 130 Hinkle, K. H. 'Molecules in the Stellar Environment, Lecture Notes in Physics' in *Molecules in the Stellar Environment, Lecture Notes in Physics*; Jorgenson, O. G., Ed.; Springer: Heidelberg, **1994**, pp 99 - 114, and references cited therein.

- 131 Omont, A. 'Molecules in the Stellar Environment, Lecture Notes in Physics' in *Molecules in the Stellar Environment, Lecture Notes in Physics*; Jorgenson, O. G., Ed.; Springer: Heidelberg, **1994**, pp 135 - 137, and references cited therein.
- 132 National Radio Astronomy Observatory, <http://www.cv.nrao.edu/~awootten/allmols.html>, **2002**
- 133 Blanksby, S. J.; Bowie, J. H. *Mass Spectrom. Rev.* **1999**, *18*, 131.
- 134 Bernath, P. F.; Hinkle, K. H.; Keady, J. J. *Science* **1989**, *244*, 562.
- 135 Ohishi, M.; Suzuki, H.; Ishikawa, S.; Yamundu, C.; Kanamori, H.; Irvine, W. M.; Brown, R. D.; Godfrey, P. D.; Kaifu, N. *Astrophys. J.* **1991**, *380*, L39.
- 136 Matthews, H. E.; Irvine, W. M.; Friberg, P.; Brown, R. D.; Godfrey, P. D. *Nature* **1984**, *310*, 125.
- 137 Herbst, E.; Klemperer, W. *Astrophys. J.* **1973**, *185*, 505.
- 138 Sims, I. R.; Smith, I. W. M. *Ann. Rev. Phys. Chem.* **1995**, *46*, 109.
- 139 Heath, J. R.; Saykally, R. J. *Science* **1996**, *274*, 1480.
- 140 Smith, I. W. M.; Rowe, B. R. *Acc. Chem. Res.* **2000**, *33*, 261.
- 141 Chastaing, D.; James, P. L.; Sims, I. R.; Smith, I. W. M. *Phys. Chem. Chem. Phys.* **1999**, *1*, 2247.
- 142 Kaiser, R. I.; Ochsenfeld, C.; Head-Gordon, M.; Lee, Y. T.; Suits, A. G. *J. Chem. Phys.* **1997**, *106*, 1729.
- 143 Sims, I. R.; Queffelec, J. L.; Defrance, A.; Travers, D.; Rowe, B. R.; Herbet, L.; Karthawer, J.; Smith, I. W. M. *Chem. Phys. Lett.* **1993**, *211*, 461.
- 144 Chaizy, P.; Reme, H.; Sauvaud, J. A.; d'Uston, C.; Lin, R. P.; Larson, D. E.; Mitchell, D. L.; Anderson, K. A.; Carlson, C. W.; Korth, A.; Mendis, D. A. *Nature* **1991**, *349*, 393.
- 145 Herbst, E. *Nature* **1981**, *289*, 656.
- 146 Dalgarno, A.; McCray, R. A. *Astrophys. J.* **1973**, *181*, 95.
- 147 Duley, W. W.; Williams, D. A. 'Negative ion reactions' in *Interstellar Chemistry*; Academic Press Inc.: London, **1984**, pp 59 - 63.
- 148 Bettens, R. P. A.; Lee, H. H.; Herbst, E. *Astrophys. J.* **1995**, *443*, 664.
- 149 Stancil, P. C.; Dalgarno, A. *Faraday Discuss.* **1998**, *109*, 61.
- 150 Petrie, S.; Herbst, E. *Astrophys. J.* **1997**, *491*, 210.
- 151 Omont, A. *Astron. Astrophys.* **1986**, *164*, 159.

- 152 Lepp, S.; Dalgarno, A. *Astrophys. J.* **1988**, *324*, 553.
- 153 Canosa, A.; Parent, D. C.; Pasquerault, D.; Gomet, J. C.; Laube, S.; Rowe, B. R. *Chem. Phys. Lett.* **1994**, *228*, 26.
- 154 Jaffke, T.; Illenberger, E.; Lezius, M.; Matejcik, S.; Smith, D.; Mark, T. D. *Chem. Phys. Lett.* **1994**, *226*, 213.
- 155 Spanel, P.; Smith, D. *Chem. Phys. Lett.* **1994**, *229*, 262.
- 156 Petrie, S. *Mon. Not. R. Astron. Soc.* **1996**, *281*, 137.
- 157 Tulej, M.; Kirkwood, D. A.; Pachkov, M.; Maier, J. P. *Astrophys. J.* **1998**, *506*, L69.
- 158 Ruffle, D. P.; Bettens, R. P. A.; Terzieva, R.; Herbst, E. *Astrophys. J.* **1999**, *523*, 678.
- 159 McCall, B. J.; York, D. G.; Oka, T. *Astrophys. J.* **2000**, *531*, 329.
- 160 Motylewski, T.; Linnartz, H.; Vaizert, O.; Maier, J. P.; Galazutdinov, G. A.; Musaev, F. A.; Krelowski, J.; Walker, G. A. H.; Bohlender, D. A. *Astrophys. J.* **2000**, *531*, 312.
- 161 Snow, T. P. *Spectrochim. Acta* **2001**, *57A*, 615.
- 162 Herbig, G. H. *Ann. Rev. Astron. and Astrophys.* **1995**, *33*, 19.
- 163 Salama, F.; Bakes, E. L. O.; Allamandola, L. J.; Tielens, A. G. G. M. *Astrophys. J.* **1996**, *458*, 621.
- 164 Cernicharo, C.; Guelin, M. *Astron. Astrophys.* **1996**, *309*, L27.
- 165 Guelin, M.; Cernicharo, C.; Travers, M. J.; McCarthy, M. C.; Gottlieb, C. A.; Thaddeus, P.; Ohishi, M.; Saito, S.; Yamamoto, S. *Astron. Astrophys.* **1997**, *317*, L1.
- 166 Takahashi, J. *Publ. Astrophys. Soc. Jpn.* **2000**, *52*, 401.
- 167 Crawford, T. D.; Stanton, J. F.; Saeh, J. C.; Schaefer, H. F. *J. Am. Chem. Soc.* **1999**, *121*, 1902.
- 168 Herbst, E.; Lee, H. H.; Howe, D. A.; Millar, T. J. *AIP Conf. Proc. (1994)*, *312 (Molecules and Grains in Space)* **1994**, 141.
- 169 Herbst, E.; Woon, D. E. *Astrophys. J.* **1997**, *489*, 109.
- 170 Chastaing, D.; James, P. L.; Sims, I. R.; Smith, I. W. M. *Faraday Discuss.* **1998**, *109*, 165.
- 171 Bettens, R. P. A.; Herbst, E. *Astrophys. J.* **1996**, *468*, 686.
- 172 Fukuzawa, K.; Osamura, Y.; Schaefer, H. F. *Astrophys. J.* **1998**, *505*, 278.

- 173 Wesdemiotis, C.; Feng, R. *Org. Mass Spectrom.* **1988**, *23*, 416.
- 174 Kaiser, R. I.; Lee, Y. T.; Suits, A. G. *J. Chem. Phys.* **1995**, *103*, 10395.
- 175 Kubitzka, C.; Schottler, M.; Homann, K. H. *Ber. Bunsen-Ges. Phys. Chem.* **1987**, *91*, 695.
- 176 Hausmann, M.; Hebgen, P.; Homann, K. H. *Symp. (Int.) Combust., [Proc.], 24th* **1992**, 793.
- 177 Muller, H. S. P.; Klaus, T.; Winnewisser, G. *Astron. Astrophys.* **2000**, *357*, L65.
- 178 Gottlieb, C. A.; Vrtilek, J. M.; Gottlieb, E. W.; Thaddeus, P.; Hjalmarsen, A. *Astrophys. J. Lett.* **1985**, *294*, L55.
- 179 Gottlieb, C. A.; Gottlieb, E. W.; Thaddeus, P. *Astron. Astrophys.* **1986**, *164*, L5.
- 180 Linnartz, H.; Motylewski, T.; Vaizert, O.; Maier, J. P.; Apponi, A. J.; McCarthy, M. C.; Gottlieb, C. A.; Thaddeus, P. *J. Mol. Spectrosc.* **1999**, *197*, 1.
- 181 Travers, M. J.; McCarthy, M. C.; Gottlieb, C. A.; Thaddeus, P. *Astrophys. J.* **1996**, *465*, L77.
- 182 McCarthy, M. C.; Travers, M. J.; Kovacs, A.; Gottlieb, C. A.; Thaddeus, P. *Astrophys. J. Suppl. Ser.* **1997**, *113*, 105.
- 183 Gottlieb, C. A.; McCarthy, M. C.; Travers, M. J.; Grabow, J.-U.; Thaddeus, P. *J. Chem. Phys.* **1998**, *109*, 5433.
- 184 Maier, J. P. *J. Phys. Chem. A.* **1998**, *102*, 3462.
- 185 Linnartz, H.; Motylewski, T.; Maier, J. P. *J. Chem. Phys.* **1998**, *109*, 3819.
- 186 Freivogel, P.; Fulara, J.; Jakobi, M.; Forney, D.; Maier, J. P. *J. Chem. Phys.* **1995**, *103*, 54.
- 187 Taylor, T. R.; Xu, C.; Neumark, D. M. *J. Chem. Phys.* **1998**, *108*, 10018.
- 188 Oakes, J. M.; Ellison, G. B. *Tetrahedron* **1986**, *42*, 6263.
- 189 Kirkwood, D. A.; Tulej, M.; Pachkov, M. V.; Schnaiter, M.; Guthe, F.; Grutter, M.; Wyss, M.; Maier, J. P.; Fischer, G. *J. Chem. Phys.* **1999**, *111*, 9280.
- 190 Grutter, M.; Wyss, M.; Maier, J. P. *J. Chem. Phys.* **1999**, *110*, 1492.
- 191 Tulej, M.; Guthe, F.; Schnaiter, M.; Pachkov, M. V.; Kirkwood, D. A.; Maier, J. P.; Fischer, G. *J. Phys. Chem. A.* **1999**, *103*, 9712.
- 192 Dua, S.; Sheldon, J. C.; Bowie, J. H. *J. Chem. Soc., Perkin Trans. 2* **1994**, 543.
- 193 Dua, S.; Sheldon, J. C.; Bowie, J. H. *J. Chem. Soc., Chem. Commun.* **1995**, 1067.

- 194 Blanksby, S. J.; Dua, S.; Bowie, J. H.; Sheldon, J. C. *J. Chem. Soc., Chem. Commun.* **1997**, 1833.
- 195 Dua, S.; Bowie, J. H.; Blanksby, S. J. *Eur. Mass Spectrom.* **1999**, *5*, 309.
- 196 Woon, D. E. *Chem. Phys. Lett.* **1995**, *244*, 45.
- 197 Natterer, J.; Koch, W. *Mol. Phys.* **1995**, *84*, 691.
- 198 McCarthy, M. C.; Gottlieb, C. A.; Thaddeus, P.; Horn, M.; Botschwina, P. *J. Chem. Phys.* **1995**, *103*, 7820.
- 199 Aoki, K.; Hashimoto, K.; Ikuta, S.; Nomura, O. *Chem. Phys. Lett.* **1995**, *242*, 527.
- 200 Botschwina, P. *55th Int. Symp. on Molecular Spectroscopy*, Ohio State University, Columbus, **2000**.
- 201 Arnold, D. W.; Bradforth, S. E.; Kitsopoulos, T. N.; Neumark, D. M. *J. Chem. Phys.* **1991**, *95*, 8753.
- 202 Schulz, S. A.; King, J. E.; Glinski, R. J. *Mon. Not. R. Astron. Soc.* **2000**, *312*, 769.
- 203 Vrtilek, J. M.; Gottlieb, C. A.; Gottlieb, E. W.; Killian, T. C.; Thaddeus, P. *Astrophys. J.* **1990**, *364*, L53.
- 204 Killian, T. C.; Vrtilek, J. M.; Gottlieb, C. A.; Gottlieb, E. W.; Thaddeus, P. *Astrophys. J.* **1990**, *365*, L89.
- 205 Cernicharo, J.; Gottlieb, C. A.; Guelin, M.; Killian, T. C.; Paubert, G.; Thaddeus, P.; Vrtilek, J. M. *Astrophys. J.* **1991**, *368*, L39.
- 206 Cernicharo, J.; Gottlieb, C. A.; Guelin, M.; Killian, T. C.; Thaddeus, P.; Vrtilek, J. M. *Astrophys. J.* **1991**, *368*, L43.
- 207 Thaddeus, P.; Vrtilek, J. M.; Gottlieb, C. A. *Astrophys. J.* **1985**, *299*, L63.
- 208 Maier, G.; Reisenauer, H. P.; Schwab, W.; Carsky, P.; Hess, B. A., Jr.; Schaad, L. J. *J. Am. Chem. Soc.* **1987**, *109*, 5183.
- 209 McCarthy, M. C.; Travers, M. J.; Kovacs, A.; Chen, W.; Novick, S. E.; Gottlieb, C. A.; P., T. *Science* **1997**, *275*, 518.
- 210 Apponi, A. J.; McCarthy, M. C.; Gottlieb, C. A.; Thaddeus, P. *Astrophys. J.* **2000**, *530*, 357.
- 211 Suelzle, D.; Schwarz, H. *Chem. Phys. Lett.* **1989**, *156*, 397.
- 212 Duran, R. P.; Amorebieta, V. T.; Colussi, A. J. *J. Am. Chem. Soc.* **1987**, *109*, 3154.
- 213 Fahr, A.; Laufer, A. H. *J. Photochem.* **1986**, *34*, 261.
- 214 Fahr, A.; Laufer, A. H. *J. Phys. Chem.* **1986**, *89*, 2906.

- 215 Levin, J.; Feldman, H.; Baer, A.; Ben-Hamu, D.; Heber, O.; Zajfman, D. *Phys. Rev. Lett.* **1998**, *81*, 3347.
- 216 Clauberg, H.; Minsek, D. W.; Chen, P. *J. Am. Chem. Soc.* **1992**, *114*, 99.
- 217 Goldberg, N.; Suelzle, D.; Schwarz, H. *Chem. Phys. Lett.* **1993**, *213*, 593.
- 218 Blanksby, S. J.; Dua, S.; Bowie, J. H.; Schröder, D.; Schwarz, H. *J. Phys. Chem. A.* **1998**, *102*, 9949.
- 219 Dua, S.; Blanksby, S. J.; Bowie, J. H. *J. Phys. Chem. A.* **2000**, *104*, 77.
- 220 Ervin, K. M.; Gronert, S.; Barlow, S. E.; Gilles, M. K.; Harrison, A. G.; Bierbaum, V. M.; DePuy, C. H.; Lineberger, W. C.; Ellison, G. B. *J. Am. Chem. Soc.* **1990**, *112*, 5750.
- 221 Bohme, D. K.; Wlodek, S.; Williams, L.; Forte, L.; Fox, A. *J. Chem. Phys.* **1987**, *87*, 6934.
- 222 Woon, D. E.; Herbst, E. *Astrophys. J.* **1996**, *465*, 795.
- 223 Van Zee, R. J.; Smith, G. R.; Weltner, W., Jr. *J. Am. Chem. Soc.* **1988**, *110*, 609.
- 224 Dibben, M.; Szczepanski, J.; Wehlburg, C.; Vala, M. *J. Phys. Chem. A.* **2000**, *104*, 3584.
- 225 Erkin, S.; Vala, M. *J. Phys. Chem. A.* **1997**, *101*, 3601.
- 226 Ortman, B. J.; Hauge, R. H.; Mulgrave, J. L.; Kafafi, Z. H. *J. Phys. Chem.* **1990**, *94*, 7973.
- 227 Ohshima, Y.; Endo, Y.; Ogata, T. *J. Chem. Phys.* **1995**, *102*, 1493.
- 228 Ogata, T.; Ohshima, Y.; Endo, Y. *J. Am. Chem. Soc.* **1995**, *117*, 3593.
- 229 Zengin, V.; Persson, B. J.; Strong, K. M.; Continetti, R. E. *J. Chem. Phys.* **1996**, *105*, 9740.
- 230 Blanksby, S. J.; Dua, S.; Bowie, J. H. *Rapid Commun. Mass Spectrom.* **1999**, *13*, 2249.
- 231 Dua, S.; Blanksby, S. J.; Bowie, J. H. *Int. J. Mass Spectrom.* **2000**, *195/196*, 45.
- 232 Dua, S.; Blanksby, S. J.; Bowie, J. H. *Rapid Commun. Mass Spectrom.* **2000**, *14*, 118.
- 233 Moazzen-Ahmandi, N.; Zerbetto, F. *J. Chem. Phys.* **1995**, *103*, 6349.
- 234 Rienstra-Kiracofe, J. C.; Ellison, G. B.; Hoffmann, B. C.; Schaefer, H. F. *J. Phys. Chem. A* **2000**, *104*, 2273.
- 235 Blanksby, S. J.; Dua, S.; Bowie, J. H.; Schröder, D.; Schwarz, H. *J. Phys. Chem. A* **1998**, *102*, 9949.

- 236 Blanksby, S. J.; Dua, S.; Bowie, J. H. *J. Phys. Chem. A* **1999**, *103*, 5161.
- 237 Dunning, T. H. *J. Chem. Phys.* **1989**, *90*, 1007.
- 238 Woon, D. E.; Dunning, T. H. *J. Chem. Phys.* **1993**, *98*, 1358.
- 239 Cizek, J. *Adv. Chem. Phys.* **1969**, *14*, 35.
- 240 Watts, J. D.; Gauss, J.; Bartlett, R. J. *J. Chem. Phys.* **1993**, *98*, 8718.
- 241 Frisch, M. J.; Trucks, G. W.; Schlegel, H. B.; Scuseria, G. E.; Robb, M. A.; Cheeseman, J. R.; Zakrzewski, V. G.; Montgomery, J. A.; Stratmann, R. E.; Burant, J. C.; Dapprich, S.; Millam, J. M.; Daniels, A. D.; Kudin, K. N.; Strain, M. C.; Farkas, O.; Tamasi, J.; Barone, V.; Cossi, M.; Cammi, R.; Mennucci, B.; Pomelli, C.; Adama, C.; Clifford, S.; Ochterski, J.; Morokuma, B.; Malich, D. K.; Rabuck, A. D.; Raghavachari, K.; Foresman, J. B.; Cioslowski, J.; Ortiz, J. V.; Stefanov, B. B.; Liu, G.; Liashenko, A.; Piskorz, P.; Komaromi, I.; Gomperts, R.; Martin, R. L.; Fox, D. J.; Keith, T.; Al-Latham, M. A.; Peng, C. Y.; Nanayakkara, A.; Gonzalez, C.; Challacombe, M.; Gill, P. M. W.; Johnson, B. G.; Chen, W.; Wong, M. W.; Andres, J. L.; Head-Gordon, M.; Replogle, E. S.; Pople, J. A. *GAUSSIAN98*; GAUSSIAN Inc.: Pittsburgh PA, **1998**.
- 242 Weltner, W.; Van Zee, R. J. *Chem. Rev.* **1989**, *89*, 1713 and references cited therein.
- 243 Van Orden, A.; Saykally, R. J. *Chem. Rev.* **1998**, *98*.
- 244 Ehrenfreund, P.; Foing, B. H. *Astron. Astrophys.* **1996**, *307*, L25.
- 245 Bettens, B. P. A.; Herbst, E. *Astrophys. J.* **1997**, *478*, 545.
- 246 Kroto, H. W.; McKay, K. *Nature* **1988**, *332*, 328.
- 247 Levi Guyer, R.; Koshland, D. E. *Science* **1990**, *250*, 1640.
- 248 Von Helden, G.; Kemper, P. R.; Gotts, N. G.; Bowers, M. T. *Science* **1993**, *259*, 1300.
- 249 Von Helden, G.; Gotts, N. G.; Bowers, M. T. *Nature* **1993**, *363*, 60.
- 250 Baddour, R. F.; Timmins, R. S. *The Application of Plasmas to Chemical Processing*; MIT Press, **1967**.
- 251 Jones, J. M.; Malcolm, R. P.; Thomas, K. M.; Botrell, S. H. *Carbon* **1996**, *34*, 231.
- 252 Kroto, H. W.; Heath, J. R.; O'Brien, S. C.; Curl, R. F.; Smalley, R. E. *Nature* **1985**, *318*, 162.
- 253 Cermak, I.; Forderer, M.; Cermakova, I.; Kalhofer, S.; Stopka-Ebeler, H.; Monninger, G.; Kratschmer, W. *J. Chem. Phys.* **1998**, *108*, 10129.
- 254 Monninger, G.; Forderer, M.; Gurtler, P.; Kalhofer, S.; Petersen, S.; Nemes, L.; Szalay, P. G.; Kratscher, W. *J. Phys. Chem. A* **2002**, *106*, 5776.

- 255 Weltner, W.; Van Zee, R. J. *Chem. Rev.* **1989**, 89, 1713.
- 256 Raghavachari, A. N. *J. Chem. Phys.* **1990**, 93, 2099.
- 257 Adamowicz, L. *Chem. Phys. Lett.* **1991**, 182, 45.
- 258 Watts, J. D.; Bartlett, R. J. *J. Chem. Phys.* **1992**, 97, 3445.
- 259 Kranz, R. H.; Graham, W. R. M. *J. Chem. Phys.* **1992**, 96, 2517.
- 260 Kranz, R. H.; Rittby, C. M. L.; Graham, W. R. M. *J. Chem. Phys.* **1995**, 103, 6841.
- 261 Sun, J.; Grutzmacherm, H.-F.; Lifshitz, C. *J. Am. Chem. Soc.* **1993**, 115, 8382, and references cited therein.
- 262 Heath, J. R.; Saykally, R. J. *On Clusters and Clustering*; Elsevier: Amsterdam, **1993**.
- 263 Van Orden, A.; Saykally, R. J. *Chem. Rev.* **1998**, 98, 2313 and references cited therein.
- 264 Schmatz, S.; Botschwina, P. *Chem. Phys. Lett.* **1995**, 235, 5.
- 265 Weltner, W.; Van Zee, R. J.; Li, S. *J. Phys. Chem.* **1995**, 99, 6277.
- 266 Schmatz, S.; Botschwina, P. *Int. J. Mass Spectrom. Ion Processes* **1995**, 149/150, 621.
- 267 Zhao, Y.; deBeer, E.; Xu, C.; Taylor, T.; Neumark, D. M. *J. Chem. Phys.* **1996**, 105, 4905.
- 268 Zhao, Y.; deBeer, E.; Neumark, D. M. *J. Chem. Phys.* **1996**, 105, 2575.
- 269 Maier, J. P. *Chem. Soc. Rev.* **1997**, 26, 21.
- 270 Blanksby, S. J.; Schröder, D.; Dua, S.; Bowie, J. H.; Schwarz, H. *J. Am. Chem. Soc.* **2000**, 122, 7105.
- 271 Dua, S.; Bowie, J. H. *J. Phys. Chem. A* **2002**, 106, 1374.
- 272 Zajfman, D.; Feldman, H.; Heber, O.; Kella, D.; Majer, D.; Vager, Z.; Naaman, R. *Science* **1992**, 258, 1129.
- 273 Algranati, M.; Feldman, H.; Kella, D.; Malkin, E.; Miklazky, E.; Naaman, R.; Vager, Z.; J., Z. *J. Phys. Chem.* **1989**, 90, 4617.
- 274 Watts, J. D.; Gauss, J.; Stanton, J. F.; Bartlett, R. J. *J. Chem. Phys.* **1992**, 97, 8372.
- 275 Xu, C.; Burton, G. R.; Taylor, T. R.; Neumark, D. M. *J. Chem. Phys.* **1997**, 107, 3428.
- 276 Huggins, W. *Proc. R. Soc. London* **1882**, 33, 1.

- 277 Swings, P. *Rev. Mod. Phys.* **1942**, *12*, 190.
- 278 Hinkle, K. H.; Keady, J. J.; Bernath, P. F. *Science* **1988**, *241*, 1319.
- 279 Giesen, T. F.; Van Orden, A. O.; Cruzan, J. D.; Provencal, R. A.; Saykally, R. J.; Gendriesch, R.; Lewen, F.; Winnewisser, G. *Astrophys. J.* **2001**, *551*, L181.
- 280 Maier, J. P.; Larkin, N. M.; Walker, G. A. H.; Bohlender, D. A. *Astrophys. J.* **2001**, *553*, 267.
- 281 Douglas, A. E. *Astrophys. J.* **1951**, *114*, 466.
- 282 Sasada, H.; Amano, T.; Jarman, C.; Bernath, P. F. *J. Chem. Phys.* **1991**, *94*, 2401 and references cited therein.
- 283 Lesieki, M. L.; Hicks, H. W.; Orenstein, A.; Guillory, W. A. *Chem. Phys. Lett.* **1980**, *71*, 72.
- 284 Szczepanski, J.; Wehlburg, C.; Vala, M. *J. Phys. Chem. A* **1997**, *101*, 7039.
- 285 Schmuttermaer, C. A.; Cohen, R. C.; Pugliano, N.; Heath, J. R.; Cooksy, A. L.; Busarow, K. L.; Saykally, R. J. *Science* **1990**, *249*, 897.
- 286 Geusic, M. E.; McIlrath, T. J.; Jarrold, M. F.; Bloomfield, L. A.; Freeman, R. R.; Brown, W. L. *J. Chem. Phys.* **1986**, *84*, 2421.
- 287 Baker, J.; Bramble, S. K.; Hamilton, P. A. *J. Mol. Spectrosc.* **1997**, *101*, 7039.
- 288 Gaumet, J. J.; Wakisaka, A.; Shimizu, Y.; Tamori, Y. *J. Chem. Soc. Faraday Trans.* **1993**, *89*, 1667.
- 289 Peric-Radic, J.; Roemelt, J.; Peyerimhoff, S. D.; Buenker, R. J. *Chem. Phys. Lett.* **1977**, *50*, 344.
- 290 Whiteside, R. A.; Krishnan, R.; Frisch, M. J.; Pople, J. A.; Schleyer, P. v. R. *Chem. Phys. Lett.* **1981**, *80*, 547.
- 291 Raghavachari, K. *Chem. Phys. Lett.* **1990**, *171*, 249.
- 292 Mladenovic, M.; Schmatz, S.; Botschwina, P. *J. Chem. Phys.* **1994**, *101*, 5891.
- 293 Martin, J. M. L.; Taylor, P. R. *J. Phys. Chem.* **1996**, *100*, 6047.
- 294 Szczepanski, J.; Ekern, S.; Vala, M. *J. Phys. Chem. A* **1997**, *101*, 1841.
- 295 Fueno, H.; Taniguchi, Y. *Chem. Phys. Lett.* **1999**, *312*, 65.
- 296 E. E. Pasqualini and M. Lopez, C. P. L., 2000, 320, 415. *Chem. Phys. Lett.* **2000**, *320*, 415.
- 297 Leonard, C.; Panten, D.; Lakin, N. M.; Chambaud, G.; Rosmus, P. *Chem. Phys. Lett.* **2001**, *335*, 97.

- 298 Grev, R. S.; Alberts, I. L.; Schaefer, H. F. *J. Phys. Chem.* **1990**, *94*, 3379 and 8744.
- 299 Watts, J. D.; Stanton, J. F.; Gauss, J.; Bartlett, R. J. *J. Chem. Phys.* **1991**, *94*, 4320.
- 300 Scuseria, G. E. *Chem. Phys. Lett* **1991**, *176*, 27.
- 301 Taylor, P. R.; Martin, J. M. L.; Francois, J. P.; Gijbels, B. *J. Phys. Chem.* **1991**, *95*, 6530.
- 302 Taylor, P. R. *J. Phys. Chem.* **1991**, *95*, 6534.
- 303 An, Y. Z.; Rubin, Y.; Schaller, C.; McElvany, S. W. *J. Org. Chem.* **1994**, *59*, 2927.
- 304 Fura, A.; Turecek, F.; McLafferty, F. W. *Int. J. Mass Spectrom.* **2002**, *217*, 81.
- 305 Wesdemiotis, C.; McLafferty, F. W. *Chem. Rev.* **1987**, *887*, 485.
- 306 Schalley, C. A.; Hornung, G.; Schröder, D.; Schwarz, H. *Chem. Soc. Rev.* **1998**, *27*, 91.
- 307 Zagorevskii, D. V.; Holmes, J. L. *Mass Spectrom. Rev.* **1999**, *18*, 87.
- 308 Billups, W. E.; Haley, M. M. *J. Am. Chem. Soc.* **1991**, *113*, 5084.
- 309 Kruithof, K. J. H.; F. Schmitz, R.; Klumpp, G. W. *Tetrahedron* **1983**, *39*, 3073.
- 310 Plattner, D. A.; Houk, K. N. *J. Am. Chem. Soc.* **1995**, *117*, 4405.
- 311 Martin, J. M. L.; El-Yazal, J.; François, J.-P. *Chem. Phys. Lett* **1995**, *242*, 570.
- 312 Martin, J. M. L.; El-Yazal, J.; François, J.-P. *Chem. Phys. Lett.* **1996**, *252*, 9.
- 313 Pasqualini, E. E.; López, M. *Chem. Phys. Lett.* **2000**, *320*, 415.
- 314 Deegan, M. J. O.; Knowles, P. J. *Chem. Phys. Lett.* **1994**, *227*, 321, and references cited therein.
- 315 Kouba, J. E.; Öhrn, Y. *J. Chem. Phys.* **1970**, *53*, 3923.
- 316 Hirsch, G.; Buenker, R. J. *J. Chem. Phys.* **1987**, *87*, 6004.
- 317 Knight, L. B.; Cobranchi, S. T.; Petty, J. T.; Earl, E.; Feller, D.; Davidson, E. R. *J. Chem. Phys.* **1989**, *90*, 690.
- 318 Oliphant, N.; Adamowicz, L. *Chem. Phys. Lett.* **1990**, *168*, 126.
- 319 Fernando, W. T. M. L.; O'Brien, L. C.; Bernath, P. F. *J. Phys. Chem.* **1990**, *93*, 8482.
- 320 Martin, J. M. L.; Taylor, P. R. *J. Chem. Phys.* **1994**, *100*, 9106.
- 321 Wyss, M.; Grutter, M.; Maier, J. P. *J. Phys. Chem.* **1998**, *102*, 9106.

- 322 Martin, J. M. L.; Taylor, P. R.; Yustein, J. T.; Burkholder, T. R.; Andrew, L. *J. Chem. Phys.* **1993**, *99*, 12.
- 323 Presilla-Marquez, J. D.; Larson, C. W.; Carrick, P. G.; Rittby, C. M. L. *J. Chem. Phys.* **1996**, *105*, 3398.
- 324 Knight, L. B.; Cabranchi, S.; Earl, E. *J. Chem. Phys.* **1996**, *104*, 4927.
- 325 Wang, C. R.; Huang, R. B.; Liu, Z. Y.; Zheng, L. S. *Chem. Phys. Lett.* **1995**, *242*, 355.
- 326 Zhan, C. G.; Iwata, S. *J. Phys. Chem.* **1997**, *101*, 591.
- 327 Léonard, C.; Rosmus, P.; Wyss, M.; Maier, J. P. *Phys. Chem. Chem. Phys.* **1999**, *1*, 1827.
- 328 Comeau, M.; Leleyter, M.; Leclercq, J.; Pastoli, G. *Amer. Inst. Phys. Conf. Proc.* **1994**, *312*, 605.
- 329 Presilla-Marquez, J. D.; Carrick, P. G.; Larson, C. W. *J. Chem. Phys.* **1999**, *110*, 5702.
- 330 Hamrick, Y. M.; Van Zee, R. J.; Godbout, J. T.; Weltner, W. J.; Lauderdale, W. J.; Stanton, J. F.; Barlett, R. J. *J. Phys. Chem.* **1991**, *95*, 2840.
- 331 Burkholder, T. R.; Andrews, L. *J. Phys. Chem.* **1992**, *96*, 2840.
- 332 Zhou, M.; Tsumori, N.; Li, Z.; Fan, K.; Andrews, A.; Xu, Q. *J. Am. Chem. Soc.* **2002**, *124*, 12936.
- 333 Sheldon, J. C.; Currie, G. J.; Bowie, J. H. *J. Am. Chem. Soc.* **1988**, *110*, 8266.
- 334 Davies, J. E.; Raithby, P. R.; Snaith, R.; Wheatley, A. E. H. *Chem. Commun.* **1997**, 1797.
- 335 Maderna, A.; Pritzkow, H.; Siebert, W.; Sommerfeld, T.; Cederbaum, L. S. *Z. Naturforsch.* **1997**, *52 b*, 1315.
- 336 Brown, H. C.; Bhat, N. G.; Srebnik, M. *Tetrahedron Lett.* **1988**, *29*, 2631.
- 337 Brown, C. D.; Chong, J. M.; Shen, L. *Tetrahedron* **1999**, *55*, 14233.

List of Publications 2000 - 2003

“Does $\text{Me}_3\text{O}^\cdot$ exist in the gas phase? A joint experimental and theoretical investigation.”

Dua, S., McAnoy, A. M., Blumenthal, T. and Bowie, J. H. *Int. J. Mass Spectrom.*, (manuscript submitted).

“The anionic, neutral and cationic rearrangements of CCCCHO and CCCHCO to HCCCCO . Generation of neutrals from anionic precursors in the gas phase.”

Fitzgerald, M., Dua, S., Bowie, J. H. and McAnoy, A. M. *Int. J. Mass Spectrom.*, (manuscript submitted).

“Gas phase generation of HCCCS and CCCHS radicals from anionic precursors. The rearrangement of CCCHS to HCCCS . A joint experimental and theoretical investigation.”

Peppe, S., Dua, S., McAnoy, A. M., and Bowie, J. H., *J. Phys. Chem. A*. (in press).

“The formation of CCBO and $[\text{CCBO}]^+$ from CCBO^- in the gas phase.”

McAnoy, A. M., Dua, S., Bowie, J. H., Schröder, D. and Schwarz, H. *J. Phys. Chem. A.*, ASAP article published on web 1/2/03.

“The formation of neutral CCC and its radical cation from the CCC radical anion in the gas phase. A joint experimental and theoretical investigation.”

McAnoy, A. M., Dua, S., Schröder, D., Bowie, J. H. and Schwarz, H. *J. Chem. Soc., Perkin. Trans. 2*, **2002**, 1647.

“Cumulenenic and heterocumulenenic anions: potential interstellar species?”

Blanksby, S. J., McAnoy, A. M., Dua, S., Bowie, J. H. *Mot. Not. R. Astron. Soc.*, **2001**, 328, 89.

“Loss of CO_2 from the *ortho* isomer of deprotonated methyl phenyl carbonate involves a methyl migration.”

McAnoy, A. M., Rees, K., Dua, S., Bowie, J. H. *Int. J. Mass Spectrom.*, **2001**, 210/211, 557.

“Negative ion fragmentations of deprotonated peptides: backbone cleavages directed through both Asp and Glu.”

Brinkworth, C. S., Dua, S., McAnoy, A. M., Bowie, J. H. *Rapid Commun. Mass Spectrom.* **2001**, 15, 1965.

“The loss of CO from the *ortho*, *meta* and *para* forms of deprotonated methyl benzoate.”

McAnoy, A. M., Dua, S., Blanksby, S. J., Bowie, J. H. *J. Chem. Soc., Perkin. Trans. 2*, **2000**, 1665.

McAnoy, A.M., Dua, S., Schröder, D., Bowie, J.H., and Schwartz, H., (2003) The formation of CCBO and [CCBO]⁺ from [CCBO]⁻ in the gas phase: a joint experimental and theoretical study.
The Journal of Physical Chemistry A, v. 107 (8), pp. 1181-1187.

NOTE:

This publication is included in the print copy of the thesis held in the University of Adelaide Library.

It is also available online to authorised users at:

<http://dx.doi.org/10.1021/jp0214920>

The formation of neutral CCC and its radical cation from the CCC radical anion in the gas phase. A joint experimental and theoretical study

Andrew M. McAnoy,^a Suresh Dua,^a Detlef Schröder,^b John H. Bowie^{*a} and Helmut Schwarz^b

^a Department of Chemistry, The University of Adelaide, South Australia, 5005.

E-mail: john.bowie@adelaide.edu.au

^b Institut für Chemie, Technische Universität Berlin, D-10623 Berlin, Germany

Received (in Cambridge, UK) 2nd July 2002, Accepted 30th July 2002

First published as an Advance Article on the web 23rd August 2002

The radical anion $[\text{CC}^{13}\text{C}]^-$ has been produced by treatment of $[(\text{CH}_3)_3\text{SiC}\equiv\text{C}^{13}\text{C}(\text{=NNHSO}_2\text{C}_6\text{H}_4\text{-}p\text{-CH}_3)\text{Si}(\text{CH}_3)_3]$ with HO^-/F^- in the ion source of a mass spectrometer. The stable anion undergoes vertical two-electron oxidation [charge reversal ($^- \text{CR}^+$)] in a collision cell to give $[\text{CC}^{13}\text{C}]^+$ which cyclises to the more stable $[\text{cyclo-CC}^{13}\text{C}]^+$ over a barrier of only 11 kJ mol^{-1} [calculated at the CCSD(T)/aug-cc-pVTZ//B3LYP/6-311G(d) level of theory], effectively scrambling the three carbon atoms of the cation radical. One-electron Franck–Condon oxidation of $[\text{CC}^{13}\text{C}]^-$ yields neutral CC^{13}C . Theoretical calculations suggest that neutral CCC may undergo a degenerate rearrangement through a cyclic C_3 transition state if the excess energy of CCC is $\geq 104 \text{ kJ mol}^{-1}$ (at the CCSD(T)/aug-cc-pVTZ//B3LYP/6-311G(d) level of theory). It is likely that at least a proportion of the CC^{13}C neutrals formed from $[\text{CC}^{13}\text{C}]^-$ should have sufficient energy to effect this reaction, resulting in the scrambling of the ^{13}C label. The neutralisation/reionisation ($^- \text{NR}^+$) spectrum of $[\text{CC}^{13}\text{C}]^-$ ($[\text{CC}^{13}\text{C}]^- \rightarrow \text{CC}^{13}\text{C} \rightarrow [\text{CC}^{13}\text{C}]^+$) shows a pronounced peak corresponding to the parent cation, confirming that neutral CC^{13}C is stable for the time of the NR experiment (10^{-6} s). However due to total scrambling of the label in the cation, possible scrambling in the neutral CCC molecule cannot be probed by this experiment. The corresponding $^- \text{NR}^-$ experiment of $[\text{CC}^{13}\text{C}]^-$ showed a recovery signal but the sensitivity of the instrument was not sufficient to detect the decomposition fragments of the final radical anion.

Introduction

The volume of scientific literature pertaining to carbon clusters is testament to the importance of these unusual species.^{1,2} The participation of carbon clusters in circumstellar and interstellar chemistry,^{3–5} combustion processes,⁶ and material sciences,⁷ is well known, but understanding the precise role in each of these systems demands detailed knowledge of the structure and reactivity of such molecules. Small carbon clusters are present in stellar media^{3–5} and are considered^{8,9} to be the precursors of large carbon molecules^{10,11} including aromatic species and fullerenes.¹² To date, C_2 , C_3 and C_5 are the only small carbon neutrals definitely identified in the stellar medium: e.g. in the circumstellar envelope of the evolved carbon star IRC+10216.³ A range of linear and cyclic carbon clusters have been made by a number of techniques, and have been characterised,^{8,9,13–28} including linear and rhombic C_4 ²⁷ and linear C_5 .²⁸

The smallest polyatomic carbon cluster (cumulene), linear C_3 , has been detected in a number of extraterrestrial sources including comets,²⁹ circumstellar envelopes,^{3,30} cold dense molecular clouds,³¹ and diffuse molecular clouds.³² Detection of this molecule in such different environments was effected by using the electronic transition at 4050 \AA (comets²⁹ and diffuse clouds³²), by the bending mode at 63.42 cm^{-1} (dense clouds³¹), and the anti-symmetrical stretching mode at 2040 cm^{-1} (circumstellar envelopes³).

Linear C_3 was first formed in the laboratory from deposited carbon vapour in 1962.³³ It has since been formed in many ways,³⁴ for example by infrared multiple photon photolysis of allene,³⁵ and by fast electric discharge in the supersonic expansion of CO .³⁶ Experimental measurements on linear CCC include the determination of electron affinity of the neutral

(1.981 eV) determined by photoelectron spectroscopy,³⁷ and other spectroscopic measurements^{13,34,38} including far infrared measurements³⁸ which were subsequently used in the successful search for linear C_3 in cold molecular clouds.³¹ The stability of C_3 has been demonstrated by it being a dominant photofragment of C_n cations ($4 < n < 20$), while in the particular case of C_3^+ , no photofragment was observed.³⁹ Laser ablation TOF mass spectrometry has been used to generate C_3 radical cations,⁴⁰ while the linear C_3 radical anion has been formed by laser ablation of graphite deposited in argon matrices and subsequently studied by infrared spectroscopy.⁴¹

There have been many theoretical studies on isomeric C_3 neutrals,^{42–49} the corresponding anions,^{23,44,48,50} and cations.^{44,51–54} As long ago as 1981, it was realised that the global minimum on the neutral potential surface corresponds to the $^1\Sigma_g^+$ ground state of linear C_3 , while the C_{2v} cyclic C_3 is a transition state for the degenerate isomerisation of linear C_3 .⁴³

In previous studies, we have synthesised small carbon clusters by converting negative ions of known connectivity into neutrals in a collision cell of a mass spectrometer and interrogating those neutral species by reionisation using the neutralisation/reionisation process ($^- \text{NR}^+$).⁵⁵ For example, we have recently made $^{13}\text{CCC}^{13}\text{C}$ ²⁷ and CC^{13}CCC ²⁸ from the corresponding anions, and shown that these energised neutrals undergo carbon scrambling within the timeframe of the NR experiment (10^{-6} s). Theoretical studies indicate that the scrambling mechanisms proceed through rhombic C_4 and a carbon substituted rhombic structure respectively.^{27,28}

The purpose of the present study is twofold, namely, (i) to make labelled linear neutral CC^{13}C from an anion precursor of known connectivity, and (ii) to determine whether the energised neutral CC^{13}C equilibrates its carbons.

Table 1 Anion geometries and energies^{a, b}

	Linear	Cyclic	TS
State	$^2\Pi_g$	2A_1	$^2A'$
Energy/Hartrees	-113.9016615	-113.8851092	-113.842067
Relative energy/kJ mol ⁻¹	0	43 (41 ^c , 60 ^d)	156 (166 ^c)
Bond lengths/Å			
C ₁ C ₂	1.306 (1.311 ^d , 1.307 ^c , 1.328 ^e , 1.310 ^f , 1.322 ^g)	1.363 (1.385 ^c , 1.369 ^d)	1.287 (1.311 ^c)
C ₂ C ₃	1.306	1.363	1.434 (1.462 ^c)
C ₁ C ₃	2.612	1.545	2.179
Angles/ ^o			
C ₁ C ₂ C ₃	180.0	69.0 (69.3 ^c , 68.9 ^d)	106.3 (104.6 ^c)

^a Geometries are optimised at the B3LYP/6-311G(d) level of theory. ^b Energies are calculated at the CCSD(T)/aug-cc-pVTZ//B3LYP/6-311G(d) level of theory and include zero point energy correction [B3LYP/6-311G(d)]. ^c MRD-CI/6-311+G(d)//CASSCF/6-31G(d). ^d B3LYP/6-31G(d). ^e CCSD(T) method (with 255 cGTOs and all electrons correlated). ^f MRCI(modified)aug-cc-pVQZ. ^g QCISD(T)/6-31G(d). ⁴⁴

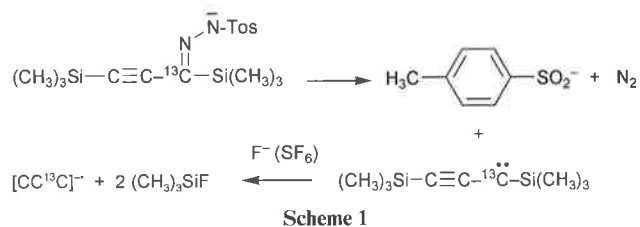
Results and discussion

The formation of linear [CC¹³C]⁻ radical anion

It has been shown previously that singlet CCC is the ground state on the C₃ potential surface and that the corresponding singlet cyclic C₃ is not a local minimum on that surface.⁴³ Triplet CCC is also a stable species, with a singlet–triplet splitting of 201 kJ mol⁻¹.³⁴ The doublet [CCC]⁻ radical anion should be a suitable precursor to effect a one-electron oxidation *via* a Franck–Condon vertical process to yield the required linear species CCC. However, there is a complication, because two stable C₃ radical anions exist. One is the required linear species [CCC]⁻, the other the cyclic C₃ radical anion. The B3LYP/6-311G(d) optimised geometries of these species are given in Table 1, together with their relative energies calculated at the CCSD(T)/aug-cc-pVTZ//B3LYP/6-311G(d) level of theory. Results from previous studies are also listed in Table 1. The highest level theoretical approach to date predicts a CC bond length of 1.307 Å for [CCC]⁻;²¹ this is in excellent agreement with our value of 1.306 Å (Table 1). While the linear C₃ anion radical is the lower in energy of the two anions, the cyclic anion radical is only higher in energy by 42 kJ mol⁻¹ at our chosen level of theory (Table 1). Based on this small difference in energy, the possibility must be considered that both anion radicals might be formed in the ion source of the mass spectrometer from a neutral precursor with linear CCC connectivity.

The rearrangement of linear [CCC]⁻ to [cyclo-C₃]⁻ has been computed at the CCSD(T)/aug-cc-pVTZ//B3LYP/6-311G(d) level of theory; geometry and energy data for the two minima and the transition states are recorded in Table 1, together with comparison data from other studies, as appropriate. There is a barrier of 156 kJ mol⁻¹ for the conversion of the linear to the cyclic anion: a barrier high enough to suggest that it is unlikely for such a rearrangement to occur in the ion source of the mass spectrometer, following the formation of [CCC]⁻. In an earlier study,²⁷ the barrier for rearrangement of [CCCC]⁻ to rhombic [C₄]⁻ was calculated to be 132 kJ mol⁻¹ at the CCSD(T)/aug-cc-pVDZ//B3LYP/6-31(d) level of theory; in fact, this rearrangement does not occur experimentally. Similarly, no rearrangement was noted for the [CCCCC]⁻ radical anion.²⁸

The synthesis of [CC¹³C]⁻ was effected by deprotonation of the ¹³C labelled tosylhydrazone [(CH₃)₃SiC≡C¹³C(NNHTos)(Si(CH₃)₃)] to yield the precursor anion shown in Scheme 1. This procedure is analogous to that used previously for the synthesis of [CC¹³CCC]⁻;²⁸ using our SF₆ modification²⁸ of the Squires double desilylation procedure⁵⁶ (which uses F⁻/NF₃), together with deprotonation of the tosylhydrazone to effect formation of the carbene intermediate.⁵⁷ We do not know



the precise sequence for this procedure (just as the intimate mechanism of the Squires bis-desilylation is not known⁵⁶). Scheme 1 shows one possible rationale of the overall reaction. [M - H]⁻, *p*-CH₃C₆H₄SO₂⁻ and [CC¹³C]⁻ species are formed in the ion source of the mass spectrometer, consistent with the process shown in Scheme 1.

The collision induced (CID) mass spectrum (MS/MS) of [CC¹³C]⁻ shows a pronounced peak due to the parent radical anion together with two weak peaks corresponding to losses of ¹²C and ¹³C. The spectrum was scanned at maximum sensitivity over the region containing *m/z* 24 and 25 (CC⁻ and C¹³C⁻) giving a peak area ratio (*m/z* 24 to *m/z* 25) of 1 : 1. This result demonstrates that the carbons of [CC¹³C]⁻ are not scrambling prior to or during the losses of ¹²C and ¹³C. This is interesting, since the dissociation process C₃⁻ → C₂⁻ + C, has Δ*H* = +603 kJ mol⁻¹,⁵⁸ similar results were obtained for linear C₄ and C₅.^{27,28}

In view of the experimental observation that [CC¹³C]⁻ may decompose (by loss of ¹²C and ¹³C) without prior or accompanying rearrangement of the carbon skeleton, is it possible that the transition state for this process is inaccessible? Renner–Teller splitting of the $^2\Pi_g$ ground state occurs upon symmetrical bending of [CCC]⁻. This effect has been studied using a number of high level procedures.^{19,48} The two Renner–Teller bending potentials (2B_2 and 2A_2) increase dramatically in energy upon symmetrical bending of the anion radical. In contrast, the cyclic anion is a local minimum on the 2A_1 surface, and this increases in energy with increasing CCC bond angle. The $^2\Pi_g$ excited state is attained some 343 kJ mol⁻¹ higher in energy than the $^2\Pi_u$ ground state (calculated at the MRD-CI/6-311+G(d)//CASSCF/6-31G(D) level of theory).⁴⁶ Thus, if only symmetrical bending is considered, theory suggests that neither ring-opening nor ring-closing is viable energetically. At first sight this appears to be at variance with the transition state detailed in Table 1. However the transition state is not symmetrical and lies on the $^2A'$ surface near the crossing point of the 2A_1 and 2B_2 surfaces. Therefore the anion rearrangement not only has a barrier, but it is also dependent on accessing the transition state on the $^2A'$ potential energy surface. In addition, rearrangement of energised [CCC]⁻ has to compete with collision-induced electron detachment.

The CR^+ and NR^+ mass spectra of $[\text{CC}^{13}\text{C}]^-$

The CR^+ and NR^+ mass spectra of $[\text{CC}^{13}\text{C}]^-$ are shown in Figs. 1 and 2 respectively. The spectra are simple, showing recovery signals and fragment peaks corresponding to losses of ^{12}C and ^{13}C together with $^{12}\text{C}_2$ and $^{12}\text{C}^{13}\text{C}$. The spectra are very similar to each other except for the peak at m/z 18.5 in the CR^+ spectrum which is due to doubly-charged CC^{13}C [this is our first observation of a peak produced by a doubly-charged cation in a CR^+ spectrum of a cumulene anion: this peak is present in the CR^+ spectra obtained from the ZAB/AMD 604 mass spectrometer (Berlin) and the VG ZAB 2HF instrument (Adelaide)]. The peaks due to losses of ^{12}C and ^{13}C (m/z 25 and 24) have an area ratio of 2 : 1, while those corresponding to losses of $^{12}\text{C}_2$ and $^{12}\text{C}^{13}\text{C}$ (m/z 13 and 12) have an area ratio of 1 : 2. These ratios indicate that the carbon chain scrambles statistically either during the formation of $[\text{C}_2^{12}\text{C}^{13}\text{C}]^+$, or accompanying decomposition of the parent radical cation.

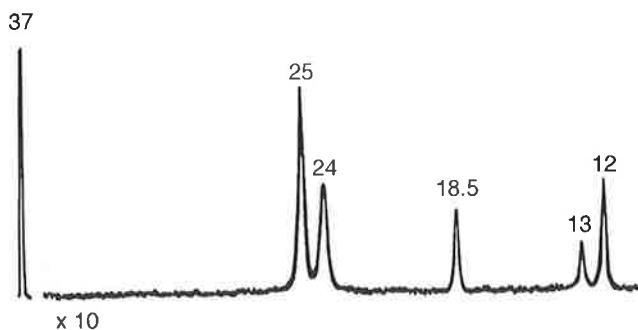


Fig. 1 CR^+ spectrum of $[\text{CC}^{13}\text{C}]^-$. HF-ZAB/AMD 604 mass spectrometer. Full experimental conditions see Experimental section.

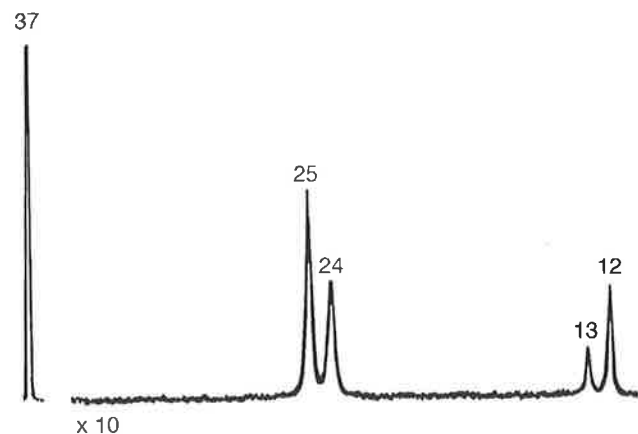


Fig. 2 NR^+ spectrum of $[\text{CC}^{13}\text{C}]^-$. HF-ZAB/AMD 604 mass spectrometer. Full experimental conditions see Experimental section.

The rearrangement of linear $[\text{CC}^{13}\text{C}]^+$ to the cyclic isomer

The cation potential energy surface has been investigated at the CCSD(T)/aug-cc-pVTZ//B3LYP/6-311(d) level of theory, and the results are listed in Table 2. There has been debate as to whether the linear $^2\Sigma_u$ or the cyclic 2B_2 structure is the ground state.^{44,45,51,53,54} Our calculations predict that the cyclic 2B_2 cation corresponds to the global minimum on the cation potential energy surface, with the linear $^2\Sigma_u$ state lying 24 kJ mol⁻¹ above the ground state. The barrier to convert the linear to the cyclic cation is only 11 kJ mol⁻¹. When $[\text{CCC}]^-$ undergoes vertical two-electron oxidation to the linear cation, the excess Franck–Condon energy (the difference in energy between the ground-state cation radical $[\text{CCC}]^+$ and the radical cation with the anion geometry on the cation potential energy surface) is only 2 kJ mol⁻¹ at the B3LYP/6-311(d) level of theory. This small energy difference can be attributed to the similar geometries of the anion and cation (*cf.* data in Tables 1 and 2). This

Franck–Condon excess energy of 2 kJ mol⁻¹ is not sufficient to surmount the 11 kJ mol⁻¹ barrier between the linear and cyclic C_3 cation radicals. However, the actual excess energy of the cation formed will be more than the excess Franck–Condon energy, either as a consequence of some formation energy of the anion radical being carried through to the cation, or by some subsequent collision process of the cation. Thus $[\text{CC}^{13}\text{C}]^+$ formed initially in the CR^+ process will rearrange over the 11 kJ mol⁻¹ barrier to yield the cyclic cation radical in which the ^{13}C label is essentially scrambled.

The conversion of $[\text{CC}^{13}\text{C}]^-$ to neutral CC^{13}C

The CR^+ and NR^+ spectra of $[\text{CC}^{13}\text{C}]^-$ show the same fragment peaks in the same ratio. The NR^+ spectrum shows the presence of a pronounced recovery signal confirming that a neutral C_3 is stable for the duration of the NR experiment (10⁻⁶ s). The similarity of the NR^+ and CR^+ spectra of $[\text{CC}^{13}\text{C}]^-$ suggests that no major decomposition of the neutral occurs on the microsecond timescale [for $\text{CCC} \rightarrow \text{CC} + \text{C}$, $\Delta H = 734$ kJ mol⁻¹⁵⁸]. Since complete ^{13}C scrambling is noted for both CR^+ and NR^+ spectra, this means that the NR^+ spectrum (Fig. 2) provides no information concerning the question of carbon scrambling of the neutral. In this context, it has been recently reported that carbon scrambling within the ^{13}C labelled $[\text{C}_3]^+$ species produced by dissociative ionisation of $[\text{CH}_3^{13}\text{C}=\text{CH}_2]^+$ precedes formation of a labelled neutral C_3 by one-electron vertical reduction in an $^+\text{NR}^+$ experiment.⁵⁹

Since the NR^+ spectrum of $[\text{CC}^{13}\text{C}]^-$ gives no data concerning the possibility of carbon scrambling occurring during or subsequent to the vertical one-electron oxidation of the anion to the neutral, the next obvious experiment is to measure the NR^- spectrum. Since the CID mass spectrum of $[\text{CC}^{13}\text{C}]^-$ shows no carbon scrambling in the anion, rearrangement of the carbon skeleton of the neutral CC^{13}C should be readily identifiable in the NR^- spectrum of $[\text{CC}^{13}\text{C}]^-$. Unfortunately, the fragment ions in the CID spectrum of $[\text{CC}^{13}\text{C}]^-$ are very weak (see earlier), and although a peak corresponding to the parent anion radical is observed in the NR^- spectrum, no fragment anions were detected using the maximum sensitivity of the instrument.

The geometry of the neutral $^1\Sigma_g$ ground state of CCC has been calculated at the B3LYP/6-311G(d) level of theory. Results are recorded in Table 3, together with data obtained from previous studies. We obtain a value of 1.291 Å for the CC bond length; this should be compared with the experimental value of 1.297 Å,³⁰ and a 'best' theoretical value of 1.295 Å obtained previously.⁴⁵

A theoretical study of the triplet C_3 neutral potential energy surface predicts the linear $^3\Pi_u$ state to be 226 kJ mol⁻¹ higher in energy than the $^1\Sigma_g$ ground state,⁴⁸ which should be compared with an experimental value of 201 kJ mol⁻¹.³⁴ There is also a cyclic neutral of D_{3h} symmetry on the triplet potential energy surface.^{41,46} At the CCSD(T)/aug-cc-pVTZ//B3LYP/6-311(d) level of theory, the energies of linear $^3\Pi_u$ and cyclic 3A_1 neutrals relative to the ground state singlet are 204 and 85 kJ mol⁻¹ respectively (Table 3).

The degenerate rearrangement of neutral $^1\Sigma_g$ CCC *via* the 1A_1 cyclic transition state is calculated to require 104 kcal mol⁻¹ (Table 3). This should be compared with the barrier of 157 kJ mol⁻¹ on the triplet neutral surface for the conversion of the $^3\Pi_u$ state to the more stable 3A_1 (Table 3). Since we cannot control the energy of the NR^+ procedure, both the $^1\Sigma_g$ and $^3\Pi_u$ CCC neutrals could be accessible in the one-electron vertical oxidation from $[\text{CCC}]^-$.⁶⁰ In our previous studies of the carbon scrambling observed for singlet forms of neutral CCCC²⁷ and CCCCC,²⁸ the respective barriers for the scrambling processes were calculated to be 120 and 224 kJ mol⁻¹ at the CCSD(T)/aug-cc-pVDZ//B3LYP/6-31(d) level of theory, energies significantly higher than the Franck–Condon excess energies

Table 2 Cation geometries and energies^{a, b}

	Linear	Cyclic	TS
State	$^2\Sigma_u$	2B_2	2B_2
Energy/Hartrees	-113.389070	-113.398386	-113.384757
Relative energy/kJ mol ⁻¹	24 (12.5 ^c , 28 ^d , 17 ^e , 22 ^f)	0	36
Bond lengths/Å			
C ₁ C ₂ , C ₂ C ₃	1.290 (1.318 ^c , 1.307 ^d , 1.283 ^e , 1.314 ^f)	1.316 (1.333 ^c , 1.324 ^d , 1.296 ^e , 1.331 ^f)	1.293
C ₁ C ₃	2.580	1.446	2.333
Angles/°			
C ₁ C ₂ C ₃	180.0	66.6 (67.2 ^c , 67.8 ^d , 71.0 ^e , 66.6 ^f)	128.9

^a Geometries are optimised at the B3LYP/6-311G(d) level of theory. ^b Energies are calculated at the CCSD(T)/aug-cc-pVTZ//B3LYP/6-311G(d) level of theory. ^c QCISD(T)/6-311+G(2df)//QCISD(T)/6-31G(d). ^d CCSD(T)/[5s4p3d2f1g]/CCSD(T)/[4s3p2d1f]. ^e CISD/TZ2P. ^f CASSCF[5s3p2d1f].⁵⁴

Table 3 Neutral geometries and energies^{a, b}

	Singlet linear	Singlet TS	Triplet linear	Triplet cyclic	Triplet TS
State	$^1\Sigma_g$	1A_1	$^3\Pi_u$	$^3A_1'$	$^3A'$
Energy/Hartrees	-113.830199	-113.797685	-113.752653	-113.797674	-113.692625
Relative energy/kJ mol ⁻¹	0	104 (125 ^c)	204 ([204] ^d , 226 ^e , 197 ^f)	85 (102 ^e , 97 ^g)	361 (367 ^g)
Bond lengths/Å					
C ₁ C ₂	1.291 ([1.297] ^g , 1.278 ^c , 1.311 ^e , 1.295 ^h , 1.310 ⁱ , 1.308 ^j)	1.260 (1.250 ^c)	1.294 ([1.298] ^d , 1.317 ^e , 1.311 ^f)	1.370 (1.346 ^e , 1.393 ^g)	1.376 (1.387 ^g)
C ₂ C ₃	1.291	1.471 (1.461 ^c)	1.294	1.370	1.301 (1.335 ^g)
C ₁ C ₃	2.582	1.471 (1.461 ^c)	2.588	1.370	2.146
Angles/°					
C ₁ C ₂ C ₃	180.0	64.7 (64.7 ^c)	180.0	60.0 (60.0 ^{c, e})	106.5 (103.2 ^g)

^a Geometries are optimised at the B3LYP/6-311G(d) level of theory. ^b Energies are calculated at the CCSD(T)/aug-cc-pVTZ//B3LYP/6-311G(d) level of theory and include zero point energy correction [B3LYP/6-311G(d)]. ^c MP4SDTQ/6-31G(d)//HF/6-31G(d). ^d Experimental value. ^e MRD-CI/6-311+G(d)//CASSCF/6-31G(d). ^f MRD-CI. ^g Experimental value. ^h CCSD(T) method (with 255 cGTOs and all electrons correlated). ⁱ QCISD(T)/6-31G(d). ^j QCISD(T)/6-31G(d).⁴⁴

imparted to those neutrals during the one-electron oxidation processes. Both of these barriers are greater than that required for the degenerate rearrangement of singlet CCC. It therefore seems likely that at least a proportion of the CC¹³C neutrals formed from [CC¹³C]⁻ will undergo the degenerate rearrangement (Table 3), with consequent randomisation of the carbons. Unfortunately we have no experimental probe to substantiate this proposal.

Conclusions

(i) The radical anion [CC¹³C]⁻ has been prepared by an unequivocal gas-phase synthesis, and this anion retains its skeletal integrity under the collision conditions necessary to effect one-electron vertical oxidation to the corresponding CCC neutral molecule.

(ii) The radical anion [CC¹³C]⁻ is converted by two-electron vertical oxidation to [CC¹³C]⁺ which requires an excess energy of only 11 kJ mol⁻¹ to interconvert to the more stable [cyclo-C₂¹³C]⁺.

(iii) The radical anion [CC¹³C]⁻ is converted to neutral CC¹³C by Franck-Condon one-electron vertical oxidation. Theoretical calculations indicate that the neutral singlet requires an excess energy of 104 kJ mol⁻¹ to effect a degenerate rearrangement through a cyclic C₂¹³C transition state; a process which essentially randomises the three carbon atoms. It is likely that some neutrals will equilibrate the carbons by this process, but no experimental probe was available to substantiate this proposal.

Experimental

A. Mass spectrometric methods

For a detailed description of the experiment and the instrument used see.⁶¹ In brief, the experiments were performed using a four-sector modified ZAB/AMD 604 mass spectrometer with BEBE configuration, where B and E represent magnetic and electric sectors respectively. The [CC¹³C]⁻ radical anion was generated by chemical ionisation (CI) in the negative ion mode, with typical source conditions as follows: source temperature 200 °C, repeller voltage -0.5 V, ion extraction voltage 8 kV, mass resolution $m/\Delta m \geq 1500$. The precursor, 1,3-bis(trimethylsilyl)-1-¹³C-prop-2-yne-1-*p*-tosylhydrazon, was placed in a small glass capillary tube which was then drawn out in a flame to create a very fine aperture, allowing for a slow steady release of sample vapour upon heating. The capillary was inserted into the CI source *via* the direct probe; the probe tip was heated to 60–80 °C to generate a background pressure of *ca.* 10⁻⁵ Torr inside the source housing. The [CC¹³C]⁻ radical anion was formed as suggested in Scheme 1, utilising a 1 : 1 mixture of H₂O and SF₆ as CI reagent gases [to liberate the reagent ions HO⁻ and F⁻ respectively—a modification²⁸ of the Squires bis S_N2(Si) reaction with F⁻/NF₃⁵⁶] at a pressure of *ca.* 10⁻⁴ Torr inside the source housing.

Collisional induced dissociation (CID) of B(1) mass selected ions was effected in the second of the tandem collision cells positioned between B(1) and E(1). Helium was used as a target gas. The pressure of the collision gas in the cell was maintained such that 80% of the parent ion beam was transmitted through

the cell. This corresponds to an average of 1.1–1.2 collisions per ion.⁶² Product ions resulting from CID were recorded by scanning E(1).

Neutralisation–reionisation⁵⁵ ($^{-}\text{NR}^{+}$ and $^{-}\text{NR}^{-}$) experiments were performed for B(1) mass-selected $[\text{CC}^{13}\text{C}]^{-}$ utilising the dual collision cells located between sectors B(1) and E(1). Neutralisation of the anions was achieved by collisional electron detachment using O_2 at 80% transmittance as collision gas, while reionisation to cations was achieved by collision of the neutrals with O_2 , again at 80% transmittance.

Reionisation to anions was effected using xenon, at 80% transmittance. Any ions remaining after the first collision event were deflected from the primary neutral beam using an electrode maintained at a high voltage (1.0 kV) positioned before the second collision cell. In order to detect a reionisation signal due to the parent, the neutral species must be stable for approximately one microsecond. Charge reversal ($^{-}\text{CR}^{+}$) spectra⁶³ were recorded using single collision conditions in collision cell 1 (O_2 , 80% transmission of main beam).

1,3-Bis(trimethylsilyl)-1-¹³C-prop-2-yne-1-*p*-tosylhydrazone was prepared by a known procedure (¹³C = 99.5%).^{64,65}

B. Theoretical methods

Geometry optimisations were carried out with the Becke 3LYP method^{66,67} using the 6-311G(d) basis set within the GAUSSIAN 98 suite of programs.⁶⁸ Stationary points were characterised as either minima (no imaginary frequencies) or transition structures (one imaginary frequency) by calculation of the frequencies using analytical gradient procedures. The minima connected by a given transition structure were confirmed by intrinsic reaction coordinate (IRC) calculations. The calculated frequencies were also used to determine zero-point vibrational energies which were used as a zero-point correction for the electronic energies. Some problems have been highlighted in the literature regarding the use of the B3LYP method for the accurate prediction of molecular energies for carbon clusters,⁶⁹ even though the method continues to be used with success.^{70,71} † More accurate energies for the B3LYP geometries were determined using the CCSD(T) method⁷² together with the Dunning aug-cc-pVTZ basis set.⁷³ The CCSD(T)/aug-cc-pVTZ//B3LYP/6-311G(d) approach used in this study computes the adiabatic electron affinity of linear C_3 to be 1.945 eV in good agreement with the experimentally measured value of 1.981 eV.³⁷ All calculations were carried out on the Alpha Server at the Australian Partnership for Advanced Computing (APAC) National Facility (Canberra).

Acknowledgements

This project was supported by an international linkage grant funded jointly by the Australian Research Council, the Deutsche Forschungsgemeinschaft and Fonds der Chemischen Industrie. A.M.McA. acknowledges the award of an APRA PhD scholarship. We thank the Australian Partnership for Advanced Computing (APAC) National Facility (Canberra) for a generous allowance of super computer time.

† A reviewer has asked that we make a statement concerning “the bias possibly introduced by the selected type of calculation in the relative energies of linear versus cyclic forms.” Plattner and Houk⁶⁹ have investigated large cyclic carbon systems and found density functional theory to incorrectly favour allenic structures over polyacetylenic structures by about 25 kJ mol⁻¹ per $\text{C}\equiv\text{C}$ to $\text{C}=\text{C}=\text{C}$ transformation. This is also true for smaller systems,⁶⁹ for example B3LYP/6-31G(d) favours allene to prop-1-yne, reversing their order of stability by 19 kJ mol⁻¹. We do not know if there is a bias towards linear over cyclic cumulenic systems of the type we are considering, because the experimental data are not available. However, we believe this perceived problem is circumvented using the CCSD(T) method together with the Dunning aug-cc-pVTZ basis set as outlined below.

References

- 1 W. Weltner and R. J. Van Zee, *Chem. Rev.*, 1989, **89**, 1713 and references cited therein.
- 2 A. Van Orden and R. J. Saykally, *Chem. Rev.*, 1998, **98**, 2313 and references cited therein.
- 3 P. F. Bernath, K. H. Hinkle and J. J. Keady, *Science*, 1989, **244**, 562.
- 4 P. Ehrenfreund and B. H. Foing, *Astron. Astrophys.*, 1996, **307**, L25.
- 5 B. P. A. Bettens and E. Herbst, *Astrophys. J.*, 1997, **478**, 545.
- 6 H. W. Kroto and K. McKay, *Nature*, 1988, **332**, 328.
- 7 R. Levi Guyer and D. E. Koshland, *Science*, 1990, **250**, 1640.
- 8 G. von Helden, P. R. Kemper, N. G. Gotts and M. T. Bowers, *Science*, 1993, **259**, 1300.
- 9 G. von Helden, N. G. Gotts and M. T. Bowers, *Nature*, 1993, **363**, 60.
- 10 R. F. Baddour and R. S. Timmins (Eds.), *The Application of Plasmas to Chemical Processing*, MIT Press, Cambridge, MA, 1967.
- 11 J. M. Jones, R. P. Malcolm, K. M. Thomas and S. H. Botrell, *Carbon*, 1996, **34**, 231.
- 12 H. W. Kroto, J. R. Heath, S. C. O'Brien, R. F. Curl and R. E. Smalley, *Nature*, 1985, **318**, 162.
- 13 (a) I. Cermac, M. Förderer, I. Cermakova, S. Kalhofer, H. Stopkaebeler, G. Monninger and W. Krätschmer, *J. Chem. Phys.*, 1998, **108**, 10129; (b) G. Monninger, M. Förderer, P. Gürtler, S. Kalhofer, S. Petersen, L. Nemes, P. G. Szalay and W. Krätscher, *J. Phys. Chem. A*, 2002, **106**, 5779.
- 14 W. Weltner and R. J. Van Zee, *Chem. Rev.*, 1989, **89**, 1713.
- 15 A. N. Raghavachari, *J. Chem. Phys.*, 1990, **93**, 2099.
- 16 L. Adamowicz, *Chem. Phys. Lett.*, 1991, **182**, 45.
- 17 J. D. Watts and R. J. Bartlett, *J. Chem. Phys.*, 1992, **97**, 3445.
- 18 (a) R. H. Kranz and W. R. M. Graham, *J. Chem. Phys.*, 1992, **96**, 2517; (b) R. H. Kranz and W. R. M. Graham, *J. Chem. Phys.*, 1993, **98**, 71; (c) R. H. Kranz, C. M. L. Rittby and W. R. M. Graham, *J. Chem. Phys.*, 1995, **103**, 6841; (d) R. H. Kranz, C. M. L. Rittby and W. R. M. Graham, *J. Chem. Phys.*, 1996, **105**, 5313.
- 19 J. Sun, H.-F. Grutzmacher and C. Lifshitz, *J. Am. Chem. Soc.*, 1993, **115**, 8382 and references cited therein.
- 20 (a) J. R. Heath and R. J. Saykally, *On Clusters and Clustering*; P. J. Reynolds, Ed.; Elsevier, Amsterdam, 1993, p. 7; (b) A. V. Orden and R. J. Saykally, *Chem. Rev.*, 1998, **98**, 2313.
- 21 S. Schmatz and P. Botschwina, *Chem. Phys. Lett.*, 1995, **235**, 8; S. Schmatz and P. Botschwina, *Chem. Phys. Lett.*, 1995, **235**, 136.
- 22 W. Weltner, R. J. Van Zee and S. Li, *J. Phys. Chem.*, 1995, **99**, 6277.
- 23 S. Schmatz and P. Botschwina, *Int. J. Mass Spectrom. Ion Processes*, 1995, **149/150**, 621.
- 24 (a) Y. Zhao, E. deBeer, C. Xu, T. Taylor and D. M. Neumark, *J. Chem. Phys.*, 1996, **105**, 4905; (b) Y. Zhao, E. deBeer and D. M. Neumark, *J. Chem. Phys.*, 1996, **105**, 2575.
- 25 J. P. Maier, *Chem. Soc. Rev.*, 1997, **26**, 21.
- 26 S. J. Blanksby and J. H. Bowie, *Mass Spectrom. Rev.*, 1999, **18**, 131.
- 27 S. J. Blanksby, D. Schröder, S. Dua, J. H. Bowie and H. Schwarz, *J. Am. Chem. Soc.*, 2000, **122**, 7105.
- 28 S. Dua and J. H. Bowie, *J. Phys. Chem. A*, 2002, **106**, 1374.
- 29 P. Swings, *Rev. Mod. Phys.*, 1942, **12**, 190.
- 30 K. W. Hinkle, J. J. Keady and P. F. Bernath, *Science*, 1988, **241**, 1319.
- 31 T. F. Giesen, A. O. Van Orden, J. D. Cruzan, R. A. Provencal, R. J. Saykally, R. Gendriesch, F. Lewen and G. Winnewisser, *Astrophys. J.*, 2001, **551**, L181.
- 32 J. P. Maier, N. M. Lakin, G. A. H. Walker and D. A. Bohlender, *Astrophys. J.*, 2001, **553**, 267.
- 33 R. H. Barger and H. P. Broida, *J. Chem. Phys.*, 1962, **37**, 1152.
- 34 H. Sasada, T. Amano, C. Jarman and P. F. Bernath, *J. Chem. Phys.*, 1991, **94**, 2401 and references cited therein.
- 35 M. L. Lesiaki, H. W. Hicks, A. Orenstein and W. A. Guillory, *Chem. Phys. Lett.*, 1980, **71**, 72.
- 36 J. Szczepanski, C. Wehlburg and M. Vala, *J. Phys. Chem. A*, 1997, **101**, 7039.
- 37 J. M. Oakes and G. B. Ellison, *Tetrahedron*, 1986, **42**, 6263.
- 38 C. A. Schumuttermaer, R. C. Cohen, N. Pugliano, J. R. Heath, A. L. Cooksy, K. L. Busarow and R. J. Saykally, *Science*, 1990, **249**, 897.
- 39 M. E. Geusic, T. J. McIlrath, M. F. Jarrold, L. A. Bloomfield, R. R. Freeman and W. L. Brown, *J. Chem. Phys.*, 1986, **84**, 2421.
- 40 J. Baker, S. K. Bramble and P. A. Hamilton, *J. Mol. Spectrosc.*, 1997, **101**, 7039.
- 41 J. J. Gaumet, A. Wakisaka, Y. Shimizu and Y. Tamori, *J. Chem. Soc., Faraday Trans.*, 1993, **89**, 1667.
- 42 J. Peric-Radic, J. Roemelt, S. D. Peyerimhoff and R. J. Buenker, *Chem. Phys. Lett.*, 1977, **50**, 344.
- 43 R. A. Whiteside, R. Krishnan, M. J. Frisch, J. A. Pople and P. v. R. Schleyer, *Chem. Phys. Lett.*, 1981, **80**, 547.
- 44 K. Raghavachari, *Chem. Phys. Lett.*, 1990, **171**, 249.

- 45 M. Mladenovic, S. Schmatz and P. Botschwina, *J. Chem. Phys.*, 1994, **101**, 5891.
- 46 J. M. L. Martin and P. R. Taylor, *J. Phys. Chem.*, 1996, **100**, 6047.
- 47 J. Szczepanski, S. Ekern and M. Vala, *J. Phys. Chem. A*, 1997, **101**, 1841.
- 48 H. Fueno and Y. Taniguchi, *Chem. Phys. Lett.*, 1999, **312**, 65.
- 49 E. E. Pasqualini and M. Lopez, *Chem. Phys. Lett.*, 2000, **320**, 415.
- 50 C. Leonard, D. Panten, N. M. Lakin, G. Chambaud and P. Rosmus, *Chem. Phys. Lett.*, 2001, **335**, 97.
- 51 R. S. Grev, I. L. Alberts and H. F. Schaefer, *J. Phys. Chem.*, 1990, **94**, 3379, 8744.
- 52 J. D. Watts, J. F. Stanton, J. Gauss and R. L. Bartlett, *J. Chem. Phys.*, 1991, **94**, 4320.
- 53 G. E. Scuseria, *Chem. Phys. Lett.*, 1991, **176**, 27.
- 54 (a) P. R. Taylor, J. M. L. Martin, J. P. Francois and B. Gijbels, *J. Phys. Chem.*, 1991, **95**, 6530; (b) P. R. Taylor, *J. Phys. Chem.*, 1991, **95**, 6534.
- 55 (a) C. Wesdemiotis and F. W. McLafferty, *Chem. Rev.*, 1987, **87**, 485; (b) D. V. Zagorevskii and J. L. Holmes, *Mass Spectrom. Rev.*, 1994, **13**, 133; (c) N. Goldberg and H. Schwarz, *Acc. Chem. Res.*, 1994, **27**, 347; (d) For more recent reviews, including NR nomenclature, see C. A. Schalley, G. Hornung, D. Schröder and H. Schwarz, *Chem. Soc. Rev.*, 1998, **27**, 91; (e) D. V. Zagorevskii and J. L. Holmes, *Mass Spectrom. Rev.*, 1999, **18**, 87.
- 56 P. G. Wenthold, J. Hu and R. R. Squires, *J. Am. Chem. Soc.*, 1994, **116**, 6961.
- 57 Y. Z. An, Y. Rubin, C. Schaller and S. W. McElvany, *J. Org. Chem.*, 1994, **59**, 2927.
- 58 <http://webbook.nist.gov/> - C₃⁻, 638; C₃, 820; C₂⁻, 525; C₂, 838; C, 717 kJ mol⁻¹. In addition, EA C₂, 3.273 ± 0.008 eV⁴⁶ and C, 1.262 eV⁵⁷.
- 59 A. Fura, F. Turecek and F. W. McLafferty, *Int. J. Mass Spectrom.*, 2002, **217**, 81.
- 60 D. W. Arnold, S. E. Bradforth, T. N. Kitsopoulos and D. M. Neumark, *J. Chem. Phys.*, 1991, **95**, 8753.
- 61 C. A. Schalley, G. Hornung, D. Schröder and H. Schwarz, *Chem. Soc. Rev.*, 1998, **27**, 91.
- 62 J. L. Holmes, *Org. Mass Spectrom.*, 1985, **20**, 169.
- 63 (a) J. H. Bowie and T. Blumenthal, *J. Am. Chem. Soc.*, 1975, **97**, 2959; (b) J. E. Szulejko, J. H. Bowie, I. Howe and J. H. Beynon, *Int. J. Mass Spectrom. Ion Phys.*, 1980, **13**, 76; (c) M. M. Bursley, *Mass Spectrom. Rev.*, 1990, **9**, 555.
- 64 W. E. Billups and M. M. Haley, *J. Am. Chem. Soc.*, 1991, **113**, 5084.
- 65 K. J. H. Kruithof, R. F. Schmitz and G. W. Klumpp, *Tetrahedron*, 1983, **39**, 3073.
- 66 A. D. Becke, *J. Phys. Chem.*, 1993, **98**, 5648.
- 67 P. J. Stevens, F. J. Devlin, C. F. Chabrowski and M. J. Frisch, *J. Phys. Chem.*, 1994, **98**, 11623.
- 68 M. J. Frisch, G. W. Trucks, H. B. Schlegel, G. E. Scuseria, M. A. Robb, J. R. Cheeseman, V. G. Zakrzewski, J. A. Montgomery, R. E. Stratmann, J. C. Burant, S. Dapprich, J. M. Millam, A. D. Daniels, K. N. Kudin, M. C. Strain, O. Farkas, J. Tamasi, V. Barone, M. Cossi, R. Cammi, B. Mennucci, C. Pomelli, C. Adama, S. Clifford, J. Ochterski, B. Morokuma, D. K. Malich, A. D. Rabuck, K. Raghavachari, J. B. Foresman, J. Cioslowski, J. V. Ortiz, B. B. Stefanov, G. Liu, A. Liashenko, P. Piskorz, I. Komaromi, R. Gomperts, R. L. Martin, D. J. Fox, T. Keith, M. A. Al-Latham, C. Y. Peng, A. Nanayakkara, C. Gonzalez, M. Challacombe, P. M. W. Gill, B. G. Johnson, W. Chen, M. W. Wong, J. L. Andres, M. Head-Gordon, E. S. Replogle and J. A. Pople, GAUSSIAN 98, Gaussian, Inc.; Pittsburgh, PA, 1998.
- 69 D. A. Plattner and K. N. Houk, *J. Am. Chem. Soc.*, 1995, **117**, 4405 and references cited therein.
- 70 (a) J. M. L. Martin, J. El-Yazal and J.-P. Francois, *Chem. Phys. Lett.*, 1995, **242**, 570; (b) J. M. L. Martin, J. El-Yazal and J.-P. Francois, *Chem. Phys. Lett.*, 1996, **252**, 9; (c) J. M. L. Martin and P. R. Taylor, *J. Phys. Chem.*, 1996, **100**, 6047.
- 71 E. E. Pasqualini and M. López, *Chem. Phys. Lett.*, 2000, **320**, 415.
- 72 (a) J. Cizek, *Adv. Chem. Phys.*, 1969, **14**, 35; (b) K. Raghavachari, G. W. Trucks, J. A. Pople and M. Head-Gordon, *Chem. Phys. Lett.*, 1989, **157**, 479; (c) M. J. O. Deegan and P. J. Knowles, *Chem. Phys. Lett.*, 1994, **227**, 321 and references cited therein.
- 73 (a) T. H. Dunning, *J. Chem. Phys.*, 1989, **90**, 1007; (b) D. E. Woon and T. H. Dunning, *J. Chem. Phys.*, 1993, **98**, 1358.

Cumulenic and heterocumulenic anions: potential interstellar species?

Stephen J. Blanksby,¹★ Andrew M. McAnoy,² Suresh Dua² and John H. Bowie²

¹Department of Chemistry and Biochemistry, University of Colorado at Boulder, Boulder, CO 80309, USA

²Department of Chemistry, University of Adelaide, SA 5005, Australia

Accepted 2001 July 16. Received 2001 June 29; in original form 2001 April 4

ABSTRACT

A recent theoretical investigation by Terzieva & Herbst of linear carbon chains, C_n where $n \geq 6$, in the interstellar medium has shown that these species can undergo efficient radiative association to form the corresponding anions. An experimental study by Barckholtz, Snow & Bierbaum of these anions has demonstrated that they do not react efficiently with molecular hydrogen, leading to the possibility of detectable abundances of cumulene-type anions in dense interstellar and circumstellar environments. Here we present a series of electronic structure calculations which examine possible anionic candidates for detection in these media, namely the anion analogues of the previously identified interstellar cumulenes C_nH and $C_{n-1}CH_2$ and heterocumulenes C_nO (where $n = 2-10$). The extraordinary electron affinities calculated for these molecules suggest that efficient radiative electron attachment could occur, and the large dipole moments of these simple (generally) linear molecules point to the possibility of detection by radio astronomy.

Key words: molecular processes – ISM: abundances – ISM: lines and bands – ISM: molecules – infrared: ISM – radio lines: ISM.

1 INTRODUCTION

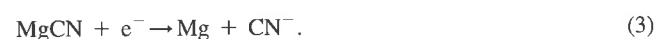
Discussions in the literature pertaining to the chemistry of interstellar and circumstellar gas clouds are dominated by the behaviours of neutrals and cations to the exclusion of anionic species. This is due largely to the fact that only neutrals and cations have thus far been unambiguously detected. Furthermore, the environments in question have long been considered hostile to anions, owing to the abundance of radiation and the generally low energy required for electron detachment (normally about 1 eV). The plausibility of formation of interstellar anions in dense interstellar clouds and the possibility for their detection were first addressed by Herbst (1981):



Based on a statistical model, Herbst suggested that the rate constant for radiative electron attachment to neutral radicals (k_{att} , equation 1) would be large when there existed a high vibrational density of states of the anion X^{-} at an internal energy equal to the electron affinity (EA) of X . Therefore interstellar molecules such as C_4H and C_3N could radiatively attach electrons at near the collision limit of $10^{-7} \text{ cm}^3 \text{ s}^{-1}$ at cloud temperatures between 10 and 50 K. Even so, Herbst predicted that the abundances of such species would be more than 1000 times lower than those of their neutral analogues. Since then it has been postulated that larger molecules

with greater vibrational densities of states may efficiently attach electrons via equation (1) (Omont 1986; Lepp & Dalgarno 1988). Examples of such molecules include carbon chains which are known to have large EAs ($> 2 \text{ eV}$) and even polycyclic aromatic hydrocarbons (PAHs) which are known to have small EAs ($\leq 1 \text{ eV}$). Consequently, recent models for the formation of large, complex interstellar molecules include such anions, and some attempts have been made to estimate the abundances of linear carbon chain anions of the form C_nH^{-} ($10 \leq n \leq 23$) in the interstellar medium (Bettens & Herbst 1996). Despite these predictions, however, experimental studies investigating the gas-phase attachment of electrons to anthracene and the fullerenes C_{60} and C_{70} suggest that there is an activation energy barrier for these species to undergo the reaction described by equation (1) (Canosa et al. 1994; Jaffke et al. 1994; Spanel & Smith 1994).

Petrie (1996) attempted to model the abundance of CN^{-} in the circumstellar envelope of the carbon-rich source IRC+10216 by including not only radiative attachment (equation 1), but also the novel pathways of charge transfer (equation 2) and dissociative electron attachment (equation 3):

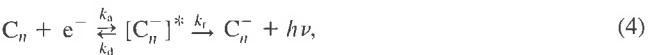


With the inclusion of these mechanisms, Petrie estimated that the abundance of CN^{-} could be as high as $2 \times 10^{-10} n(H_2)$, rendering it a possible candidate for detection by radio astronomy.

Terzieva & Herbst (2000) have recently modelled the

★E-mail: Stephen.Blanksby@Colorado.edu

efficiencies of radiative electron attachment,



for increasing molecular size, using the carbon chains C_n (where $n = 4-9$). They find that once the carbon chain contains six or more carbon atoms the rate of radiative relaxation of the excited anion complex is higher than the rate of electron detachment (i.e. $k_r \gg k_d$). Thus they conclude that for such molecules formation of a stable anion occurs for every collision. The flowing afterglow experiments of Barckholtz et al. (2001) demonstrate that C_n^- anions react only very slowly with molecular hydrogen and, as such, interstellar reservoirs are unlikely to be significantly depleted by this reaction. However, this study also measures efficient reactions between C_n^- anions and atomic hydrogen (see later discussion). Polycarbon anions have also recently been suggested as possible carriers of the diffuse interstellar bands (Tielens & Snow 1995), with some of these lines showing good agreement with the optical transitions of C_7^- that have been studied in the matrix and the gas phase (Tulej et al. 1998; Ruffle et al. 1999; McCall, York & Oka 2000; Motylewski et al. 2000). However, more unequivocal identification of anions in the interstellar medium would come from radio astronomical detection. For such an investigation to have the greatest possibility of success, a target anion or series of anions must be found that fulfil the following requirements: (i) the parent neutral should be an identified interstellar molecule or part of a homologous series of molecules known to be abundant in interstellar sources; (ii) the parent neutral should have a large electron affinity and sufficient molecular size to attach electrons efficiently; and (iii) the anion itself should be structurally simple (i.e. possess a high degree of symmetry) and possess a permanent electric dipole moment in order to make radio astronomical detection a possibility.

In our laboratory we have used mass spectrometry to generate and investigate unsaturated cumulene anions (C_nH^- and $C_{n-1}CH_2^-$) and heterocumulenes (C_nO^-) in the gas phase (Blanksby & Bowie 1999). These anions represent the charged analogues of identified interstellar molecules. We present here the results of a systematic theoretical investigation into the structure and properties of the anions C_nH^- , $C_{n-1}CH_2^-$ and C_nO^- with increasing carbon chain length ($2 \leq n \leq 10$). We pay particular attention to those properties that pertain to their likely presence and detectability in the interstellar medium.

2 THEORETICAL CALCULATIONS

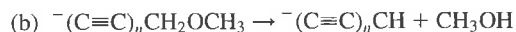
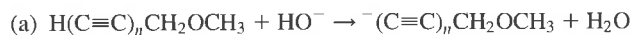
For this study we have adopted the Becke 3LYP (B3LYP) hybrid density functional approach as implemented within the GAUSSIAN98 suite of programs (Frisch et al. 1998), with the relatively modest 6-31G(d) basis set to calculate the geometries of the neutrals and anions. This approach allows calculation of the increasingly large molecules investigated in this study (up to 11 heavy atoms). Further, the B3LYP method has been shown previously to give molecular geometries that agree well with more computationally expensive approaches (Blanksby et al. 1998; Blanksby, Dua & Bowie 1999b). In order to model the electron affinities and dipole moments of these species more accurately, single-point calculations were carried out employing the larger correlation consistent Dunning basis set aug-cc-pVDZ which includes diffuse functions (Dunning 1989; Woon & Dunning 1993). In some cases the coupled cluster CCSD(T) method (Cizek

1969; Watts, Gauss & Bartlett 1993) was employed as a further check of the calculated electronic energies. Electron affinities were determined by calculation and comparison of the electronic energies, including the scaled (0.9806) zero-point energy correction (Wong 1996), of the ground-state anion and neutral species. Many of the calculated data for the neutral species have previously been reported, and are presented here in Tables A1–A6. Electronic energies, zero-point energies and rotational constants for the anions discussed here are also tabulated in Tables A1–A6.

3 TRENDS IN THE PHYSICAL PROPERTIES WITH INCREASING CHAIN LENGTH

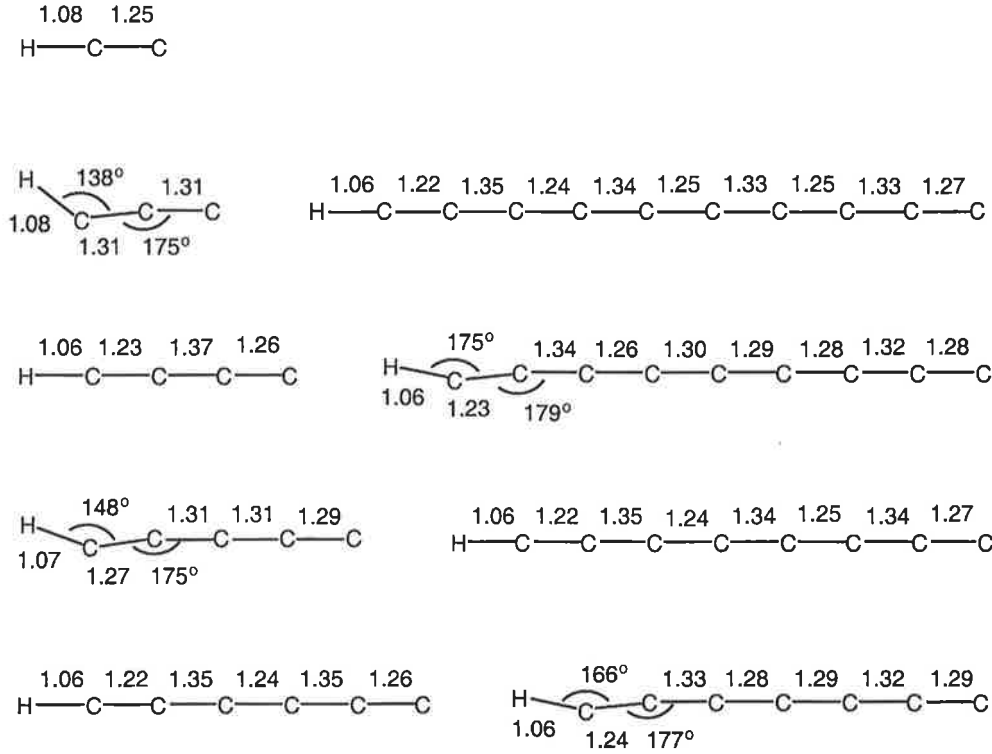
3.1 C_nH^- anions

Neutrals of the form C_nH (where $2 \leq n \leq 14$) have been extensively studied both theoretically and experimentally. The neutral polyynes C_2H to C_8H have been detected in interstellar environments (Cernicharo & Guelin 1996; Guelin et al. 1997). Of the corresponding negative ions, the photoelectron spectra of C_2H^- , C_3H^- , C_4H^- , C_6H^- and C_8H^- have been measured (Oakes & Ellison 1986; Taylor, Cangshan & Neumark 1998), providing the electron affinity of the neutrals and allowing a useful comparison for the calculated data presented here. In these experiments, C_nH^- , where n is even, were generated in a pulsed discharge of acetylene ($HC \equiv CH$) and carbon dioxide in neon (Taylor et al. 1998), whilst C_3H^- was produced from allene ($H_2C=C=CH_2$) and molecular oxygen in a Branscomb discharge source (Oakes & Ellison 1986). Gas-phase preparation of C_3H^- , C_5H^- and C_7H^- in a mass spectrometer has also been reported (Dua, Bowie & Sheldon 1994; Blanksby et al. 1997; Dua, Bowie & Blanksby 1999). These procedures are outlined in Scheme 1 and involve (a) deprotonation of a synthesized polyacetylide precursor in the gas phase, followed by (b) decomposition of the parent anion.



Scheme 1

The calculated geometries of the anions C_nH^- where $n = 2-10$ are shown in Scheme 2 (where bond lengths are given in ångströms and bond angles in degrees). At short chain lengths there are clear structural distinctions between anions with even versus odd numbers of carbons. For example, the structure of the C_4H^- anion is very much like a linear polyacetylene with alternating short (~ 1.24 Å) and long (~ 1.37 Å) carbon–carbon bonds which may be considered as triple and single bonds, respectively. In contrast, C_3H^- has a more allene-like structure with a bent geometry and nearly equivalent carbon–carbon bond lengths (~ 1.31 Å) which are close to double-bond in character. As the chain length increases, however, the structures of odd and even homologues become more similar, with the C_9H^- structure deviating only very slightly from linearity. The linear even- n anions have a $^1\Sigma$ ground state which corresponds to the additional electron being tightly bound in a σ -orbital on the terminal carbon. Such a configuration would be expected to be very stable and hence give rise to large electron binding energies. In contrast, the odd- n species adopt a $^3A''$ electronic configuration which corresponds to two unpaired electrons occupying orthogonal half-filled π -orbitals which would



Scheme 2

Table 1. The electron affinities (eV) of the neutral C_nH cumulenes and dipole moments (debye) of the corresponding anions C_nH^- . These properties are calculated at the B3LYP/aug-cc-pVDZ//B3LYP/6-31G(d) level of theory. Experimental data are presented where available, with experimental uncertainties given in parentheses.

	C_2H	C_3H	C_4H	C_5H	C_6H	C_7H	C_8H	C_9H	$C_{10}H$
EA theory	3.15	1.96	3.46	2.56	3.65	2.97	3.78	3.28	3.90
EA exp.	2.956 ^a (0.020)	1.858 ^b (0.027)	3.558 ^a (0.015)	NA ^c	3.809 ^a (0.015)	NA	3.966 ^a (0.010)	NA	NA
μ	3.4	3.7	5.9 ^d	5.7	8.2	8.2	10.4	10.3	12.7

^a Taylor et al. (1998); ^bOakes & Ellison (1986); ^cNA: not available; ^dagreement with, 6.19 debye, calculated by Botschwina (2000).

be expected to give lower electron binding energies and, by electron repulsion considerations, the observed bent geometries.

Aoki et al. (1995) have previously investigated some of the properties of the C_3H^- anion by high-level *ab initio* calculation. The calculated geometries for the $^3A''$ ground state using both CASSCF/D95** and QCISD(T)/D95** methods agree with our reported geometry to within 0.02 Å and 3°. Botschwina (2000) has conducted large-scale coupled cluster calculations on the C_4H^- anion, and reports a ground-state rotational constant $B_0 = 4658$ MHz, which is in very good agreement with $B_0 = 4639$ MHz calculated from our equilibrium geometry. The agreement between the B3LYP/6-31G(d) geometries for C_3H^- and C_4H^- anions (Scheme 2) and those calculated at higher levels of theory suggests that this method is a rather good approach for calculating the structures of cumulenenic anions at relatively low computational cost.

The binding energies of the C_nH^- anions (i.e. the EAs of their corresponding neutrals) have been determined by calculating the structure and electronic energy of the corresponding neutrals at the same level of theory, and calculating the

difference in energy between neutral and anionic ground states. Where possible these EAs are compared with experimental values in Table 1.

The agreement between experimental and calculated data appears reasonable (most differ by < 0.2 eV) given the well-known difficulties in accurately calculating EAs. Both the calculated and measured EAs show a clear increase with increasing carbon chain length. The even- n homologues rise more sharply than their odd- n counterparts, as would be expected given their polyacetylenic structures. This observation is also consistent with the experimentally measured EAs of the naked carbon chains C_n ($2 \leq n \leq 9$) (Arnold et al. 1991). These are shown for comparison along with the calculated C_nH values in Fig. 1.

3.2 $C_{n-1}CH_2$ anions

The microwave spectra of the linear carbenes $C_{n-1}CH_2$, where $3 \leq n \leq 9$, have been recorded in the laboratory (Killian et al. 1990; Vrtilek et al. 1990; McCarthy et al. 1997; Apponi et al. 2000); however, currently only C_2CH_2 , C_3CH_2 and C_5CH_2 have been

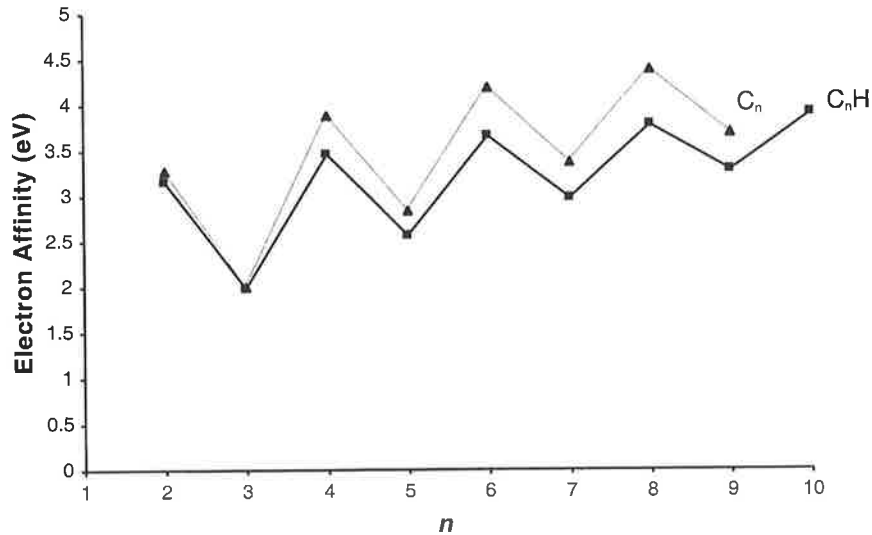


Figure 1. A plot of the calculated electron affinity in electron volts, $EA(C_nH)$, versus the number of carbons in the carbon chain, n (shown as squares). The experimentally determined $EA(C_n)$ values are also included for comparison (shown as triangles).

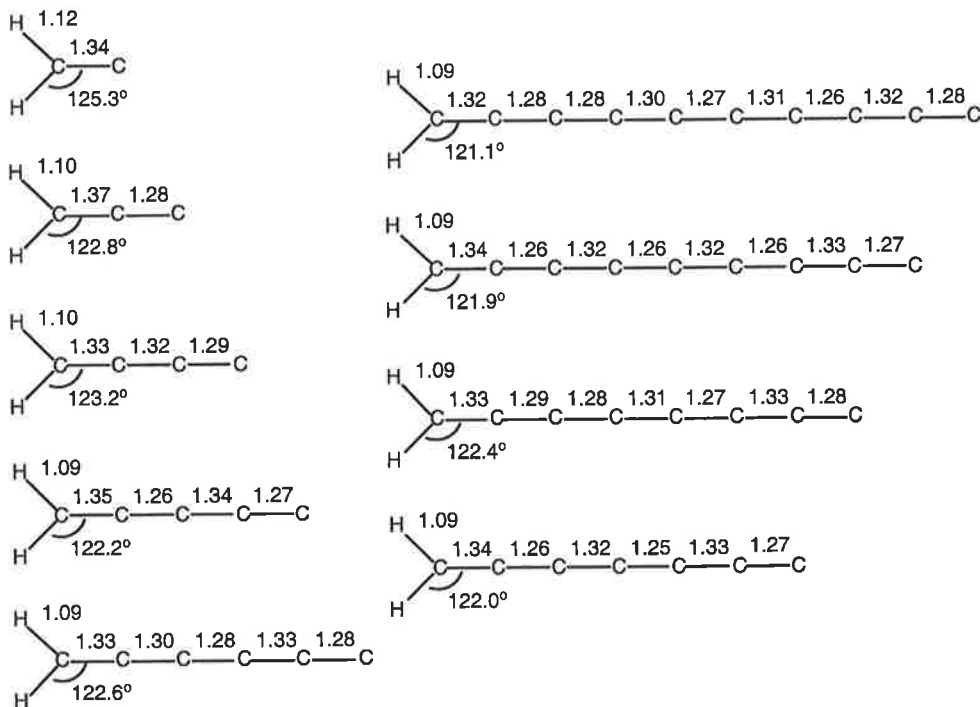
identified in interstellar and circumstellar clouds (Cernicharo et al. 1991a,b; Langer, in preparation). Of the corresponding negative ions, the photoelectron spectra of CCH_2^- and $C_2CH_2^-$ have been measured, providing the electron affinity of the neutrals and allowing some comparison for the calculated data presented here. In these experiments CCH_2^- was produced by gas-phase reaction of atomic oxygen radical anion (O^-) with ethylene (Ervin et al. 1990), whilst $C_2CH_2^-$ was generated from an allene ($H_2C=C=CH_2$) and oxygen mixture in a Branscomb ion source (Oakes & Ellison 1986). Gas-phase preparation of $C_2CH_2^-$, $C_4CH_2^-$ and $C_6CH_2^-$ in a mass spectrometer has also been reported (Dua et al. 1994; Blanksby et al. 1998; Dua, Blanksby & Bowie 1998). These

procedures are outlined in Scheme 3 and involve (a) deprotonation of a synthesized polyacetylide precursor in the gas phase, followed by (b) decomposition of the parent anion.

- (a) $H(C\equiv C)_nCH_2OCH_3 + HO^- \rightarrow ^-(C\equiv C)_nCH_2OCH_3 + H_2O$
 (b) $^-(C\equiv C)_nCH_2OCH_3 \rightarrow ^-(C\equiv C)_nCH_2 + CH_3O$

Scheme 3

The calculated geometries of the anions $C_{n-1}CH_2^-$ where $n=2-10$ are shown in Scheme 4. The structures of these anions are quite similar with little variation in bond lengths and angles with



Scheme 4

Table 2. The electron affinities (eV) of the neutral $C_{n-1}CH_2$ cumulenes and dipole moments (debye) of the corresponding anions $C_{n-1}CH_2^-$. These properties are calculated at the B3LYP/aug-cc-pVDZ//B3LYP/6-31G(d) level of theory. Experimental data are presented where available, with experimental uncertainties given in parentheses.

	CCH ₂	C ₂ CH ₂	C ₃ CH ₂	C ₄ CH ₂	C ₅ CH ₂	C ₆ CH ₂	C ₇ CH ₂	C ₈ CH ₂	C ₉ CH ₂
EA theory	0.70	1.94	1.85	2.60	2.53	3.02	2.96	3.32	3.24
EA exp.	0.447 ^a (0.002)	1.794 ^b (0.008)	NA ^c	NA	NA	NA	NA	NA	NA
μ	3.5	5.0	5.7	7.0	7.7	9.0	9.6	10.9	11.6

^aErvin et al. (1990); ^bOakes & Ellison (1986); ^cNA: not available.

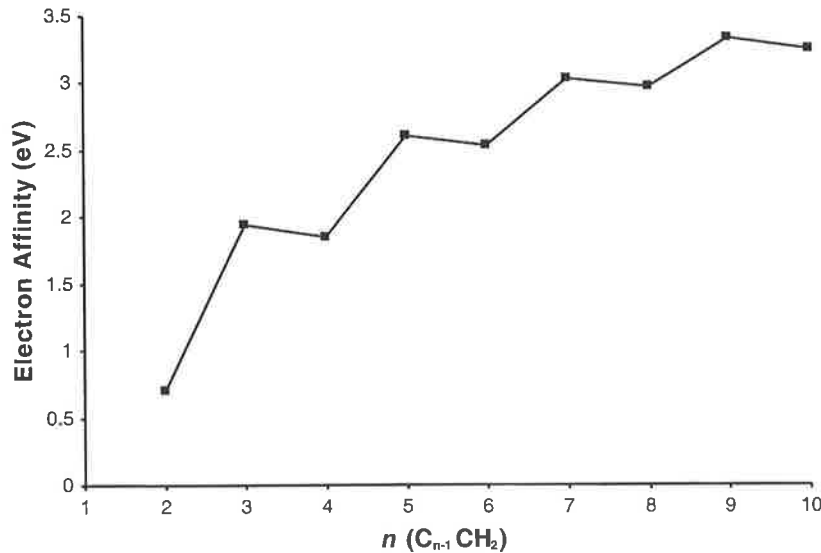


Figure 2. A plot of the calculated electron affinity in electron volts, EA($C_{n-1}CH_2$), versus the number of carbons in the carbon chain, n .

Table 3. The electron affinities (eV) of the neutral C_nO cumulenes and dipole moments (debye) of the corresponding anions C_nO^- . These properties are calculated at the B3LYP/aug-cc-pVDZ//B3LYP/6-31G(d) level of theory. Experimental data are presented where available, with experimental uncertainties given in parentheses.

	C ₂ O	C ₃ O	C ₄ O	C ₅ O	C ₆ O	C ₇ O	C ₈ O	C ₉ O	C ₁₀ O
EA theory	2.28	1.25	2.91	2.11	3.28	2.71	3.54	3.11	3.73
EA theory		[1.03] ^a 0.93 ^e (0.10)	2.99 ^e (0.10)						
EA exp.	2.289 ^b (0.018)	1.34 ^c (0.15)	2.05 ^c (0.15)	NA ^d	NA	NA	NA	NA	NA
μ	3.6	3.8	4.9	5.5	6.0	6.6	7.1	7.6	8.3

^aCalculated at CCSD(T)/aug-cc-pVDZ//B3LYP/6-31G(d); ^bZengin et al. (1996); ^cOakes & Ellison (1986); ^dNA: not available; ^eRienstra-Kiracofe et al. (2000).

increasing carbon chain length. For longer chain lengths in particular there appears to be little structural variation upon adding additional carbons to the chain, and one might well predict that this trend will continue toward still higher n and thus allow sensible structural predictions without further calculation. The ground state of the $C_{n-1}CH_2$ neutrals is 1A_1 , which corresponds to a singlet carbene with the lone electron pair localized on the terminal carbon. Forming the anions may be considered as adding an electron to the π -system of orbitals either (i) in the C-C-H plane in the case of even n giving 2B_2 anions (e.g. CCH₂⁻), or (ii)

orthogonal to the C-C-H plane in the case of odd n giving 2B_1 anions (e.g. C₂CH₂⁻). The relative stability of these different ground electronic states may explain the observed stepwise increase in electron affinities with increasing carbon chain length.

The binding energies of these anions are presented in Table 2. This homologous series of compounds demonstrates a clear increase in electron affinity with increasing carbon chain length. Although the rate of this increase appears to taper somewhat toward larger n , our data suggest that further homologues will have

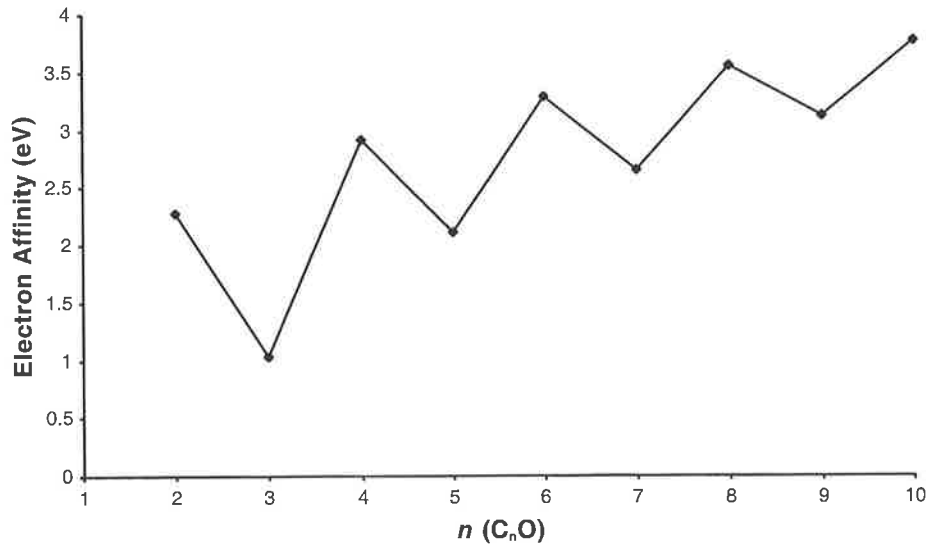
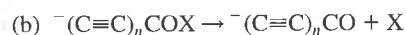
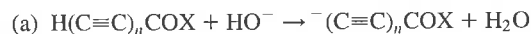


Figure 3. A plot of the calculated electron affinity in electron volts, $EA(C_nO)$, versus the number of carbons in the carbon chain, n .

still larger electron affinities. This is demonstrated most clearly in the plot of electron affinity versus n presented in Fig. 2.

3.3 C_nO anions

The microwave spectra of the polycarbon monoxides C_nO have been recorded for $2 \leq n \leq 8$ (Ogata, Ohshima & Endo 1995; Ohshima, Endo & Ogata 1995) with some of these species, $n = 2, 3$ and 5, having been identified in interstellar environments. Of the corresponding negative ions, photoelectron spectra have been recorded for C_2O^- , C_3O^- and C_4O^- , giving the electron affinities presented in Table 3 (Oakes & Ellison 1986; Zengin et al. 1996). These ions were generated from carbon suboxide (C_3O_2) either in a pulsed discharge (Zengin et al. 1996) or in a Branscomb ion source (Oakes & Ellison 1986). Gas-phase preparation of C_3O^- , C_5O^- and C_7O^- in a mass spectrometer has also been reported (Blanksby, Dua & Bowie 1999a; Dua, Blanksby & Bowie 2000a,b). These procedures are outlined in Scheme 5 and involve (a) deprotonation of a synthesized polyacetylide precursor in the gas phase, followed by (b) decomposition of the parent anion.



(where $X = \text{OCH}_3$ or $t - \text{C}_4\text{H}_9$)

Scheme 5

Interestingly, the values $EA(C_3O)$ and $EA(C_4O)$ have recently been the subject of a rigorous theoretical study by Rienstra-Kiracofe et al. (2000) who suggest that the experimental values may be erroneous. The theoretical work suggests values of $EA(C_3O) = 0.93 \pm 0.10$ eV and $EA(C_4O) = 2.99 \pm 0.10$ eV (these values are also listed for comparison in Table 3). The latter value seems in good agreement (< 0.1 eV) with our B3LYP/aug-cc-pVDZ//B3LYP/6-31G(d) calculations. The $EA(C_3O)$ of Rienstra-Kiracofe et al. appears noticeably different (> 0.3 eV) from that obtained using our approach. Using the CCSD(T)/aug-cc-pVDZ//B3LYP/6-31G(d) method, we calculate an electron

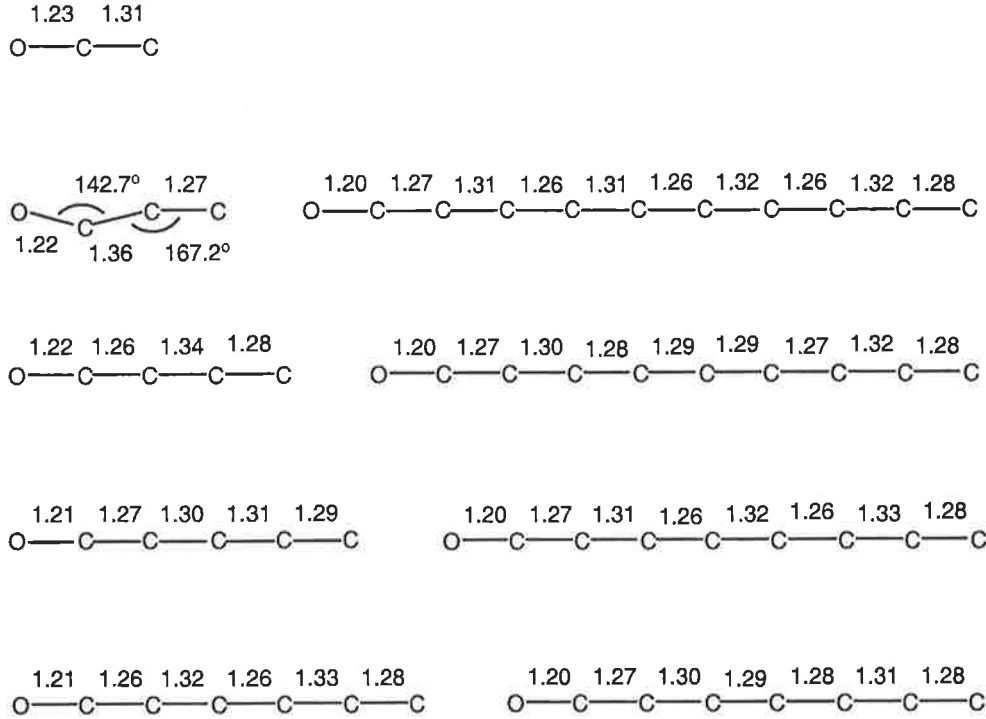
affinity of $EA(C_3O) = 1.03$ eV which agrees well with the Rienstra-Kiracofe et al. value, and we therefore suggest that this is probably closer to the true EA. Once again there is a clear trend of increasing electron affinity with increasing carbon chain length, which is best described in Fig. 3.

The structures of the C_nO^- anions are presented in Scheme 6. With the exception of C_3O^- , the anions have linear structures which appear to become more cumulene-like with increasing chain length. That is to say, the carbon-carbon bonds tend to approach a uniform bond length near 1.30 \AA . All the anions have a linear $^2\Pi$ ground state, except for C_3O^- which displays some Renner-Teller distortion (see Rienstra-Kiracofe et al. 2000 for discussion) giving it a $^2A'$ ground state. The corresponding neutrals have ground electronic states of $^3\Sigma$ for even n and $^1\Sigma$ for odd n .

4 THE POSSIBILITY OF C_nH , $C_{n-1}CH_2$ AND C_nO ANIONS AS DETECTABLE INTERSTELLAR SPECIES

The anions presented in this paper represent the charged counterparts of either (i) identified interstellar molecules or (ii) molecules that form part of an homologous series of molecules of which several members have been identified. The calculations presented here demonstrate that the electron affinities of the parent neutrals C_nH , $C_{n-1}CH_2$ and C_nO are quite large and (for $n \geq 3$) increase from 1 up to nearly 4 eV with increasing length of the carbon chain. Further, it seems likely from the examination of the plots of n versus EA shown in Figs 1–3 that this trend will extend further than the scope of this study, and larger molecules may yet be shown to have still larger EAs.

Terzieva & Herbst (2000) estimated the rate of radiative attachment of electrons (i.e. the overall rate for equation 4) to naked carbon chains (C_4 – C_9) to approach and surpass $2 \times 10^{-7} \text{ cm}^3 \text{ s}^{-1}$ where there were six or more carbons in the chain. The estimated increase in efficiency of electron attachment with increasing carbon chain length may be considered as the result of two effects. Increasing the carbon chain length (i) increases the electron affinity (Fig. 1), thus increasing the lifetime of the



Scheme 6

intermediate electron-neutral complex ($[C_n^-]^*$ in equation 4) against electron detachment, and (ii) increases the degrees of freedom in the molecule which provides for a greater density of states at the electron affinity threshold and thus a more effective distribution of the excess internal energy in the complex. This also delays electron detachment. In light of these considerations, it would be expected that the neutrals C_nH , $C_{n-1}CH_2$ and C_nO would also be likely to attach electrons efficiently in the interstellar environment. We have demonstrated that these cumulenenes have large electron affinities which increase with increasing carbon chain length in much the same way as C_n molecules (Fig. 1). Further, the additional hydrogen or oxygen atom in the C_nH , $C_{n-1}CH_2$ and C_nO species will provide additional degrees of freedom compared with their respective C_n analogues. In the case of C_nH and $C_{n-1}CH_2$ these additional degrees of freedom will be made up in part of low-frequency C-H bending modes which will further increase the density of states and thus the lifetime of the excited electron-neutral complex (equation 4). Therefore a qualitative analysis of the data presented here suggests that (i) neutral C_nH , $C_{n-1}CH_2$ and C_nO are likely to attach electrons efficiently in interstellar clouds, and (ii) once formed, C_nH^- , $C_{n-1}CH_2^-$ and C_nO^- anions are likely to have lifetimes against electron detachment in the interstellar medium comparable to those estimated for C_n^- anions (up to 2 weeks for C_9^-) (Terzieva & Herbst 2000).

Barckholtz et al. (2001) have experimentally examined the reactions of C_nH^- anions (where $n=2, 4, 6$ and 7) with molecular hydrogen, the most abundant interstellar gas. Their work demonstrates that depletion of C_nH^- anions occurs very slowly ($k_{ad} < 10^{-13} \text{ cm}^3 \text{ s}^{-1}$) by what is assumed to be associative detachment (equation 5):



It might be expected that $C_{n-1}CH_2^-$ and C_nO^- anions would also be

unreactive toward H_2 , and therefore it seems unlikely that populations of these anions would be substantially depleted by reaction with dihydrogen in interstellar clouds. Barckholtz et al. (2001) further demonstrated that poly-carbon anions (C_n^- , $n=2-10$) react with atomic hydrogen in two ways depending on chain length. For carbon chains where $n < 7$ the reaction proceeds exclusively by associative electron detachment (equation 6), whereas for $n \geq 7$ both detachment and the association product anion (C_nH^-) are observed (equation 7):



It is also noted that as n increases further the branching ratio between reactions (6) and (7) increases to favour production of the hydrocarbon anion. These results suggest that if indeed C_n^- ($n \geq 7$) anions are present in the interstellar environment, reactions with atomic hydrogen could provide a further pathway to formation of the C_nH^- anions discussed here. However, C_nH^- anions ($n=2, 4, 6, 7$) were also found to react efficiently with atomic hydrogen by associative electron detachment (cf. equation 6). This suggests that these anions may be depleted in interstellar regions of high atomic hydrogen density (Barckholtz et al. 2001).

Neutral C_nH and C_nO molecules have simple linear structures with significant permanent electric dipole moments. These properties have aided their characterization by microwave spectroscopy in the laboratory and subsequent detection in astronomical sources. Similarly, the neutral $C_{n-1}CH_2$ cumulenenes are simple, slightly asymmetric tops, with electric dipole moments increasing up to 10 debye, for $n=10$ (McCarthy et al. 1997). Our electronic structure calculations predict similar properties for the corresponding anions. C_nH^- and C_nO^- anions are linear structures, with the exception of odd- n members of the C_nH^- series and C_3O^- , while $C_{n-1}CH_2^-$ anions are slightly asymmetric tops. The calculated electric dipole moments of all these anions are listed

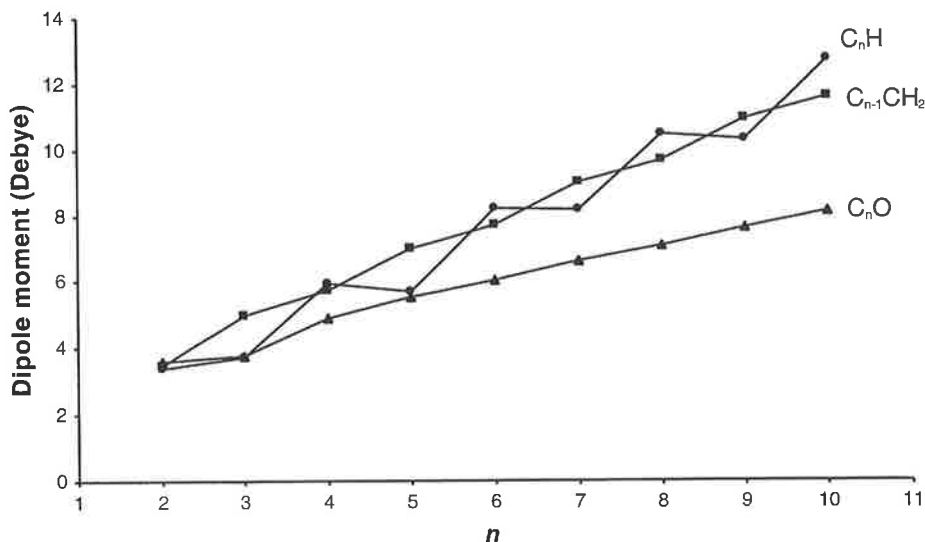


Figure 4. A plot of the dipole moments of the anions in debye, C_nH^- (circles), $C_{n-1}CH_2^-$ (squares) and C_nO^- (triangles), versus the number of carbons in the carbon chain, n .

in Tables 1–3 and are also plotted in Fig. 4 as a function of n . This figure clearly demonstrates the increasing dipole moment with increasing carbon chain length.

Theoretical calculation of the physical properties of molecules (e.g. geometries, electron affinities, dipole moments and rotational constants), particularly at the relatively modest levels of theory used in this study, are most often of insufficient quality for use in direct astronomical searches. However, such calculations may be a useful guide to laboratory experiments which could produce data of the necessary precision. Several methodologies for the gas-phase formation of some of these anions have been summarized above.

5 CONCLUSIONS

The electronic structure calculations presented here predict that the cumulenes C_nH and C_nCH_2 and heterocumulenes C_nO have large electron affinities which increase with increasing carbon chain length (n). Such properties suggest that molecules of this type may efficiently attach electrons in interstellar gas clouds, producing the corresponding negative ions which are likely to be stable to electron detachment. Sufficient populations of these anions may be produced by this mechanism to allow astronomical detection. The calculated structures and physical properties of C_nH^- , $C_nCH_2^-$ and C_nO^- anions ($2 \leq n \leq 10$) presented here may serve as a guide to laboratory experiments which should precede astronomical detection.

ACKNOWLEDGMENTS

This work was carried out with the aid of a grant from the Australian Research Council. SD thanks the ARC for a research associate stipend. We thank the Australian National University Supercomputing Facility (Canberra, ACT) for generous time allocation. SJB acknowledges Professors Diethard Böhme, Veronica Bierbaum and Chuck DePuy for their advice and encouragement.

REFERENCES

- Aoki K., Hashimoto K., Ikuta S., Nomura O., 1995, *Chem. Phys. Lett.*, 242, 527
- Apponi A. J., McCarthy M. C., Gottlieb C. A., Thaddeus P., 2000, *ApJ*, 530, 357
- Arnold D. W., Bradforth S. E., Kitsopoulos T. N., Neumark D. M., 1991, *J. Chem. Phys.*, 95, 8753
- Barckholtz C., Snow T. P., Bierbaum V. M., 2001, *ApJ*, 547, L171
- Bettens R. P. A., Herbst E., 1996, *ApJ*, 468, 686
- Blanksby S. J., Bowie J. H., 1999, *Mass Spectrom. Rev.*, 18, 131
- Blanksby S. J., Dua S., Bowie J. H., Sheldon J. C., 1997, *Chem. Commun.*, 1833
- Blanksby S. J., Dua S., Bowie J. H., Schroder D., Schwarz H., 1998, *J. Phys. Chem. A*, 102, 9949
- Blanksby S. J., Dua S., Bowie J. H., 1999a, *Rapid Commun. Mass Spectrom.*, 13, 2249
- Blanksby S. J., Dua S., Bowie J. H., 1999b, *J. Phys. Chem. A*, 103, 5161
- Botschwina P. 2000, in Miller T. A., ed., 55th Int. Symp. on Molecular Spectroscopy. Ohio State University, Columbus
- Canosa A., Parent D. C., Pasquero D., Gomet J. C., Laube S., Rowe B. R., 1994, *Chem. Phys. Lett.*, 228, 26
- Cernicharo J., Guelin M., 1996, *A&A*, 309, L27
- Cernicharo J., Gottlieb C. A., Guelin M., Killian T. C., Paubert G., Thaddeus P., Vrtilek J. M., 1991a, *ApJ*, 368, L39
- Cernicharo J., Gottlieb C. A., Guelin M., Killian T. C., Thaddeus P., Vrtilek J. M., 1991b, *ApJ*, 368, L43
- Cizek J., 1969, *Adv. Chem. Phys.*, 14, 35
- Dua S., Bowie J. H., Sheldon J. C., 1994, *J. Chem. Soc. Perkin Trans.*, 2, 543
- Dua S., Blanksby S. J., Bowie J. H., 1998, *Chem. Commun.*, 1767
- Dua S., Bowie J. H., Blanksby S. J., 1999, *Eur. Mass Spectrom.*, 5, 309
- Dua S., Blanksby S. J., Bowie J. H., 2000a, *Int. J. Mass Spectrom.*, 196, 45
- Dua S., Blanksby S. J., Bowie J. H., 2000b, *Rapid Commun. Mass Spectrom.*, 14, 118
- Dunning T. H., Jr, 1989, *J. Chem. Phys.*, 90, 1007
- Ervin K. M. et al., 1990, *J. Am. Chem. Soc.*, 112, 5750
- Frisch M. J. et al., GAUSSIAN 98. GAUSSIAN Inc., Pittsburgh, PA
- Guelin M., Cernicharo J., Travers M. J., McCarthy M. C., Gottlieb C. A., Thaddeus P., Ohishi M., Saito S., 1997, *A&A*, 317, L1
- Herbst E., 1981, *Nat*, 289, 656

- Jaffke T., Illenberger E., Lezius M., Matejcik S., Smith D., Mark T. D., 1994, *Chem. Phys. Lett.*, 226, 213
- Killian T. C., Vrtilik J. M., Gottlieb C. A., Gottlieb E. W., Thaddeus P., 1990, *ApJ*, 365, L89
- Lepp S., Dalgarno A., 1988, *ApJ*, 324, 553
- McCall B. J., York D. G., Oka T., 2000, *ApJ*, 531, 329
- McCarthy M. C., Travers M. J., Kovács A., Chen W., Novick S. E., Gottlieb C. A., Thaddeus P., 1997, *Sci*, 275, 518
- Motylewski T. et al., 2000, *ApJ*, 531, 312
- Oakes J. M., Ellison G. B., 1986, *Tetrahedron*, 42, 6263
- Ogata T., Ohshima Y., Endo Y., 1995, *J. Am. Chem. Soc.*, 117, 3593
- Ohshima Y., Endo Y., Ogata T., 1995, *J. Chem. Phys.*, 102, 1493
- Ormont A., 1986, *A&A*, 164, 159
- Petrie S., 1996, *MNRAS*, 281, 137
- Rienstra-Kiracofe J. C., Ellison G. B., Hoffman B. C., Schaefer H. F., 2000, *J. Phys. Chem. A*, 104, 2273
- Ruffe D. P., Bettens R. P. A., Terzieva R., Herbst E., 1999, *ApJ*, 523, 678
- Spanel P., Smith D., 1994, *Chem. Phys. Lett.*, 229, 262
- Taylor T. R., Cangshan X., Neumark D. M., 1998, *J. Chem. Phys.*, 108, 10018
- Terzieva R., Herbst E., 2000, *Int. J. Mass Spectrom.*, 201, 135
- Tielens A. G. G. M., Snow T. P., 1995, *The Diffuse Interstellar Bands*. Kluwer, Dordrecht
- Tulej M., Kirkwood D. A., Pachkov M., Maier J. P., 1998, *ApJ*, 506, L69
- Vrtilik J. M., Gottlieb C. A., Gottlieb E. W., Killian T. C., Thaddeus P., 1990, *ApJ*, 364, L53
- Watts J. D., Gauss J., Bartlett R. J. J., 1993, *J. Chem. Phys.*, 98, 8718
- Wong M. W., 1996, *Chem. Phys. Lett.*, 256, 391
- Woon D. E., Dunning T. H., Jr, 1993, *J. Chem. Phys.*, 98, 1358
- Zengin V., Persson B. J., Strong K. M., Continetti R. E., 1996, *J. Chem. Phys.*, 105, 9740

Table A1. Electronic states, electronic energies (hartrees), unscaled zero-point energies (hartrees) and molecular geometries for the neutral cumulenes C_nH (where $n=2-10$).

	C_2H	C_3H	C_4H	C_5H	C_6H	C_7H	C_8H	C_9H	$C_{10}H$
Ground electronic state	$^2\Sigma$	$^2A'$	$^2\Pi$	$^2\Pi$	$^2\Pi$	$^2\Pi$	$^2\Pi$	$^2\Pi$	$^2\Pi$
Electronic energy (hartrees)									
B3LYP/6-31G(d)	-76.604 28	-114.677 07	-152.770 69	-190.848 06	-228.936 71	-267.014 17	-305.100 24	-343.177 97	-381.262 64
B3LYP/aug-cc-pVDZ//	-76.615 69	-114.693 72	-152.790 48	-190.871 33	-228.963 08	-267.044 05	-305.133 39	-343.214 60	-381.301 08
B3LYP/6-31G(d)									
ZPE	0.014 39	0.017 33	0.025 07	0.029 96	0.036 32	0.041 32	0.047 52	0.052 47	0.058 68
Molecular geometries (ångströms, degrees)									
H-C ₁	1.07	1.07	1.07	1.07	1.07	1.07	1.07	1.07	1.07
C ₁ -C ₂	1.21	1.26	1.23	1.23	1.22	1.22	1.22	1.22	1.23
C ₂ -C ₃		1.33	1.33	1.33	1.34	1.34	1.34	1.34	1.35
C ₃ -C ₄			1.29	1.27	1.25	1.25	1.24	1.24	1.24
C ₄ -C ₅				1.31	1.32	1.30	1.32	1.32	1.33
C ₅ -C ₆					1.29	1.28	1.26	1.26	1.25
C ₆ -C ₇						1.31	1.31	1.29	1.31
C ₇ -C ₈							1.29	1.29	1.26
C ₈ -C ₉								1.30	1.31
C ₉ -C ₁₀									1.29
H ₁ -C ₂ -C ₃		150.8							
C ₂ -C ₃ -C ₄		174.7							

Table A2. Electronic states, electronic energies (hartrees), unscaled zero-point energies (hartrees) and rotational constants for the cumulenec anions C_nH^- (where $n=2-10$).

	C_2H	C_3H	C_4H	C_5H	C_6H	C_7H	C_8H	C_9H	$C_{10}H$
Ground electronic state	$^1\Sigma$	$^3A''$	$^1\Sigma$	$^3A''$	$^1\Sigma$	$^3A''$	$^1\Sigma$	$^3A''$	$^1\Sigma$
Electronic energy (hartrees)									
B3LYP/6-31G(d)	-76.682 55	-114.716 73	-152.870 66	-190.917 08	-229.047 70	-267.100 44	-305.219 40	-343.276 95	-381.388 03
B3LYP/aug-cc-pVDZ//	-76.731 65	-114.764 22	-152.916 68	-190.963 40	-229.096 39	-267.151 00	-305.272 61	-343.332 67	-381.445 04
B3LYP/6-31G(d)									
ZPE	0.014 59	0.016 44	0.024 15	0.027 96	0.035 49	0.039 26	0.047 86	0.050 06	0.059 56
Molecular symmetry	$C_{\infty v}$	C_s	$C_{\infty v}$	C_s	$C_{\infty v}$	C_s	$C_{\infty v}$	C_s	$C_{\infty v}$
Rotational constants (GHz)									
From B3LYP/6-31G(d)	41.531	1204.155	4.639	2026.106	1.371	10371.559	0.581	56777.098	0.299
geometry		11.052		2.359		0.863		0.408	
		10.952		2.356		0.863		0.408	

Table A3. Electronic states, electronic energies (hartrees), unscaled zero-point energies (hartrees) and molecular geometries for the neutral cumulenes $C_{n-1}CH_2$ (where $n = 2-10$).

	CCH ₂	C ₂ CH ₂	C ₃ CH ₂	C ₄ CH ₂	C ₅ CH ₂	C ₆ CH ₂	C ₇ CH ₂	C ₈ CH ₂	C ₉ CH ₂
Ground electronic state	¹ A ₁	¹ A ₁	¹ A ₁	¹ A ₁	¹ A ₁	¹ A ₁	¹ A ₁	¹ A ₁	¹ A ₁
Electronic energy (hartrees)									
B3LYP/6-31G(d)	-77.259 79	-115.332 48	-153.420 16	-191.492 86	-229.577 12	-267.651 96	-305.734 85	-343.810 97	-381.893 06
B3LYP/aug-cc-	-77.274 64	-115.348 55	-153.439 66	-191.515 08	-229.603 07	-267.680 94	-305.767 56	-343.846 78	-381.932 55
pVDZ//B3LYP/6-31G(d)									
ZPE	0.023 87	0.031 29	0.036 20	0.042 03	0.047 23	0.052 94	0.058 26	0.063 88	0.069 15
Molecular geometries (ångströms, degrees)									
H-C ₁	1.09		1.09	1.09	1.08	1.09	1.09	1.09	1.09
C ₁ -C ₂	1.30	1.09	1.31	1.32	1.31	1.32	1.31	1.32	1.31
C ₂ -C ₃		1.29	1.29	1.27	1.28	1.27	1.28	1.27	1.28
C ₃ -C ₄			1.29	1.30	1.27	1.29	1.28	1.29	1.28
C ₄ -C ₅				1.29	1.30	1.27	1.29	1.27	1.28
C ₅ -C ₆					1.29	1.30	1.27	1.29	1.28
C ₆ -C ₇						1.29	1.30	1.27	1.29
C ₇ -C ₈							1.29	1.30	1.27
C ₈ -C ₉								1.29	1.30
C ₉ -C ₁₀									1.29
H-C ₁ -C ₂	120.9	122.0	121.0	121.8	121.2	121.67	121.3	121.6	121.3

Table A4. Electronic states, electronic energies (hartrees), unscaled zero-point energies (hartrees) and rotational constants for the cumulenic anions $C_{n-1}CH_2^-$ (where $n = 2-10$).

	CCH ₂	C ₂ CH ₂	C ₃ CH ₂	C ₄ CH ₂	C ₅ CH ₂	C ₆ CH ₂	C ₇ CH ₂	C ₈ CH ₂	C ₉ CH ₂
Ground electronic state	² B ₂	² B ₁	² B ₂	² B ₁	² B ₂	² B ₁	² B ₂	² B ₁	² B ₂
Electronic energy (hartrees)									
B3LYP/6-31G(d)	-77.249 49	-115.373 18	-153.462 20	-191.564 16	-229.648 14	-267.742 11	-305.824 17	-343.914 15	-381.995 19
B3LYP/aug-cc-	-77.299 35	-115.418 23	-153.506 11	-191.609 27	-229.694 68	-267.791 09	-305.875 46	-343.968 30	-382.050 79
pVDZ//B3LYP/6-31G(d)									
ZPE	0.022 92	0.029 59	0.034 63	0.040 79	0.046 00	0.052 12	0.057 31	0.063 36	0.068 33
Molecular symmetry	C _{2v}	C _{2v}	C _{2v}	C _{2v}	C _{2v}	C _{2v}	C _{2v}	C _{2v}	C _{2v}
Rotational constants (GHz)									
From B3LYP/6-31(d)	299.858	295.411	296.088	293.822	294.719	293.225	294.453	292.848	293.384
geometry	35.893	10.256	4.356	2.253	1.318	0.836	0.564	0.398	0.292
	32.056	9.912	4.293	2.236	1.312	0.834	0.563	0.398	0.292

Table A5. Electronic states, electronic energies (hartrees), unscaled zero-point energies (hartrees) and molecular geometries for the neutral cumulenes C_nO (where $n = 2-10$).

	C_2O	C_3O	C_4O	C_5O	C_6O	C_7O	C_8O	C_9O	$C_{10}O$
Ground electronic state	$^3\Sigma$	$^1\Sigma$	$^3\Sigma$	$^1\Sigma$	$^3\Sigma$	$^1\Sigma$	$^3\Sigma$	$^1\Sigma$	$^3\Sigma$
Electronic energy (hartrees)									
B3LYP/6-31G(d)	-151.257 56	-189.392 24	-227.422 67	-265.539 68	-303.587 81	-341.693 67	-379.750 31	-417.849 66	-455.911 50
B3LYP/aug-cc-pVDZ// B3LYP/6-31G(d)	-151.283 52	-189.420 21	-227.454 40	-265.574 25	-303.626 06	-341.735 06	-379.795 35	-417.897 95	-455.961 79
ZPE	0.008 71	0.015 74	0.019 71	0.026 54	0.030 77	0.037 89	0.042 07	0.049 10	0.053 01
Molecular geometries (ångströms, degrees)									
O-C ₁	1.17	1.16	1.17	1.17	1.17	1.17	1.17	1.17	1.17
C ₁ -C ₂	1.37	1.30	1.29	1.29	1.29	1.29	1.29	1.29	1.28
C ₂ -C ₃		1.28	1.29	1.27	1.28	1.27	1.28	1.27	1.28
C ₃ -C ₄			1.31	1.30	1.28	1.29	1.28	1.28	1.28
C ₄ -C ₅				1.28	1.29	1.27	1.28	1.27	1.28
C ₅ -C ₆					1.30	1.30	1.28	1.29	1.28
C ₆ -C ₇						1.29	1.30	1.27	1.29
C ₇ -C ₈							1.30	1.30	1.28
C ₈ -C ₉								1.29	1.30
C ₉ -C ₁₀									1.30

Table A6. Electronic states, electronic energies (hartrees), unscaled zero-point energies (hartrees) and rotational constants for the cumulenec anions C_nO^- (where $n = 2-10$).

	C_2O	C_3O	C_4O	C_5O	C_6O	C_7O	C_8O	C_9O	$C_{10}O$
Ground electronic state	$^2\Pi$	$^2A'$	$^2\Pi$	$^2\Pi$	$^2\Pi$	$^2\Pi$	$^2\Pi$	$^2\Pi$	$^2\Pi$
Electronic energy (hartrees)									
B3LYP/6-31G(d)	-151.313 48	-189.408 46	-227.507 84	-265.594 33	-303.689 69	-341.772 88	-379.863 41	-417.945 01	-456.032 80
B3LYP/aug-cc-pVDZ// B3LYP/6-31G(d)	-151.367 97	-189.463 44	-227.561 68	-265.649 89	-303.747 12	-341.832 90	-379.926 04	-418.010 54	-456.099 74
ZPE	0.009 33	0.012 86	0.020 04	0.024 53	0.031 27	0.036 08	0.042 74	0.047 29	0.053 91
Molecular symmetry	$C_{\infty v}$	C_s	$C_{\infty v}$	$C_{\infty v}$	$C_{\infty v}$	$C_{\infty v}$	$C_{\infty v}$	$C_{\infty v}$	$C_{\infty v}$
Rotational constants (GHz)									
From B3LYP/6-31(d) geometry	11.383	306.822 4.772 4.698	2.294	1.322	0.832	0.559	0.393	0.288	0.217

McAnoy, A.M., Dua, S., Rees, K., and Bowie, J.H., (2001) Loss of CO₂ from the *ortho* isomer of deprotonated methyl phenyl carbonate involves a methyl migration. *International Journal of Mass Spectrometry*, v. 210-211, pp. 557-562.

NOTE:

This publication is included in the print copy of the thesis held in the University of Adelaide Library.

It is also available online to authorised users at:

[http://dx.doi.org/10.1016/S1387-3806\(01\)00419-5](http://dx.doi.org/10.1016/S1387-3806(01)00419-5)

The loss of CO from the *ortho*, *meta* and *para* forms of deprotonated methyl benzoate in the gas phase

2 PERKIN

Andrew M. McAnoy, Suresh Dua, Stephen J. Blanksby and John H. Bowie*

Department of Chemistry, The University of Adelaide, South Australia, 5005

Received (in Cambridge, UK) 7th April 2000, Accepted 2nd June 2000

Published on the Web 12th July 2000

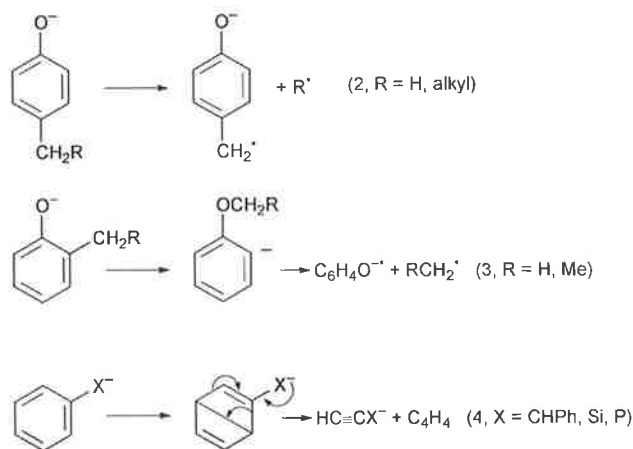
The *ortho*, *meta* and *para* anions of methyl benzoate may be made in the source of a mass spectrometer by the $S_N2(Si)$ reactions between HO^- and methyl (*o*-, *m*-, and *p*-trimethylsilyl)benzoate respectively. All three anions lose CO upon collisional activation to form the *ortho* anion of anisole in the ratio *ortho* \gg *meta* $>$ *para*. The rearrangement process is charge directed through the *ortho* anion. Theoretical calculations at the B3LYP/6-311++G(d,p)//HF/6-31+G(d) level of theory indicate that the conversion of the *meta* and *para* anions to the *ortho* anion prior to loss of CO involve 1,2-H transfer(s), rather than carbon scrambling of the methoxycarbonylphenyl anion. There are two mechanisms which can account for this rearrangement, *viz.* (A) cyclisation of the *ortho* anion centre to the carbonyl group of the ester to give a cyclic carbonyl system in which the incipient methoxide anion substitutes at one of the two equivalent ring carbons of the three membered ring to yield an intermediate which loses CO to give the *ortho* anion of anisole, and (B) an elimination reaction to give an intermediate benzyne–methoxycarbonyl anion complex in which the $MeOCO^-$ species acts as a MeO^- donor, which then adds to benzyne to yield the *ortho* anion of anisole. Calculations at the B3LYP/6-311++G(d,p)//HF/6-31+G(d) level of theory indicate that (i) the barrier in the first step (the rate determining step) of process A is 87 kJ mol $^{-1}$ less than that for the synchronous benzyne process B, and (ii) there are more low frequency vibrations in the transition state for benzyne process B than for the corresponding transition state for process A. Stepwise process A has the lower barrier for the rate determining step, and the lower Arrhenius factor: we cannot differentiate between these two mechanisms on available evidence.

Introduction

The negative ion spectra of deprotonated neutral organic molecules are generally quite characteristic and diagnostic of structure.¹ In the majority of cases, the spectra are simple, involving either loss of a radical, or a neutral accompanied by a hydrogen transfer reaction. When these cleavage reactions are energetically unfavourable, three scenarios may pertain, *viz.* (i) the initially formed $(M - H)^-$ ion rearranges (often by H transfer) to another anion which is able to undergo facile cleavage, (ii) the initial anion may undergo a skeletal rearrangement which is often identical to the reaction which occurs for the same system under basic conditions in solution,² and (iii) a reaction may take place which occurs remote from and uninfluenced by the anionic centre.^{3,4}

Deprotonated phenyl systems containing substituents illustrate a number of these fragmentation types. For example, the benzyloxy anion fragments by the simple cleavage shown in eqn. (1) (Scheme 1),⁵ while alkylphenoxide anions fragment by simple homolytic cleavage (eqn. (2)), or following rearrangement (eqn. (3)).⁶ When there is no simple fragmentation that can occur through the substituent, specific retro-cleavage of the phenyl ring occurs (see eqn. (4)).⁷

The collision induced mass spectrum of deprotonated (methyl-*d*₃) benzoate is shown in Fig. 1. The spectrum is unusual in that the major fragmentation involves loss of carbon monoxide from the even-electron parent anion. This paper addresses the following questions: (i) does loss of CO from deprotonated methyl benzoate only occur when the deprotonation occurs at the *ortho* position, or does the process also occur for the isomeric anions formed by deprotonation at the *meta* and *para* positions on the phenyl ring? (ii) Is the loss of CO a charge-remote reaction, *i.e.* a fragmentation not directed by the negative charge on the ring? (iii) If the loss of CO process is not a charge-remote process, what is the mechanism?



Scheme 1

Results and discussion

The reaction between (methyl-*d*₃) benzoate and HO^- in the ion source of the mass spectrometer produces only an $(M - H)^-$ ion. Collisional activation of this anion results in loss of CO (Fig. 1). The only deprotonated esters that have been reported to lose CO are dimethyl succinate (where the loss is a minor process)⁸ and acyloxy acetates (where the loss constitutes the base peak of the spectrum).⁹ In both cases, an incipient $MeOCO^-$ ion acts as a MeO^- donor within an anion–neutral–ion complex (the reaction $MeOCO^- \rightarrow MeO^- + CO$ is exothermic by 2 kJ mol $^{-1}$).¹⁰ The latter reaction occurs following the (acyloxy)acetate–acylhydroxyacetate rearrangement (eqn. (5), Scheme 2).⁹ We have also, for comparison, measured the

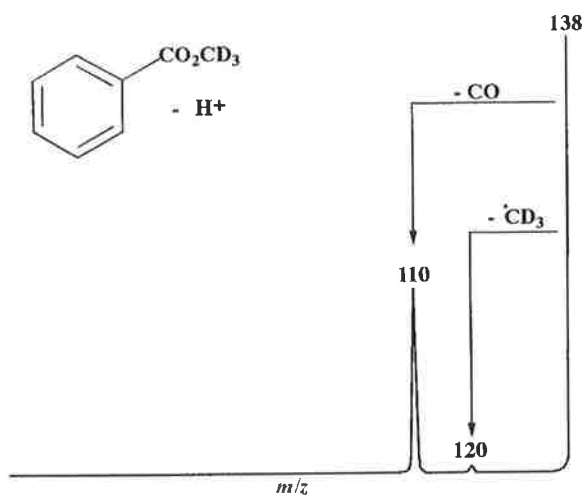
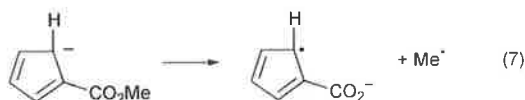
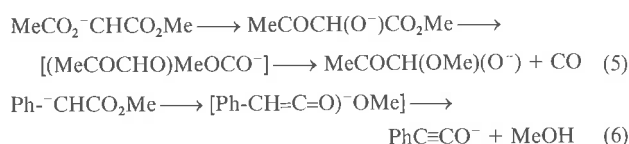


Fig. 1 Collisional activation (CA) mass spectrum (MS/MS) of deprotonated (methyl- d_3) benzoate. VG ZAB 2HF mass spectrometer. For experimental conditions see Experimental section.

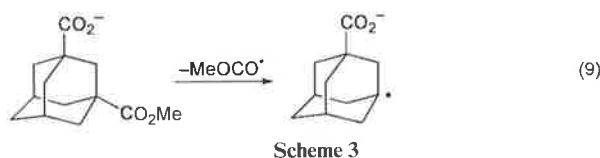
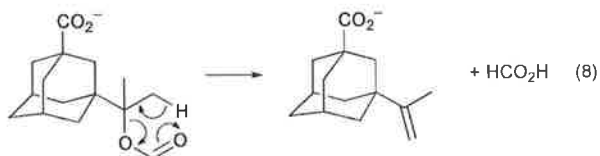
mass spectra of several deprotonated esters which contain unsaturation: these show simple fragmentation processes, for example, deprotonated methyl phenylacetate fragments as shown in eqn. (6), Scheme 2, while the major fragmentation of deprotonated cyclopentadienyl ester is loss of the ester substituent (eqn. (7), Scheme 2). Neither of these examples show



Scheme 2

loss of CO. It is also of interest to note that the fragmentation behaviour of deprotonated methyl benzoate (an even-electron anion) is quite different from that of radical anions (odd-electron anions) of the general formula $\text{ArCO}_2\text{R}^{\cdot-}$: these show the characteristic cleavage sequence $\text{M}^{\cdot-} - \text{R}^{\cdot} - \text{CO}_2$.¹¹

There has been much debate recently concerning charge-remote reactions, *i.e.* reactions that occur remote from and uninfluenced by the charged centre.^{3,4} Such reactions may occur when simple fragmentations are energetically unfavourable. We have studied charge-remote reactions using 1,3-disubstituted adamantanes, systems where the charged centre and the reacting centre are separated by a rigid saturated ring system, and cannot approach through space. A particular example of a charge-remote reaction is the facile loss of formic acid from the species shown in eqn. (8), Scheme 3.⁵ Perhaps the loss of CO from deprotonated methyl benzoate is a charge-remote reac-



Scheme 3

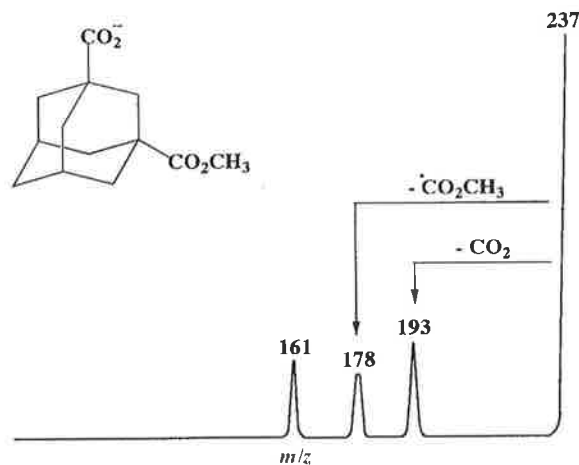


Fig. 2 CA MS/MS of the carboxylate anion produced by the $\text{S}_{\text{N}}2$ reaction between HO^- and 1,3-bis(methoxycarbonyl)adamantane in the ion source of the VG 2HF mass spectrometer. The peak at m/z 161 in this spectrum is formed by the sequence $[(\text{M} - \text{H})^- - (\text{CO}_2 + \text{MeOH})]$.

tion? In order to test this proposal, we have measured the collision induced mass spectrum of the adamantane ester shown in Fig. 2. A charge-remote radical cleavage reaction occurs (eqn. (9), Scheme 3), but no loss of CO is noted. We conclude from all the above data that the loss of CO from deprotonated methyl benzoate is charge initiated and that the aryl ring system is a prerequisite for this reaction.

If the loss of CO from deprotonated (methyl- d_3) benzoate is charge initiated, is the reaction initiated by the charge being at the *ortho* position of the ring, or can it also occur for those isomers where the charges are localised on *meta* or *para* positions? Deprotonation of the phenyl ring of (methyl- d_3) benzoate with HO^- , can, in principle, occur at any ring position, so the spectrum shown in Fig. 1 does not answer this question. We have approached this problem both indirectly and directly. First, we examined the collision induced mass spectrum of an analogous compound which has *ortho* and *para* positions blocked so that deprotonation can only occur in the *meta* positions. The compound chosen was methyl 2,4,6-trifluorobenzoate: the spectrum of the $(\text{M} - \text{H})^-$ ion shows the two major fragmentations $[(\text{M} - \text{H})^- - \text{HF}]$ and $[(\text{M} - \text{H})^- - \text{MeCO}_2^-]$ in the ratio of 2:1. Both of these fragmentations are high energy processes [even though the electron affinity of F^- is 3.4 eV,¹² the C-F bond energy is high (543.9 kJ mol⁻¹)¹³]. Since no loss of CO from this parent anion is observed, this might suggest that (methyl- d_3) benzoate deprotonated at the *meta* position should not fragment by loss of carbon monoxide. On the other hand it may be that in the trifluoro system, loss of CO is not observed because it is energetically unfavourable with respect to the competing reactions, *viz.* the loss of HF.

In order to confirm this proposal it is necessary to prepare the required three isomeric anions unequivocally and to obtain their mass spectra. We chose to use the $\text{S}_{\text{N}}2(\text{Si})$ procedure (initially proposed by DePuy *et al.*¹⁴) for this purpose, *viz.* $\text{RSiMe}_3 + \text{Nu}^- \rightarrow \text{R}^- + \text{Me}_3\text{SiNu}$. The neutral precursors methyl (*ortho*-, *meta*- and *para*-trimethylsilyl)benzoate were synthesised and the collision induced mass spectra of the three isomeric anions are shown in Figs. 3–5. The mass spectrum of the *ortho* isomer (Fig. 3) is dominated by loss of CO, and is comparable with that shown in Fig. 1. This confirms that the *ortho* isomer undergoes pronounced loss of CO. The most surprising feature of these experiments is that the *meta* and *para* isomers also lose carbon monoxide. A qualitative estimate of the CO loss from each of the isomeric anions can be obtained by comparing the abundances of the peaks formed from $[(\text{M} - \text{H})^- - \text{CO}]$ and $[(\text{M} - \text{H})^- - \text{Me}^{\cdot}]$ processes in the three

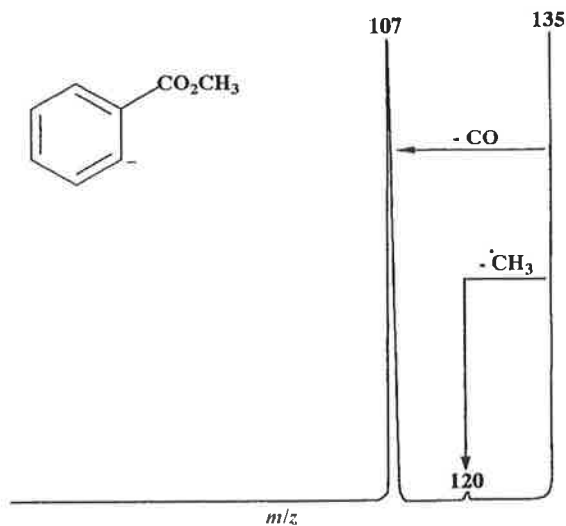


Fig. 3 CA MS/MS of the methyl *o*-benzoate anion formed by the $S_N2(Si)$ reaction between HO^- and methyl *o*-trimethylsilylbenzoate.

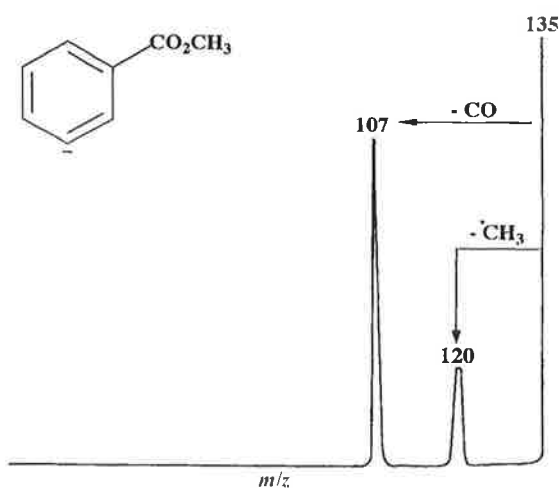


Fig. 4 CA MS/MS of the methyl *m*-benzoate anion formed by the $S_N2(Si)$ reaction between HO^- and methyl *m*-trimethylsilylbenzoate. VG ZAB 2HF mass spectrometer.

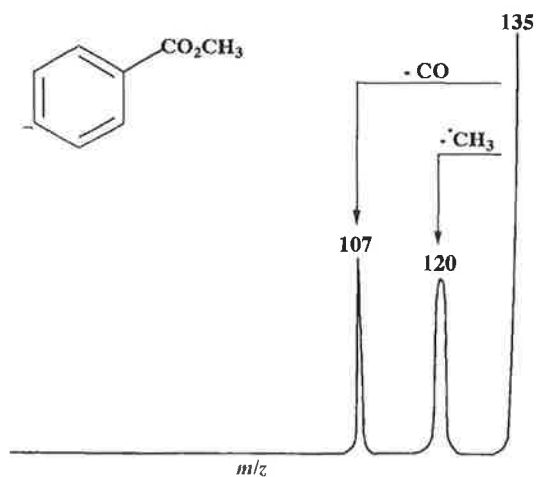


Fig. 5 CA MS/MS of the methyl *p*-benzoate anion formed by the $S_N2(Si)$ reaction between HO^- and methyl *p*-trimethylsilylbenzoate. VG ZAB 2HF mass spectrometer.

spectra, *viz.* *ortho* (100:3), *meta* (100:28) and *para* (100:91). The energy required for loss of Me^\cdot is comparable in each case, so the relative extent of CO loss is *ortho* \gg *meta* $>$ *para*. The peak widths at half height of the three *m/z* 107 ions in Figs. 2 to 4 are different [*ortho* (28.0 V), *meta* (32.9 V) and *para* (35.7 V)].

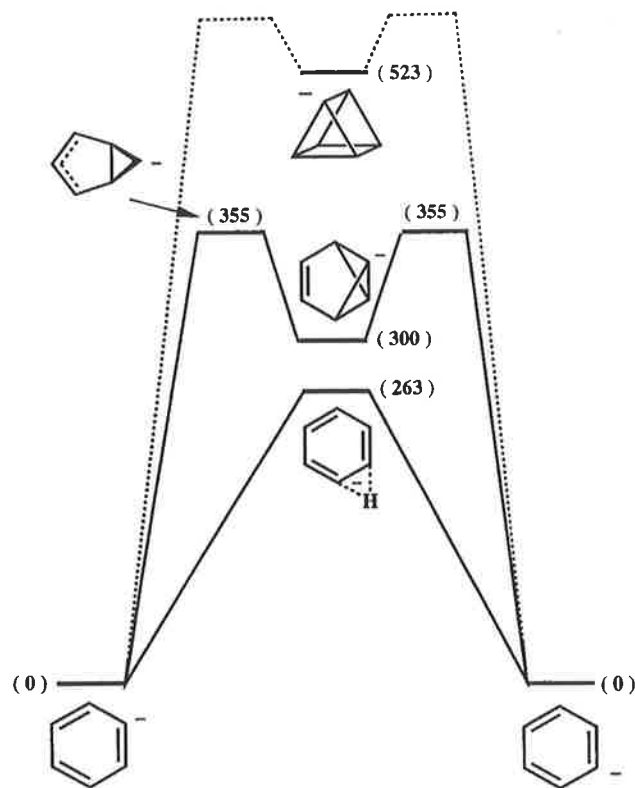


Fig. 6 Possible phenyl anion interconversions. B3LYP/6-311++G(d,p)//HF/6-31+G(d) level of theory. Full details of energies and geometries and species shown in the figure are listed in Table 1.

This means that either the structures and/or energies of the three *m/z* 107 ions are different, or their modes of formation are different.¹⁵ The three *m/z* 107 ions are also formed in the ion source of the mass spectrometer. These three ions show the characteristic loss of CH_2O from the $(M - H)^-$ ion of anisole.^{16,17} Not only that, but the peak widths of the three *m/z* 77 ($C_6H_5^-$) species formed by loss of CH_2O from the three source-formed *m/z* 107 ions are the same within experimental error (33.5 ± 0.5 V) and the same as the peak formed by loss of CH_2O from *ortho*-(C_6H_4)OMe [formed by the $S_N2(Si)$ reaction between HO^- and *ortho*-trimethylsilylanisole]. The experimental measurements indicate that the three product ions (*m/z* 107) formed by losses of CO from the *ortho*, *meta*, and *para* isomers of $[(C_6H_4)CO_2Me]^-$ have the same structure [the *ortho* anion of $(C_6H_4)OMe$], but the energetics of formation of this anion from each precursor are different. We propose from the available data, that the loss of carbon monoxide is a reaction of the *ortho* anion $[(C_6H_4)CO_2Me]^-$, and that the losses of CO observed in the spectra of *meta* and *para* isomers are a consequence of rearrangement of these isomers to the *ortho* anion prior to loss of CO.

Mechanisms which may account for the interconversion of the *ortho*, *meta* and *para* forms of deprotonated methyl benzoate are, (i) C scrambling *via* a prismane-type anion, (ii) C scrambling *via* stepwise formation and cleavage of benzvalene anions, (iii) a process by which H is transported around the phenyl ring leaving the carbon framework unchanged, or (iv) a combination of some of the above. Some data concerning the energetics of C scrambling in neutral benzene have been examined by theoretical and experimental studies indicating that these are energetically unfavourable processes.¹⁸⁻²⁰ The relative energies [at the RMP2/6-31G(d) level of theory] of benzvalene and prismane relative to benzene are 313 and 492 kJ mol⁻¹ respectively.¹⁸ The energy of the transition state for ring opening of benzvalene is calculated to be 116 kJ mol⁻¹ above benzvalene (at the B3LYP/DZP level of theory)^{19,20} and measured experimentally to be 122.6 kJ mol⁻¹.²¹

Table 1 Geometries (bond lengths/Å, angles/° and dihedral angles/°) and energies for species in Fig. 6 (geometries—HF/6-31+G(d), energies—B3LYP/6-311++G(d,p))

	1	2	3
Energy/hartree	-231.6593903	-231.5529727	-231.5431464
Zero pt correction	0.091767	0.084772	0.089399
Relative Energy/ kJ mol ⁻¹	0.0	262.6	299.5

	4	5
Energy/hartree	-231.5163550	-231.4574589
Zero pt correction	0.085732	0.088729
Relative Energy/ kJ mol ⁻¹	355.4	522.9

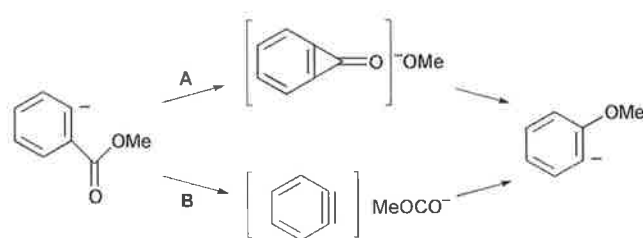
	1	2	3	4	5
C2-C1	1.417	1.435	1.580	1.504	1.545
C3-C2	1.394	1.394	1.500	1.455	1.546
C4-C3	1.391	1.397	1.332	1.386	1.503
C5-C4	1.391	1.391	1.501	1.383	1.507
C6-C5	1.394	1.397	1.495	1.502	1.546
H7-C2	1.084	1.288	1.080	1.083	1.082
H8-C3	1.082	1.082	1.077	1.074	1.081
H9-C4	1.080	1.081	1.077	1.079	1.082
H10-C5	1.082	1.081	1.080	1.076	1.081
H11-C6	1.084	1.082	1.086	1.093	1.082
C3-C2-C1	124.8	119.4	111.3	129.6	92.7
C4-C3-C2	120.3	120.2	105.1	107.5	89.1
C5-C4-C3	117.9	120.4	105.1	111.7	60.8
C6-C5-C4	120.3	120.4	109.6	113.1	89.1
H7-C2-C1	118.7	56.1			129.7
H7-C2-C3				121.5	118.7
H8-C3-C2	120.1	121.1	126.4	124.0	133.8
H9-C4-C3	121.0	120.1	128.4	125.4	127.8
H10-C5-C4	119.5	119.5	121.5	125.7	130.4
H11-C6-C5	116.4	118.7	135.3	119.6	130.2
C4-C3-C2-C1			31.8	40.7	-1.2
C5-C4-C3-C2			0.0	8.3	-90.2
C6-C2-C3-C4			-29.1	4.5	59.6
H7-C2-C3-C4			179.5	-166.1	-152.5
H8-C3-C4-C5			178.8	155.6	116.2
H9-C4-C3-H8			0.0	-171.0	-0.8
H10-C5-C4-H9			-0.7	-176.7	0.8
H11-C6-C5-H10			-24.0	139.2	0.5

We have calculated the reaction coordinates for the interconversion of the phenyl and benzvalene anions at the modest B3LYP/6-311++G(d,p)//HF/6-31+G(d) level of theory and the results are summarised in Fig. 6 and Table 1. At this level of theory, the benzvalene anion lies 300 kJ mol⁻¹ above the phenyl anion, and the transition state for interconversion of the two is 355 kJ mol⁻¹ above the phenyl anion. The corresponding prismane anion is 523 kJ mol⁻¹ less stable than the phenyl anion. The formation of this anion is clearly not feasible in comparison to formation of the benzvalene anion, thus we have not calculated the transition state for this interconversion.

Anion scrambling *via* a degenerate H transfer mechanism is also shown in Fig. 6. The transition state is 263 kJ mol⁻¹ above the phenyl anion at the B3LYP/6-311++G(d,p)//HF/6-31+G(d) level of theory, making this a more energetically favoured process than that involving C scrambling through a

benzvalene anion. We have also computed the transition state energies for the equivalent H migration reactions of deprotonated methyl benzoate at the same level of theory, and these reactions are summarised in Fig. 7. It appears that there is no significant difference in the energetics of the H transfer process for the phenyl anion and deprotonated methyl benzoate. On the basis of these calculations, we propose that the interconversions of *ortho*, *meta* and *para* anions occur by H transfers. The interconversions *meta* to *ortho*, and *para* to *ortho* require one and two steps respectively, explaining the observed CO loss ratio *meta* > *para*.†

There are two possible mechanisms which could account for the loss of CO from deprotonated methyl benzoate. The first, route A (Scheme 4), involves a cyclisation and nucleophilic



Scheme 4

substitution prior to loss of CO. The second involves the formation of a [benzynes-MeOCO⁻] ion complex, followed by a cine substitution with MeOCO⁻ acting as a MeO⁻ donor. We have investigated the reaction coordinates of both of these reaction pathways using calculations at the B3LYP/6-311++G(d,p)//HF/6-31G+(d) level of theory. The two mechanistic pathways are shown in Figs. 8 and 9; structures and energies of the reactant, transition states, reactive intermediates and products are shown in Table 2.

The cyclisation process A shown in Fig. 8 has four steps, with the initial cyclisation step together with the subsequent attack of the incipient MeO⁻ at a ring carbon being rate determining with a barrier of 202 kJ mol⁻¹ at this level of theory. The benzyne cine substitution mechanism B is shown in Fig. 9. This is a simpler process than that shown in Fig. 8, but the barrier to the transition state for the benzyne mechanism is 289 kJ mol⁻¹, some 87 kJ mol⁻¹ more than that for cyclisation process A. Thus the cyclisation process is favoured in terms of the relative barriers to the respective transition states of the rate determining steps. There is however, a second factor which must be taken into account when determining the relative rates of these two processes, *viz.* the relative pre-exponential Arrhenius factors for both processes. In other words, there may be entropy bottlenecks in such reactions. In principle, the larger the number of steps, the greater the probability of such bottlenecks. In order to access these factors properly, we need to know the potential surfaces for both processes, *i.e.* the width of the pathways of each step into and out of each transition state and reactive intermediate, together with the curvature of the reaction coordinate pathway. Unfortunately, such calculations are not feasible with a system of this size using our supercomputing facilities. What we can do however, is to compare the relative vibrational partition functions of the first transition state in each of the two mechanisms: this will give some insight into the relative values of the pre-exponential factors for each of the processes A and B. We have described this method (together

† A reviewer has suggested that the anion interconversion could be due to H exchange within an anion-water complex, *viz.* [(*m*-C₆H₄CO₂Me)⁻(H₂O)] → [(*C*₆H₅CO₂Me)(HO⁻)] → [(*o*-C₆H₄CO₂Me)⁻(H₂O)] → [(*o*-C₆H₄-CO₂Me)⁻ + H₂O]. We have tested this proposal by allowing the *o*, *m* and *p* anions formed by the respective S_N2(S_i) reactions to be exposed to D₂O in the ion source. No incorporation of D into the anions is observed, thus this process is not operable.

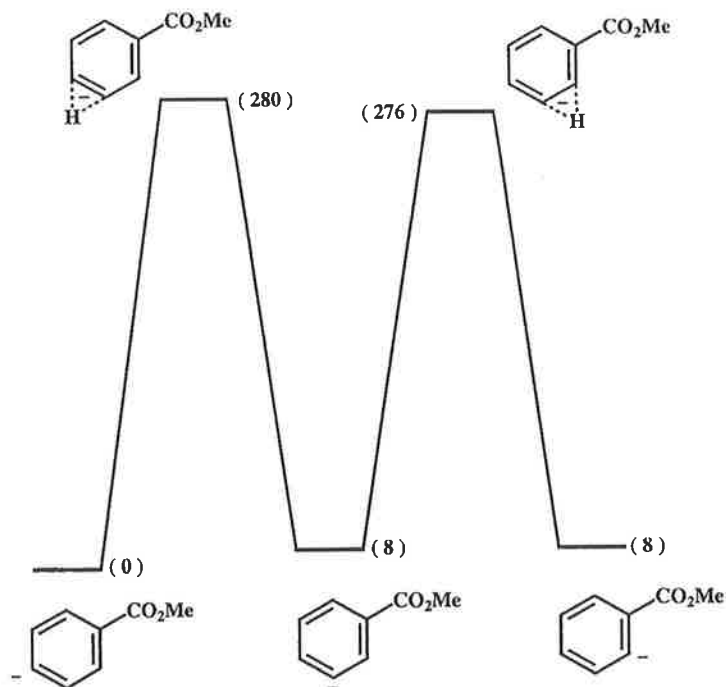


Fig. 7 H transfer reactions within deprotonated methyl benzoate. B3LYP/6-311++G(d,p)//HF/6-31+G(d) level of theory.

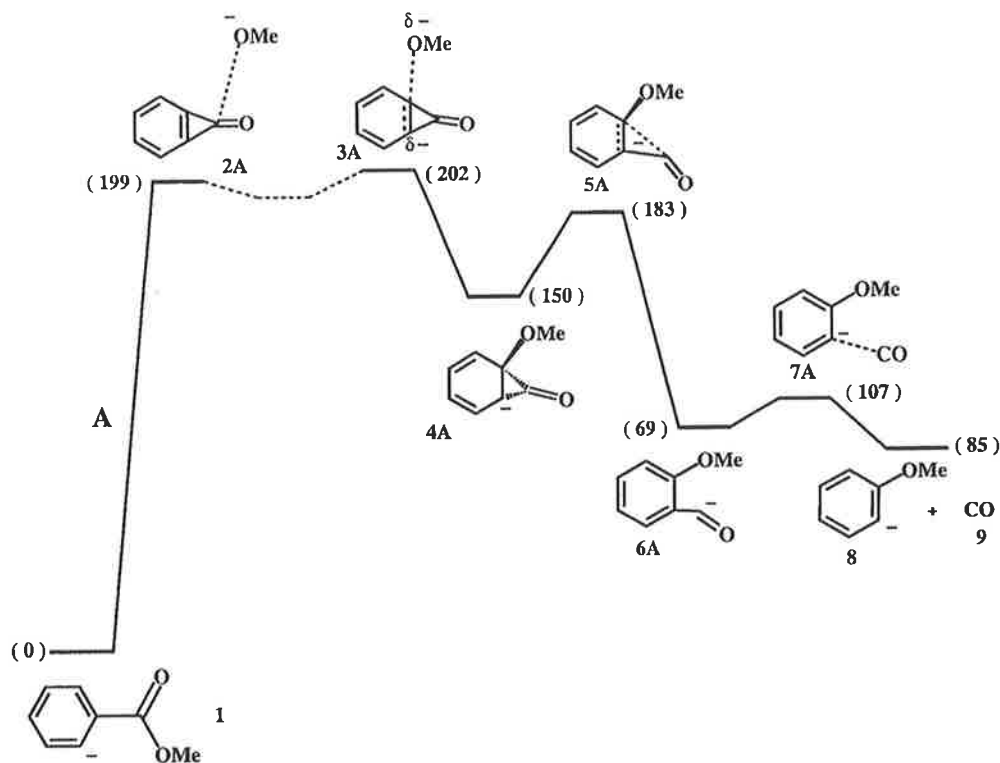


Fig. 8 Loss of CO from the methyl *o*-benzoate anion. The cyclisation mechanism A. B3LYP/6-311++G(d,p)//HF/6-31+G(d) level of theory. Full details of energies and geometries of reactant, reactive intermediates, transition states and products are listed in Table 2.

with its approximations) in detail previously²² (see also ref. 23). These data are recorded in Table 3.

There is a difficulty in knowing precisely which of the low frequency vibrations (shown in Table 3) to use, but if all of the listed values are considered, the Arrhenius factor for the benzyne process B is some four times larger than that for process A. This is clearly a maximum value, but it is in the correct direction, since the first transition state for dissociative process A has a number of low frequency modes for which there are no counterparts in the first transition state for B.

In conclusion, the loss of carbon monoxide from deprotonated

ated methyl benzoate to form deprotonated anisole, is initiated from an anion in which the charge is localised on the *ortho* position of the phenyl ring. If the initial anion centre is situated *meta* or *para* to the methoxycarbonyl substituent, 1,2-H transfer(s) effects formation of the *ortho* anion prior to fragmentation of the substituent. We are not able, using the available data, to differentiate between the two mechanisms shown in Scheme 4. The barrier to the first transition state for the cyclisation process A is 87 kJ mol⁻¹ lower than that for benzyne process B at the level of theory used, but this is counteracted by the Arrhenius factor for the process A being the smaller of the two.

Table 2 Geometries and energies of all species in Figs. 8 and 9 (geometries—HF/6-31+G(d), energies—B3LYP/6-311++G(d,p))

A Reactants and products

Energy/hartree	-459.6162298	-346.2297129	-113.3485635
Zero pt correction	0.138628	0.126984	0.005542
Relative Energy of Reactant/kJ mol ⁻¹	0.0		
Relative Energy of Product/kJ mol ⁻¹		85.0	

	1	8	9
O2-C1			1.113
C2-C1	1.425	1.409	
C3-C2	1.413	1.399	
C4-C3	1.408	1.393	
C5-C4	1.377	1.389	
C6-C5	1.401	1.389	
C7-C3	1.487		
O7-C3		1.388	
O8-C7	1.209		
C8-O7		1.390	
O9-C7	1.332		
C10-O9	1.399		
C3-C2-C1	112.2	112.0	
C4-C3-C2	124.4	125.4	
C5-C4-C3	120.3	119.5	
C6-C5-C4	118.2	119.3	
C7-C3-C2	121.3		
O7-C3-C2		121.8	
O8-C7-C4	125.0		
C8-O7-C3		118.3	
O9-C7-C8	119.7		
C10-O9-C7	117.1		

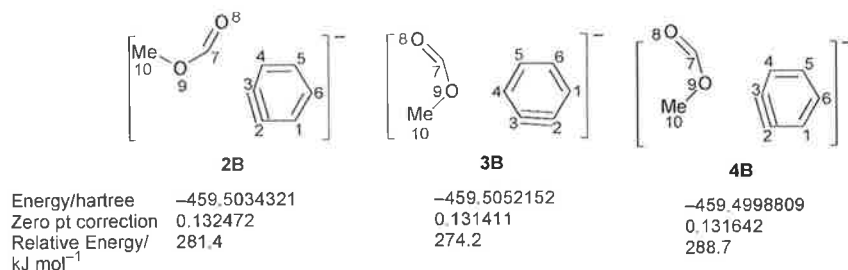
B Other species in Fig. 8

Energy/hartree	-459.5353556	-459.5348882	-459.5577180	-459.5421810	-459.5883092	-459.5719478
Zero pt correction	0.133144	0.13364	0.137261	0.134011	0.136638	0.134734
Relative Energy/kJ mol ⁻¹	199.2	201.6	150.3	183.3	68.5	106.9

	2A	3A	4A	5A	6A	7A
C2-C1	1.395	1.426	1.442	1.477	1.396	1.481
C3-C2	1.352	1.370	1.496	1.511	1.397	1.474
C4-C3	1.395	1.435	1.493	1.424	1.394	1.346
C5-C3	1.378	1.351	1.341	1.370	1.385	1.436
C6-C5	1.420	1.454	1.466	1.458	1.389	1.397
C7-C2	1.440	1.389	1.355	1.296	1.614	1.313
C8-C7	1.194	1.207	1.222	1.181	1.223	1.181
O9-C3	2.666	2.102	1.422	1.412	1.370	1.380
C10-O9	1.346	1.348	1.389	1.391	1.406	1.383
C3-C2-C1	123.6	123.8	123.8	120.3	116.5	114.9
C4-C3-C2	123.6	121.2	113.3	112.4	121.4	121.8
C5-C4-C3	114.0	114.6	119.2	121.9	120.5	122.6
C6-C5-C4	122.4	123.1	121.9	119.9	119.3	116.6
C7-C2-C3	62.0	62.1	62.5	86.4	123.4	121.2
O8-C7-C2	147.8	151.0	151.9	173.3	110.0	177.2
O9-C3-C2	75.3	118.7	121.6	120.5	123.1	111.9
C10-O9-C3	144.4	116.6	114.7	115.2	116.7	118.8
C4-C3-C2-C1	0.0	-11.7	-21.4	-30.6	-0.9	0.0
C5-C4-C3-C2	-2.1	8.7	17.8	8.2	0.9	0.0
C6-C5-C4-C3	2.1	-1.0	-3.8	14.5	-0.2	0.0
C7-C2-C3-C4	-175.6	148.9	113.2	114.0	-179.4	180.0
O8-C7-C2-C3	-147.5	-172.2	-171.1	-171.2	-162.8	180.0
O9-C3-C2-C1	115.2	99.0	117.3	113.3	-178.0	180.0
C10-O9-C3-C2	111.5	27.7	-58.0	-64.8	-67.6	180.0

Table 2 (continued)

C Other species in Fig. 9



	2B	3B	4B
C2-C1	1.417	1.408	1.418
C3-C2	1.251	1.366	1.250
C4-C3	1.360	1.400	1.359
C5-C4	1.398	1.408	1.397
C6-C5	1.405	1.394	1.409
C7-C4		3.581	3.320
O8-C7	1.221	1.203	1.204
O9-C7	1.416	1.492	1.480
C10-O9	1.397	1.391	1.392
C3-C2-C1	110.1	114.0	109.6
C4-C3-C2	105.6	140.0	143.4
C5-C4-C3	121.3	105.5	105.7
C6-C5-C4	121.9	121.9	121.2
C7-C3-C2	146.0		
C7-C4-C3		169.1	96.8
O8-C7-C4		174.9	175.1
O8-C7-C3	98.4		
O9-C7-C8	113.1	11.9	112.3
C10-O9-C7	118.7	118.4	118.5

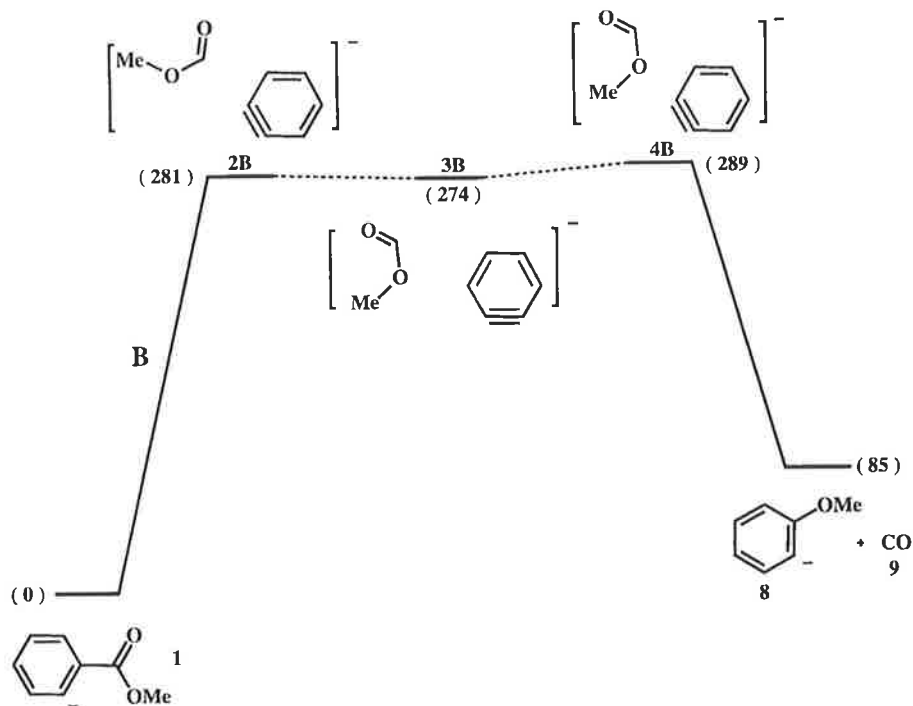


Fig. 9 Loss of CO from the methyl *o*-benzoate anion. The benzyne mechanism B. B3LYP/6-311G(d,p)//HF/6-31+G(d) level of theory. Details of energies and geometries of species shown in the figure are listed in Table 2.

Experimental

A. Synthetic procedures

Methyl benzoate and methyl phenylpropiolate were commercial samples used without further purification. The following compounds were made by reported procedures: 1-methoxycarbonylcyclopenta-1,3-diene,²⁴ methyl *o*-trimethylsilylbenzoate,²⁵

methyl *m*-trimethylsilylbenzoate,²⁶ methyl *p*-trimethylsilylbenzoate,²⁷ and *o*-trimethylsilylanisole.²⁸ (Methyl-*d*₃) benzoate (*d*₃ = 99%) was prepared by esterification of benzoyl chloride with methanol-*d*₄.²⁹

B. Computational methods

Geometry optimisations were carried out at the HF/6-31+G(d)

Table 3 Vibrational partition functions (Q' vib) for transition states **2A** and **2B**

Transition state 2A		Transition state 2B	
Frequency/cm ⁻¹	Q' vib	Frequency/cm ⁻¹	Q' vib
63	4.1394	38	6.5088
92	3.0050	59	4.3730
100	2.8028	99	2.8205
112	2.5641	105	2.6986
183	1.8067	134	2.2487
269	1.4412	185	1.7914
293	1.3802	342	1.2851
394	1.2144	361	1.2553
499	1.1251	443	1.1657
548	1.0984	466	1.1473
584	1.0827	480	1.1373
688	1.0507	666	1.0560
771	1.0347	691	1.0501
807	1.0295	759	1.0366
823	1.0274	845	1.0248
843	1.0250	902	1.0192
972	1.0140	926	1.0172
1063	1.0094	966	1.0144
1079	1.0087	1074	1.0089
1103	1.0078	1075	1.0088
1113	1.0075	1096	1.0081
1181	1.0055	1122	1.0072
1242	1.0042	1158	1.0061
1244	1.0042	1204	1.0050
1247	1.0041	1227	1.0045
1282	1.0035	1274	1.0037
1289	1.0034	1309	1.0031
1399	1.0021	1340	1.0027
1401	1.0021	1411	1.0020
1584	1.0009	1530	1.0012
1607	1.0008	1594	1.0009
1609	1.0008	1596	1.0009
1626	1.0008	1630	1.0008
1626	1.0008	1644	1.0007
1770	1.0004	1649	1.0007
1785	1.0004	1724	1.0005
1980	1.0002	1997	1.0002
2870	1.0000	3178	1.0000
2907	1.0000	3225	1.0000
2976	1.0000	3230	1.0000
3325	1.0000	3321	1.0000
3345	1.0000	3343	1.0000
3375	1.0000	3362	1.0000
3378	1.0000	3374	1.0000

level of GAUSSIAN 94.³⁰ Energies were optimised by the Becke 3LYP method^{31,32} *i.e.* B3LYP/6-311++G(d,p)//HF/6-31+G(d). The calculated frequencies were also used to determine the zero-point vibrational energies which were then scaled by 0.9135³³ and used as a zero-point energy correction for the electronic energies calculated at this and higher levels of theory. Stationary points were characterised as either minima (no imaginary frequencies) or transition states (one imaginary frequency) by calculation of the frequencies using analytical gradient procedures. The minima connected by a given transition structure were confirmed by intrinsic reaction coordinate (IRC) calculations. Calculations were carried out using the Power Challenge Super Computers at the South Australian Super Computing Centre (The University of Adelaide), and the Beowulf computing cluster at the South Australian Computational Chemistry Facility (The University of Adelaide).

C. Mass spectrometric methods

Collisional activation mass spectra (CA MS/MS) were measured using a two-sector reversed geometry VG ZAB 2HF spectrometer. This instrument and the typical experimental conditions of negative ion chemical ionisation (NICI) have

been described in detail elsewhere.³⁴ Samples were introduced into the source *via* a heated septum inlet, producing a measured pressure of 5×10^{-6} Torr inside the source housing. Typical ionization conditions were: source temperature, 200 °C; ionising energy, 70 eV (tungsten filament); accelerating voltage, -7 kV. All slits were fully open in order to minimize mass discrimination effects due to energy resolution.^{35,36} The reagent ion HO⁻ was generated from electron impact on H₂O (introduced through the heated septum inlet to give an operating pressure inside the source housing of *ca.* 5×10^{-5} Torr, and thus an estimated pressure inside the ion source of close to 0.1 Torr). Negative ion chemical ionisation of the sample either effected (i) deprotonation, or (ii) desilylation of a neutral trimethylsilylated substrate, by analogy to the method originally developed by DePuy *et al.*¹⁴ Collisional activation (CA) spectra were obtained by collision of the incident anions with argon in the first of two collision cells at a pressure typically around 10^{-7} Torr. This reduces the main beam to 90% of its initial value, producing essentially single collision conditions in the collision cell.³⁷ Peak width (at half height) values are a mean of ten measurements and are correct to within ± 0.5 V.

Acknowledgements

We thank the Australian Research Council for funding this work. S. D. thanks the ARC for a research associate stipend. We thank Mark S. Taylor (University of Colorado, Boulder) for helpful discussion concerning the calculation of vibrational partition functions.

References

- 1 J. H. Bowie, The Fragmentations of (M - H)⁻ Ions Derived from Organic Compounds: an Aid to Structure Determination, in *Topics in Mass Spectrometry. Vol. 1. Experimental Mass Spectrometry*, ed. D. H. Russell, pp. 1-34, Plenum Press, New York and London, 1994.
- 2 S. Dua, P. C. H. Eichinger, G. W. Adams and J. H. Bowie, *Int. J. Mass Spectrom. Ion Processes*, 1994, **133**, 1.
- 3 J. Adams, *Mass Spectrom. Rev.*, 1990, **9**, 141; M. L. Gross, *Int. J. Mass Spectrom. Ion Processes*, 1992, **118/119**, 137.
- 4 S. Dua, J. H. Bowie, B. A. Cerda and C. Wesdemiotis, *J. Chem. Soc., Perkin Trans. 2*, 1998, 1443.
- 5 M. J. Raftery, J. H. Bowie and J. C. Sheldon, *J. Chem. Soc., Perkin Trans. 2*, 1988, 563.
- 6 L. B. Reeks, P. C. H. Eichinger and J. H. Bowie, *Rapid Commun. Mass Spectrom.*, 1993, **7**, 286.
- 7 J. H. Bowie, *Mass Spectrom. Rev.*, 1990, **9**, 349, and references cited therein.
- 8 M. J. Raftery and J. H. Bowie, *Aust. J. Chem.*, 1987, **47**, 711.
- 9 P. C. H. Eichinger, R. N. Hayes and J. H. Bowie, *J. Am. Chem. Soc.*, 1991, **113**, 1949.
- 10 Thermochemical data from <http://webbook.nist.gov>
- 11 A. C. Ho, J. H. Bowie and A. Fry, *J. Chem. Soc. B*, 1971, 530.
- 12 P. L. Jones and R. D. Mead, *J. Chem. Phys.*, 1980, **73**, 4419.
- 13 S. W. Benson, *Thermochemical Kinetics*, Wiley, New York, 1968.
- 14 C. H. DePuy, V. M. Bierbaum, L. A. Flippin, J. J. Grabowski, G. K. King, R. J. Schmitt and S. A. Sullivan, *J. Am. Chem. Soc.*, 1980, **102**, 5012.
- 15 For discussions of metastable and collision induced ions see, R. G. Cooks, J. H. Beynon, R. M. Caprioli and G. R. Lester, *Metastable Ions*, Elsevier, Amsterdam, London and New York, 1973.
- 16 T. C. Kleingeld and N. M. M. Nibbering, *Tetrahedron*, 1983, **39**, 4193.
- 17 P. C. H. Eichinger, J. H. Bowie and R. N. Hayes, *Aust. J. Chem.*, 1989, **42**, 865.
- 18 J. M. Schulman and R. L. Disch, *J. Am. Chem. Soc.*, 1985, **107**, 5059.
- 19 K. E. Wilzbach, J. S. Ritcher and J. L. Kaplan, *J. Am. Chem. Soc.*, 1971, **93**, 3782; M. J. S. Dewar and S. J. Krischner, *J. Am. Chem. Soc.*, 1975, **97**, 2932.
- 20 H. F. Bettinger, P. R. Schriener, H. F. Schaefer and P. von R. Schleyer, *J. Am. Chem. Soc.*, 1998, **120**, 5741.
- 21 N. J. Turro, C. A. Renner, T. J. Katz, K. B. Wiberg and H. A. Connon, *Tetrahedron Lett.*, 1976, 4133.
- 22 J. M. Hevko, S. Dua, J. H. Bowie and M. S. Taylor, *J. Chem. Soc., Perkin Trans. 2*, 1999, 457.

- 23 R. G. Gilbert and S. C. Smith, *Theory of Unimolecular and Recombination Reactions*, Blackwell Scientific, Cambridge, UK, 1990; A. P. Scott and L. Radom, *J. Phys. Chem.*, 1996, **100**, 16502.
- 24 G. N. Grunewald and D. P. Davis, *J. Org. Chem.*, 1978, **43**, 3075.
- 25 A. G. Schultz and E. G. Antoulinakis, *J. Org. Chem.*, 1996, **61**, 4555.
- 26 C. Earborn and P. M. Jackson, *J. Chem. Soc. B*, 1969, 21.
- 27 J. C. Amedio, G. T. Lee, K. Prasad and O. Repic, *Synth. Commun.*, 1995, **25**, 2599.
- 28 D. S. Wilbur, W. E. Stone and W. S. Aderson, *J. Org. Chem.*, 1983, **48**, 1544.
- 29 R. A. McClelland and G. Patel, *J. Am. Chem. Soc.*, 1981, **103**, 6912.
- 30 GAUSSIAN 94, Revision C3, M. J. Frisch, G. W. Trucks, H. B. Schlegel, P. M. W. Gill, B. G. Johnson, M. A. Robb, J. R. Cheeseman, T. Keith, G. A. Petersson, J. A. Montgomery, J. B. Foresman, J. Cioslowski, B. B. Stefanov, A. Nanayakkara, M. Challacombe, C. Y. Peng, P. V. Ayala, W. Chen, M. W. Wong, J. L. Andres, E. S. Replogle, R. Gomperts, R. L. Martin, D. J. Fox, J. S. Binkley, D. J. Defrees, J. Baker, J. P. Stewart, M. Head-Gordon, C. Gonzales and J. A. Pople, Gaussian Inc., Pittsburgh, PA, 1995.
- 31 A. D. Becke, *J. Chem. Phys.*, 1993, **98**, 5648.
- 32 P. J. Stevens, F. J. Devlin, C. F. Chabrowski and M. J. Frisch, *J. Phys. Chem.* 1994, **98**, 11623.
- 33 M. W. Wong, *Chem. Phys. Lett.*, 1996, **256**, 391.
- 34 M. B. Stringer, J. H. Bowie and J. L. Holmes, *J. Am. Chem. Soc.*, 1986, **108**, 3888.
- 35 J. K. Terlouw, P. C. Burgers and J. L. Holmes, *Org. Mass Spectrom.*, 1979, **14**, 307.
- 36 P. C. Burgers, J. L. Holmes, A. A. Mommers and J. E. Szulejko, *J. Am. Chem. Soc.*, 1984, **106**, 521.
- 37 J. L. Holmes, *Org. Mass Spectrom.*, 1985, **20**, 169.

An examiner has questioned the interpretation of some results described in chapter three. These comments, which are dealt with below, in no way affect the conclusions of the research.

Questions 1 and 2 [see Fig 3.2 and pg 47]

“If these anion calculations [referring to Figs 3.4, 3.5 and 3.6] are meaningful, then I would expect to observe here a large kinetic energy release. Why is it not seen? What reason can there be for this?”

“If the benzyne cine-substitution were active, then the peak widths at half height should surely be all the same?”

The phenomenon of *kinetic energy release* is introduced on pg 15, while on pg 47 peak width measurements are used to deduce valuable mechanistic information for the loss of CO from the $(\text{C}_6\text{H}_4)^-\text{CO}_2\text{Me}$ system. Kinetic energy may be released in a dissociation process from two sources: (i) the reverse activation energy of the process and (ii) the excess energy of the transition state for the dissociation. Energy from both sources is partitioned between internal and translational energy of the products. It is this translational energy which may be observed as peak broadening. However, this partitioning of energy is dependent on the detailed energetics and dynamics and is intrinsic to the particular process. It is not necessarily dependent solely on the exothermicity of the reaction. Therefore the relationship between peak widths and excess energy is a complicated one and any predictions of peak broadening, such as those indicated by the examiner, may only be made in a general sense.

Summarising what is described in the text (p 47), the peak width measurements on the m/z 107 fragment ions from the three $(\text{C}_6\text{H}_4)^-\text{CO}_2\text{Me}$ isomers are not the same. Thus, either (i) the structures and/or the energies of the m/z 107 are different, or (ii) the modes of formation of the ions are different. Further results described indicate that the m/z 107 ions do have the same structure. This observation supports our proposal that a rearrangement of the *para* and *meta* isomers to the *ortho* isomer occurs before any rearrangement resulting in loss of CO.

Questions 3 and 4

“Page 47 states that, ‘the energy of the methyl loss is comparable in each case’, How is this known or inferred?”

“The CH₃ loss peaks in Fig 3.2 are extremely broad. Are they the same width? Why was this major competing reaction not discussed at all? Why is this channel (almost) closed the *ortho* isomer?”

The reaction involving methyl radical loss from (C₆H₄)CO₂Me, shown in Fig 3.2, is a charge remote process occurring from all three isomers and is of no importance to the investigation into the loss of CO from this system. The three isomers are essentially isoenergetic, it therefore follows that these radical losses are comparable. As for this competing radical reaction being closed to the *ortho* isomer, this is not the case. The *ortho* isomer is set up for the facile rearrangement reaction, which occurs in preference to the radical reaction. This is in contrast to the *meta* and *para* isomers which must first rearrange to the *ortho* isomer. Therefore, the rearrangement reaction is less competitive with respect to the methyl radical loss in these isomers.

Questions 5 and 6

“Possibly the level of theory used is inadequate for determining TS energies for such anions?”

“The CO₂ loss from methyl phenyl carbonate, Fig 3.9, is, according to the calculations, hugely exothermic, by about 112 kcal mol⁻¹. The *m/z* 107 peak in Fig 3.7 shows no significant broadening. Before doubting the experiments, I would doubt the utility of the calculations. Some sensible, critical remarks about these discrepancies are very necessary.”

Statements such as these may be put forward for most theoretical calculations at the levels of theory used in chapter three. While being modest, the optimisation calculations do include both diffuse and polarisation functions in their basis set definitions. The diffuse functions, in particular, allow better description of long range interactions, such as those within ion-neutral complexes. Accurate energies require more sophisticated methods to be employed. Due to the size of the systems studied the use of high-level methods, such as CCSD(T) and MP4(STDQ), are not feasible and therefore the B3LYP method coupled with the large 6-311++G(d,p) basis set was used. While higher-level calculations would result in more accurate energies, and possibly lower energy barriers, this would not alter the arguments described in the text. As for the broadening of peaks in the methyl phenyl carbonate based on exothermicity see above.